FLEXURAL DUCTILITY OF
REINFORCED CONCRETE BEAMS

ALFREDO ROBERTO DONOSO DI DONATO

A dissertation submitted to the Faculty of Engineering, University of the Witwatersrand, Johannesburg in partial fulfilment for the Degree of Master of Science in Engineering.

JULY, 1984

ABSTRACT

This report describes a study of variables affecting the flexural ductility of simply-supported singly-reinforced concrete beams subjected to a concentrated load at midspan. Such an investigation is aimed at improving the appreciation of factors which influence the redistribution of moments in the vicinity of ultimate load of statically indeterminate reinforced concrete structures. Although the inelastic response of reinforced concrete members has been recognized for a long time, its adoption in design practice is still a controversial matter.

Initial tests were made to establish the section geometry and percentage of steel to be used subsequently. The purpose of the fourteen tests was to study the effect of tension reinforcement, binders and span to depth ratio over rotation capacity. An assessment of the influence of sectional width was also made.

Although shear reinforcement must ensure that the strength in shear must exceed the strength in flexure, the tests suggested that binders alone , without compression reinforcement, do not have a beneficial influence on rotation capacity.

As the amount of steel in tension decreases, or the percentage of tension steel x yield stress decreases, the inelastic rotation and rotation capacity increases.

Rotation capac[illegible] seems not to be a function of the span-to-depth ratio[illegible]though if span decreases the inelastic rotation and rotation capacity seems to increase.

Although it was not possible in a six-month project to reach definite conclusions, a number of interesting and important features were observed during the project.

DECLARATION

I, Alfredo Roberto Donoso Di Donato, declare that this dissertation is my own, unaided work. It is being submitted in partial fulfilment for the degree of Master of Science in Engineering to the University of the Witwatersrand, Johannesburg. It has not been submitted before for any degree or examination in any other University.

____

ALFREDO ROBERTO DONOSO DI DONATO

Signed at ______________ this ________ day of ________ 1984

DEDICATION

All the effort spent in the realization of this dissertation leading towards the degree of Master of Science in Engineering, is dedicated to my father and to the memory of my beloved mother.

ACKNOWLEDGEMENTS

I would like to express my appreciation to the following:

My supervisor, Professor A.R.Kemp, whose assistance, guidance and advice I gratefully acknowledge.

Rotary Foundation of Rotary International for granting me a graduate scholarship, which enabled me to come to South Africa and further my studies, providing me with educational and living expenses from February 1983 to November 1983.

The University of the Witwatersrand, Johannesburg, for assigning me a senior bursary award, which gave me financial support from January 1984 to June 1984.

The academic and workshop staff of the Department of Civil Engineering, who were involved in one way or another in providing advice, ideas and support.

My colleagues at the University for their friendship and help.

My family for the much appreciated moral support and encouragement.

TABLE OF CONTENTS

TABLE OF CONTENTS (CONT'D)

NOTATION

A_s = Area of tensile reinforcement

A'_s = Area of compressive reinforcement

a = Depth of the equivalent rectangular stress block

b = Width of rectangular section

C = The neutral axis depth

C_u = Distance from extreme compressive fibre to neutral axis at ultimate strength, or neutral axis depth at ultimate strength.

C_y = Distance from extreme compressive fibre to neutral axis that satisfies force equilibrium at first yield of tension steel

d = Distance from extreme compressive fibre to centroid of tensile reinforcement, or effective depth

d' = Distance from extreme compressive fibre to centroid of compressive reinforcement

E_s = Modulus of elasticity of steel

E_c = Secant modulus of elasticity of concrete

E_{c2} = Maximum concrete compressive strain calculated according to CEB-FIP

E'_s = Modulus of strain-hardening

E_{SH} = Strain at beginning of strain-hardening

EI = Flexural rigidity

F = Bond factor

f_c = Strength of a concrete cylinder of diameter 150mm

f_{cu} = Cube crushing strength of concrete

f_{ct} = Maximum tensile strength for concrete

NOTATION (CONT')

f_{cy} = Maximum concrete compressive stress at yield of tension reinforcement

f'_c = Cylinder crushing strength of concrete

f'_s = Stress in compression reinforcement

f_y = Yield point stress of tension reinforcement

f_{ys} = Yield point of the stirrup steel

L = Span of the beam

l_p = Hypothetical length of the member over which a uniform inelastic curvature is assumed to be spread, creating an equivalent rectangle with an area equal to the value of the inelastic rotation for half span of the beam

M = Moment

M_u = Ultimate moment of resistance

M_{u1} = Design moment at ultimate strength according to ACI

M_{u2} = Design moment at ultimate strength according to CP110

M_y = Moment at first yield of tension reinforcement

n = ratio of modulus of elasticity of steel to that of concrete : Es/Ec

P = Midspan load

p = Tensile steel ratio, As/bd

p' = compressive steel ratio, A's/bd

p_b = Steel ratio at balanced ultimate strength conditions in a beam without compression reinforcement according to ACI code

p" = Binding ratio expressed as the ratio of the

NOTATION (CONT')

volume of the binding reinforcement (one stirrup plus compressive steel) to the volume of the concrete bound (area enclosed by one stirrup multiplied by the stirrup spacing)

R = Radius of curvature

w = Plate width

x_{pu} = Plastic neutral axis calculated according to CP110

z = Distance between the points of zero and maximum moment

z_1 = Distance between neutral axis depth and the centroid of the tension reinforcement, that is : lever arm.

β_1 = Reduction factor equal to 0,85 for $f'_c \leq$ 27,6MPa, which reduces continuously by 0,05 for each 6,89MPa of strength of concrete in excess of 27,6MPa.

dx = Small element of length of a member

ϵ_c = Concrete strain in the extreme compressive fibre

ϵ_{c1} = Maximum strain in axial compression(average of 0,0022 adopted in code)

NOTATION (CONT')

ε_{cu}	=	Maximum concrete compressive strain
ε_s	=	Tension steel strain
ε_y	=	Steel strain at commencement of yield of the tension reinforcement
η	=	Ratio of $\varepsilon_c/\varepsilon_{c1}$
θ	=	Total rotation
θ_e	=	Elastic rotation
$\theta_i=\theta_p$	=	Inelastic rotation
σ_c	=	Concrete stress at strain Ec in N/mm²
$\emptyset$	=	Curvature
$\emptyset_p$	=	Plastic curvature
$\emptyset_u$	=	Curvature at ultimate strength
$\emptyset_y$	=	Curvature at commencement of yield of the tension reinforcement

LIST OF FIGURES

LIST OF FIGURES (CONT'D)

LIST OF FIGURES (CONT')

LIST OF FIGURES (CONT')

LIST OF FIGURES (CONT')

LIST OF TABLES

CHAPTER 1

INTRODUCTION

In order to establish the extent to which the concept of plastic theory may be applied to the analysis of reinforced concrete structures, a greater understanding of the inelastic response of reinforced concrete is necessary. Both limit design of structural concrete and plastic design of structural steel are based on the inelastic behaviour of structures at high loads. The inelastic behaviour results in a readjustment of the relative magnitudes of internal moments and forces at various points within a structure; but these two design methods differ in an important aspect.

The plastic design methods for structural steel concentrate on the formation of a sufficient number of plastic sections to transform all or part of a structure into a mechanism and therefore causes its collapse; but little attention is given to the magnitude of the strains at the individual yielded sections as redistribution of moments proceeds. The strain at maximum stress of concrete in compression in a reinforced concrete member is smaller than those which develop in a mild steel member. Consequently, it could occur that the strain capacity of a reinforced concrete yielded section is exhausted before full redistribution of bending moments takes place. It is this reasoning that makes it necessary to consider the deformation of the yielded regions in any theory of limit design for structural concrete, and more specifically to limit their rotation to known safe values.

While the inelastic flexural behaviour of reinforced concrete members and structures has been recognized for a long time, its adoption in design practice is still a controversial matter since the distribution of moments in this phase are no longer proportional to the distribution of moments in the elastic range. This is explained by the fact that, after cracking has reached a significant degree at one or more sections of a member, the moment that results from the application of additional loads is carried in greater proportion by the portion of the member that remains uncracked.

Once the ultimate moment of resistance is reached at one critical section of a reinforced concrete structure, the extent to which further load can be carried by the structure depends on the rotation capacity of that one critical section; provided that this one critical section is ductile, moment redistribution will occur until a collapse mechanism is formed in that structure. Rotation capacity known as the ratio of inelastic rotation to elastic rotation is an important parameter that indicates quantitatively the behaviour of the inelastic response as a multiple of the well known elastic response.

The investigation described in this report studies the influence of several variables on the rotation capacity of simply-supported singly-reinforced concrete beams subjected to a concentrated load at midspan. The analysis of the results will lead to a better understanding of the inelastic response and therefore to the rotation capacity of reinforced concrete members in indeterminate structures. A full knowledge of rotation capacity will eventually lead to inelastic design methods which will reflect as closely as possible the actual behaviour of reinforced concrete structures.

In the second chapter a description is given of the basis for quantifying ductility of reinforced-concrete members, as well as a discussion of the results of earlier research on this subject. The fourteen tests which were undertaken in this project are described in Chapter 3. Four of the tests were aimed at assessing the effect of binders, five of the tests enables an assessment to be made of the influence of span and three tests were used to assess the influence of the strength properties of reinforcing steel. The remaining two experiments of the total fourteen are the control tests.

The results are analyzed and discussed in Chapter 4 and the conclusions summarized in the fifth chapter.

CHAPTER 2

FLEXURAL DUCTILITY OF CONCRETE MEMBERS

2.1 INTRODUCTION

Ductility has been considered a main factor influencing rotation capacity of yielded zones, and also governs the redistribution of moments in a structure.

In general terms, ductility of a concrete section is the ability to deform beyond the elastic range without major alteration of its resistant capacity.

In order for reinforced concrete members to undergo large deformations and rotations for loads near to failure, limitations on the percentage of reinforcement and geometry of the members become necessary.

2.2 MOMENT-CURVATURE RELATIONSHIP

2.2.1 Curvature of a member

A typical element of a reinforced concrete member is illustrated in Fig.2.1, where the radius of curvature R, the neutral axis depth C, concrete strain in the extreme compressive fibre ε_c, and tension steel strain ε_s will vary along the member due to the fact that the concrete will carry some tension between the cracks in the member.

Considering a small element of the member, and using the notations of Fig. 2.1, the rotation that occurs between the ends of the element is given by:

$$\frac{dx}{R} = -\frac{\varepsilon_c dx}{C} = \frac{\varepsilon_s dx}{d-C}$$

$$\therefore \quad \frac{1}{R} = -\frac{\varepsilon_c}{C} = \frac{\varepsilon_s}{d-C} = \emptyset = -\frac{\varepsilon_c + \varepsilon_s}{d} \qquad \text{Eqn.2.1}$$

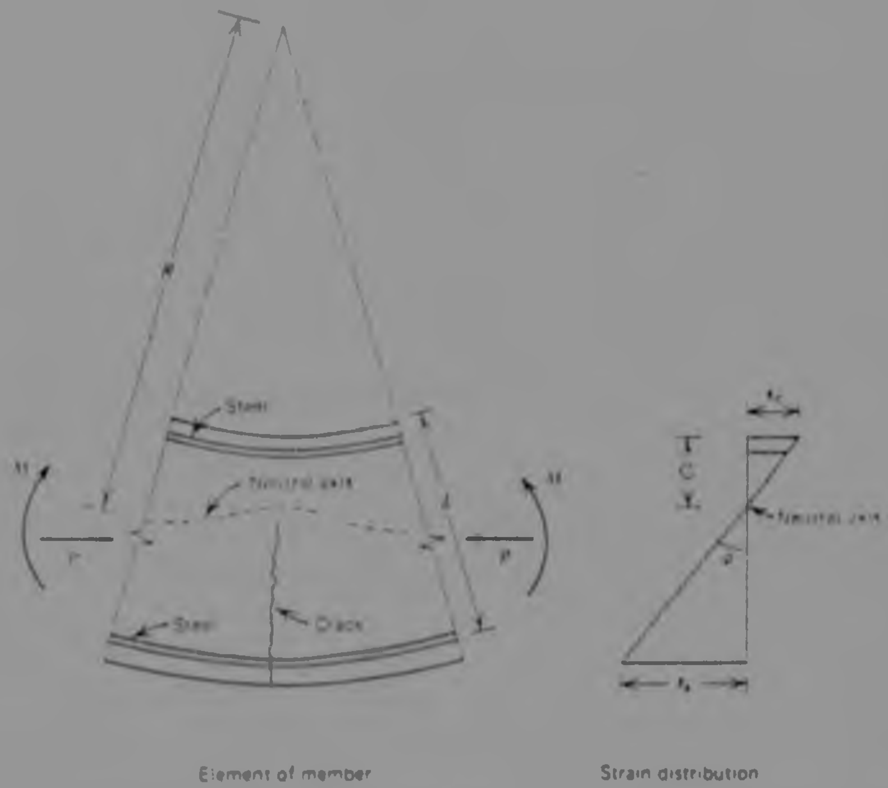

FIGURE 2.1 Deformation of a flexural member
(Refer to Bibliography: Park[9])

where $\frac{1}{R}$ is the curvature at the element

d is the effective depth.

If strains are measured at two levels of a section of a reinforced concrete beam, the curvature can be calculated from Eqn.2.1 permitting the moment-curvature relationship for the section to be obtained, as the bending moment is increased to failure.

Fig.2.2 shows two moment-curvature relationships for singly reinforced beams failing in tension and compression. Both curves are linear in the initial stages for which the flexural rigidity of the section can be obtained by applying Eqn.2.2

$$EI = M.R = \frac{M}{\emptyset} \qquad \text{Eqn.2.2}$$

where M = moment
Ø = curvature
EI = flexural rigidity

With increase in moment, cracking of the concrete reduces the flexural rigidity of the sections. This decrease of rigidity is greater for lightly reinforced sections than for the more heavily reinforced sections.

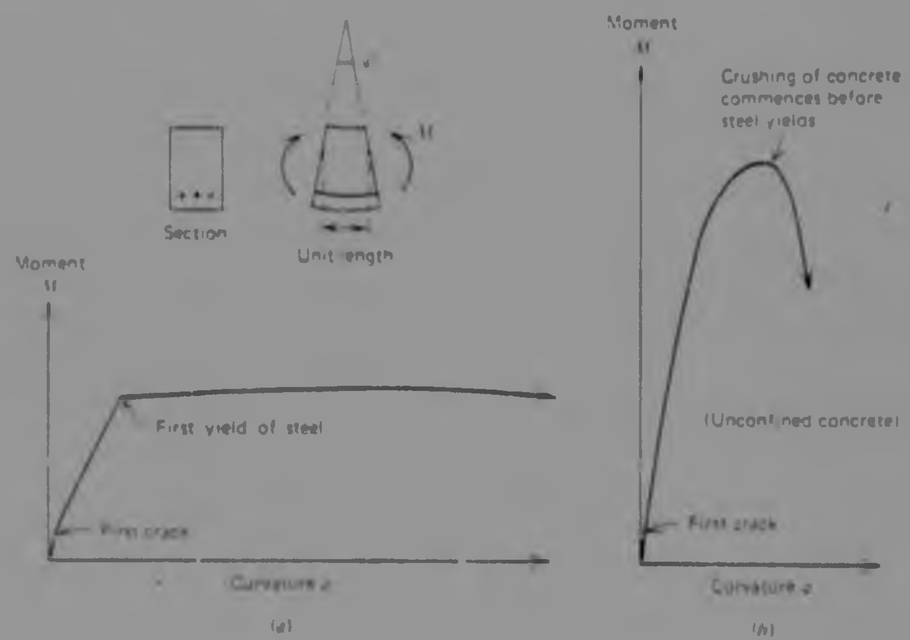

FIGURE 2.2 : Moment-Curvature relationships for singly reinforced beam sections (a) Section failing after yielding of the reinforcement, $p < p_b$.(b) Section failing in compression $p > p_b$.(Refer to Bibliography: Park[9]).

Lightly reinforced sections have practically a linear relation between moment and curvature up to the point at which the steel yields as shown in Fig. 2.2a. As the steel yields, a large increase in curvature occurs as the bending moment rises slightly due to a small increase of the level arm and strain hardening and finally for the last stage of the curve the moment continues to decrease.

Heavily reinforced sections, as in Fig 2.2b, show that the moment-curvature relation becomes non-linear when the concrete enters the inelastic part of its stress-strain relationship and failure can be quite brittle unless the concrete is appropriately confined by transverse reinforcement.

If the concrete is not confined, it crushes at a relatively low curvature before the steel yields, causing an immediate decrease in the moment-carrying capacity. To ensure ductile behaviour, steel contents of beam members are limited by various codes.

The moment-curvature relation for a beam, in which the tension steel yields, can be idealized to a tri-linear relationship as presented in Fig.2.3a where the first stage ends at cracking of the concrete, the second stage at the yielding of the tension steel, and the third stage at the limit of the strain in the concrete.

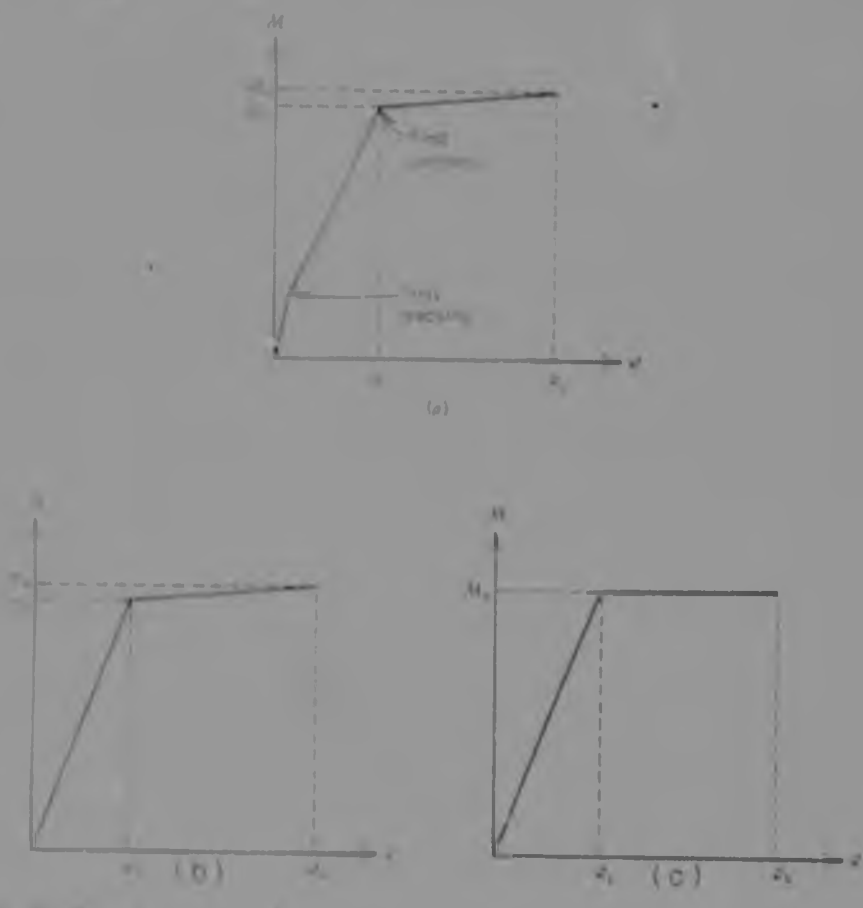

FIG.2.3 Idealized moment-curvature curves for a singly reinforced section failing after yielding of the reinforcement. (Refer to Bibliography: Park 9).

It is often sufficient to idealise the moment-curvature relationship to a bilinear relationship as shown in Fig. 2.3b. For design purposes the simplified curve of Fig.2.3b is generally adopted.

2.2.2 Theoretical Moment and Neutral Axis Ratios Vs. Curvature.

For the calculation of moment-curvature curves for reinforced concrete sections, it is assumed that plane sections before bending remain plane after bending, and that the stress-strain curves for concrete and steel are known. Given a maximum concrete strain for the extreme fibre in compression, and an assessment of the depth of the plastic neutral axis required for the concrete to resist the yielded forces in the reinforcement, it is possible to calculate the maximum curvature to be adopted for this curve.

This maximum curvature is divided into a number of small increments, and for each increment a depth of neutral axis is assumed. The strain is determined at increments of depth over the section and, from the material stress-strain properties, the resulting axial force and bending moment across the section is determined. For a beam not subjected to axial force, the neutral axis is adjusted progressively until the net axial force across the section is negligible. Once this condition of equilibrium has been reached at a particular increment of curvature, the neutral axis depth and the resulting bending moment of internal forces may be used to plot the relationship between moment or neutral axis depth and curvature. The trial and error calculations involved in this process are lengthy and therefore it is convenient to undertake them using a digital computer. An example of

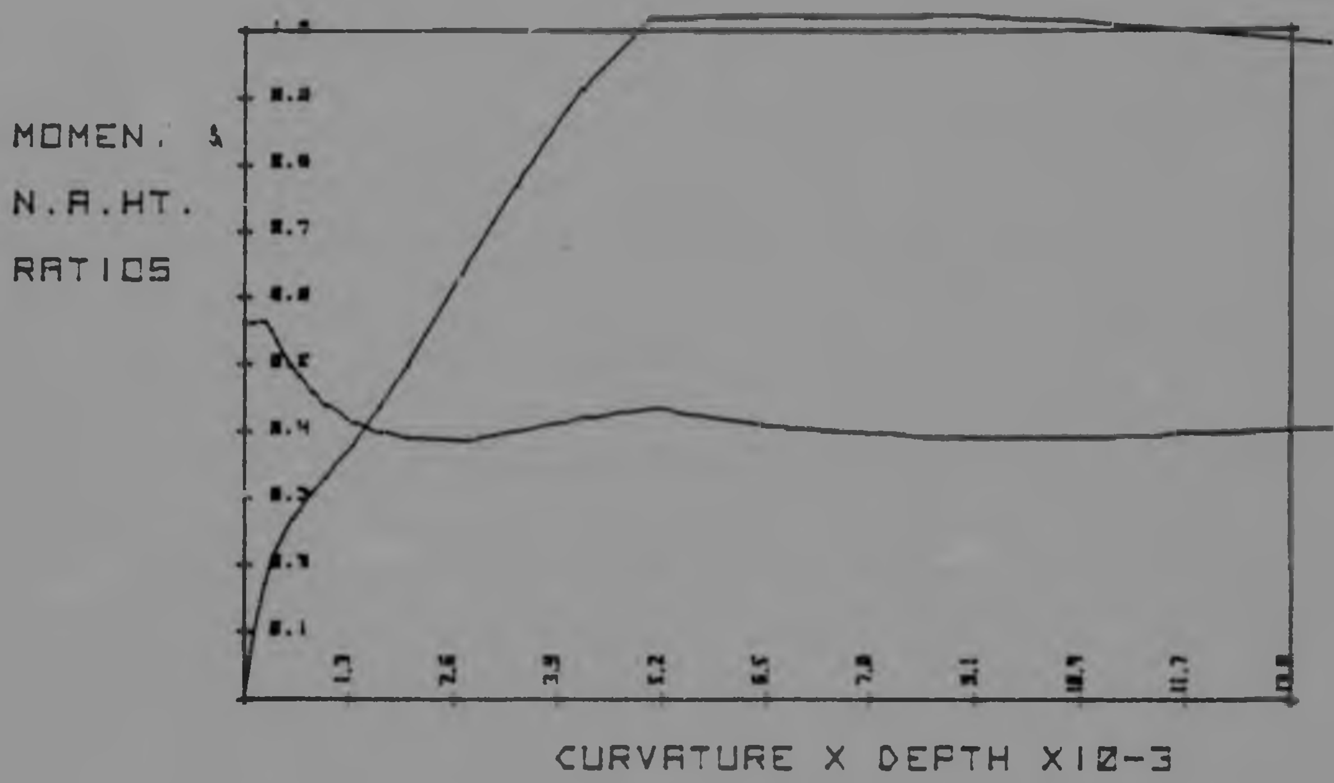

FIGURE 2.4

MOMENT AND NEUTRAL AXES HE .T RATIOS VS. CURVATURE moment and neutral axis ratios vs. curvature is illustrated in Fig.2.4 corresponding to a cross-section with steel percentage of 1,571%.

The idealized non-dimensional stress-strain curve for concrete in compression under short-term duration loading used in evaluating this theoretical moment-curvature relationship is as proposed by CEB-FIP[1] code shown in Fig. 2.5a, and is represented by the following function :

$$\frac{\sigma_c}{f_c} = \frac{K\eta - \eta^2}{1+(K-2)\eta} \qquad \text{Eqn.2.3}$$

where σ_c = concrete stress at strain ε_c in N/mm^2

f_c = strength of a concrete cylinder of diameter 150mm in N/mm^2

$\eta = \dfrac{\varepsilon_c}{\varepsilon_{c1}}$

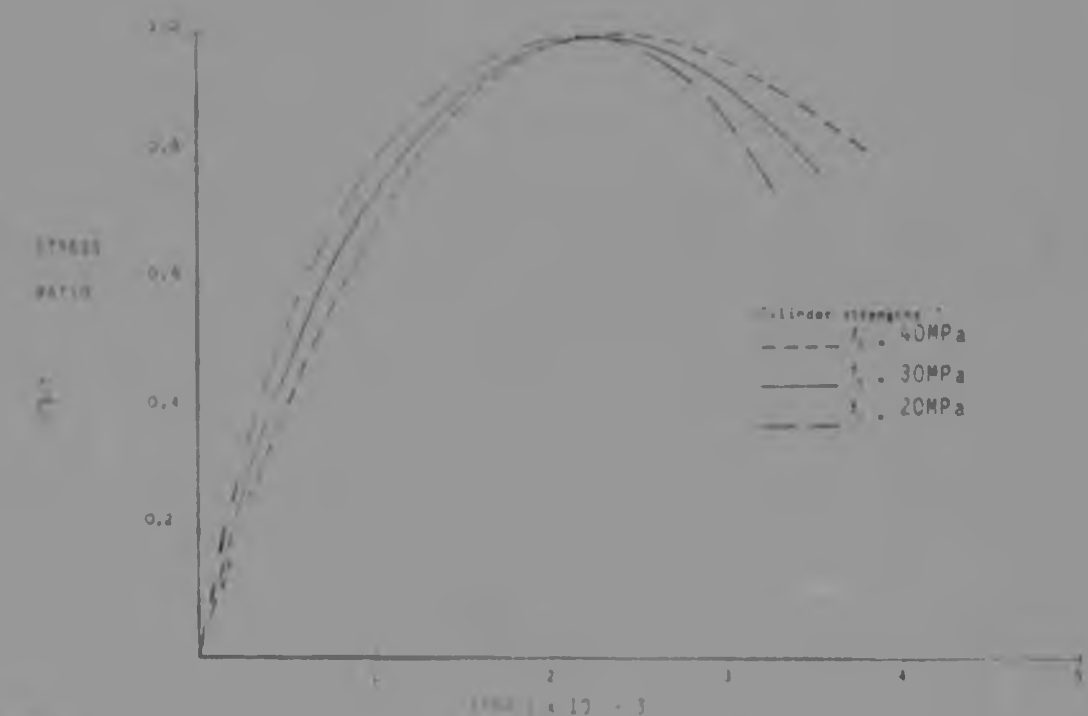

FIG.2.5a :Concrete stress-strain curves (Refer to **Bibliography:Kemp**[6])

ε_{c1} = maximum strain in axial compression (average of 0,0022 adopted in calcualtions)

$$K = \frac{1.1 \times E_c \times \varepsilon_{c1}}{f_c}$$

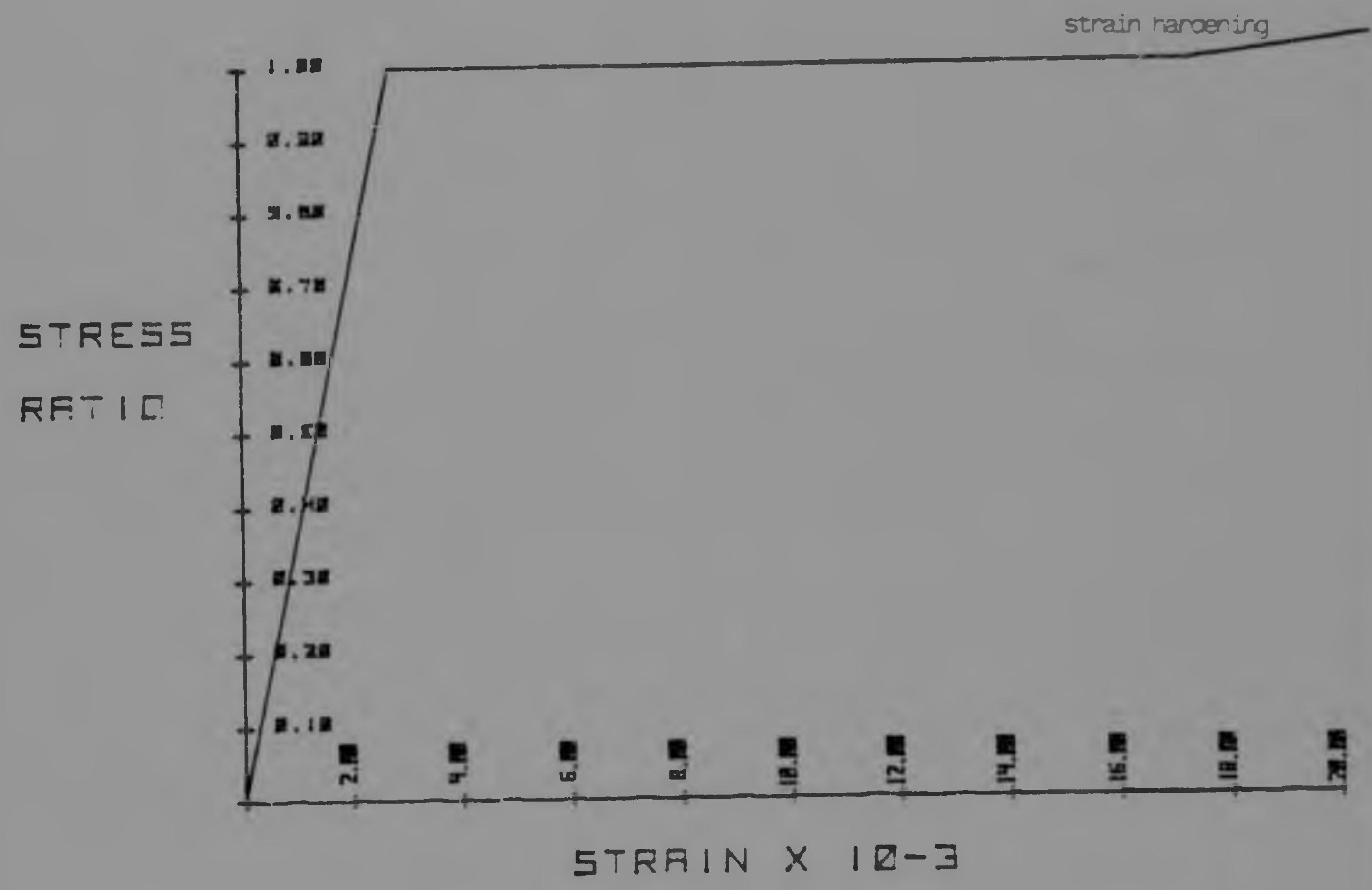

FIGURE 2.5b : IDEALIZED STRESS RATIO-STRAIN CURVE FOR STEEL

E_c = secant modulus of elasticity = $9{,}5(f_c)^{1/3}$ kN/mm²

The stress ratio - strain curve for concrete in tension was also taken into account although its influence is small and almost negligible. A linear relationship is adopted up to failure at which the maximum tensile strength according to CEB-FIP is :

$$f_{ct} = 0{,}3\ f_c^{2/3} \qquad \text{Eqn.2.4}$$

The idealized stress ratio-strain curve for the steel is shown in Fig. 2.5b, high strength steels used exhibited a well-defined yield point whereas the mild steel did not. The modulus of elasticity of the steel, according to the CP110[2] code, is defined as 200GPa up to the yield point; after which measured hardening is taken into account.

2.3 DUCTILITY OF UNCONFINED BEAM SECTIONS

Although unconfined reinforced concrete beams are unusual in practical conditions, concrete is generally considered to be unconfined unless special beneficial measurements are taken to confine it by means of transverse reinforcement.

In the design of structural sections in flexure, it is common practice to evaluate the ultimate moment of resistance of a reinforced concrete section on the basis of a rectangular stress block in compression, which has the same stress resultant located at the same level as the actual stress distribution.

The curvature, neutral axis depth, and moment of resistance at the ultimate strength for a reinforced concrete beam can be calculated using the equations derived from the concepts of compatibility of strains and equilibrium of forces.

Fig.2.6 illustrates a general case of a doubly reinforced concrete beam in flexure. The equations defining neutral axis, moment and curvature are :

<u>At first yield :</u> (Refer to Bibliobraphy: Mattock[8])

$$C_y = \{[(p + p')^2 n^2 + 2(p + p'\frac{d'}{d})n]^{\frac{1}{2}} - (p+p')n\}d \qquad \text{Eqn.2.5}$$

$$f_{cy} = \frac{pf_y}{\frac{C_y}{2d} + np'(1-d'/C_y)} \qquad \text{Eqn.2.6}$$

$$M_y = \frac{1}{2} f_{cy} \times C_y \times b(d - \frac{C_y}{3}) + A'_s f'_s (d-d') \qquad \text{Eqn.2.7}$$

$$f'_s = f_{cy} n(1 - \frac{d'}{C_y}) \qquad \text{Eqn.2.8}$$

$$\emptyset_y = \epsilon_y/(d - C_y) \qquad \text{Eqn.2.9}$$

where :

C_y = distance from extreme compressive fibre to neutral axis that satisfies force equilibrium at first yield of tension steel

f_y = yield stress of tension reinforcement

f_{cy} = maximum concrete compression stress at yield of tension reinforcement

A_s = area of tensile reinforcement

A'_s = area of compressive reinforcement

b = width of rectangular section

p = tensile steel ratio, A_s/bd

p' = compressive steel ratio, A'_s/bd

n = ratio of modulus of elasticity of steel to that of concrete, E_s/E_c

d' = distance from extreme compressive fibre to centroid of compressive reinforcement.

f'_s = stress in compression reinforcement

M_y = moment at yield of tension reinforcement

ϵ_y = steel strain at commencement of yield

$\emptyset_y$ = curvature at commencement of yield of the tension reinforcement.

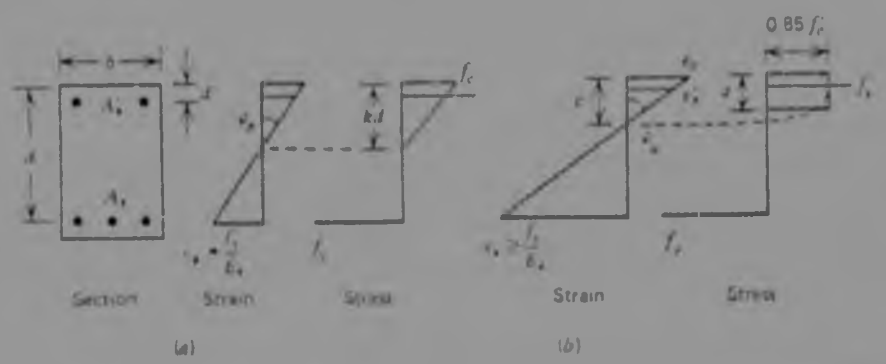

Doubly reinforced beam section with flexure (a) At first yield (b) At ultimate.

FIGURE 2.6: Doubly reinforced beam section with flexure (Refer to Bibliography: Park[9]).

At ultimate strength : (Refer to Bibliography : Park[9]).

$$a = \frac{A_s f_y - A'_s f_y}{0,85 f'_c b} \qquad \text{Eqn 2.10}$$

$$M_u = 0,85 f'_c ab\left(d - \frac{a}{2}\right) + A'_s f_y (d - d') \qquad \text{Eqn.2.11}$$

$$\emptyset_u = \frac{\epsilon_c}{C_u} \; ; \quad C_u = a/\beta_1 \qquad \text{Eqns.2.12 and 2.13}$$

where :

a = depth of the equivalent rectangular stress block

M_u = ultimate moment of resistance

C_u = distance from extreme compressive fibre to neutral axis at ultimate strength

$\emptyset_u$ = curvature at ultimate strength

β_1 = reduction factor equal to 0,85 for $f'_c \leq 27,6$MPa which reduces continuously by 0,05 for each 6,89MPa of strength in excess of 27,6MPa

ϵ_y = steel strain at commencement of yield

ϕ_y = curvature at commencement of yield of the tension reinforcement.

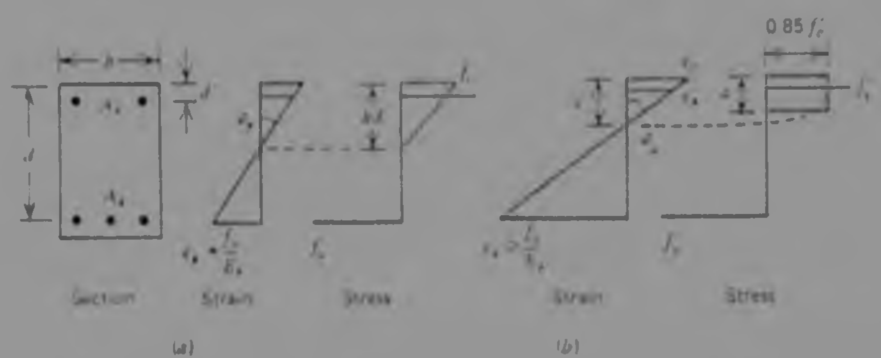

Doubly reinforced beam section with flexure (a) At first yield (b) At ultimate.

FIGURE 2.6: Doubly reinforced beam section with flexure (Refer to Bibliography: Park[9]).

At ultimate strength : (Refer to Bibliography : Park[9]).

$$a = \frac{A_s f_y - A'_s f_y}{0,85 f'_c b} \qquad \text{Eqn 2.10}$$

$$M_u = 0,85 f'_c ab(d - \frac{a}{2}) + A'_s f_y (d - d') \qquad \text{Eqn.2.11}$$

$$\phi_u = \frac{\epsilon_c}{C_u} \quad ; \quad C_u = a / \beta_1 \qquad \text{Eqns.2.12 and 2.13}$$

where :

a = depth of the equivalent rectangular stress block

M_u = ultimate moment of resistance

C_u = distance from extreme compressive fibre to neutral axis at ultimate strength

ϕ_u = curvature at ultimate strength

β_1 = reduction factor equal to 0,85 for $f'_c \leq 27,6$MPa which reduces continuously by 0,05 for each 6,89MPa of strength in excess of 27,6MPa

Therefore the ductility ratio f[illegible] section may be written as

$$\frac{\emptyset_u}{\emptyset_y} = \frac{\varepsilon_c (d - C_y)}{(f_y/E_s)(a/\beta_1)} = \frac{0{,}85\beta_1 E_s \varepsilon_c f'_c}{(p-p')f_y^2} \left\{ 1 + (p+p')n - \sqrt{(p+p')^2 n^2 + 2\left(p + \frac{p'd'}{d}\right)n} \right\}$$

Eqn. 2.14

(Refer to Bibliography: Park[9])

According to this formula as illustrated in Figs. 2.7 and 2.8, it is possible to appreciate the influence of the following variables on ductility:

- An increase in the percentage of steel in tension decreases the ductility, because both K and a are increased, therefore $\emptyset_y$ increases and $\emptyset_u$ decreases.
- An increase in the percentage of steel in compression increases the ductility, because both K and a are decreased, therefore $\emptyset_y$ decreases and $\emptyset_u$ increases.
- As a result of an increase of the yield strength of the steel, the ductility decreases since both f_y/E_s and a are increased causing $\emptyset_y$ to increase and $\emptyset_u$ to decrease.
- The ductility is increased as a result of increasing the strength of the concrete because both K and a decrease causing $\emptyset_y$ to decrease and $\emptyset_u$ to increase.
- If the concrete strain at the extreme fibre of compression increases, the ductility increases since $\emptyset_u$ increases.

According to Cohn[1], the principal factors affecting the ductility of a reinforced concrete section are classified as : Material, geometrical and loading variables.

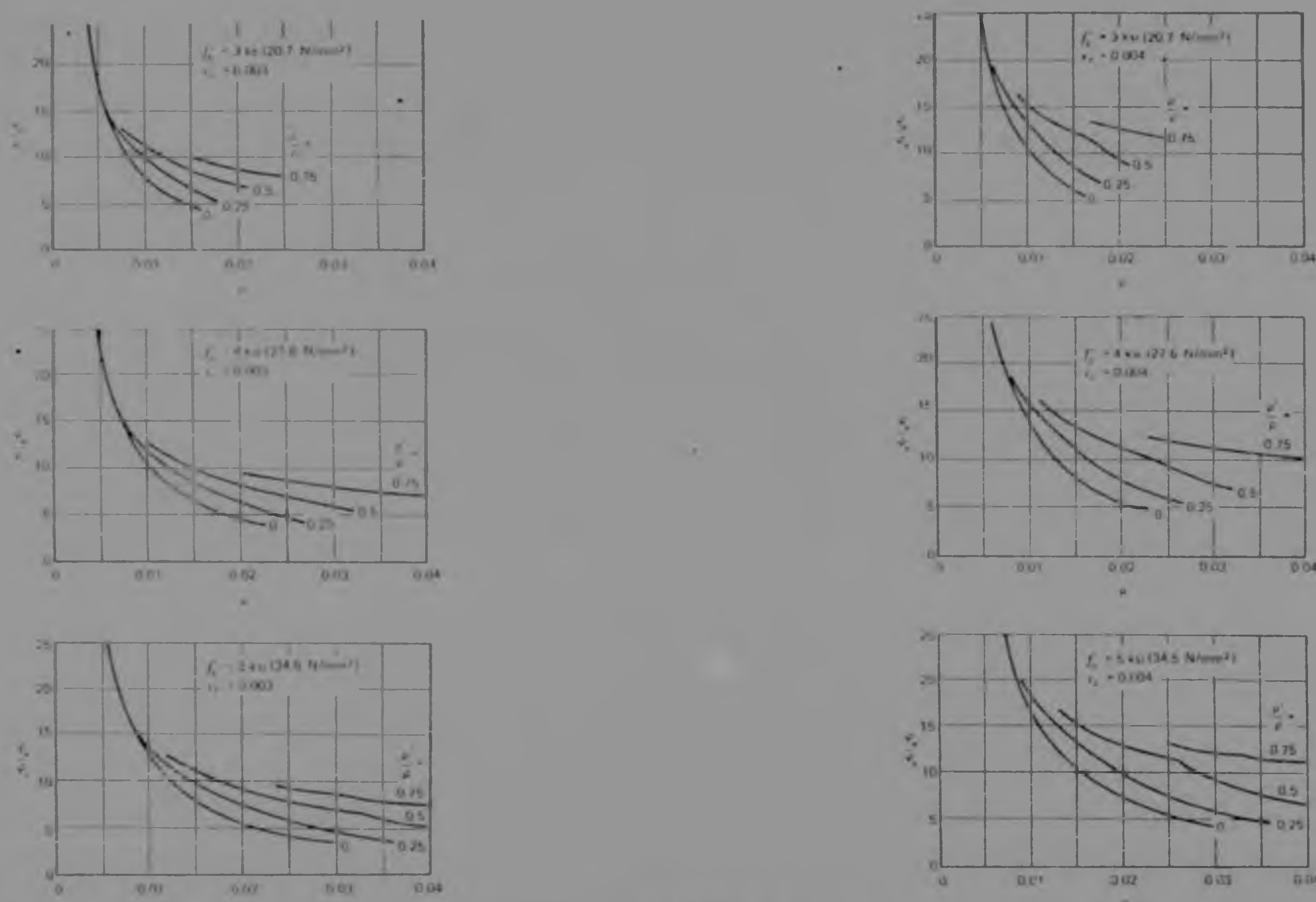

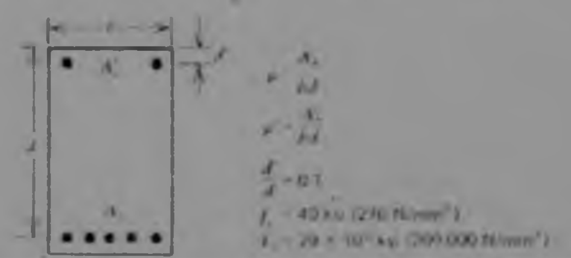

FIGURE 2.7: Variation of ϕ_u/ϕ_y for beams with unconfined concrete and f_y = 40 ksi (276 N/mm²).
(Refer to Bibliography: Park[9]).

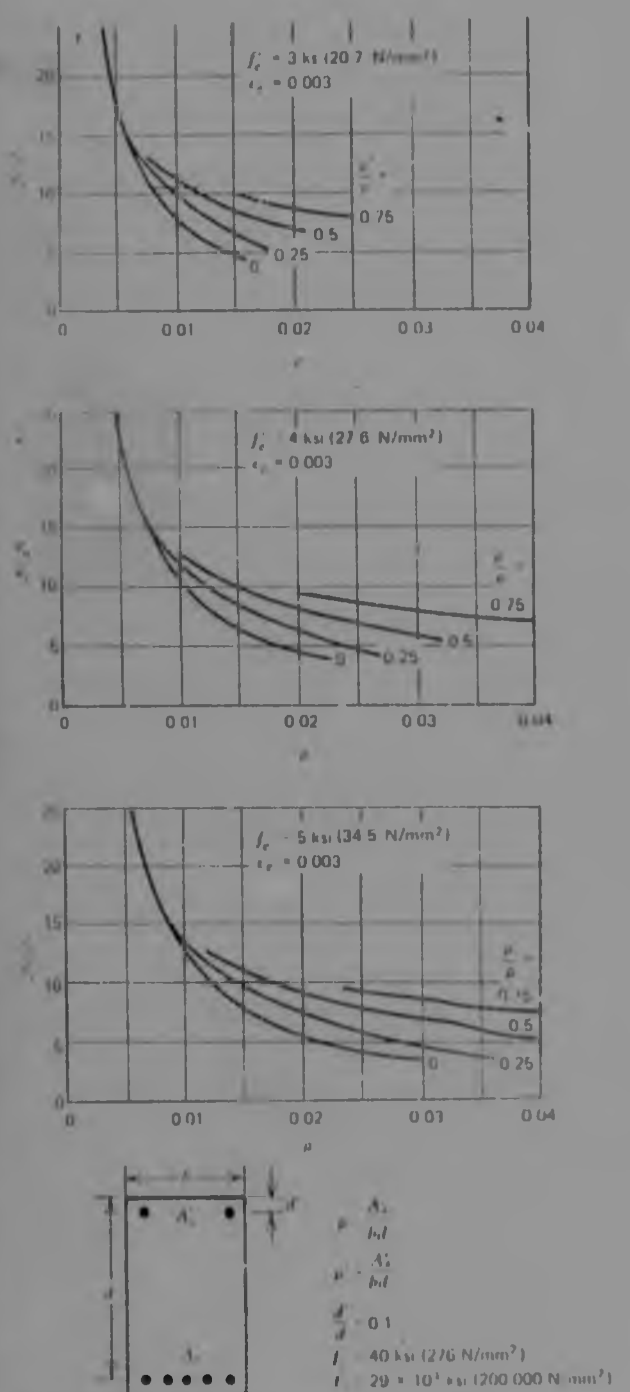

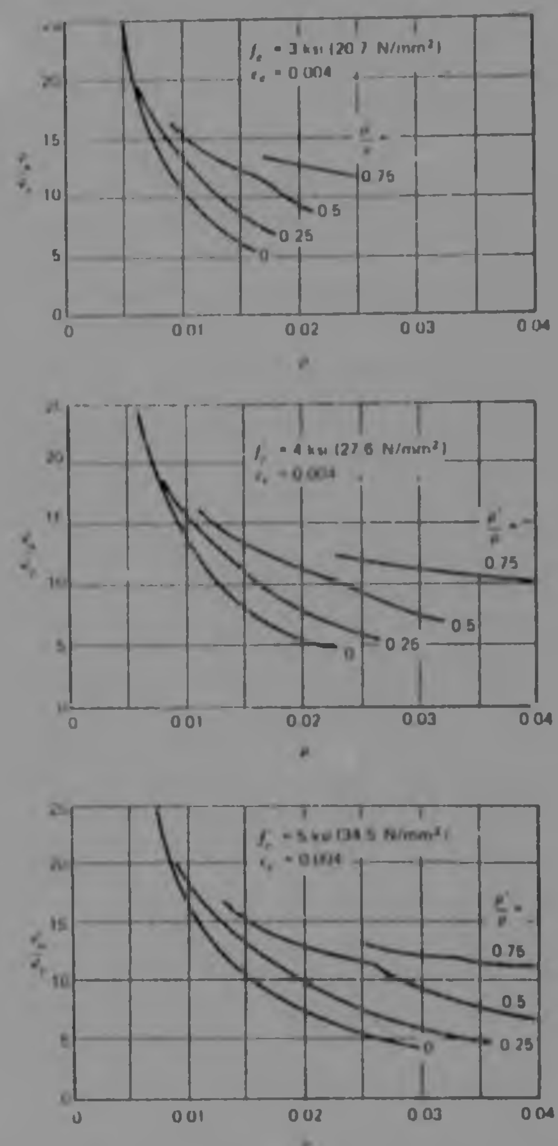

FIGURE 2.7: Variation of φ_u/φ_y for beams with unconfined concrete and $f_y = 40$ ksi (276 N/mm²) (Refer to Bibliography: Park[9]).

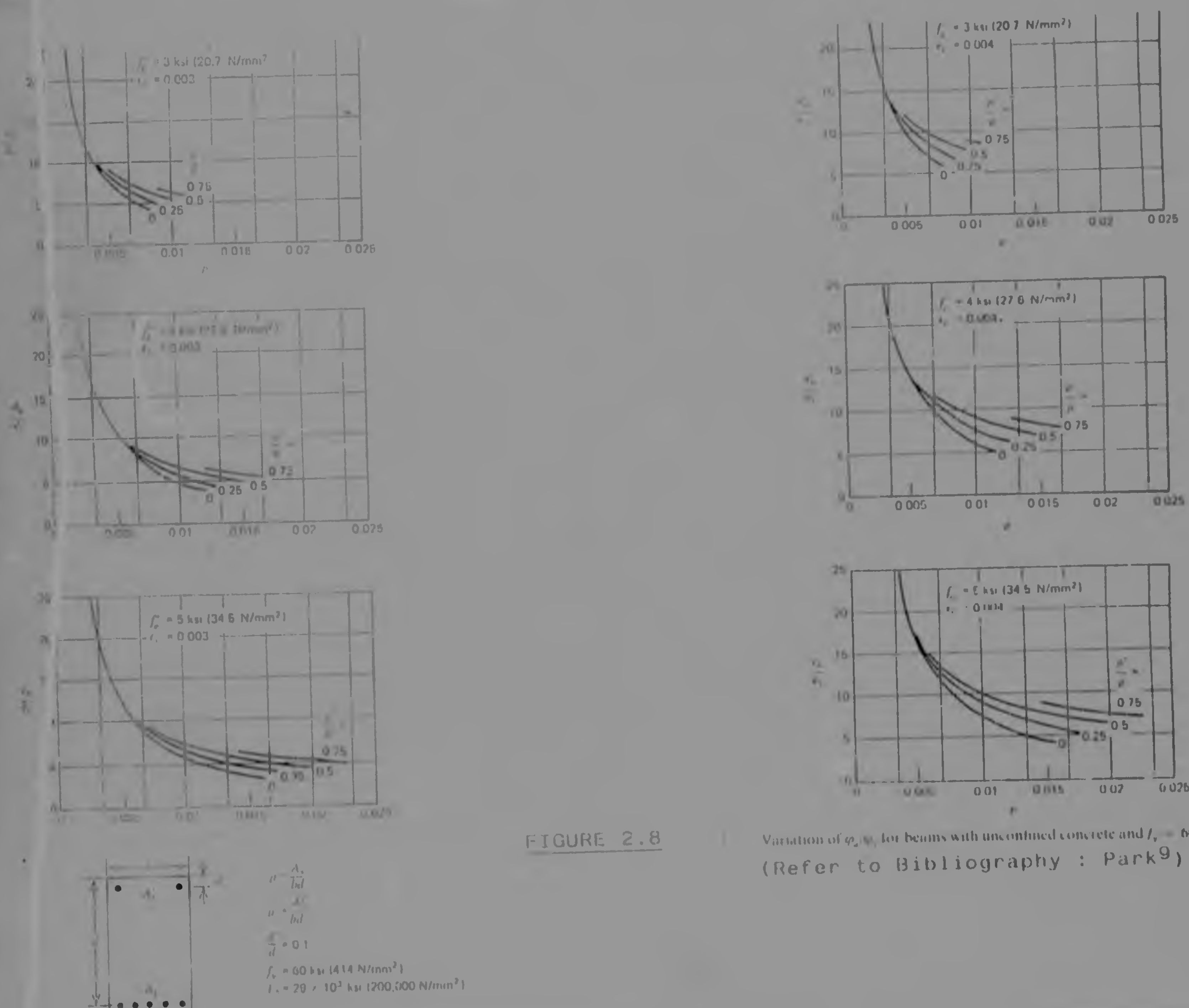

FIGURE 2.8 Variation of φ_u/φ_y for beams with unconfined concrete and f_y = 60 ksi (414 N/mm²) (Refer to Bibliography : Park[9]).

Material variables take into consideration the concrete quality, grades of tension and compression reinforcement, strength of lateral reinforcement, strain-hardening of steel, bond and tensile strength of concrete.

Geometric variables consider the shape and size of sections, percentage of tension and compression reinforcement, amount and spacing of transverse reinforcement and cover thickness of concrete to steel.

Finally the loading variables include the duration of loading, axial loading, prestressing, repetition of loading and loading reversal.

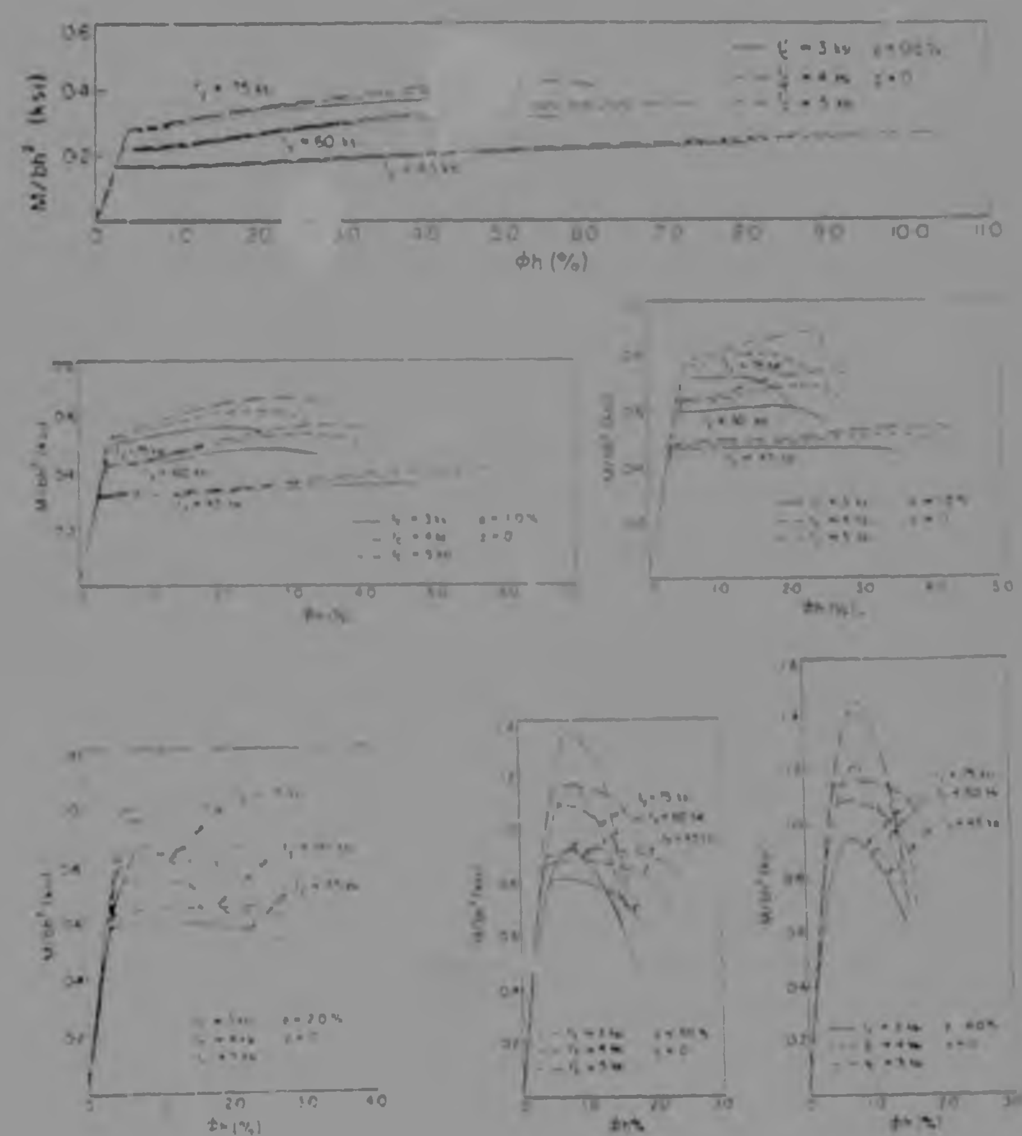

FIGURE 2.9: Effect of concrete and steel grades of steel percentages on ductility : M-Ø diagrams. (Refer to Reference: Cohn[3])

Figure 2.9 shows that ductility, as a ratio of ultimate to yield curvatures, increases as a result of increasing the concrete strength or decreasing the strength of the longitudinal reinforcements, independent of the percentage of steel in the section.

Ductility increases for lightly reinforced sections when strain-hardening is taken into consideration, but its effect on heavily reinforced sections is small and negligible, as can be seen from Fig.2.10

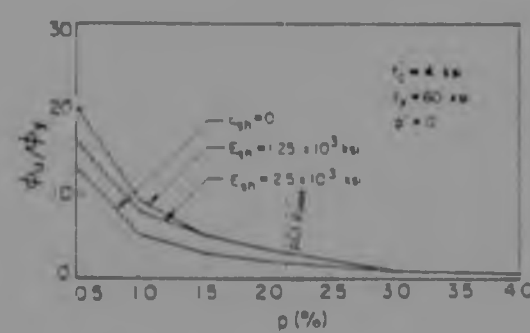

FIGURE 2.10 Effect of strain-hardening of steel on ductility: $\varnothing_u/\varnothing_y$-p diagrams.(Refer to Reference:Cohn[3])

From Fig.2.11 which is for singly reinforced sections with nominal amounts of lateral reinforcement, it can be seen that although for low reinforcement percentages fairly hich ductility ratios are reached by most concrete and steel strengths, this ratio may be as low as 2,5 for some steel and concrete strengths as p reaches the maximum value specified in ACI[4]. In this figure each curve has a little arrowhead attached to it which corresponds to the maximum percentage of tensile reinforcement (pmax).

The tensile strength of concrete has almost no effect on the ductility since moment-curvature relationships for sections that included and neglected tensile strength of concrete have been found to be almost identical.

Among the geometric variables the percentages of tension and compression reinforcement are the most important; the ductility of a section increases as the amount of tension reinforcement decreases. This is confirmed in Fig.2.12 which shows that almost no ductility is available for sections **with** very high steel percentages, this is precisely why many codes impose an upper limit on the amount of tension reinforcement to be used in design.

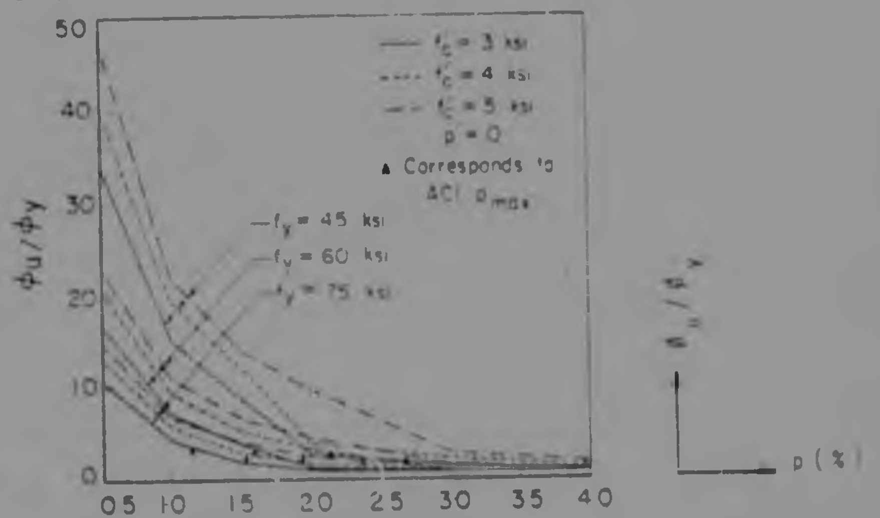

FIGURE 2.11: Effect of concrete and steel grades and steel percentages on ductility $\emptyset_u / \emptyset_y$-p diagrams. (Refer to Reference: Cohn [3])

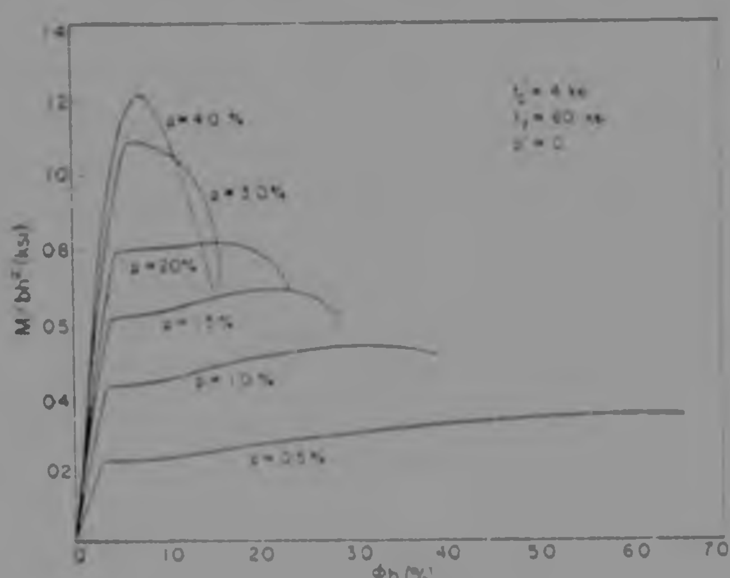

FIGURE 2.12: Effect of tension steel percentage on ductility : M-Ø diagrams. (Refer to Reference : Cohn [3])

Fig 2.13 shows that an increase in the percentage of compression reinforcement increases significantly the ductility of the section for a given strength of concrete and steel.

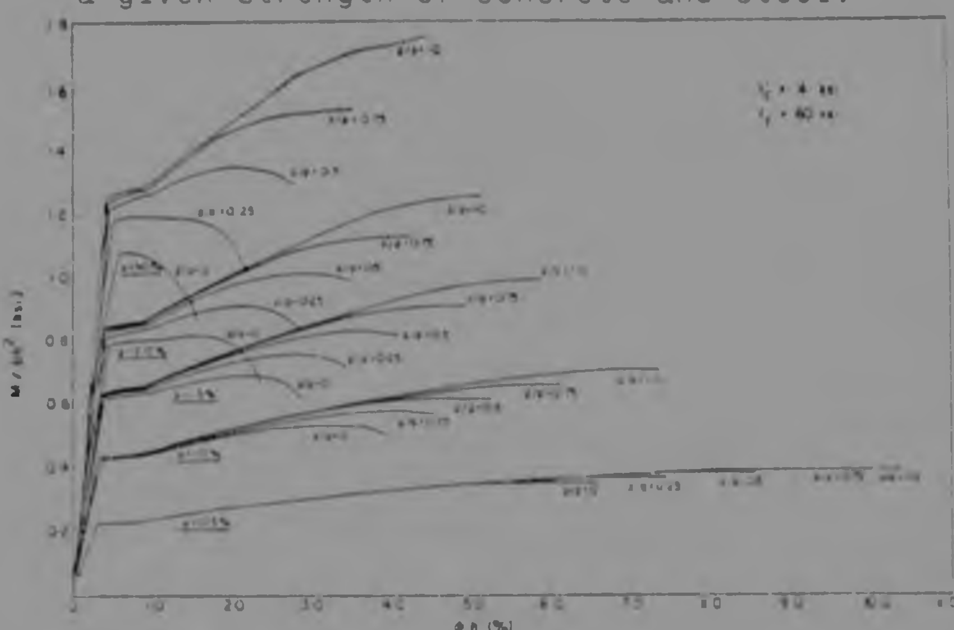

FIGURE 2.13 Effect of Compression reinforcement on ductility M -Ø diagrams (Refer to Reference : Cohn[3])

Ductility can be improved by decreasing the spacing and increasing the amount of lateral reinforcement as shown in Figs. 2.14, 2.15 and 2.16.

The effect of duration of loading on ductility is not very significant according to Fig.2.17.

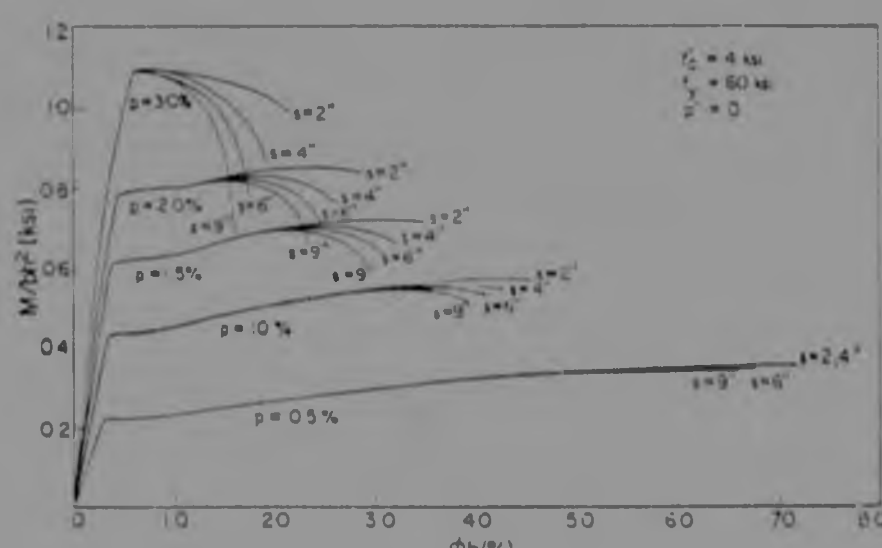

FIGURE 2.14 Effect of tie spacing on ductility M-Ø diagrams. (Refer to Reference: Cohn[3])

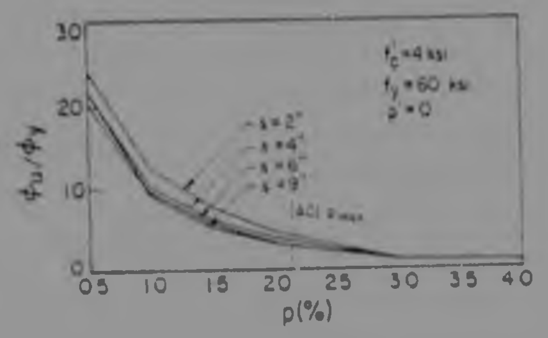

FIGURE 2.15 Effect of tie spacing ductility $\emptyset_u/\emptyset_y$-p diagrams (Refer to Reference: Cohn[3])

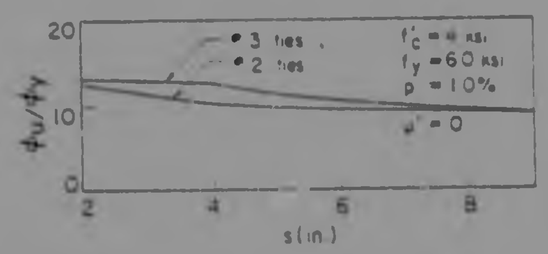

FIGURE 2.16 Effect of tie size on ductility $\emptyset_u/\emptyset_y$-p diagrams (Refer to Reference: Cohn[3])

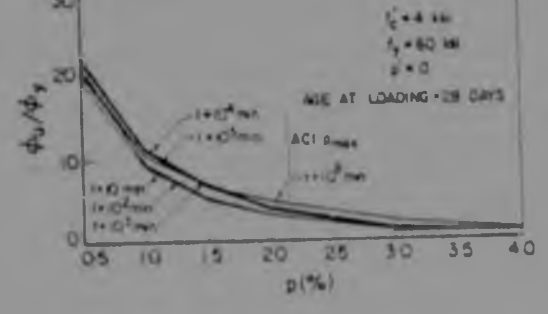

FIGURE 2.17 Effect of loading duration on ductility $\emptyset_u/\emptyset_y$-p diagrams (Refer to Reference: Cohn[3])

2.4 EFFECTS OF CONFINING THE CONCRETE

The ductility of a reinforced concrete member may be significantly increased by means of confining the compressive zone by closely spaced transverse reinforcement.

At low levels of compressive stress, the effect of transverse reinforcement is negligible since the strains in the concrete are very small; hence the concrete is unconfined.

At higher compressive stresses, near uniaxial strength, the concrete is under progressive internal cracking because its strains increase rapidly and therefore the concrete expands against the transverse reinforcement. At this point, the stress-strain properties of the concrete improve because the lateral reinforcement applies a triaxial constraint to the concrete, allowing the member to increase its strength.

Fig. 2.18 illustrates a number of tests reported by Base and Read [5], that indicate the beneficial effects of confinement by transverse reinforcement on the ductility of reinforced flexural members.

Confinement has a greater effect on heavily rather than on lightly reinforced concrete beams, since the latter already has adequate ducility. Concrete may also receive some confinement from the loading and supporting conditions. Figs. 2.19 and 2.20 contain results of investigations by Chandrasekhar [8] which indicate that a loading plate introduces a confining effect on the failing concrete zone under the plate which affects the deformations and the carrying capacity of flexural members. Several beams with a cross section of 101,6mm x 152,4mm were loaded through steel plates having widths varying from W1 (6,4mm) to W5 (152,4mm). It was concluded

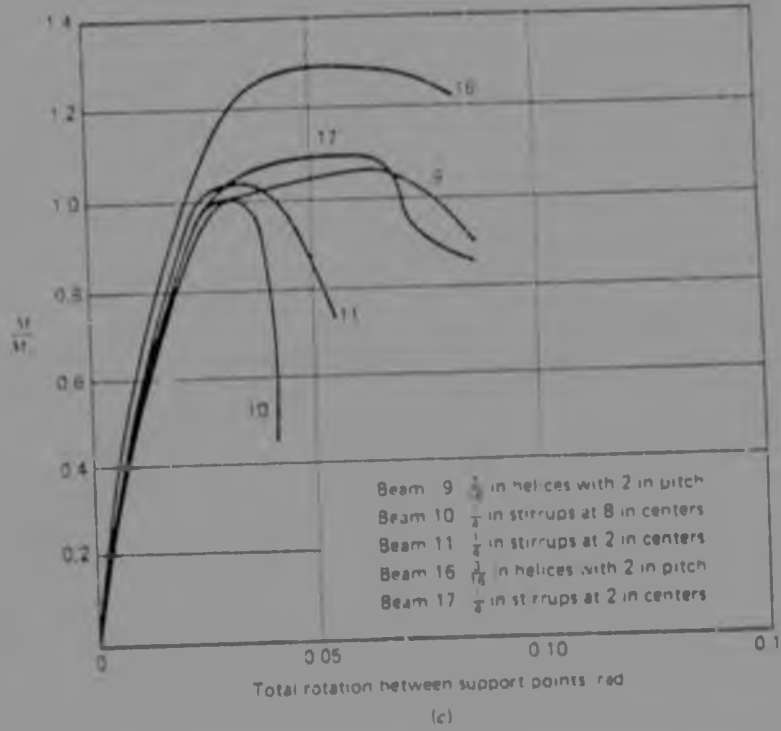

FIGURE 2.18: Experimental moment-rotation curves for reinforced concrete beams. (a) Beams failing after yielding of the reinforcement.(b) Balanced beams.(c) Beams failing in Compression. (Refer to Reference : Base and Read[5])

that the width of the loading plate significantly influences the rotation capacity, which was considerably reduced when loads were applied to test beams through narrow bearing plates. Nevertheless when the bearing stresses to which the concrete under the plate is subjected are small (less than $0{,}10f'_c$) then this influence is not significant.

Another important point to be mentioned is the fact that the presence of strain gradient along the length of a flexural member also confines the concrete at its critical section. Because the strains change rapidly with the length of the member due to different bending moments along the member or due to a shallow neutral axes depth, the highly stressed concrete at critical sections will receive confinement from the adjacent less highly stressed sections.

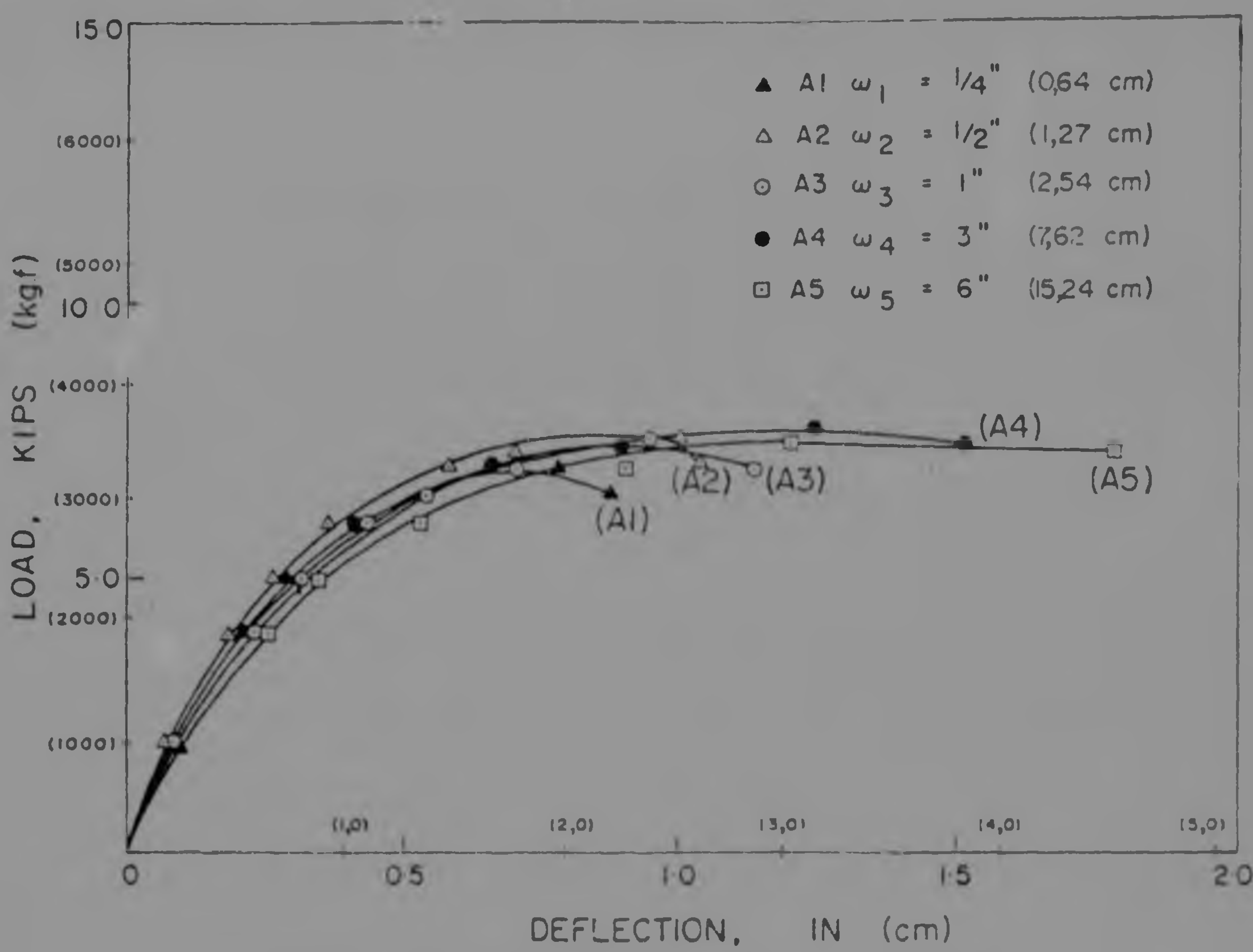

FIGURE 2.19 Load-deflection curves on test beams
(Refer to Reference: Chandrasekhar[6])

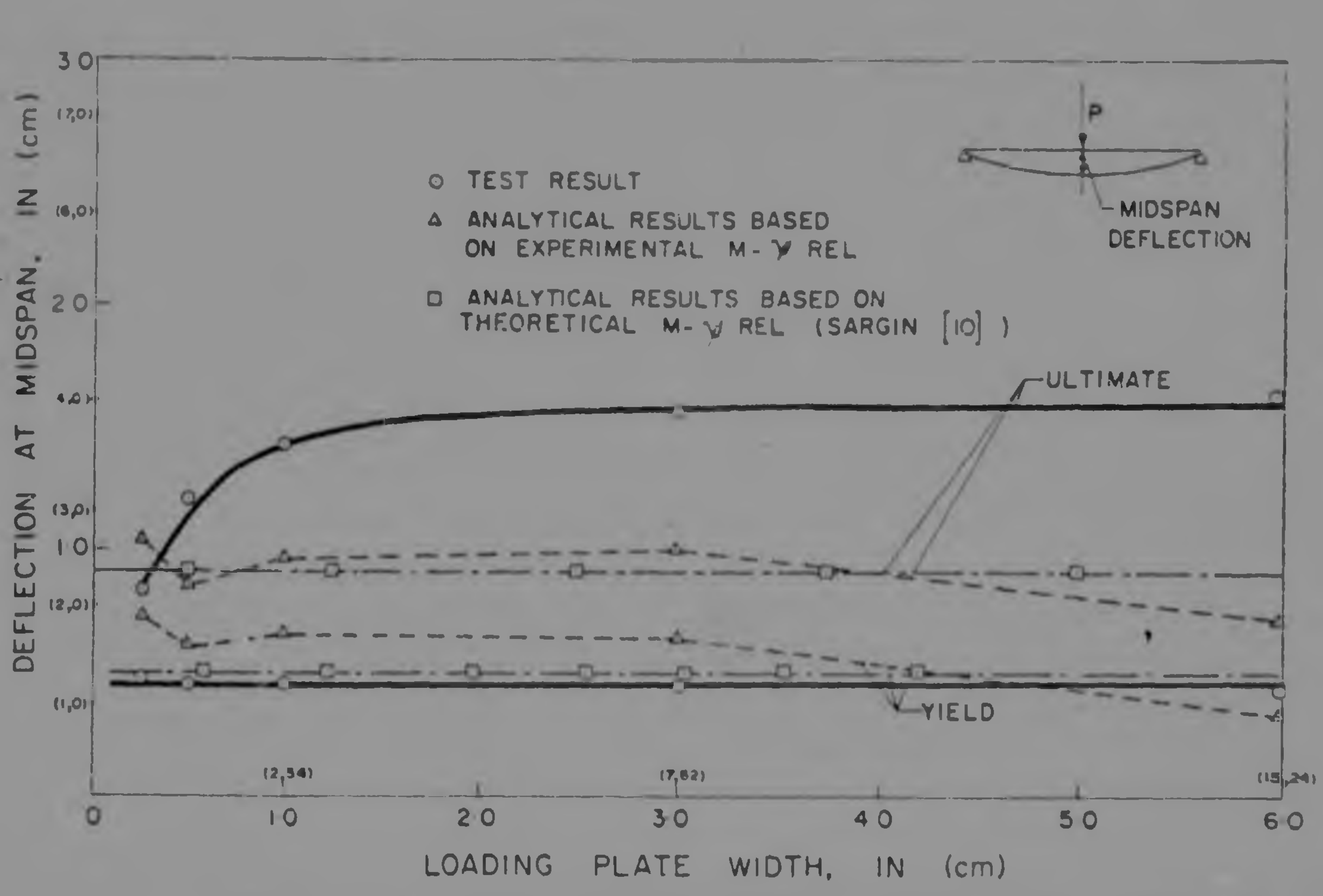

FIGURE 2.20 Influence of loading plate width on deflections
(Refer to Reference: Chandrasekhar[6]).

2.5 FLEXURAL ROTATION OF A MEMBER

Since the curvature is defined as rate of change of rotation with length of member, the total rotation for the entire length of a member is given by the integration of the curvature for the entire length of the member.

$$\theta = \int_0^l \phi dx \qquad \text{Eqn. 2.15}$$

where dx = element of length of the member

ϕ = curvature at the element

In Fig.2.21 Burnett[7] displays the curvature distribution for a member reinforced with mild steel, which is likely to occur in the following loading stages :

A : Well before yield of steel
B : At first yield of the steel
C : At maximum strength of the member
D : At a stage where the critical section may be considered to have ruptured.

It is extremely difficult, if not impossible, to predict the value of the precise curvature at or very near to the critical section after the steel has yielded.

The rotation over a portion of member depends not only on the properties of the member at that critical section but also on other factors such as : loading distribution; length of member, position of the member in the structural system, i.e. amount of fixity, etc.

The first moment-area theorem, a semigraphical method, may be used to calculate the rotation for a simply supported member under a central point load; this theorem established that the rotation between any two points on the elastic line or deflection curve of a member is equal to the total area of the corresponding portion of the bending moment diagram

Figure 1: Loading diagram.

Figure 2: Bending moment distribution

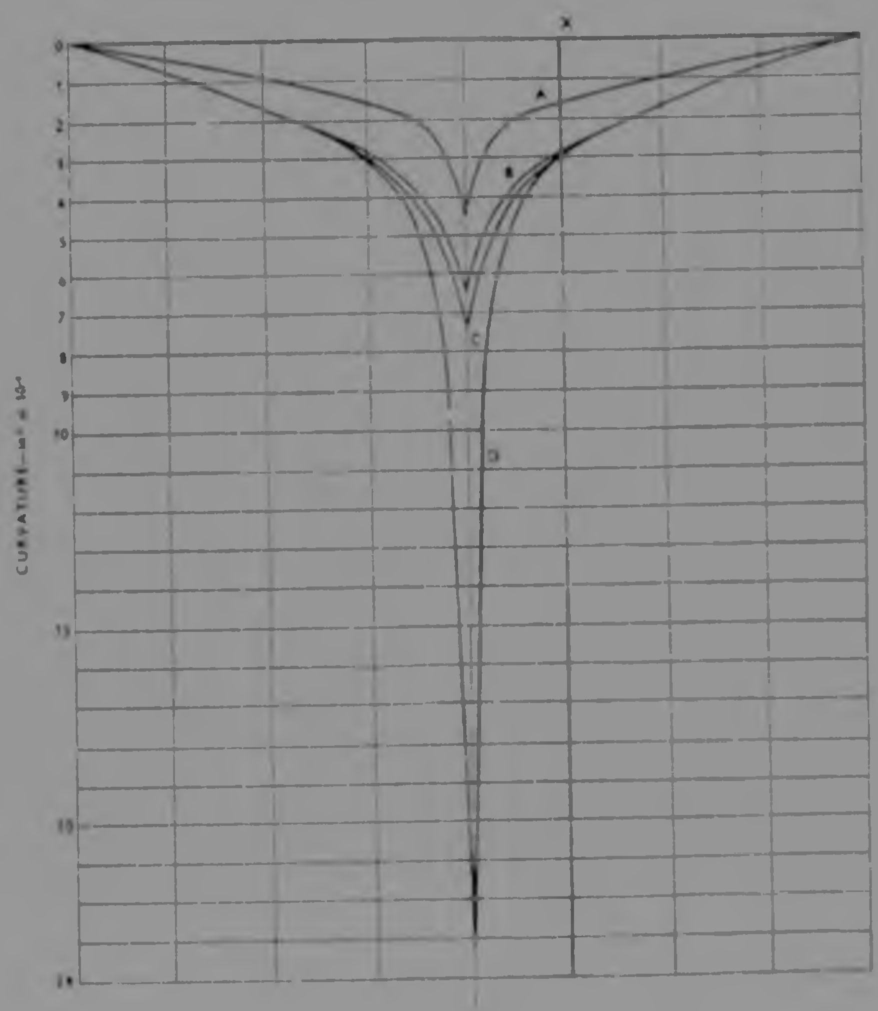

FIGURE 2.21 CURVATURE DISTRIBUTION FOR LOADING STAGES A,B,C and D. (Refer to Reference : Burnett[7]).

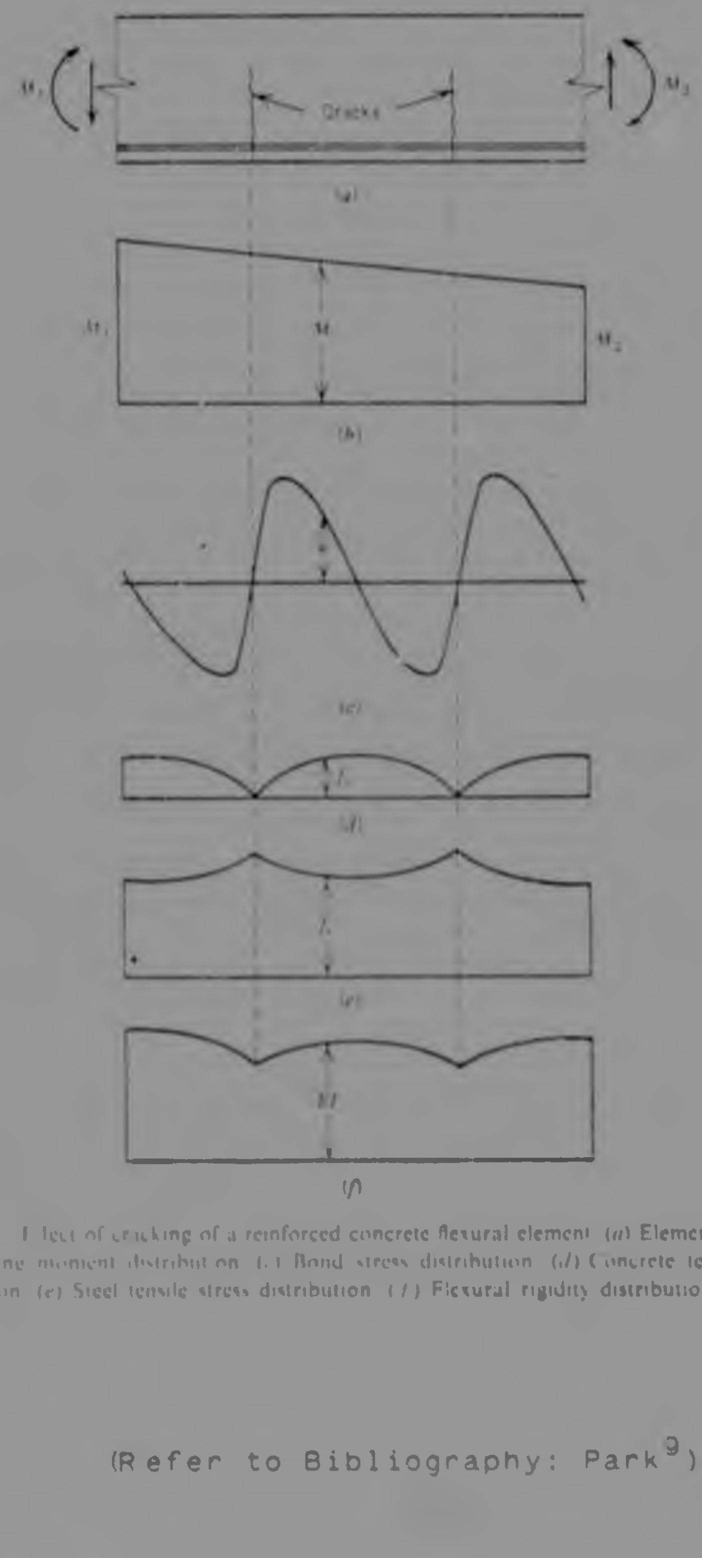

Figure 2.22 Effect of cracking of a reinforced concrete flexural element. (a) Element of beam. (b) Bending moment distribution. (c) Bond stress distribution. (d) Concrete tensile stress distribution. (e) Steel tensile stress distribution. (f) Flexural rigidity distribution in elastic range.

(Refer to Bibliography: Park[9]).

between these points, divided by the flexural rigidity (EI).
Replacing the curvature ϕ by $\frac{M}{EI}$ in Eqn. 2.15, the following expression is obtained :

$$\theta = \int_{0}^{l} \frac{M}{EI} dx \qquad \text{Eqn.2.16}$$

The establishment of the precise flexural rigidity to be used remains a major problem since the flexural rigidity is not constant throughout the total length of any loaded member.

Cracks in members appear at very early stages and at these cracked sections the tension is carried by the steel reinforcement.

Some tensile stress is carried by the concrete between the cracks due to the effect of bond stresses that transfer some tension from the steel to the concrete. It is the bond stresses that determine the tension stresses in the concrete and steel between the cracks. Fig. 2.22 shows the effect of cracking of a reinforced concrete beam on its flexural rigidity.

As the flexural rigidity fluctuates between cracks, the curvature also fluctuates along the member. Since curvature is inversely proportional to flexural rigidity, each peak of a typical curvature distribution curve will correspond to a cracked section in the member. The choice of a meaningful flexural rigidity, vital to the calculations, has been a variable discussed by Burnett , and the major results emphasized in his work can be seen in Fig. 2.23. This figure illustrates a comparison between the actual curvature distribution over a member at yield, with other curvatures calculated with different flexural rigidities.

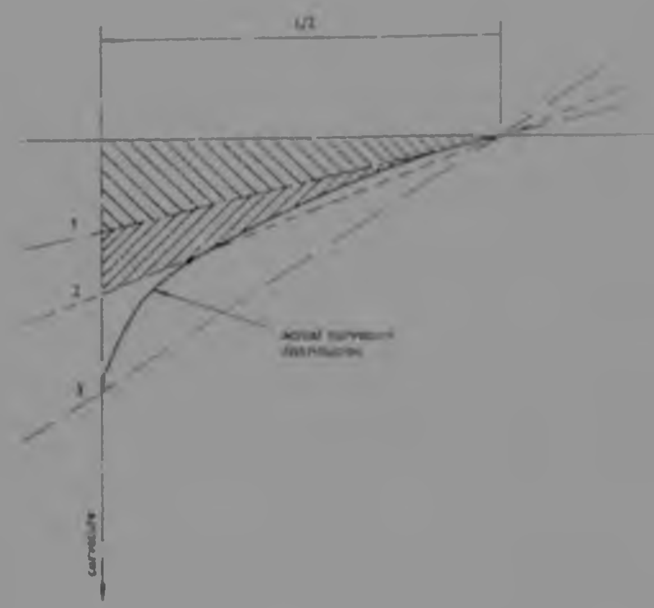

FIGURE 2.23 The actual curvature distribution over the member at yield compared with the equivalent elastic contributions calculated for the following values of flexural rigidity (Refer to Reference : Burnett[7]).

(1) F_r max. based on the "uncracked" behaviour of the member.

(2) F_r mean based on the overall behaviour of the member

(3) F_r min. based on the behaviour of the critical section

Where F_r = Flexural rigidity : F_r=EI

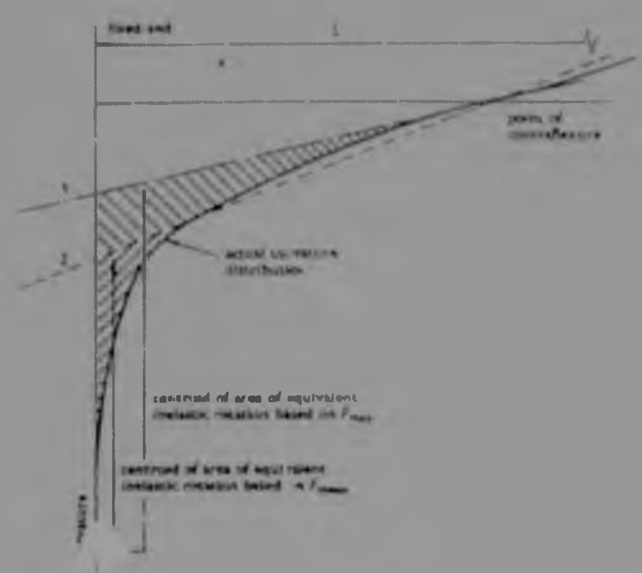

FIGURE 2.24 Curvature distribution near the support section of a member with fixed ends after yield has occurred: (Refer to Reference : Burnett[7]).

(1) Elastic curvature distribution based on F_r max.

(2) Elastic curvature distribution based on F_r mean

Where F_r= Flexural rigidity = F_r= EI

If the uncracked flexural rigidity is to be used in the calculations for curvature, then small values are obtained, which are much less than those which actually occur.

On the other hand, if it is proposed to use the minimum value for the flexural rigidity, the results for curvature, and therefore rotation, will be overestimated.

If the mean flexural rigidity based on the overall behaviour of the member is used then, for the vicinity of the critical section, the actual curvature is greater than that calculated with the mean flexural rigidity.

The areas under the curves 1,2 and 3 in Fig 2.23 represent the elastic rotations calculated on the basis of these maximum, mean and minimum flexural rigidities.

The main advantage of including the inelastic behaviour of a concrete member in its structural design is that the strength of the members can increase above that calculated by the elastic theory. This additional strength is limited mainly by the rotation capacity of the member.

A fundamental assumption for the purpose of design is that the inelastic rotation may be considered to be concentrated at critical sections. The validity of this assumption is dependent on the spread of inelastic effects over the member.

Fig.2.24 illustrates the curvature distribution at the end of a fixed-end beam under some general type of load, at a time when yielding has already occurred.

This figure shows that the spread of inelasticity is much greater if the uncracked value for flexural rigidity is used than that when the mean value is used; this is because the distance from the centroid of the inelastic area is further from the critical section, therefore when considering inelastic rotation concentrated at critical sections, the use of the uncracked value rather than the mean value for flexural rigidity would create an appreciable error.

The use of the correct value for flexural rigidity of members is much more critical in ultimate strength theory than it is in a conventional elastic theory.

Assuming that the curvature for a small region of a hinged zone is constant and equal to the difference between ultimate and yield curvature, the plastic rotation can be calculated as

$$\theta p_u = \int_y^u \varnothing \, dl = (\varnothing_u - \varnothing_y)\, l_p = \varnothing_p l_p \qquad \text{Eqn.2.17a}$$

where l_p = hypothetical length of the member over which a uniform inelastic curvature is assumed to be spread, creating an equivalent rectangle with an area equal to the value of the inelastic rotation for half span of the beam.

$\varnothing_u$ = curvature at ultimate strength

$$\varnothing_u = \frac{\varepsilon_{cu}}{C_u}$$

C_u = neutral axis depth at ultimate

$\varnothing_y$ = curvature at yield of steel $= \dfrac{\varepsilon_y}{d-C_y}$

the plastic rotation can be rewritten as

$$\theta p_u = \left[\frac{\varepsilon_{cu}}{C_u} - \frac{\varepsilon_y}{(d-C_y)}\right] l_p \qquad \text{Eqn.2.18}$$

Use is made subsequently of this hypothetical length l_p to compare the experimental results with other results and equations established by Corley [8] and Mattock [9]. In fact it would make more sense to create an equivalent triangle instead of a rectangle and then Eqn.2.17a would be rewritten as

$$\theta_{pu} = \int_y^u \phi dl = \tfrac{1}{2} (\phi_u - \phi_y)\, l_p \qquad \text{Eqn.2.17b}$$

where l_p = length of the member over which the hinge is assumed to be concentrated.

From the analysis of Figs. 2.25 and 2.26, Corley [8] shows the effects of the binding reinforcement and depth width ratios on the maximum concrete compressive strain; he proposed that the maximum compressive strain be calculated as

$$\epsilon_{cu} = 0{,}003 + 0{,}02 \frac{b}{z} + \left(\frac{p'' fys}{20}\right)^2 \qquad \text{Eqn.2.19}$$

where p'' = binding ratio expressed as the ratio of the volume of the binding reinforcement (one stirrup plus compressive steel) to the volume of the concrete bound(area enclosed by one stirrup multiplied by the stirrup spacing).

fys = yield point of the stirrup steel

z = distance between the points of zero and maximum moment.

b = width of beam

In a discussion of Corley's paper, Mattock [9], proposed that the maximum compressive concrete strain be calculated using a slightly modified version

$$\epsilon_{cu} = 0{,}003 + 0{,}02 \frac{b}{z} + 0{,}2p'' \qquad \text{Eqn. 2.20}$$

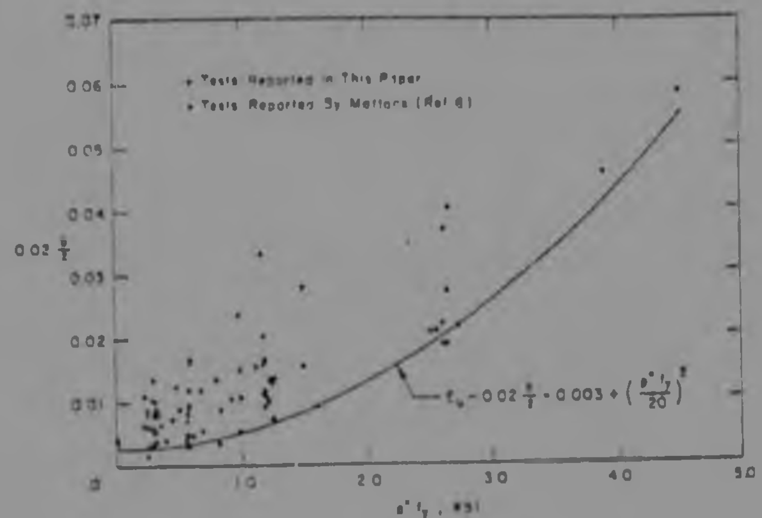

FIGURE 2.25 Effect of binding reinforcement (Refer to Reference : Corley[8]).

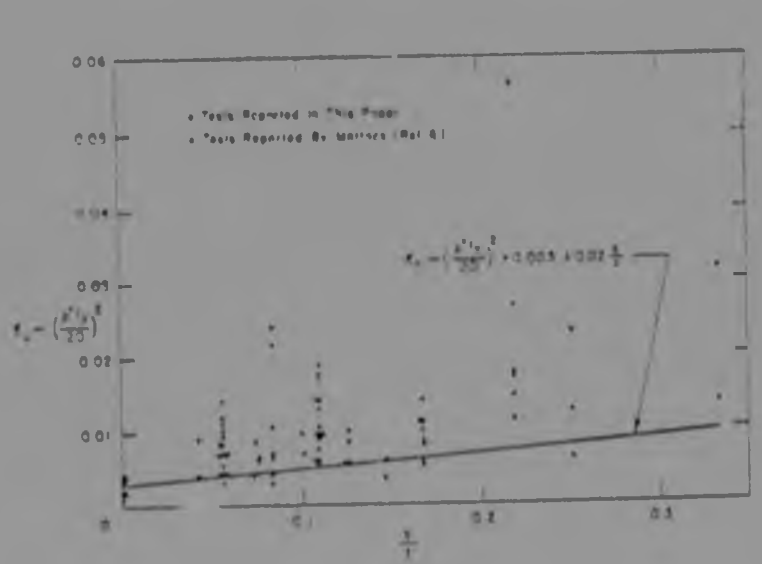

FIGURE 2.26 Effect of b/z Ratio (Refer to Reference : Corley[8]).

This was done to make calculations easier and also to be more conservative for high values of p". Mattock also suggested that, according to the terminology of Corley's paper, the effective hinging length may be calculated reasonably following the trend indicated in Fig.2.27 where

$$l_o = 0{,}5d + 0{,}05z \qquad \text{Eqn.2.21}$$

One of Corley's[8] principal variables investigated was the effect of size on rotational capacity in critical regions in reinforced concrete beams. To isolate the effect of size, beams with the same amount of binding were compared because stirrups show a pronounced influence on the rotational capacity. Since rotation depends on curvature and curvature is the ratio of maximum concrete compressive strain to neutral axes depth, the influence in size was established by a comparison of the maximum concrete compressive strain for beams with similar width to half span ratios and similar amount of stirrups.

Table 2.1 illustrates that although average values indicate there is a trend for slightly more concrete strain with smaller size, the smallest maximum strains are quite similar. Corley concludes that the direct effect of size on rotational capacity is not significant but he points out that there is an important indirect effect which is that, for design purpose, shear reinforcement requires closer spacing of stirrups with decreasing beam depth and therefore the maximum concrete compressive strain of a small beam may be greater than that of a larger beam of similar design because of concrete confinement.

CEB-code[1] recommends permissible local plastic rotations which are shown in Fig. 2.28 and which relate the angle of plastic rotation to the c/d ratio where c is the height of the plastic neutral axes. This diagram by the CEB commission on

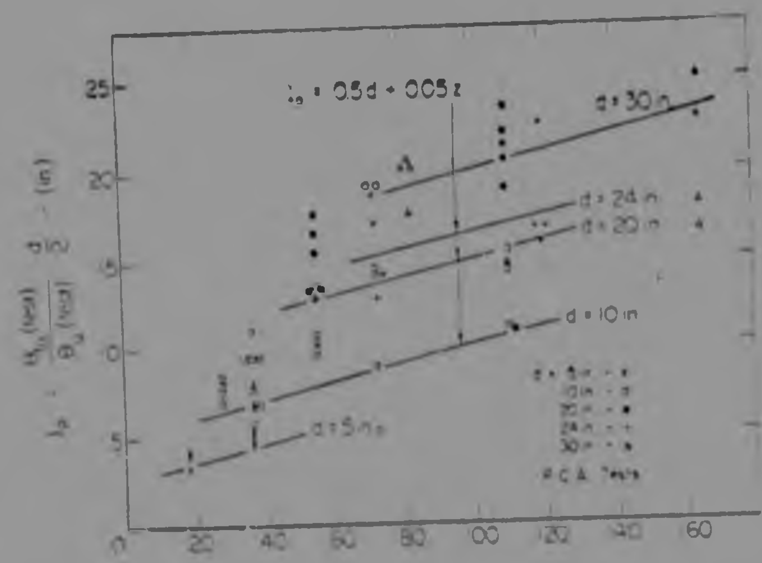

FIGURE 2.27: Variation of effective hinging, l_p, with distance from section of maximum moment to section of zero moment, z. (Refer to Reference : Mattock[9]).

Beam depth, in inches	Smallest maximum strain	Average maximum strain	Beams included in average[a]
10	0,007	0,013	A2,A5,C2,C5,E2, F2,K6,K8
20	0,011	0,015	B1,B3,D1,D3,G1,G3
24	0,007	0,010	M1,M3,M6,M8
30	0,006	0,008	N1,N3

[a] Tests on beams in Series A,B,C,D,E,F & G are reported by Mattock

TABLE 2.1: Comparison of measured maximum concrete compressive strain for beams with similar amounts of stirrup steel. (Refer to Reference : Corley[8]).

hyperstatic structures does not include the beneficial effect of confinement of concrete.

The influence of breadth is considered to be another important aspect affecting rotation and this effect has been studied by Clements[10] by testing a series of simply-supported under-reinforced beams. The results of these tests were plotted in Figs. 2.29, 2.30 and 2.31 which indicate that there is a trend for an increase of the steepness of the falling branch as the ratio $\left(\frac{b}{h}\right)$ decreases.

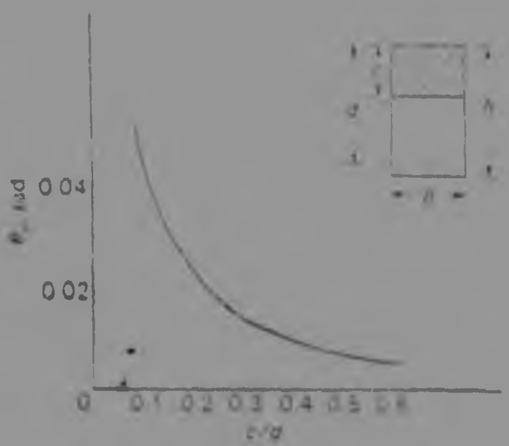

(b)

FIGURE 2.28: Permissible local plastic rotation disregarding confinement. (Refer to Bibliography: Kong[7])

Also from Fig. 2.32 Clements[10] shows that, apart from the beneficial effect on rotation of increasing sectional breadth, another aspect which opens new perspectives can be seen slightly and that is that very wide beams, more like slab-type, show a greater rotation.

effect has been studied by Clements[10] by testing a series of simply-supported under-reinforced beams. The results of these tests were plotted in Figs. 2.29, 2.30 and 2.31 which indicate that there is a trend for an increase of the steepness of the falling branch as the ratio $\left(\frac{b}{h}\right)$ decreases.

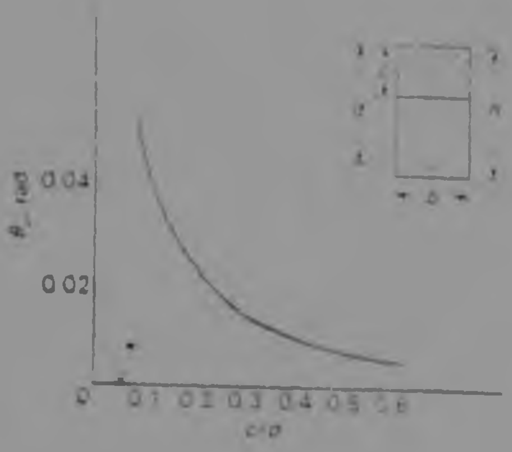

(b)

FIGURE 2.28: Permissible local plastic rotation disregarding confinement. (Refer to Bibliography: Kong[7])

Also from Fig. 2.32 Clements[10] shows that, apart from the beneficial effect on rotation of increasing sectional breadth, another aspect which opens new perspectives can be seen slightly and that is that very wide beams, more like slab-type, show a greater rotation.

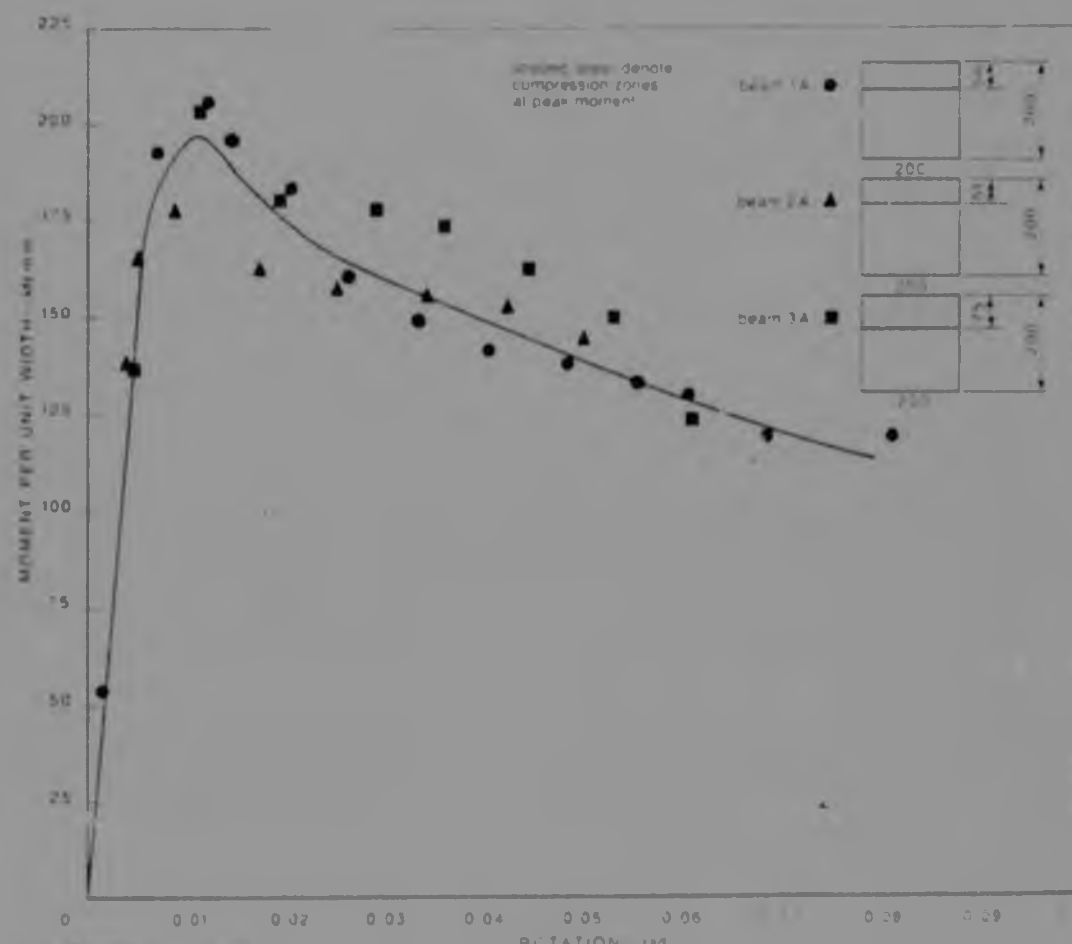

(a) Beams with b/h = 1

FIGURE 2.29 Plots of moment per unit width against rotation beams with b/h = 1,0. (Refer to Reference: Clements[10])

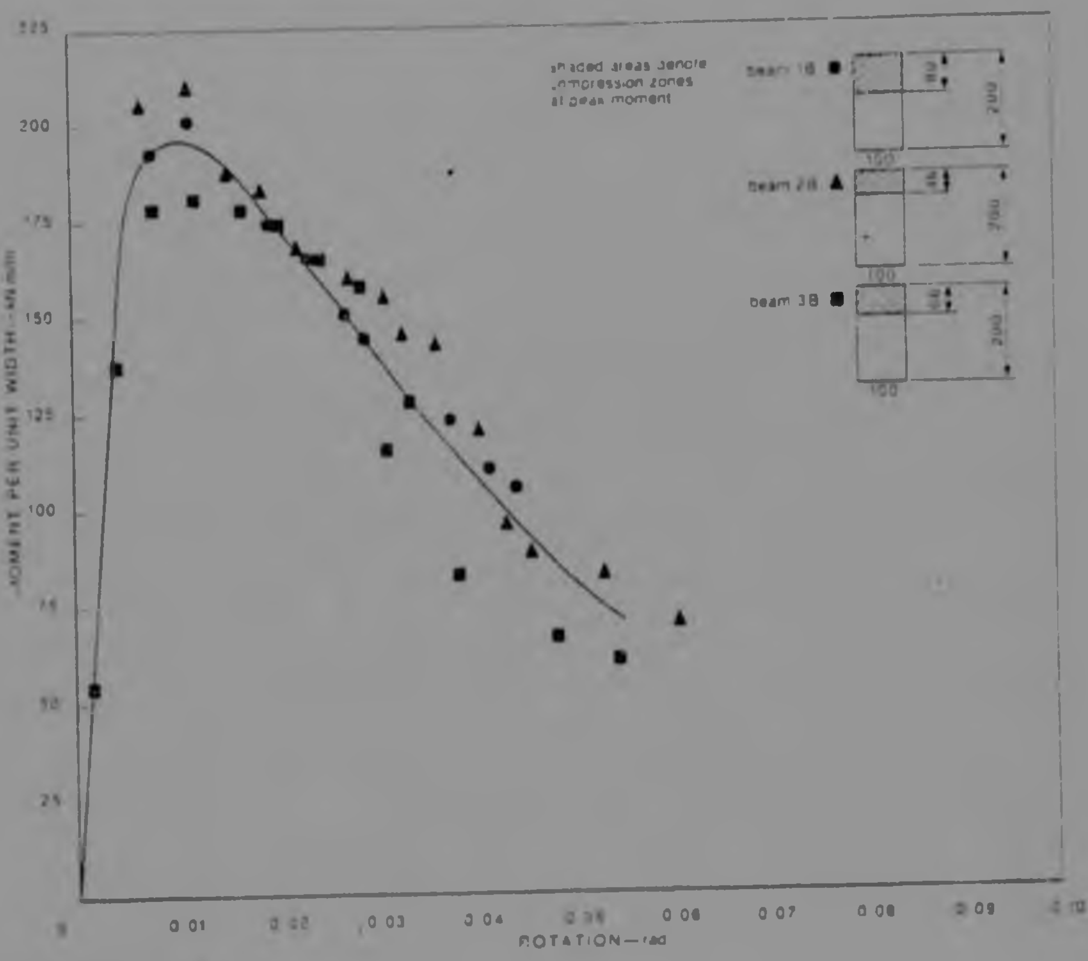

(b) Beams with b/h = ½

FIGURE 2.30 : Plots of Moment per unit width against rotation. beams with b/h : ½.(Refer to Reference : Clements[10]).

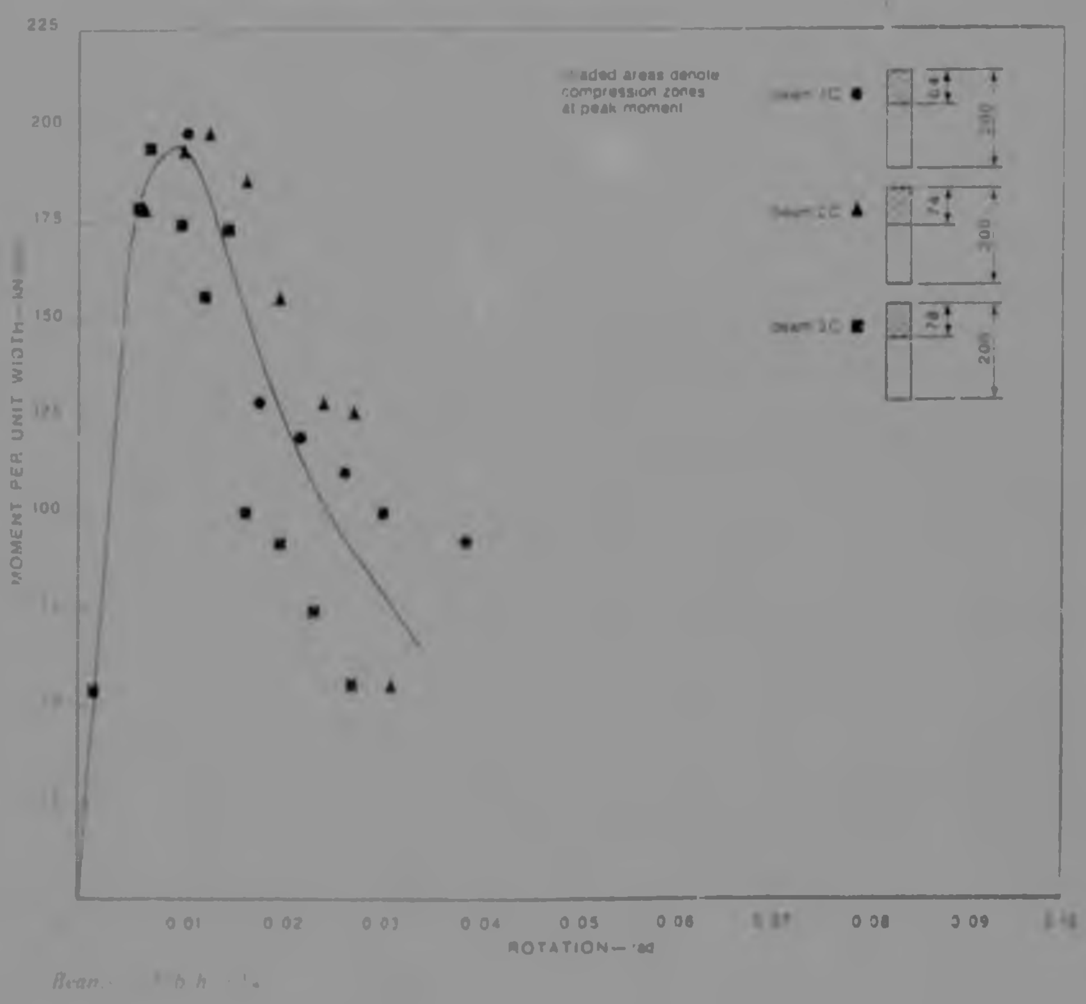

FIGURE 2.31 Plots of Moment per unit width against rotation, beams with b/h = 1/4 (Refer to Reference : Clements[10]).

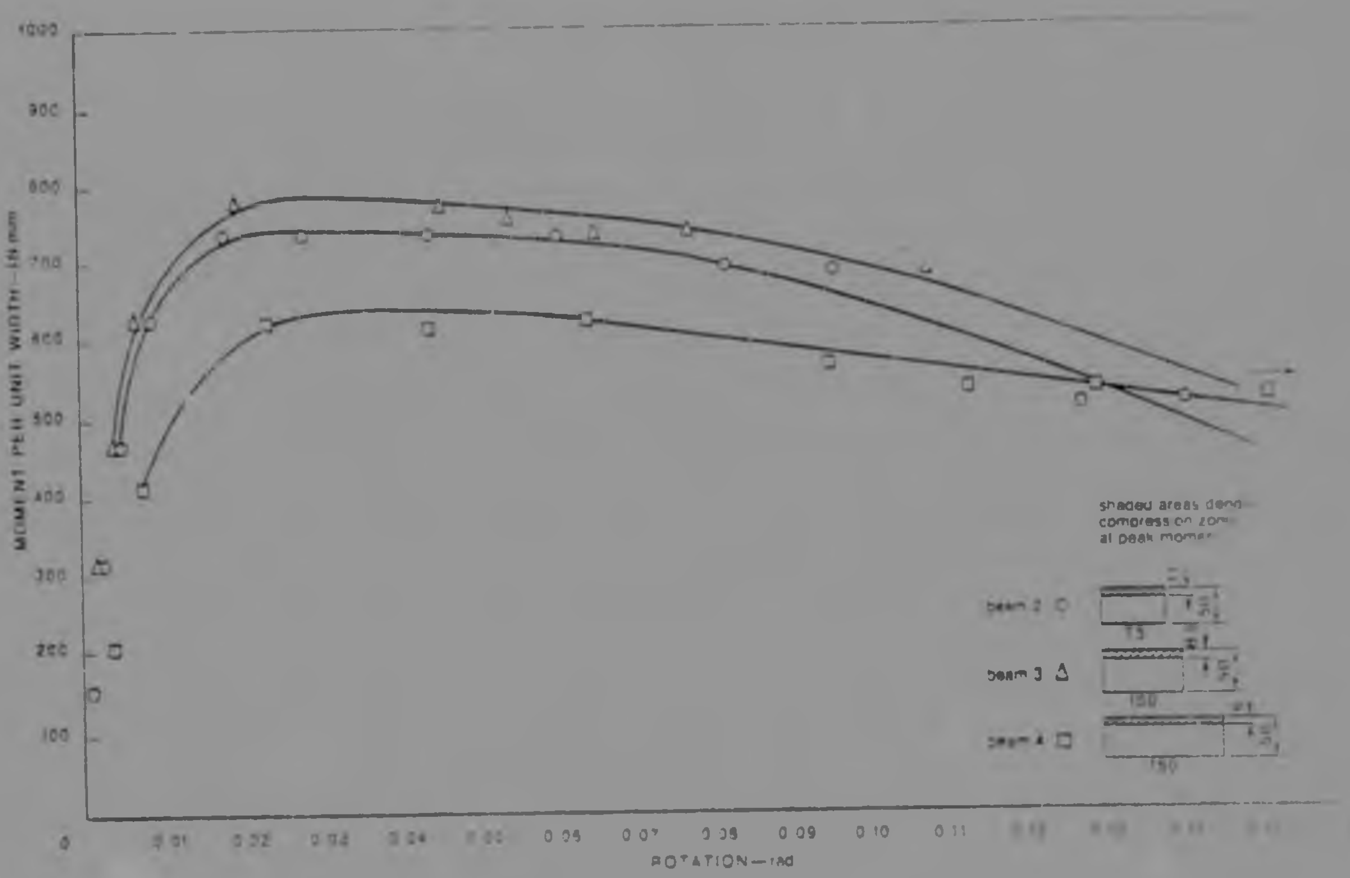

FIGURE 2.32: Plots of moment per unit width against [illegible] beams with $b/h \geq 1,0$. (Refer to Refere[illegible] Clements[10]).

CHAPTER 3

EXPERIMENTAL PROGRAMME

3.1 TEST SPECIMENS

Fourteen singly reinforced concrete beams were tested up to failure; these specimens were simply-supported beams subjected to a concentrated load at midspan. Free rollers were used to support the test beams at each end.

The half span of a simply-supported beam may represent that part of a continuous beam between a support and an adjacent point of contraflexure, as shown in Fig.3.1.

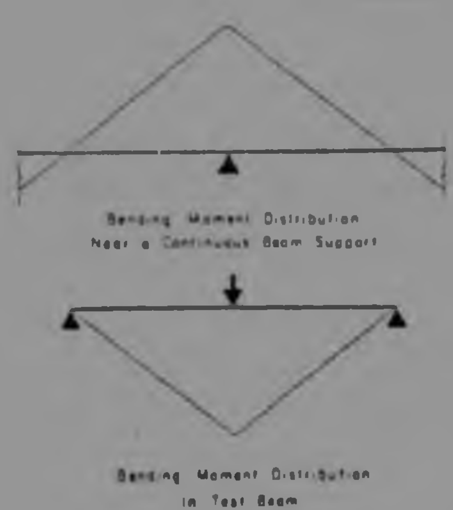

FIGURE 3.1

Relationship Between Distribution of Moments in the Test Beams and those near a support in a Continuous Beam. Refer to Bibliography : Mattock[8].

In the tests, three major variables are to be studied, and these are : the effects of binders, span-to-depth ratio, and type of reinforcing.

The concrete cylinder and cube strength were held approximately constant for all the beams.

For the design of beams with transverse reinforcement, closed links perpendicular to the main tension reinforcement were used.

All the beams tested were 102mm wide except two which were both 153mm, to include the study of the effect of width. Other properties of the test beams are illustrated in Table 3.1.

3.2 MATERIALS AND FABRICATION OF SPECIMENS

3.2.1 Concrete

The fine aggregate used for the concrete was a coarse grained weathered granite, and the coarse aggregate was a 13mm quartzite stone. Further details of the trial mix design, fine mechanical analysis for the sand, aggregate grading analysis, and relative density of the sand can be found in Appendix 1.

Standard 6 inch control cylinders and 150mm cubes were taken from each batch, and a total of 15 cylinders and 3 cubes were made for each beam. 5 Cylinders were tested at 7, 14 and 28 days, and 3 cubes were tested at 14 days at the same age at which the beams were tested.

During casting, the concrete was compacted by a hand held vibrator, and after 24 hours of being in moulds, the beams, cylinders and cubes were removed from their moulds and cured in air, wrapped in wet hessian and covered with plastic bags and stored in a room where the environment was controlled to maintain temperature constant at 21°C.

BEAM	b mm	d mm	SPAN L mm	TENSION REINFORCEMENT BARS	AREA mm²	As/bd p(%)	L/d	CONCRETE STRENGTH CYLINDER	CUBE	BINDING CODE CP110	SPACING mm
A1	102	125	1500	2Y10	157,08	1,232	12	23,94	29,78	Minimum binding**	90
A2 *	102	125,35	1500	3Y10	235,62	1,84	11,97	33,78	42,36	Minimum binding**	90
B1	102	123,6	1500	2Y10	157,08	1,25	12,14	22,28	30,53	2xMinimum binding	45
B2	102	123	1500	2Y10	157,08	1,25	12,2	20,03	25,51	NO LINKS	-
B3	153	127,725	1500	3Y10	235,62	1,21	11,75	20,94	27,23	Minimum binding**	90
B4	153	123,7	1500	3Y10	235,62	1,24	12,13	21,21	27,44	NO LINKS	-
C1	102	193,6	2250	3Y10	235,62	1,19	11,62	21,23	25,95	Minimum binding**	135
C2	102	126	1000	2Y10	157,08	1,22	7,94	25,51	31,03	Minimum binding**	90
C3	102	187	1500	3Y10	235,62	1,24	8,02	20,56	26,29	Minimum binding**	135
C4	102	133	2250	2Y10	157,08	1,16	16,92	19,52	27,48	Minimum binding**	90
C5	102	65	1125	1Y10	78,54	1,18	17,31	20,38	27,59	Minimum binding**	45
D1	102	128	1500	4R8	201,06	1,54	11,72	19,67	24,60	Minimum binding**	90
D2	102	126,85	1500	6R8	301.59	2,33	11,82	23,07	29,88	Minimum binding**	90
D3	102	127,35	1500	3Y10	235,62	1,81	11,78	22,23	26,09	Minimum binding**	90

** or maximum spacing

* ALL BEAMS WERE TESTED AT 14 DAYS EXCEPT BEAM A2 WHICH WAS TESTED AT 59 DAYS.

TABLE 3.1

The hessian was always maintained wet so as to keep the specimens moist.

The value of the mean cylinder strength of concrete at 14 days, used as constant for all beams except A2, was 21,6MPa; this value was obtained as the mean of all the average values for each beam. Each average value was the mean of the 5 standard 6 inch control cylinders tested for each beam at 14 days.

For the purpose of design $f'c$ = 21,6 and fcu = 27,5MPA were used for all the beams except A2 since these values were the mean values giving a reasonable coefficient of variation of 7,9% and 7,3% respectively. Only beam A2, which was tested at 59 days had a $f'c$ = 33,8 and fcu = 42,4MPa.

Further details of strength of concrete at 7,14 and 28 days can be seen in Appendix 1.

3.2.2 Steel

The tension reinforcement used for these test beams were high tensile bars (Y10), or mild tensile bars (R8).

The R8 bars are hot-rolled bars of plain round cross-section, and Y10 bars are hot-rolled deformed bars.

According to the S.A.B.S.920[11], the R8 bars should have a yield stress of 250MPa and an ultimate tensile strength of at least 430MPa; the Y10 bars should have a yield stress or 0,25% proof stress of 450MPa and an ultimate tensile strength 15% higher than the actual yield or 0,25% proof stress.

From the tests of steel in tension, the stress-strain curve for a bar taken from each beam was made; and it was found that the Y10 bars had a mean yield stress of 551,8MPa, with a coefficient of variation of 1,5%; the R8 bars had a mean yield stress of 401,5MPa with a coefficient of variation of 8,2%. In the theoretical assessments, each beam was given its measured value of yield stress.

The experimental stress-strain curves for the steel bars corresponding to each beam are shown in Appendix 2. The tension reinforcement stress-strain curve parameters are given in Table 3.2.

The tensile steel percentage (p), the balanced value of tensile steel percentage (p_b) established by ACI code, and the ratio (p/p_b) as a percentage are shown in Table 3.3.

The transverse reinforcement used in the test beams were rectangular closed links of cold drawn indented wire with a diameter of 6,3mm and a very high yield stress of 642 MPa. Links were designed to comply with the requirements of the CP110 code for which the limiting value for the yield strength of the link is not to be taken over 425MPa which was the value used for the design.

Links when used were tied to the tension reinforcement by 1,25mm galvanised wire. After each reinforcement cage was fabricated, small pieces of steel were attached to the bottom to maintain the level of effective depth and to ensure a cover to the tension reinforcement during placing of the concrete. In addition two vertical hooks were located each at a reasonable distance from midspan in order to maintain the level of effective depth while casting and also to be able to carry the beams.

Each beam was cast in a metallic mould using a total of three batches, and from each batch, 5

BEAM	fy MPa	Es GPa	E's MPa	εsH x10^{-4}
A1	550	211,5	4480	156
A2	550	203	4552	169
B1	551	208	4379	140
B2	550	203,7	4616	149
B3	567	198	4619	174
B4	561	200,3	4515	179,2
C1	562	202	4584	165
C2	543	186	2341,33	76
C3	550	167	4549	126
C4	551	203,8	4176	125
C5	535	194	4584	120
D1	425	212,5	2387	123
D2	378	189	2493	40
D3	552	190,3	4144	156

fy = Yield stress in MPa

Es = Modulus of Elasticity in GPa

E's = Modulus of strain hardening in GPa

εsH = Strain at beginning of strain hardening

TABLE 3.2

BEAM	p %	p_b %	$\frac{p}{p_b}$ (%)
A1	1,232	1,469	83,88
A2	1,84	2,293	80,25
B1	1,25	1,465	85,33
B2	1,25	1,469	85,10
B3	1,21	1,404	86,19
B4	1,24	1,426	86,94
C1	1,19	1,422	83,66
C2	1,22	1,406	86,79
C3	1,24	1,469	84,42
C4	1,16	1,465	79,19
C5	1,18	1,530	77,12
D1	1,54	2,14	72,12
D2	2,33	2,518	92,54
D3	1,81	1,461	123,89

p = Tension steel ratio: As/bd

p_b = Steel ratio at balanced ultimate strength conditions in a beam without compression reinforcement according to ACI code

TABLE 3.3

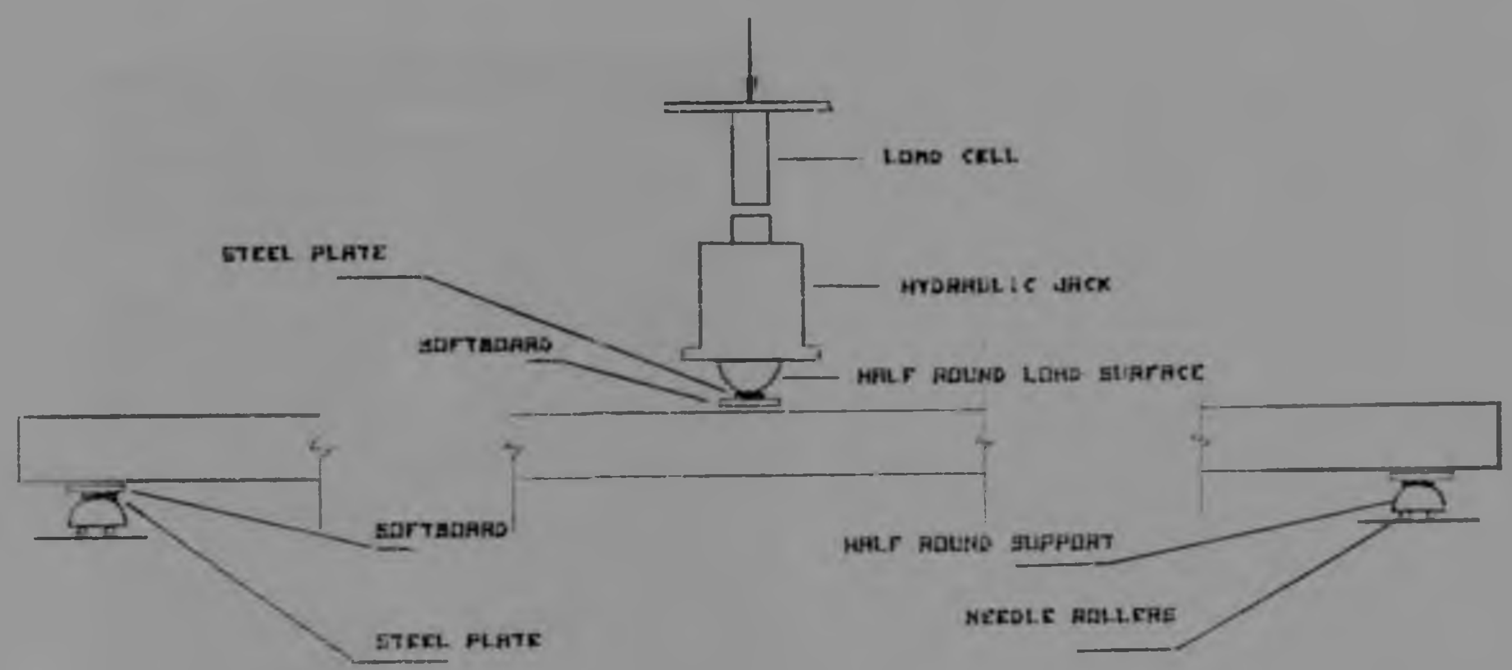

FIGURE 3.2
Diagrammatic Representation of the Test Specimen.

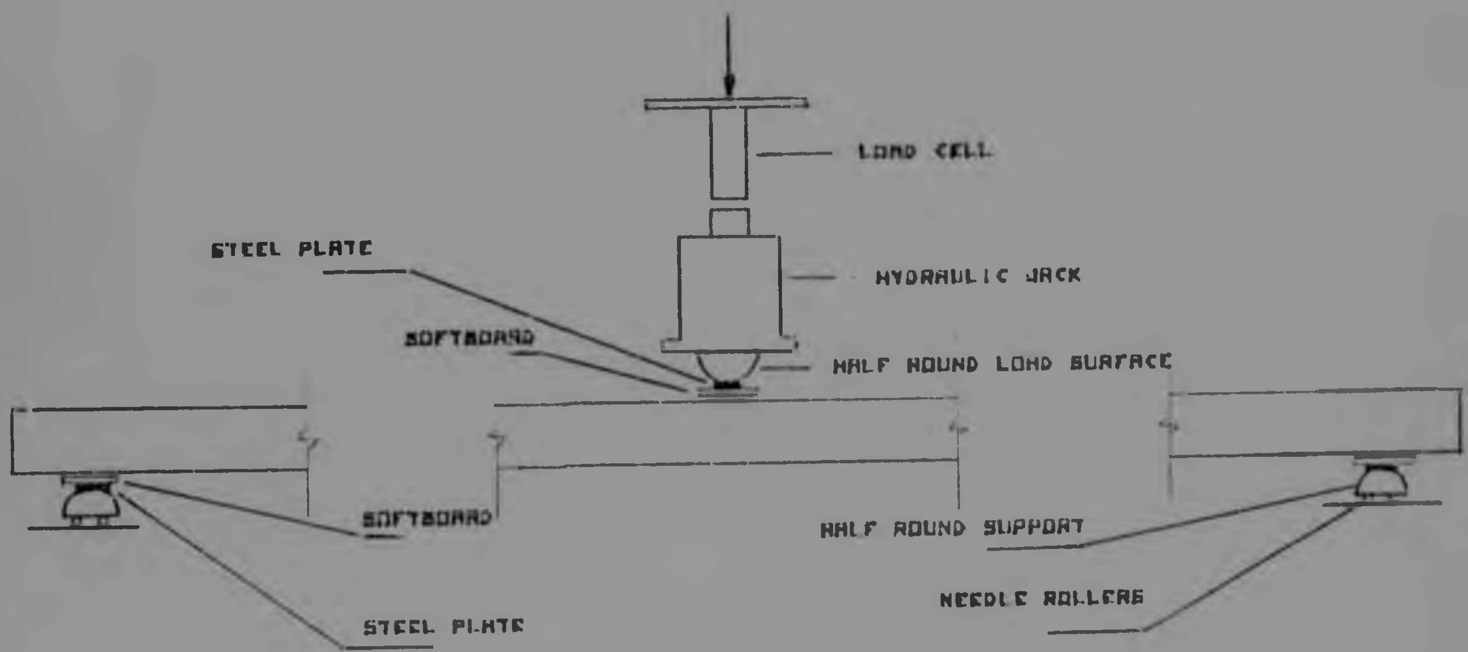

FIGURE 3.2
Diagrammatic Representation of the Test Specimen.

cylinders and 1 cube were made, the entire process was completed in a single operation lasting 75 minutes.

3.2.3 Instruments

Some of the main instruments and items involved in the experiments can be seen in a diagrammatic representation of the test specimen in Figure 3.2.

Two inch demountable mechanical strain gauge(demec), three deformation dial gauges : Baty : 0,01mm - 20mm; and rotation gauges over a length of 100mm: Mitutoyo : 0,01-10mm No.2048 were used for recording main results.

The tests were carried out under the general set-up shown in Figure 3.3

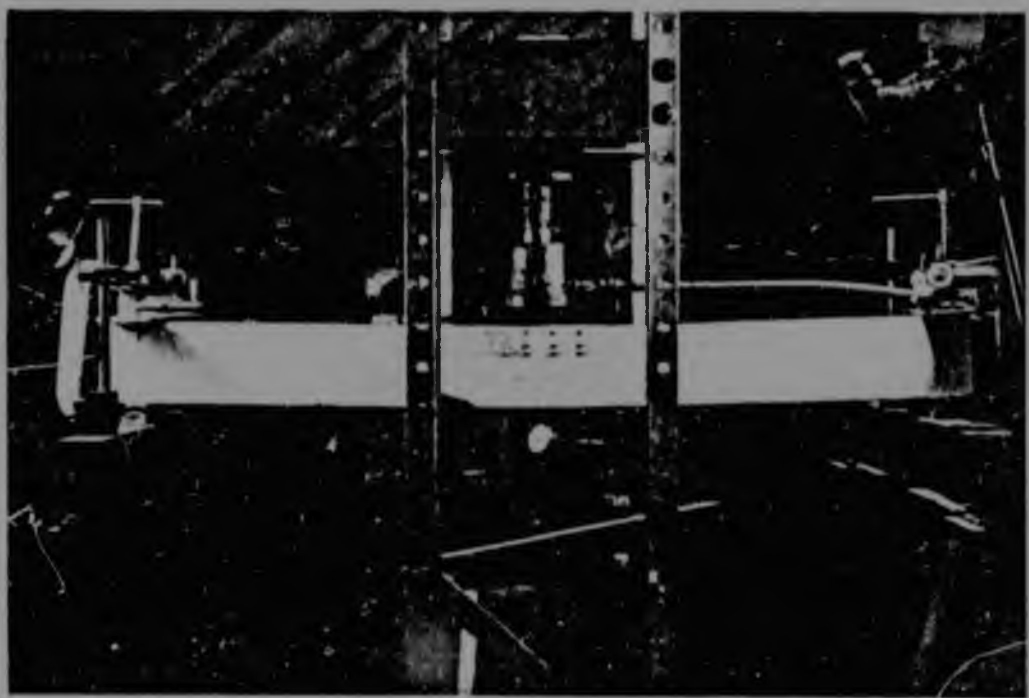

FIGURE 3.3

A small rectangular softboard 10mm high was located at the supports to distribute the reaction smoothly and thereby avoid concentration of stresses. Underneath the softboard was a steel plate 25mm wide and 10mm high also for the purpose of distributing the pressures equally. The thickness of the steel plates used in the test was sufficiently large so as not to cause any significant deformation in the steel plate itself. Finally, the small steel plate was located on a half round metallic support, which was placed on top of two needle rollers FF2535ZW, spread at a distance equal to the test beam span.

The settlements at the supports were checked by deformation dial gauges one on top of each support, and the average deflection at support was subtracted from the displacement measured at midspan by means of another deformation dial gauge located underneath the beam. The central load consisted of a device including a loading cell and a hydraulic jack. The load cell was connected to a Huggenburger strain bridge.

Demec strain-measurement targets were located in three rows at different levels in the compressive zone of the beam. The first row was located as near as possible to the top of the beam; the second row was placed at the calculated plastic neutral axis, and the third row at the neutral axis corresponding to the conditions at commencement of yield of the tension steel.

The targets for each row were spaced at a distance of two inches (50mm) in such a way as to obtain strains at midspan and at a section two inches (50mm) away from midspan. Targets were placed on both sides of the beam.

The following measurements were recorded during the test :

(a) amount of deflection at midspan
(b) amount of deflection of softboard at each support
(c) total rotations at both supports
(d) strains at three different levels in the compressive zone on the two sides of the beams by means of a two-inch demountable mechanical strain gauge.

The maximum compressive strain, neutral axis level and curvature at each section was calculated assuming a linear relationship between the measurements of the strains on the first two rows from the compression face. The third row was not included directly in the calculations because, at loads higher than that of commencement of yielding of steel, these readings included tension cracks.

3.3 TEST PROCEDURE

Each test beam was removed from cure the day before the experiment was to take place. After placing the Demec targets on the beam, it was placed on its supports and the loading equipment was positioned.

It was planned to apply the load in 13 increments. The first 5 increments were each made equal to 15% of the calculated ultimate load; then 3 increments each made equal to 5%, and the last 5 increments each made equal to 2% of the calculated ultimate load.

Each increment of load was applied over less than a minute, and the load held constant for 6 minutes, then the measurements of strain readings, deflections and rotations were taken during the next 5 minutes, so that the time required for each increment of load was about 12 minutes. Each test for a beam would take at least two and a half hours.

CHAPTER 4

RESULTS AND DISCUSSION

4.1 INTRODUCTION

The test beams were divided into four groups . group A consisted of 2 beams regarded as the basic tests, group B was composed of 4 beams which were tc determine the effect of binders and beam width, group C consisted of 5 beams in which the effect of span would be highlighted and finally group D which consisted of 3 beams which would take into account the effect of the properties of the reinforcement on the rotational capacity of beams.

All beams in these tests were under-reinforced and failed by crushing of the concrete after the tension reinforcement had yielded.

The first visible flexural cracks appeared at between 15% and 30% of the ultimate load of failure. These cracks grew wider and slowly extended towards the compression zone as the load was increased.

4.2 IDEALIZED LOADING SYSTEM

The load at midspan was spread to the beam by a 20mm wide and 10mm thick steel plate, and therefore the load was assumed to be spread as shown in Fig. 4.1. The moment at midspan was assumed to be :

$$M = B1 \frac{PL}{4} \qquad \text{Eqn.4.1}$$

$$\text{wnere} \quad B1 = 1 - \left(\frac{w + 2c}{2L} \right)$$

w = plate width
L = span of beam

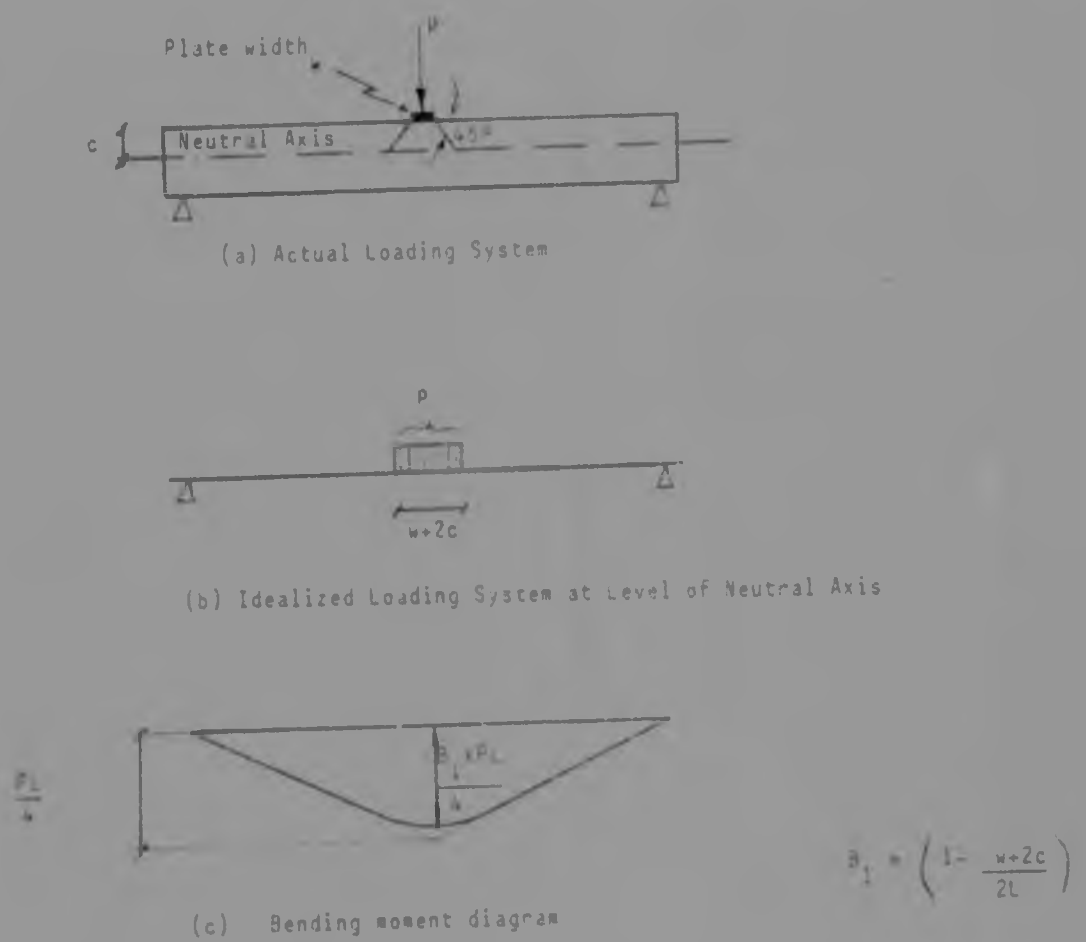

FIGURE 4.1 Spread of Load at Midspan

The moment at 50mm away from midspan was assumed to be :

$$M = B2 \; \frac{P}{2} \left(\frac{L}{2} - 0{,}0508 \right) \qquad \text{Eqn.4.2}$$

$$\text{where} \quad B2 = \left[1 - \frac{\left(\frac{w + 2C}{2} - 0{,}0508 \right)}{\left(\frac{L}{2} - 0{,}0508 \right)(w + 2C)} \right]$$

Table 4.1 shows the reduction factors for both sections and by comparing these results it can be seen that the values assumed for a section 50mm away from midspan are almost identical to the values corresponding to that section using the straight line bending moment diagram based on a maximum moment at midspan of PL/4.

BEAM	MAXIMUM LOAD P [kN]	SPAN [mm]	MOMENTS AT MIDSPAN Straight Line(PL/4) [kN.M]	MOMENTS AT MIDSPAN Assumed Eqn.4.1 [kN.M]	B1	MOMENTS 50mm FROM MIDSPAN Straight Line [kN.M]	MOMENTS 50mm FROM MIDSPAN Assumed Eqn.4.2 [kN.M]	B2
A1	23,94	1500	8,97	8,68	0,96	8,36	8,36	0,99
A2	36,40	1500	13,65	13,07	0,95	12,72	12,69	0,99
B1	23,32	1500	8,74	8,44	0,96	8,15	8,14	0,99
B2	28,47	1500	10,67	10,33	0,96	9,95	9,93	0,99
B3	49,00	1500	18,37	17,76	0,96	17.13	17,11	0,99
B4	49,50	1500	18,56	18,01	0,97	17,30	17,30	0,99
C1	45,50	2250	25,59	24,55	0,95	24,43	23,86	0,97
C2	35,29	1000	8,82	8,48	0,96	7,92	7,91	0,99
C3	60,48	1500	22,68	21,35	0,94	21,14	20,98	0,99
C4	17.42	2250	9,79	9,56	0,97	9,35	9,35	0,99
C5	9,86	1125	2,77	2,68	0,96	2,52	2,52	1,00
D1	26,66	1500	9,99	9,68	0,96	9,32	9,31	0,99
D2	37,20	1500	13,95	13,34	0,95	13,00	12,92	0,99
D3	29,44	1500	11,04	10,50	0,95	10,29	10,23	0,99

TABLE 4.1 : Moments and Reduction Factors for Two Sections : At Midspan and at 50mm away from Midspan

For midspan section, the assumed moments are slightly lower than the corresponding straight line maximum moments which was logical to expect. This means that provided the length of the loading plate is small, the loading pattern has little effect on the maximum moment.

4.3 TERMINOLOGY USED IN INTERPRETING RESULTS

4.3.1 Theoretical Values

The theoretical ultimate moment was evaluated on the basis of the ACI code[4] according to the following formula

$$M_u = A_s f_y (d - \frac{a}{2}) \qquad \text{Eqn.4.3}$$

$$\text{where} \quad a = \frac{A_s f_y}{0{,}85 . f'_c b}$$

The hypothetical value of theoretical elastic rotation at ultimate moment at either end of the beam, corresponding to the onset of plastic rotation, was obtained by means of the first moment-area theorem. An average flexural rigidity was obtained from the theoretical moment-curvature curve, corresponding to the slope between two points representing 0,4 and 0,6 of the ultimate moment.

4.3.2 Experimental Results

Where experimental results for maximum values of compressive strain of concrete, curvature, neutral axis depth and rotation are reported, they correspond to the instant at which the maximum load on the beam was reached under increasing load; or to the load just before this ultimate load was achieved at the preceding loading increment.

The hypothetical value of experimental elastic rotation at ultimate moment at either end of the beam was calculated in the following way. It was assumed that the load-deflection curve at mid-span could be divided into two regions : one region representing elastic deformation and another region associated with inelastic or plastic deformation. The load was identified at which plastic deformation began, and the corresponding moment evaluated. A secant line was drawn from the origin through the point on the moment-end rotation curve corresponding to this moment, and this line was extended to give the elastic rotation at a moment equal to the moment of resistance calculated according to the ACI code. This rotation was regarded as the experimental elastic rotation associated with the onset of plastic rotation for half span of the beam. This procedure is illustrated in the load-deflection curve and the moment-end rotation curve for beam A1, shown in Figs. 4.4a and 4.4b respectively.

The experimental inelastic end rotation was obtained by subtracting the experimental elastic rotation from the total experimental rotation for the half span of the beam at maximum load.

4.4 GENERAL RESULTS

Failure of the concrete compressive zone in flexure did not occur until the maximum concrete compressive strain exceeded 0,003. A photograph showing the response of a beam as the load approaches 42,8% of the ultimate load and a compressive strain equal to 1446×10^{-6} is displayed in Fig. 4.2a, and Fig. 4.2b shows the same beam under a load corresponding to 78,6% of the ultimate load with a concrete compressive strain of 3196×10^{-6}; and finally Fig.4.2c displays the same beam at the end of the test. At ultimate load the concrete compressive strain was 9585×10^{-6}.

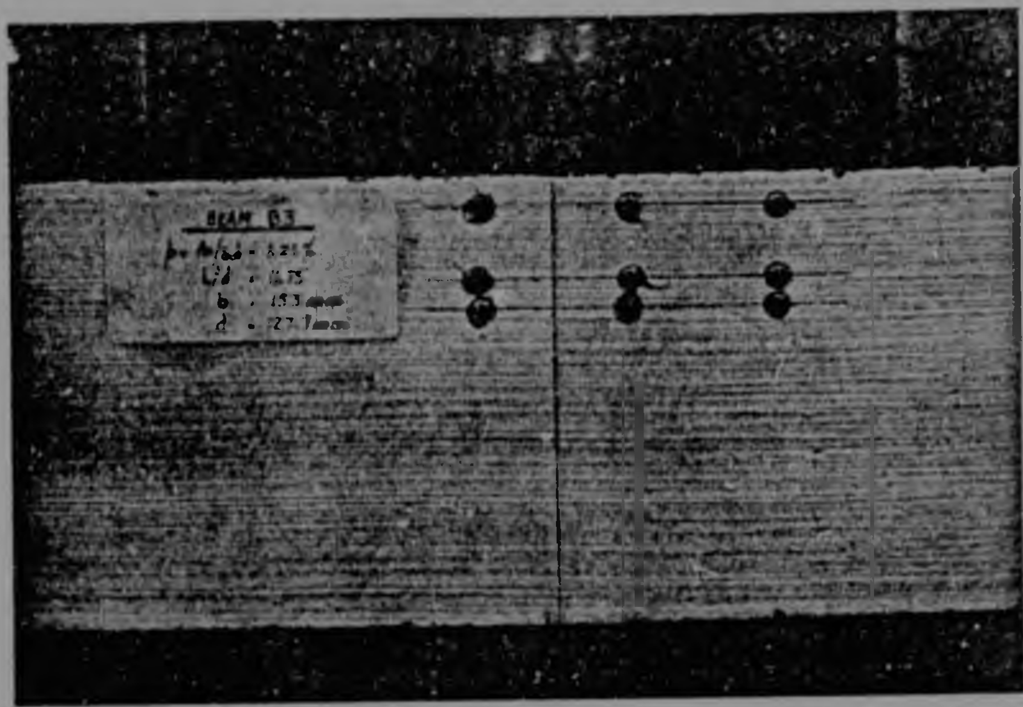

FIGURE 4.2a

Beam B3 at 42,8% of ultimate load.

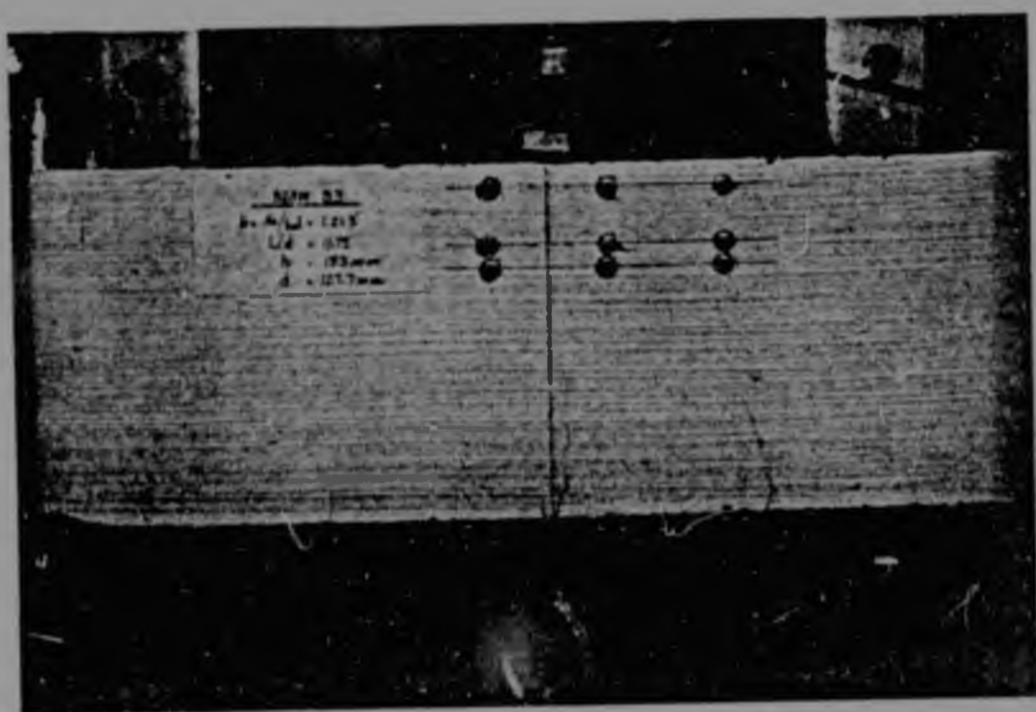

FIGURE 4.2b

Beam B3 at 78,6% of ultimate load.

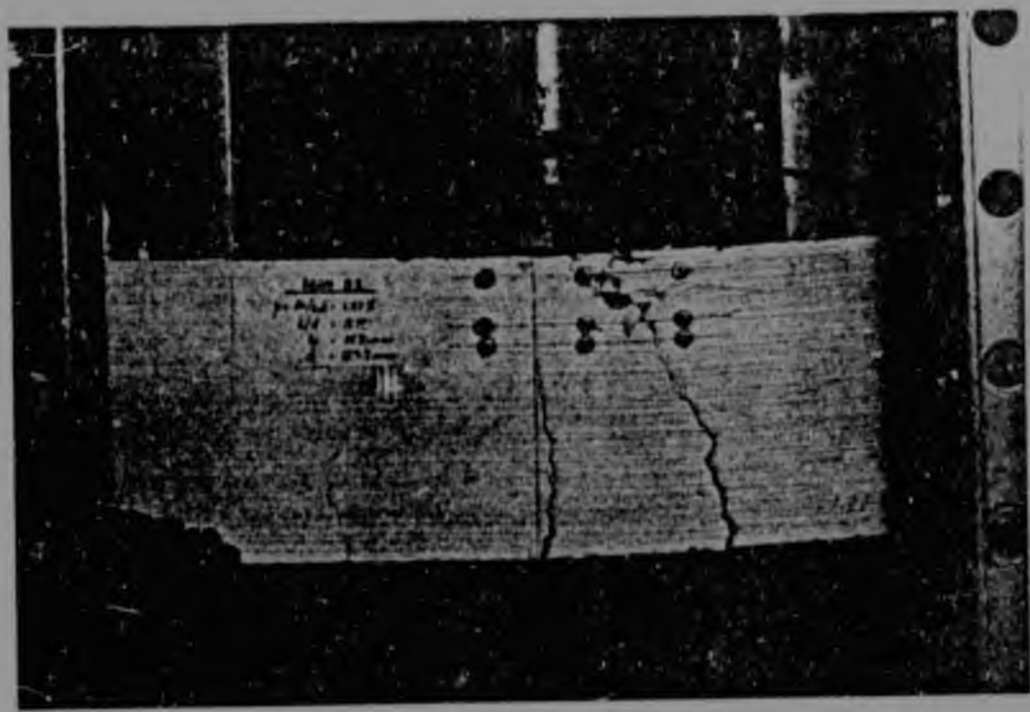

FIGURE 4.2c

Beam B3 at the end of the test

Figure 4.3 illustrates the theoretical values and experimental results for the relationship between moment or neutral axis height and curvature for beam A1. For the same moment ratio, the experimental results of curvature were found to be greater than the theoretical values, indicating that more ductility was obtained than was expected.

For convenience, test results for each beam of experimental load-deflection and moment-end rotation curves, together with theoretical and experimental plots of the ratio of moment to theoretical ultimate moment and the ratio of neutral axis depth to effective depth as a function of curvature are shown in Appendix 3
The properties of the different beams are summarised in Table 3.1 and the main test results are tabulated as follows :

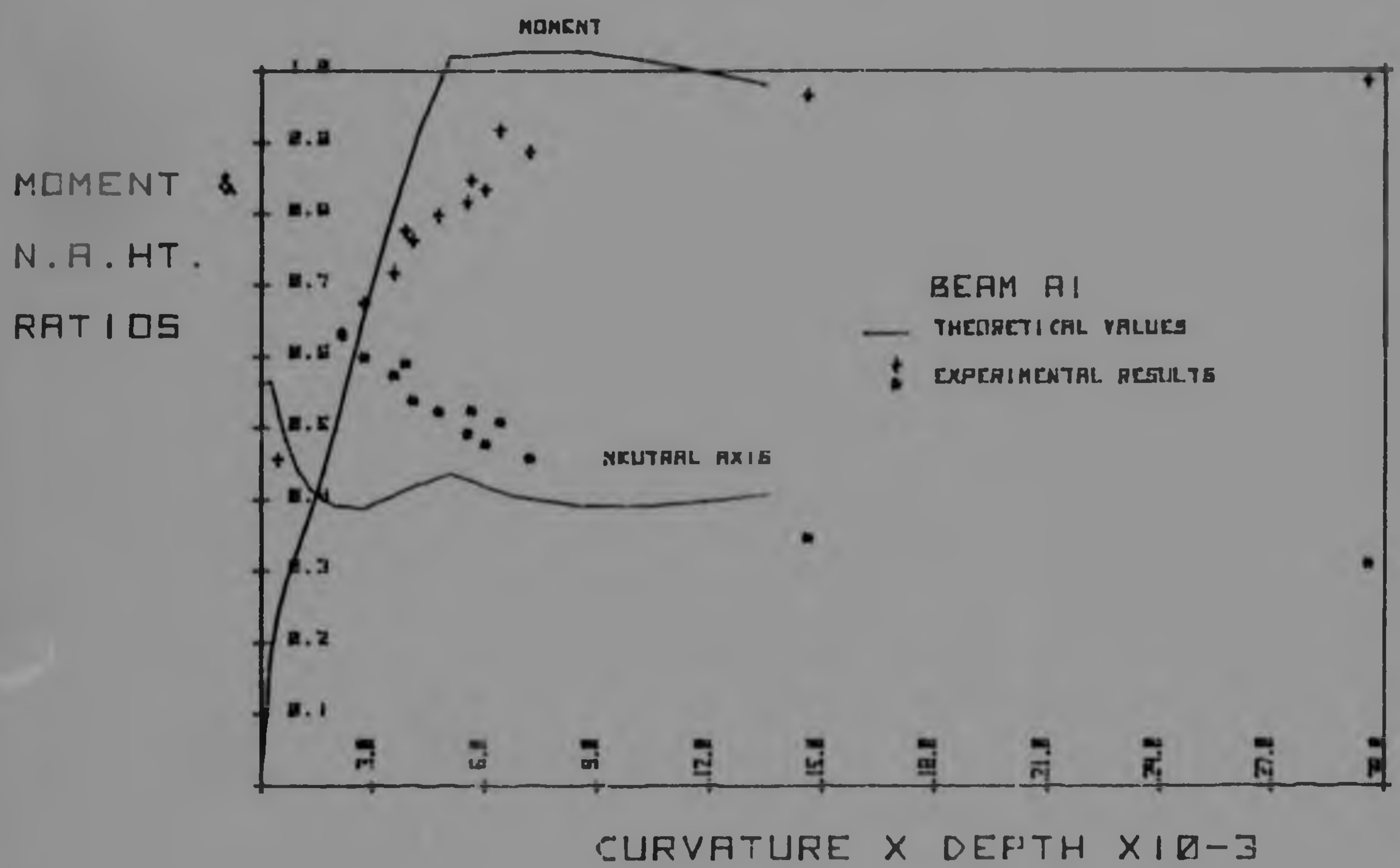
MOMENT
MOMENT &
N.A.HT.
RATIOS
BEAM A1
THEORETICAL VALUES
EXPERIMENTAL RESULTS
NEUTRAL AXIS
CURVATURE X DEPTH X10-3

FIGURE 4.3

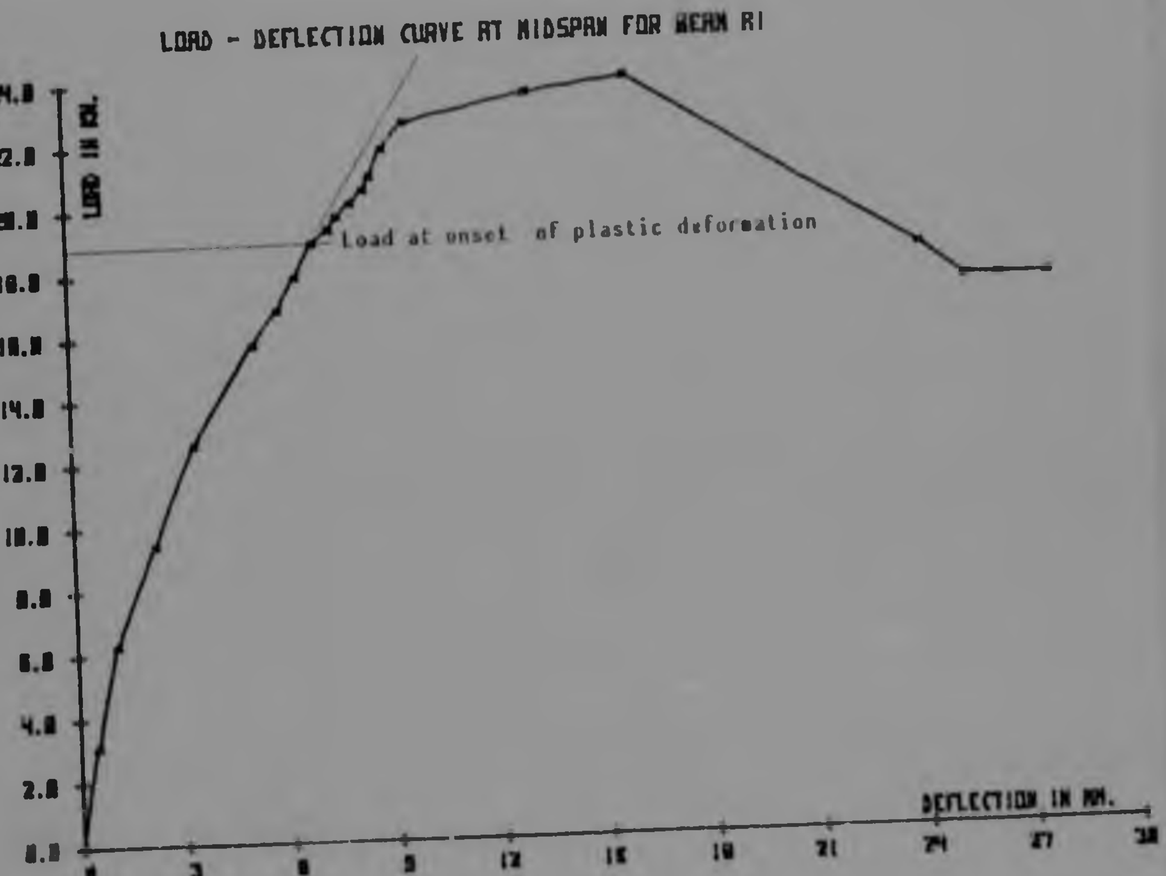
LOAD - DEFLECTION CURVE AT MIDSPAN FOR BEAM R1
LOAD IN KN.
DEFLECTION IN MM.
Load at onset of plastic deformation
24.0
22.0
20.0
18.0
16.0
14.0
12.0
10.0
8.0
6.0
4.0
2.0
0.0
0
3
6
9
12
15
18
21
24
27
30

FIGURE 4.4a

MOMENT - ROTATION CURVE FOR HALF SPAN FOR BEAM A1

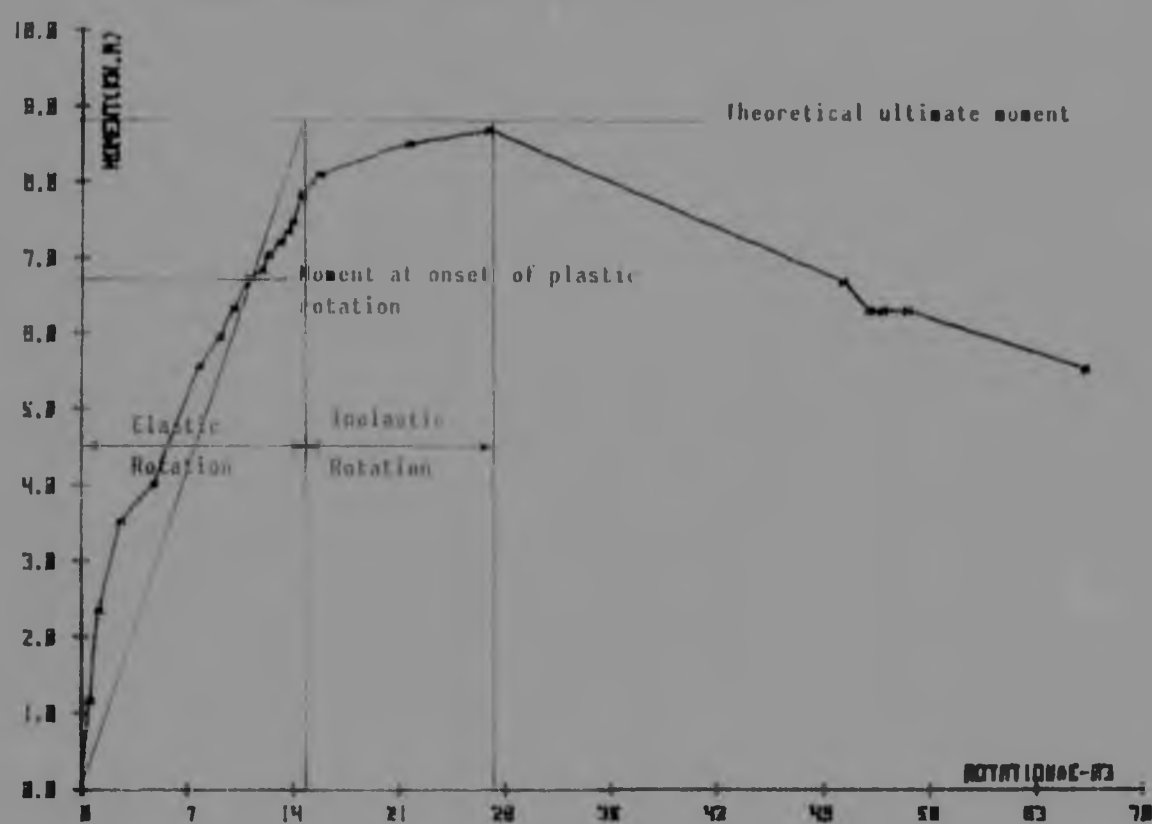

FIGURE 4.4b

Table 4.2 Comparison between different expressions for maximum concrete compressive strains at ultimate moment with the results obtained in the experiment.

Table 4.3 Comparison between different expressions for the ratio of neutral axis depth to effective depth at ultimate moment with the results obtained in the experiment.

Table 4.4. Comparison between theoretical ultimate moments and the experimental maximum moments.

Table 4.5 Total, elastic and plastic rotations for half span of each beam.

Table 4.6 Ductility expressed as the ratio of maximum curvature to curvature at first yield of the tension reinforcement, and rotation capacity (ratio of inelastic to elastic end rotation) for each beam.

Table 4.7 Comparison of spread of plasticity (l_p) according to Corley-Mattock (Eqn.2.21) and the experimental results evaluated using Eqn.2.[illegible]

From Table 4.2 it can be seen that the values for maximum concrete compressive strain obtained by using Corley's and Mattock's equation (Eqn.2.20 in Chapter 2) are too optimistic but the results obtained by using the CEB-FIP expression and the theoretical program are definitely too conservative. The CEB-FIP expression used is as follows :

$$\varepsilon_{c2} = 0{,}003 + 0{,}0002(50 - f_c) \qquad \text{Eqn.4.4}$$

where f_c is : the cylinder strength in MPa.

Table 4.3 shows that the theoretical neutral-axis depth ratios that are closer to the experimental results are those obtained by Kemp's[13] expression. The plastic neutral axis expression used according to Kemp[13] was :

$$x_{pu} = \frac{f_y A_s}{0{,}93 \times (0{,}86 \times f_{cu}) \times b} = \frac{f_y A_s}{0{,}93 \times f'_c b} \qquad \text{Eqn.4.5a}$$

The neutral axis depth ratios for ultimate load obtained by using the ACI code (Eqns. 2.10 and 2.13 in Chapter 2) and the theoretical moment-curvature program gave higher values than those that resulted in the experiment. This difference was largest in the tests where the highest compressive strains in the concrete were observed.

Table 4.4 shows that although all the design moments are very similar, there are, in some cases, differences with the experimental maximum moments; this can be a result of small changes in level arm, stress-strain properties of concrete in beams not being the same as obtained from cylinder and cube specimens, strength of steel varying from one bar to another, strain-hardening properties of steel and other effects discussed subsequently. The moment at ultimate strength according to ACI design code was evaluated using Eqn. 4.3 and the CP110 was calculated from the following expression :

$$M_{u2} = f_y . A_s z_1 \qquad \text{Eqn.4.5b}$$

$$\text{where} \quad z_1 = d \left(1 - \frac{f_y A_s}{2 \times 0{,}6 \times f_{cu} \times b \times d} \right)$$

and the value 0,6 does not include the partial material factor of 1,5 for concrete.

Table 4.5 shows that the theoretical values of elastic rotation are higher than the experimental elastic rotation results. This is probably due to the different bases of defining the elastic curvatures in the two cases. This comparison is reasonably consistent except in tests B2 and C5.

BEAM	MAXIMUM CONCRETE COMPRESSIVE STRAINS AT ULTIMATE MOMENT									
	Experimental Results	Theoretical Program Values		Corley-Mattock	CEB-FIP	SPAN	WIDTH	EFFECTIVE Depth	STRESS Block Depth [mm]
	Strainx10^{-6}	Strainx10^{-6}	Ratio	RATIOS		[mm]			
	ε_c Max.	ε_{cTH}	$\varepsilon_c MAX/\varepsilon_{cTH}$	$\varepsilon_c MAX/\varepsilon_{c1}$	$\varepsilon_c MAX/\varepsilon_{c2}$	L	b	d	a(ACI)
A1	9151	2738	3,34	0,93	2,56	1500	102	125,00	46,0
A2	3451	2752	1,25	0,35	1,03	1500	102	125,35	44,2
B1	9340	2766	3,37	0,95	2,61	1500	102	123,60	46,1
B2	6370	2773	2,29	1,11	1,78	1500	102	123,00	46,0
B3	9585	2757	3,47	0,96	2,68	1500	153	127,725	47,5
B4	9375	2804	3,34	1,32	2,62	1500	153	123,70	47.0
C1	4856	2715	1,78	0,68	1,36	2250	102	193,60	70,6
C2	11279	3247	3,47	1,00	3,16	1000	102	126.00	45,5
C3	4045	2743	1,47	0,50	1,13	1500	102	187,00	68.9
C4	5757	3135	1,83	0,64	1,61	2250	102	133.00	46,1
C5	6416	3116	2,05	0,33	1,79	1125	102	65.00	22,4
D1	9190	3207	2,86	0,93	2,57	1500	102	128,00	45,5
D2	7404	2688	2,75	0,75	2,07	1500	102	126,85	60,8
D3	6806	3912	1,74	0,69	1,90	1500	102	127,35	69,2

TABLE 4.2: Maximum concrete compressive strains at ultimate moment.

BEAM	NEUTRAL AXIS DEPTH RATIOS AT ULTIMATE MOMENT					SPAN	WIDTH	EFFECTIVE DEPTH	STRESS BLOCK DEPTH
	Experimental Results	Theoretical Program	KEMP	ACI	STRESS BLOCK HEIGHT / EFFECTIVE DEPTH	[mm]			
	NA/d	NA/d	x_{pu}/d	c/d	a/d (ACI)	L	b	d	a (ACI)
A1	0,310	0,406	0,337	0,433	0,368	1500	102	125,00	46,0
A2	0,427	0,408	0,323	0,415	0,353	1500	102	125,35	44,2
B1	0,332	0,410	0,341	0,439	0,373	1500	102	123,60	46,1
B2	0,308	0,411	0,342	0,440	0,374	1500	102	123,00	46,0
B3	0,315	0,408	0,340	0,438	0,372	1500	153	127.725	47,5
B4	0,278	0,415	0,347	0,447	0,380	1500	153	123,70	47,0
C1	0,422	0,402	0,333	0,429	0,365	2250	102	193,60	70,6
C2	0,228	0,385	0,330	0,425	0,361	1000	102	126,00	45,5
C3	0,415	0,406	0,338	0,434	0,369	1500	102	187,00	68,9
C4	0,328	0,372	0,317	0,408	0,347	2250	102	133,00	45,1
C5	0,406	0,369	0,315	0,406	0,345	1125	102	65,00	22,4
D1	0,287	0,380	0,325	0,419	0,356	1500	102	128,00	45,5
D2	0,435	0,531	0,438	0,564	0,479	1500	102	126,85	60,8
D3	0,428	0,580	0,498	0,640	0,544	1500	102	127,35	69,2

TABLE 4.3 Neutral axis depth ratios at ultimate moment

BEAM	MOMENTS AT ULTIMATE STRENGTH IN [kNxM]				SPAN	WIDTH	EFFECTIVE DEPTH	STRESS BLOCK DEPTH
	Experimental Results	Theoretical Values	ACI	CP110	[mm]			
	M.Max	M.PG	Mu1	Mu2	L	b	d	a (ACI)
A1	8,68	9,04	8,81	8,58	1500	102	125,00	46,0
A2	13,07	13,67	13,37	13,00	1500	102	125,35	44,2
B1	8,44	8,93	8,70	8.47	1500	102	123,60	46,1
B2	10,33	8,87	8,63	8,41	1500	102	123,00	46,0
B3	17,76	14,26	13,89	13,53	1500	153	127,725	47,5
B4	18,01	13,61	13,24	12,89	1500	153	123,70	47,0
C1	24,55	21,46	20,96	20,43	2250	102	193,60	70,6
C2	8,48	9,03	8.80	8.58	1000	102	126,00	45,5
C3	21,35	20,24	19,75	19,24	1500	102	187,00	68,9
C4	9,56	9,75	9,51	9,28	2250	102	133,00	46,1
C5	2,68	2,32	2,26	2,20	1125	102	65,00	22,4
D1	9,68	9,22	8.99	8.77	1500	102	128,00	45,5
D2	13,34	11,38	10,99	10,60	1500	102	126,85	60,8
D3	10,50	12,35	12,05	11,54	1500	102	127,35	69,2

TABLE 4.4 Moments at ultimate strength in [kNxm]

BEAM	ROTATIONS FOR EACH HALF SPAN OF BEAM x 10^{-3}				SPAN	WIDTH	EFFECTIVE DEPTH	STRESS BLOCK DEPTH
	TOTAL ROTATION	ELASTIC ROTATION, θ_e		INELASTIC ROTATION, θ_i	[mm]			
	Experimental Results	Theoretical Values	Experimental Results	Experimental Results	L	b	d	a (ACI)
A1	26,7	15,2	14,75	12.00	1500	102	125,09	46,0
A2	15,9	15,3	13,42	2,48	1500	102	125,35	44,2
B1	23,4	15,4	14,28	9,12	1500	102	123,60	46,1
B2	20,9	15,4	10.86	10,11	1500	102	123,00	46,0
B3	25,2	15,2	13,36	11,91	1500	153	127,725	47,5
B4	25,9	15,7	13,75	12,22	1500	153	123,70	47,0
C1	24,7	15,5	12,14	12,59	2250	102	193,60	70,6
C2	38,5	9,9	9,00	29,50	1000	102	126,00	45,5
C3	13,1	10,6	8,57	4,60	1500	102	187,00	68,9
C4	33,7	22,2	22,63	11.09	2250	102	133,00	46,1
C5	40,3	20,4	5,25	35,07	1125	102	65,00	22,4
D1	26,8	13,9	10,92	15,88	1500	102	128,00	45,5
D2	24,3	12,7	10,08	14,25	1500	102	126,85	60,8
D3	24,2	15,9	15,52	8,73	1500	102	127,35	69,2

TABLE 4.5 ROTATIONS FOR EACH HALF SPAN OF BEAM x 10^{-3}

BEAM	% STEEL x YIELD STRESS of STEEL	SPAN L [mm]	STRESS BLOCK HEIGHT / EFFECTIVE DEPTH $a/_d$ (ACI)	DUCTILITY RATIO $\emptyset_u/\emptyset_y$ (Eqn.2.14) Experimental Results	DUCTILITY RATIO $\emptyset_u/\emptyset_y$ (Eqn.2.14) Theoretical Values	ROTATION CAPACITY θ_i/θ_e (Table 4.5) Experimental Results
A1	667,60	1500	0,368	7,29	1,64	0,814
A2	1012,00	1500	0,353	1,78	1,62	0,185
B1	688,75	1500	0,373	4,70	1,61	0,639
B2	687,50	1500	0,374	4,29	1,61	0,931
B3	686,07	1500	0,372	4,04	1,58	0,892
B4	695,64	1500	0,380	2,41	1,56	0,889
C1	668,78	2250	0,365	1,05	1,63	1,037
C2	662,46	1000	0,361	12,55	1,70	3,278
C3	682,00	1500	0,369	2,86	1,64	0,537
C4	639,16	2250	0,347	6,10	1,76	0,490
C5	631,30	1125	0,345	4,00	1,82	6,681
D1	654,50	1500	0,356	8,48	2,09	1,454
D2	880,74	1500	0,479	3,96	1,57	1,413
D3	999,12	1500	0,544	3,25	1,01	0,563

TABLE 4.6: Ductility expressed as the ratio of maximum curvature to curvature at first yield of the tension reinforcement, and rotation capacity for each beam.

BEAM	SPREAD OF PLASTICITY (LP)					
	EXPERIMENTAL RESULTS					LP ACCORDING TO CORLEY & MATTOCK [mm]
	CURVATURES x [mm^{-1}] x 10^{-6}			PLASTIC ROTATION	L_p [mm]	
	ELASTIC	MAXIMUM	PLASTIC	θ_p x 10^{-3}	θ_p/ϕ_p	(Eqn.2.21)
	ϕ_y	ϕ Max	ϕ_p			
A1	32,42	236,33	203,91	12,00	58,85	100,00
A2	36,25	64,50	28,25	2,48	87,79	
B1	48,50	227,75	179,25	9,12	50,88	99,30
B2	39,25	168,25	129,00	10,115	78,41	99.00
B3	59,00	238,50	179,50	11,915	66,38	101,363
B4	113,25	272,50	159,25	12,225	76,77	99,35
C1	56,63	N.A.*	–	12,595	–	153.050
C2	31,25	392,31	361,06	29,50	81,70	88,00
C3	18,19	52,08	33,89	4,605	135,88	131,00
C4	21,63	131,97	110,34	11,095	100,55	122,75
C5	60,71	242,86	182,15	35,075	192,56	60,625
D1	29,50	250,25	220,75	15,88	71,94	101,50
D2	33,91	134,22	100,31	14,25	142,06	100,925
D3	38,48	125,00	86,52	8,73	100,90	101,175

N.A.* Not available

TABLE 4.7 : Spread of plasticity (l_p)

BEAM	SPREAD OF PLASTICITY (LP) EXPERIMENTAL RESULTS					LP ACCORDING TO CORLEY & MATTOCK [mm]
	CURVATURES $\times [mm^{-1}] \times 10^{-6}$			PLASTIC ROTATION	L_p [mm]	
	ELASTIC $Ø_y$	MAXIMUM $Ø_{Max}$	PLASTIC $Ø_p$	$\theta_p \times 10^{-3}$	$\theta_p/Ø_p$	(Eqn.2.21)
A1	32,42	236,33	203,91	12,00	58,85	100,00
A2	36,25	64,50	28,25	2,48	87,79	
B1	48,50	227,75	179,25	9,12	50,88	99,30
B2	39,25	168,25	129,00	10,115	78,41	99.00
B3	59,00	238,50	179,50	11,915	66,38	101,363
B4	113,25	272,50	159,25	12,225	76,77	99,35
C1	56,63	N.A.*	—	12,595	—	153.050
C2	31,25	392,31	361,06	29,50	81,70	88,00
C3	18,19	52,08	33,89	4,605	135,88	131,00
C4	21,63	131,97	110,34	11,095	100,55	122,75
C5	60,71	242,86	182,15	35,075	192,56	60,625
D1	29,50	250,25	220,75	15,88	71,94	101,50
D2	33,91	134,22	100,31	14,25	142,06	100,925
D3	38,48	125,00	86,52	8,73	100,90	101,175

N.A.* Not available

TABLE 4.7 : Spread of plasticity (l_p)

4.5 VARIABLES AFFECTING ROTATION CAPACITY

4.5.1 Theoretical and Experimental Moment and Neutral Axis Ratio-Curvature Curves

The comparison between theoretical and experimental moment and neutral axis ratio-curvature curves is shown in Appendix 3, and from these curves it can be noticed that the moment ratio-curvature curves differ significantly once flexural cracking occurs. At a particular value of moment the experimental curvatures are considerably greater than the theoretical curvatures. As the comparison between theoretical and experimental neutral axis depths is reasonably good, it can be concluded that the differences relate to the compressive strain on the outer fibre of the concrete at which the moment reaches its maximum value.

The main parameters that affect the maximum compressive strain of a singly-reinforced simply-support concrete beam are the concrete strength and stress-strain curve, the tensile steel strength and strain-hardening properties, amount of tensile reinforcement, the span and width of the beam and also the rate of loading. The differences between experimental and theoretical values of these variables together with others such as effect of binding may explain part of these observed differences in maximum concrete strain.

It should be mentioned that there could have been a possible bond failure which would reduce the strain in the steel as shown in Fig 4.5, and therefore for the same curvature in the concrete a lower value of moment would be

4.5 VARIABLES AFFECTING ROTATION CAPACITY

4.5.1 Theoretical and Experimental Moment and Neutral Axis Ratio-Curvature Curves

The comparison between theoretical and experimental moment and neutral axis ratio-curvature curves is shown in Appendix 3, and from these curves it can be noticed that the moment ratio-curvature curves differ significantly once flexural cracking occurs. At a particular value of moment the experimental curvatures are considerably greater than the theoretical curvatures. As the comparison between theoretical and experimental neutral axis depths is reasonably good, it can be concluded that the differences relate to the compressive strain on the outer fibre of the concrete at which the moment reaches its maximum value.

The main parameters that affect the maximum compressive strain of a singly-reinforced simply-support concrete beam are the concrete strength and stress-strain curve, the tensile steel strength and strain-hardening properties, amount of tensile reinforcement, the span and width of the beam and also the rate of loading. The differences between experimental and theoretical values of these variables together with others such as effect of binding may explain part of these observed differences in maximum concrete strain.

It should be mentioned that there could have been a possible bond failure which would reduce the strain in the steel as shown in Fig 4.5, and therefore for the same curvature in the concrete a lower value of moment would be [illegible] bond is made up of three components: (a) chemical adhesion, (b) friction, and (c) mechanical interaction between concrete and steel. Bond of plain bars depends primarily on the first two elements, while bond of deformed bars depend mainly on mechanical interlocking of concrete and steel. At cracks, in reinforced concrete members, the stress in the steel rises while at positions in between cracks the stress in the steel has a lower value; therefore bond conditions at cracks and in the immediate surrounding concrete are more severe and local bond failure may take place.

A bond factor F was introduced by Baker[12] where the strain of steel is related to the strain of the concrete at the outer compression surface of the concrete. i.e.:

$$F = \frac{\varepsilon_s C}{\varepsilon_c (d-C)} \qquad \text{Eqn.4.6}$$

This bond factor is equal to one (1) for full bond conditions and as this factor decreases, its negative influence upon the steel strain increases.

Also from Fig. 4.6 which corresponds to beam C3 it can be seen that bond failure seems to affect a section near midspan more than at the midspan itself, this is reasonable since major cracks sometimes develop at sections near midspan and occur symmetrically on both sides of the midspan section. However this was the only beam for which curvatures were reported to be significantly lower at midspan than for a section near midspan.

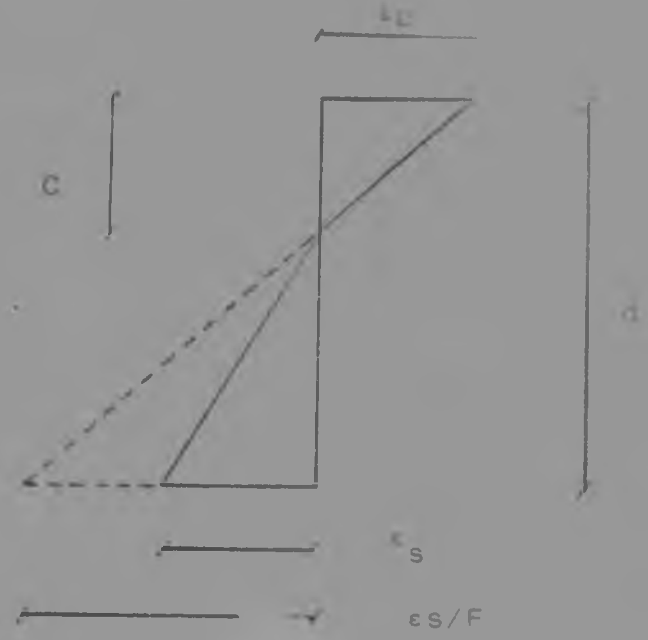

FIGURE 4.5

From Fig.4.7 it can be seen that, as expected, the moment ratio-curvature curves for a section at midspan and at a section near midspan (50mm) have a similar trend and similar results were obtained in all the other tests except for beam C[illegible]

4.5.2 Effect of Tension Reinforcement

Fig.4.8 displays the load ratio-deflection curves at midspan for beams A1, D1, D2 and D3. All these beams are capable of undergoing large deflections near maximum load and therefore show a ductile behaviour. Beams A1 and D3 are reinforced by high tensile steel with a percentage of steel x yield stress of steel equal to 667,[illegible] and 999,12 respectively; beams D1 and D2 are reinforced with mild steel and have a percentage of steel x yield stress of steel equal to 654,5 and 880,74 respectively.

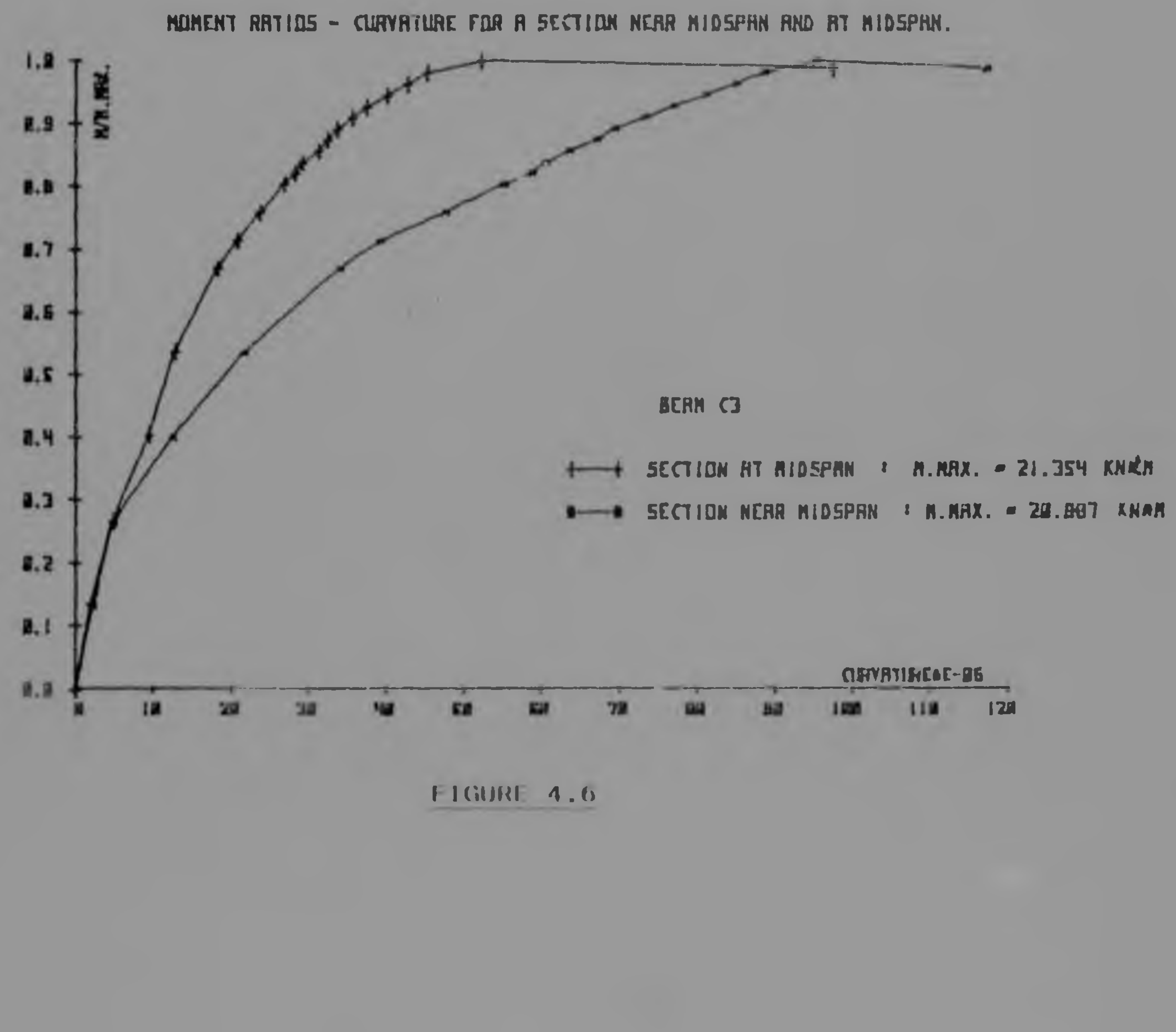
MOMENT RATIOS - CURVATURE FOR A SECTION NEAR MIDSPAN AND AT MIDSPAN.
M/M.MAX.
1.0
0.9
0.8
0.7
0.6
0.5
0.4
0.3
0.2
0.1
0.0
0
10
20
30
40
50
60
70
80
90
100
110
120
BEAM C3
SECTION AT MIDSPAN : M.MAX. = 21.354 KN*M
SECTION NEAR MIDSPAN : M.MAX. = 20.807 KN*M

FIGURE 4.6

MOMENT RATIOS - CURVATURE FOR A SECTION NEAR MIDSPAN AND AT MIDSPAN.

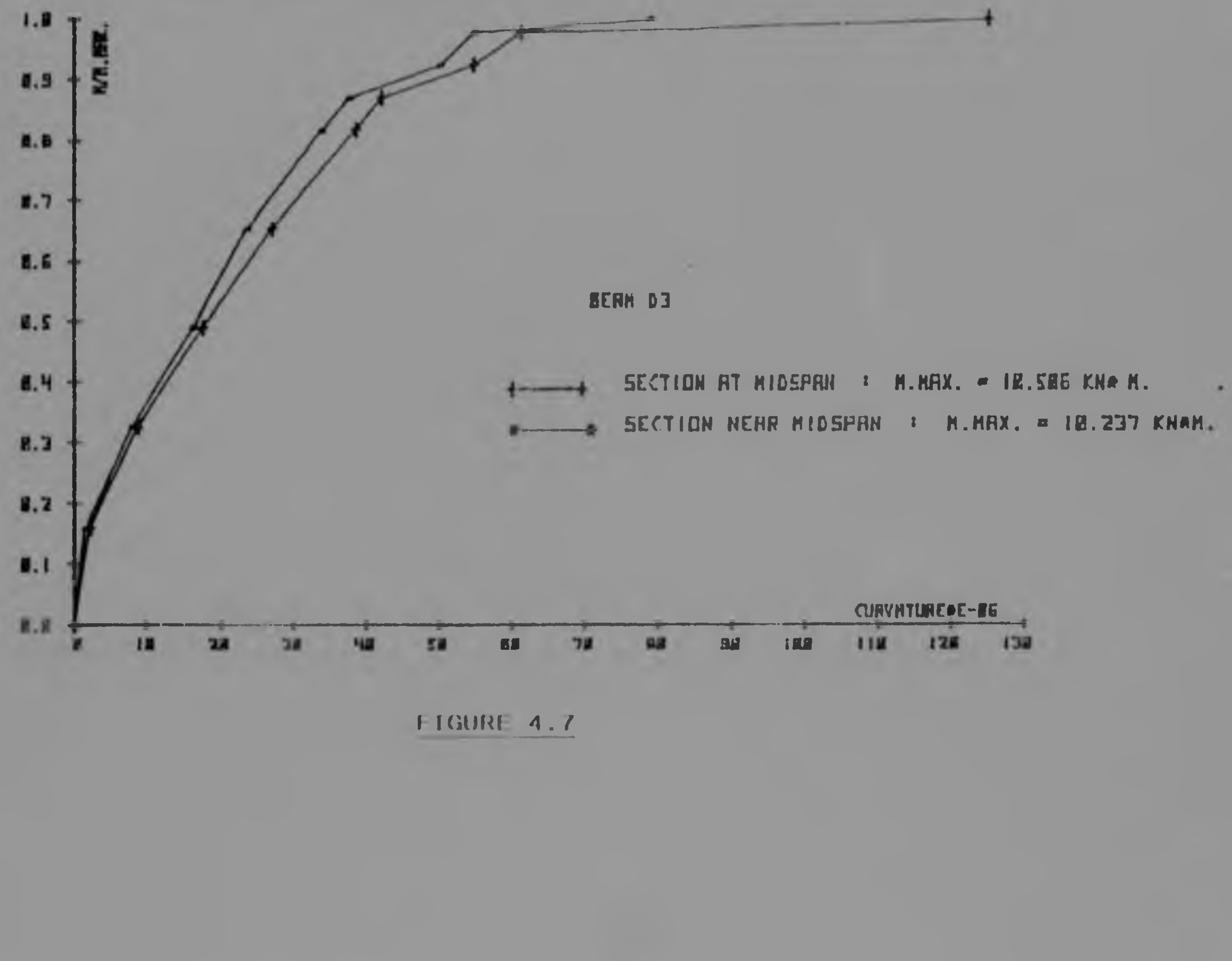

FIGURE 4.7

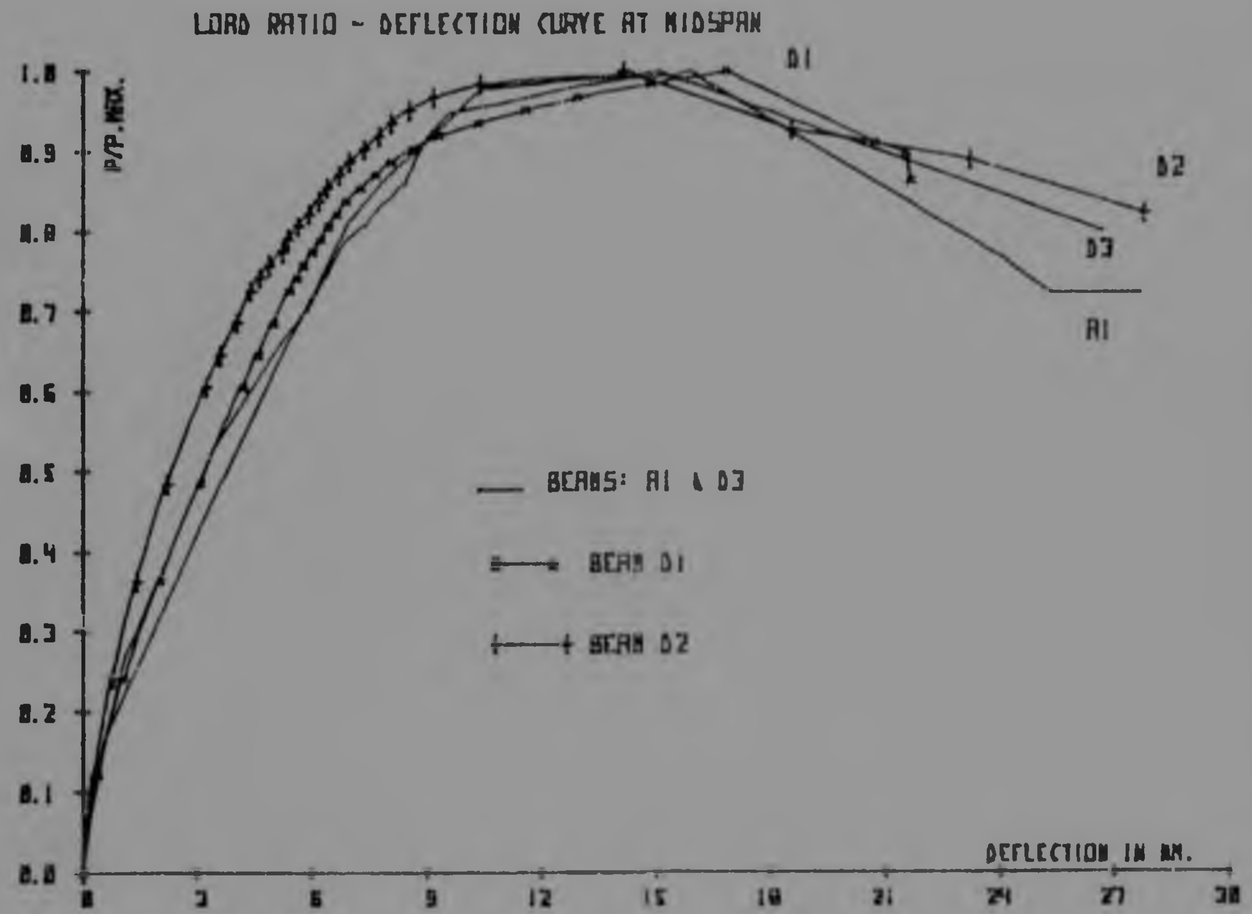

LOAD RATIO - DEFLECTION CURVE AT MIDSPAN
P/P.MAX.
1.0
0.9
0.8
0.7
0.6
0.5
0.4
0.3
0.2
0.1
0.0
0
3
6
9
12
15
18
21
24
27
30
DEFLECTION IN MM.
D1
D2
D3
A1
BEAMS: A1 & D3
BEAM D1
BEAM D2

FIGURE 4.8

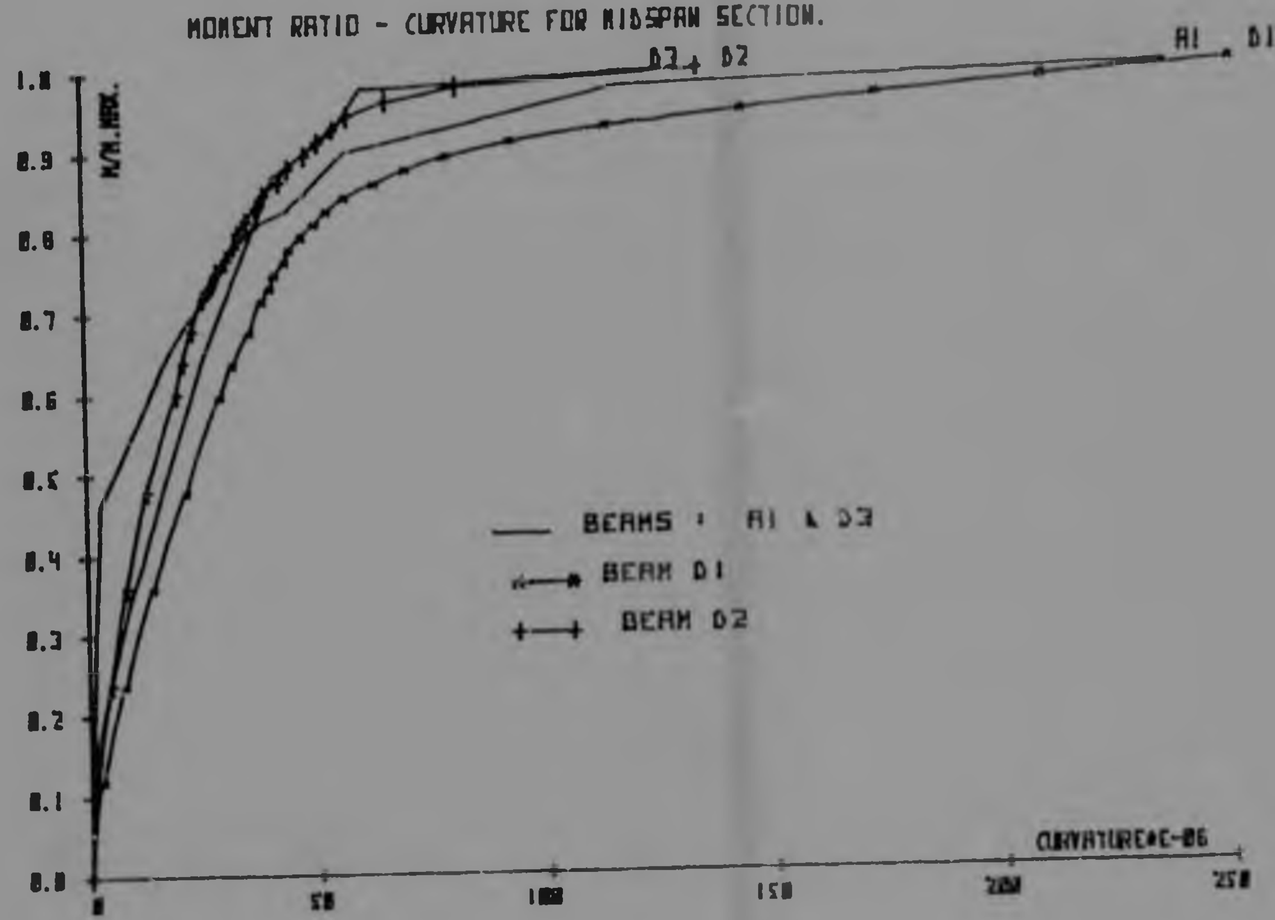
MOMENT RATIO - CURVATURE FOR MIDSPAN SECTION.
M/M.MAX.
1.0
0.9
0.8
0.7
0.6
0.5
0.4
0.3
0.2
0.1
0.0
0
50
100
150
200
250
CURVATURE*E-06
BEAMS : A1 & D3
BEAM D1
BEAM D2
A1
D1
D3
D2

FIGURE 4.9

TOTAL ROTATION FOR HALF SPAN VS. PERCENTAGE OF STEEL * YIELD STRESS.

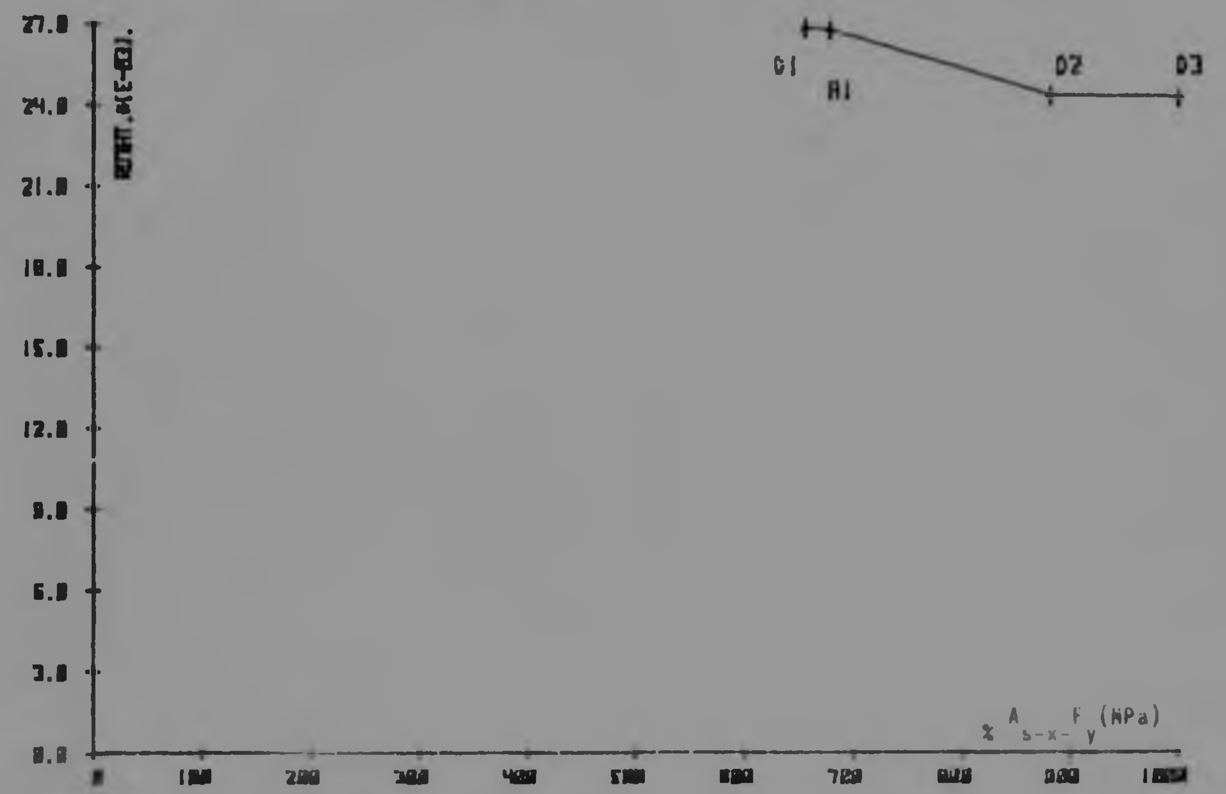

FIGURE 4.10

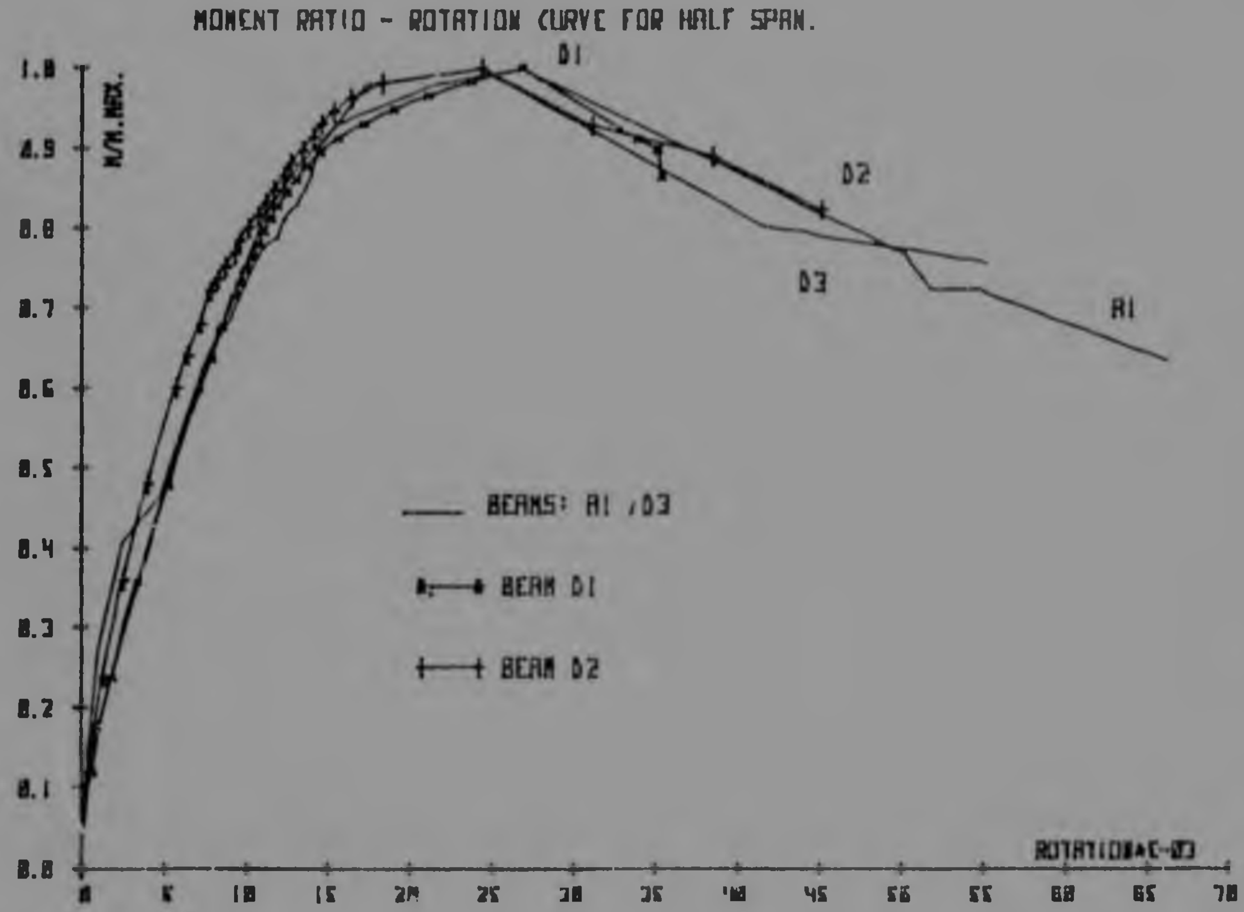
MOMENT RATIO - ROTATION CURVE FOR HALF SPAN.
M/M.MAX.
D1
D2
D3
A1
BEAMS: A1 /D3
BEAM D1
BEAM D2
0 5 10 15 20 25 30 35 40 45 50 55 60 65 70
0.0 0.1 0.2 0.3 0.4 0.5 0.6 0.7 0.8 0.9 1.0

FIGURE 4.11

INELASTIC ROTATION FOR HALF SPAN VS. PERCENTAGE OF STEEL * YIELD STRESS.

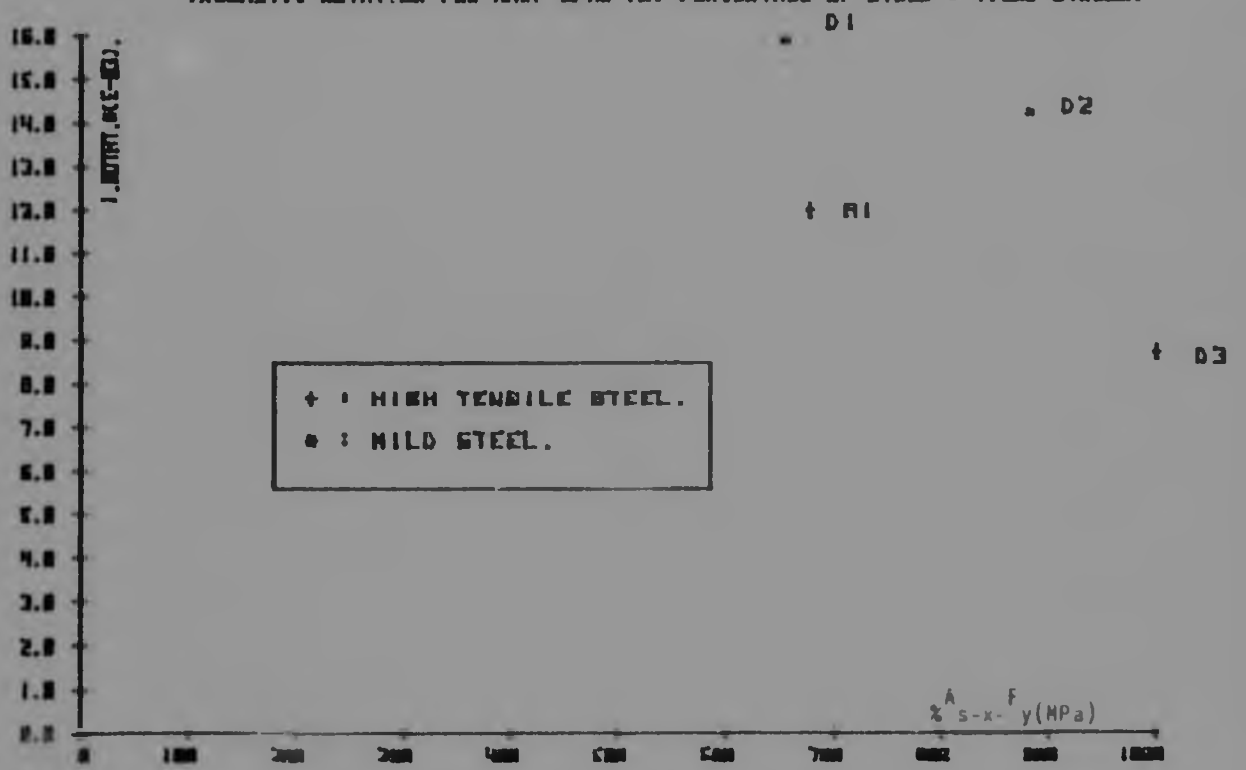

FIGURE 4.12

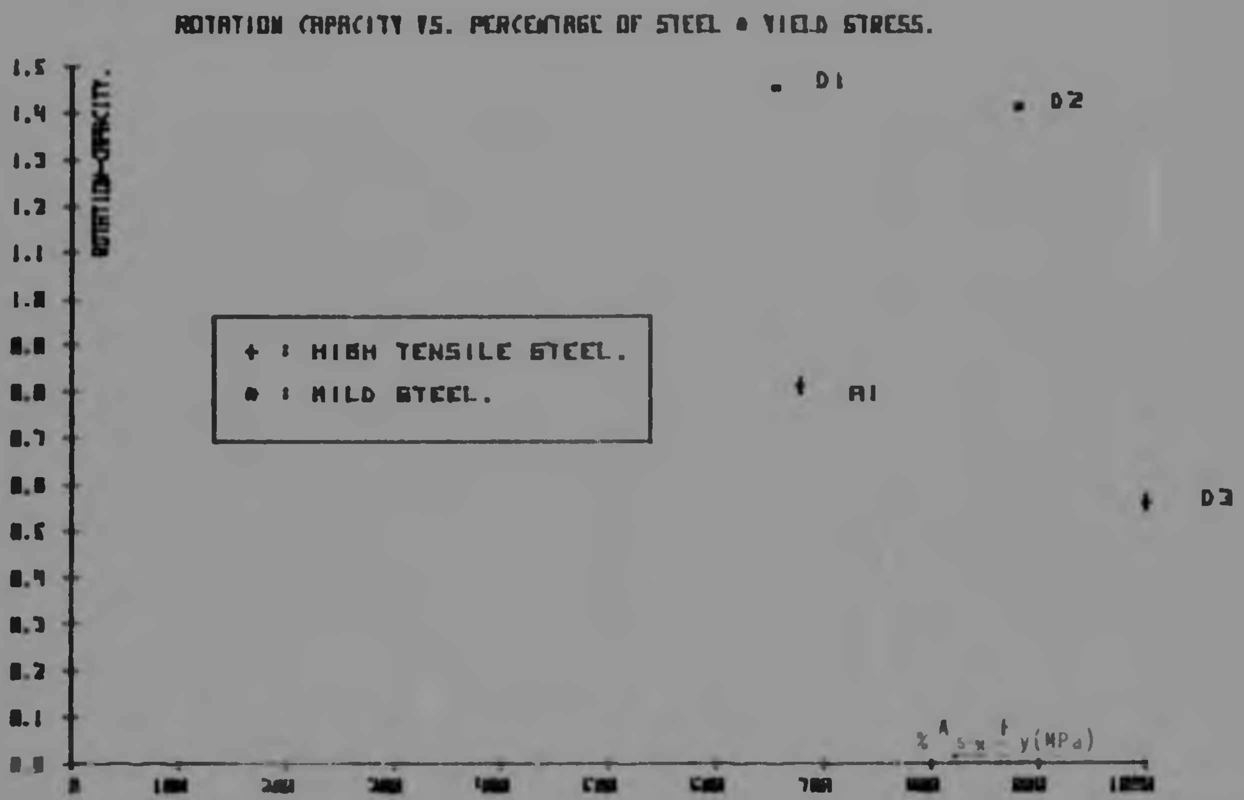
ROTATION CAPACITY VS. PERCENTAGE OF STEEL * YIELD STRESS.
ROTATION-CAPACITY.
+ : HIGH TENSILE STEEL.
* : MILD STEEL.
D1
D2
A1
D3
% As x fy (MPa)
1.5
1.4
1.3
1.2
1.1
0.1
0
700

FIGURE 4.13

From Fig.4.9 it can be seen that at maximum moment at midspan, greater curvatures are reached by beams D1, then A1, followed by beams D2 and D3. This was expected because at lower values of percentage of steel x yield stress of the steel (D1 and A1), the curvature is expected to be greater.

Fig. 4.10 shows clearly that as the percentage of steel x yield stress is increased, the total rotation for half span of the beam is reduced. Beams A1 and D1 had a very similar percentage of steel x yield stress varying only by 3,5%, and beams D2 and D3 had also a similar amount varying by 13,5%, but about 40% higher than beams A1 and D1.

Fig. 4.11 shows that beams A1 and D1 have a similar and higher total rotation than beams D2 and D3 for the maximum moment ratio.

Fig. 4.12 illustrates the inelastic rotation for half span and shows not only that as percentage of steel x yield stress of the reinforcing decreases the inelastic rotation increases, but also highlights the important aspect that beams D1 and D2 which are reinforced with mild steel bars, display higher inelastic rotations than beams A1 and D3 with high tensile steel. These findings are magnified when considering rotation capacity as shown in Fig. 4.13.

4.5.3 Effect of Span

Initially it was thought that rotation capacity was a function of span to depth ratio and therefore three different ratios for L/d were tested. Ratios of 8 (beams C2 and C3), 12 (beams A1 and C1), and 18 (beams C4 and C5) were chosen and both beams for each ratio were tested and compared.

In beams C2 (span = 1000mm), A1 (span = 1500mm) and C4 (span = 2250mm) all variables were kept the same except span. It can be seen from Figure 4.14 and Table 4.6 that the rotation capacity of these three beams reduces significantly as the span is increased. A similar trend is observed in the maximum concrete compressive strain, as recorded in Table 4.2. This important observation may be expressed in terms of a greater strain capacity existing in beams with higher strain gradients along the length of the beam. An alternative way of expressing this may be that crushing occurs in a beam where the compressive strain exceeds the strain at maximum stress over a limited length, which does not increase with span.

In beams C3, A1 and C5 the l/d ratio was increased by changing the effective depth (and to a lesser degree the span) while maintaining the same A_s/bd and x/d ratios. It can be seen in Figures 4.14, 4.15 and 4.16 that no clear relationship exists between ductility and either the span or the effective depth in these three beams. It is a pity that the rotation measurements in test C5 appear somewhat in doubt in terms of the comparison of theoretical and experimental elastic rotations in Table 4.5. In this test the l/d ratio was increased to 18 but the span was reduced to 1125mm. It therefore appears that the improved ductility achieved in tests C2, A1 and C4 as the span is reduced, is not so much a function of l/d as span itself. The maximum compressive strain achieved is influenced by both span and effective depth.

Figs. 4.17a, 4.17b and 4.18 indicate that there seems to be no clear relationship between the ratios span to height of stress block and span to effective depth with respect to rotation capacity. It is indicated subsequently that this

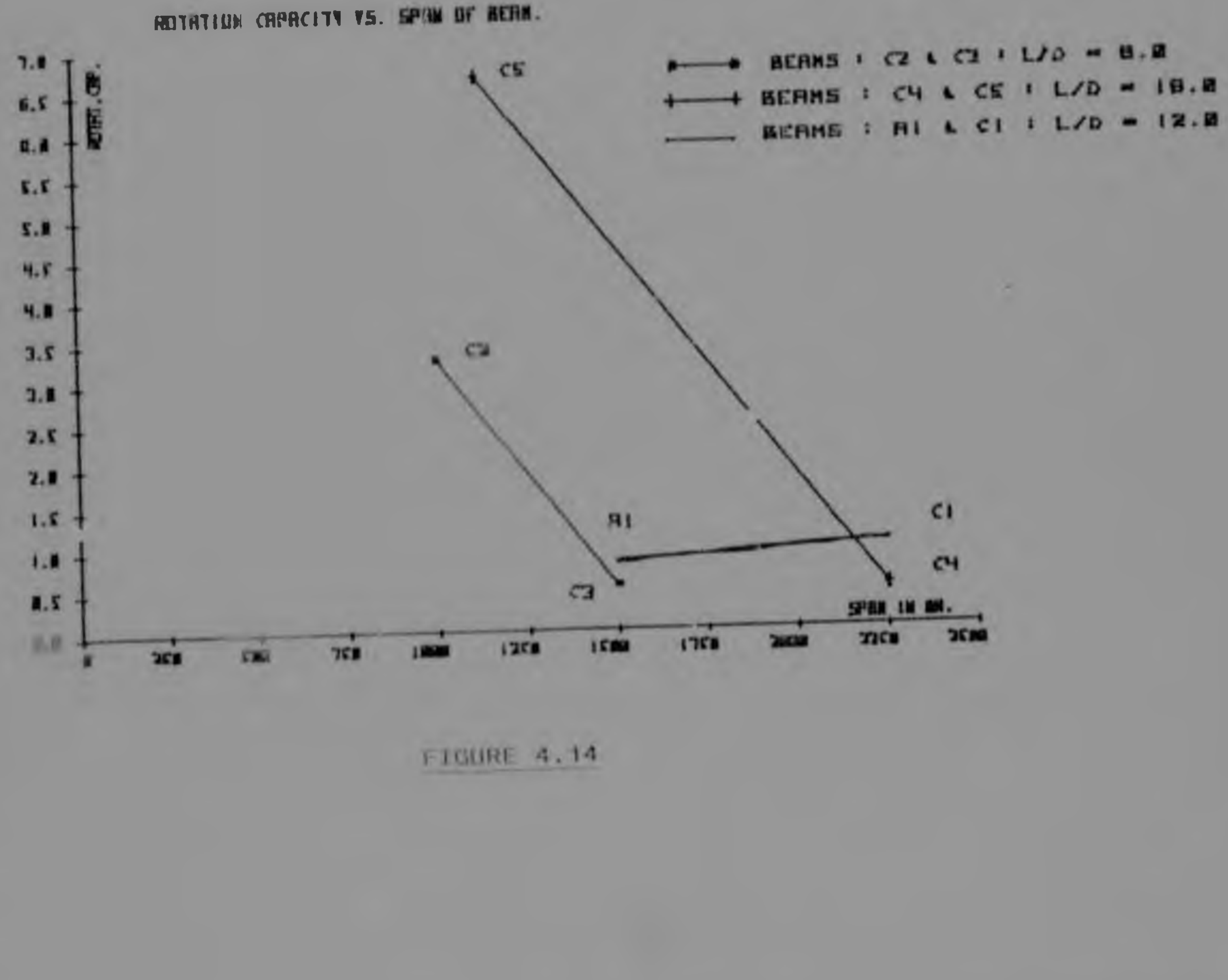
ROTATION CAPACITY VS. SPAN OF BEAM.
BEAMS : C2 & C3 : L/D = 8.0
BEAMS : C4 & C5 : L/D = 10.0
BEAMS : A1 & C1 : L/D = 12.0
ROTAT.CAP.
SPAN IN MM.
C5
C2
A1
C1
C4
C3

FIGURE 4.14


INELASTIC ROTATION FOR HALF SPAN VS. SPAN OF BEAM.
C5
C2
B1
C1
C4
C3
SPAN IN MM.

FIGURE 4.15

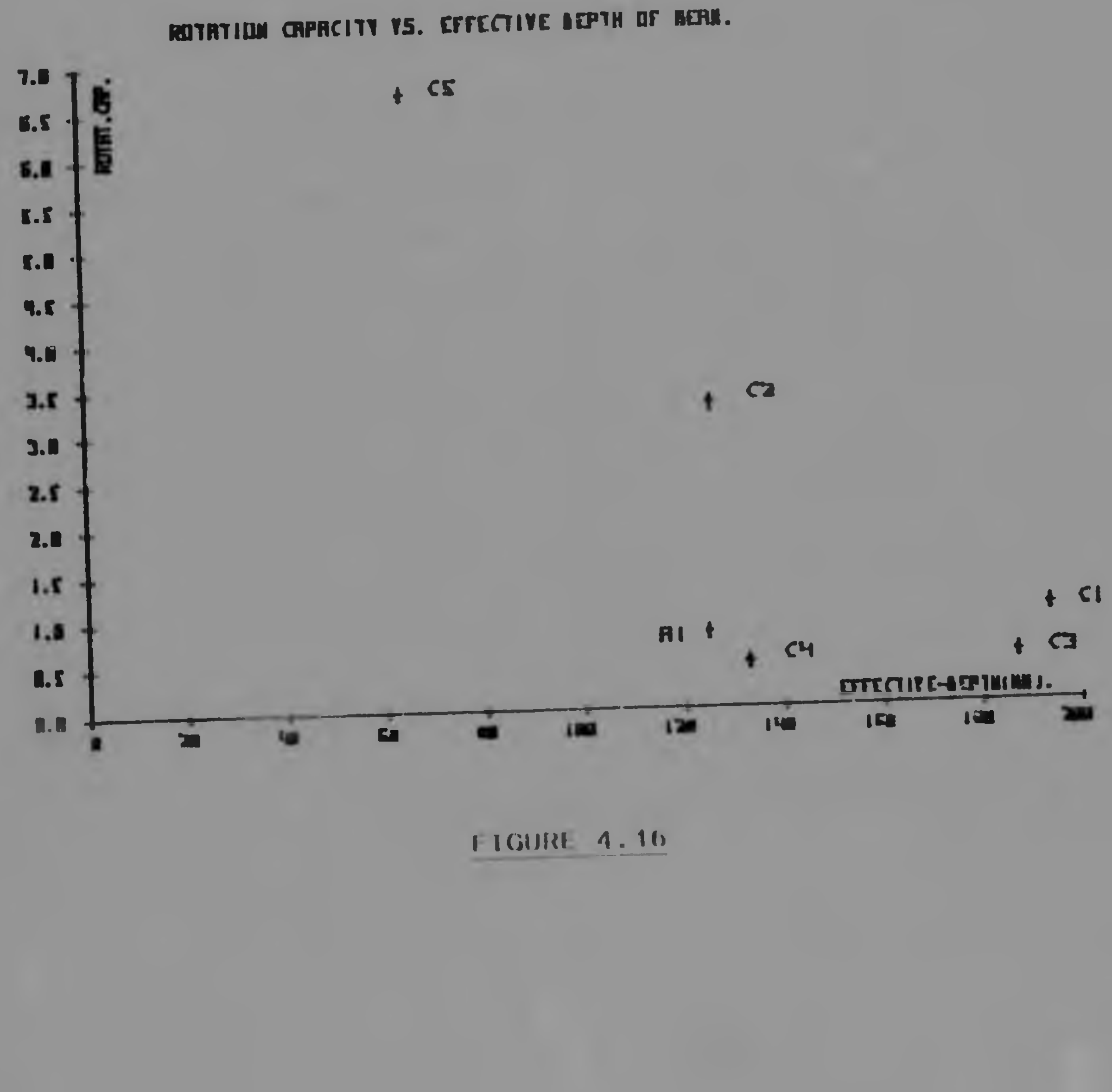
ROTATION CAPACITY VS. EFFECTIVE DEPTH OF BEAM.
ROTAT.CAP.
7.0
6.5
6.0
5.5
5.0
4.5
4.0
3.5
3.0
2.5
2.0
1.5
1.0
0.5
0.0
C5
C2
C1
A1
C4
C3
EFFECTIVE-DEPTH(MM).
0
20
40
60
80
100
120
140
160
180
200

FIGURE 4.16

ROTATION CAPACITY VS. SPAN / HEIGHT OF STRESS BLOCK.

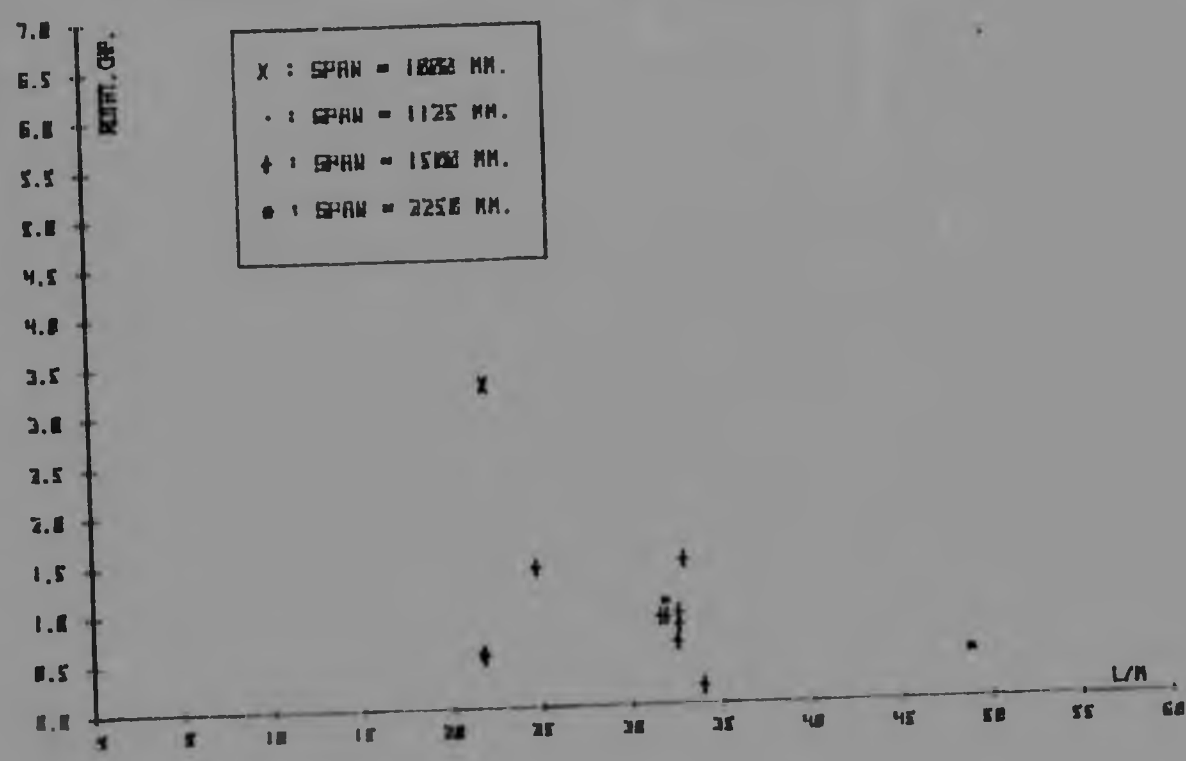

FIGURE 4.17a

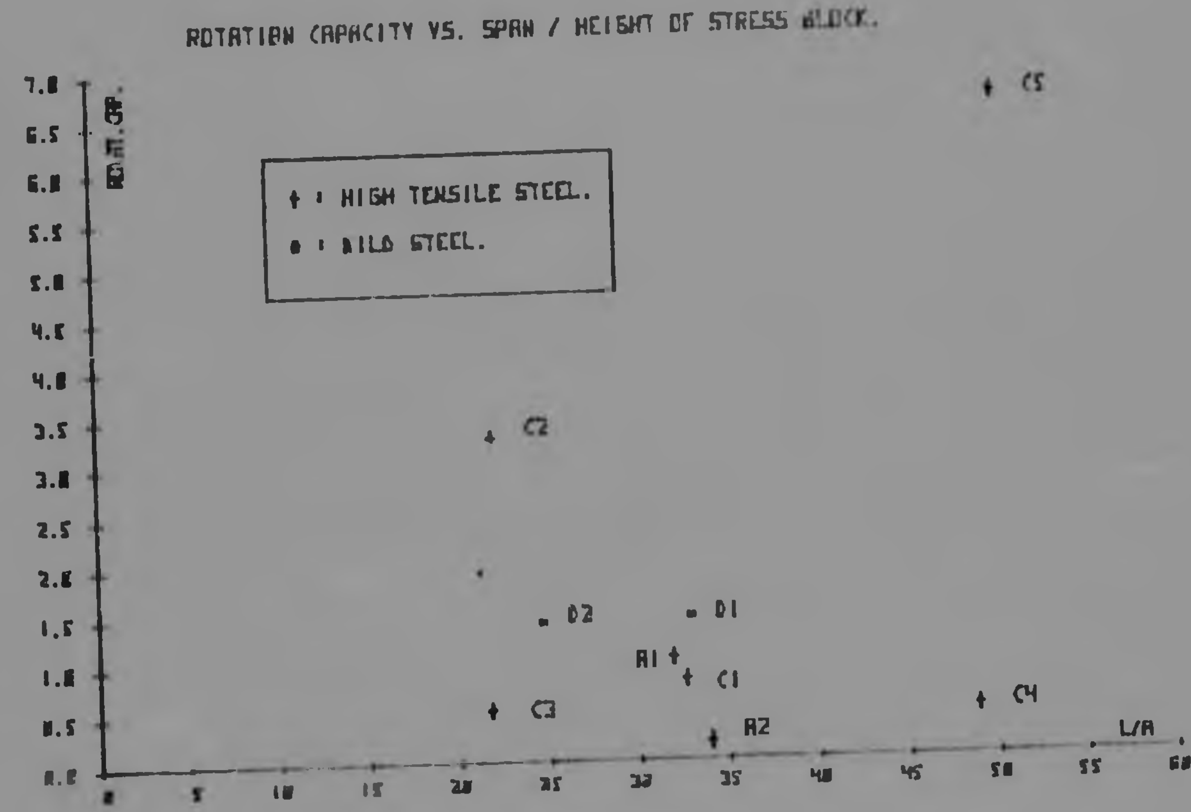
ROTATION CAPACITY VS. SPAN / HEIGHT OF STRESS BLOCK.
ROTAT.CAP.
+ : HIGH TENSILE STEEL.
• : MILD STEEL.
C5
C2
D2
D1
A1
C1
C3
A2
C4
L/A
7.0
6.5
6.0
5.5
5.0
4.5
4.0
3.5
3.0
2.5
2.0
1.5
1.0
0.5
0.0
0
5
10
15
20
25
30
35
40
45
50
55
60

FIGURE 4.17b

ROTATION CAPACITY VS. SPAN / EFFECTIVE DEPTH.

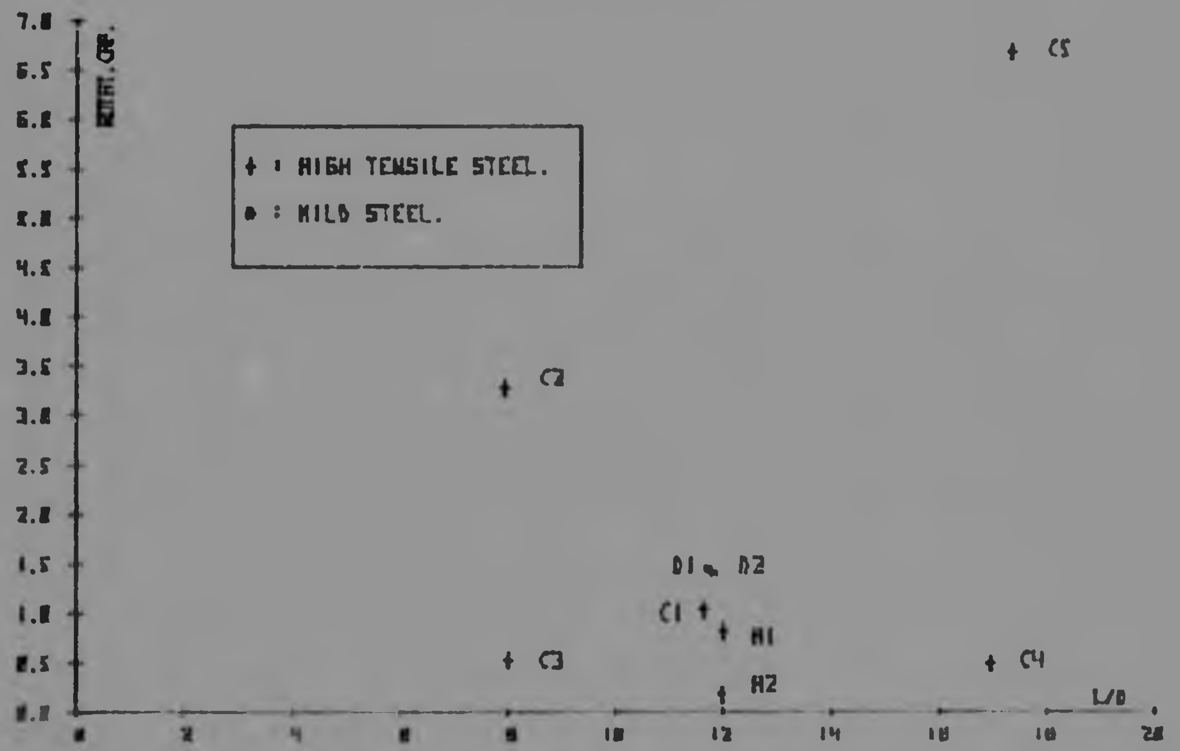

FIGURE 4.18

may be related to weaknesses caused when the depth of the stress block and cover to the binders are of similar dimensions (test C5).

Table 4.7 compares the experimental results of the spread of plasticity with the formula derived by Corley and Mattock (Eqn.2.21 in Chapter 2), and it appears that there is really no evidence that this formula can be regarded as a general expression. Apparently effective depth and span alone are not the only main parameters as can be seen in Figs. 4.19a and 4.19b.

4.5.4 Effect of Height and Stress Block

Figs. 4.20, 4.21a, and 4.21b show that the ratio height of stress block to effective depth give a scattered result with respect to inelastic rotation and rotation capacity, although ductility appears to increase as this ratio decreases.

CEB-FIP code has modelled a curve for the ratio neutral axis to effective depth-inelastic rotation, and this curve has been superimposed in Fig.4.22 which uses a ratio of height of stress block to effective depth. This slight change does not affect the results significantly, since the ratio of neutral axis depth to height of stress block is reasonably constant. It can be seen from Fig. 4.22 that the CEB-FIP relationship represents a fairly good lower boundary for the expected inelastic rotation. It should be noted that in Figs. 4.21 and 4.22 the highest rotation capacities were observed in beams C2 and C5 which were the shortest spans tested.

4.5.5 Effect of Binders and Width of Specimens

From Tables 4.5 and 4.6 it can be seen that by comparing a beam with no binders at all (B2), to a beam with minimal amount of binders according to CP110 code design (A1) and to a beam

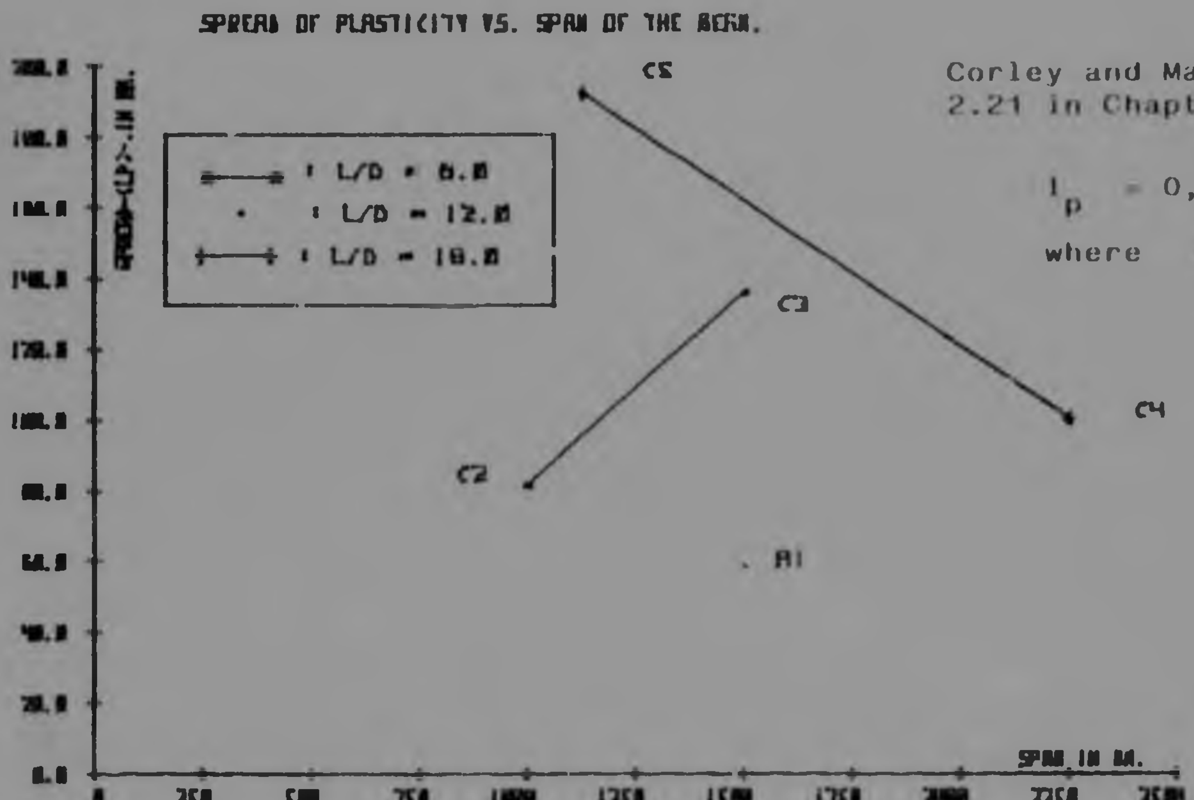

Corley and Mattocks's equation (Eqn. 2.21 in Chapter 2)

$$l_p = 0,05d + 0,05Z$$

where $Z = \frac{l}{2}$

FIGURE 4.19a

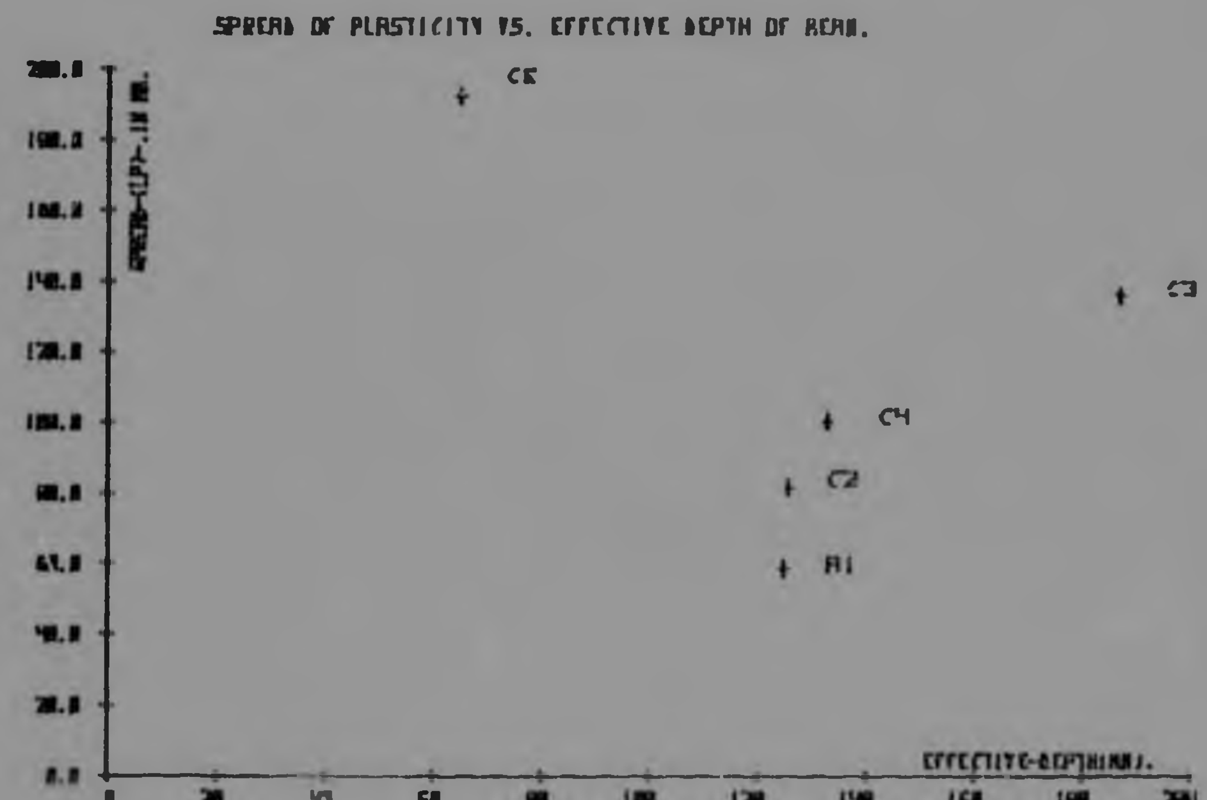

FIGURE 4.19b

INELASTIC ROTATION VS. HEIGHT OF STRESS BLOCK / EFFECTIVE DEPTH.

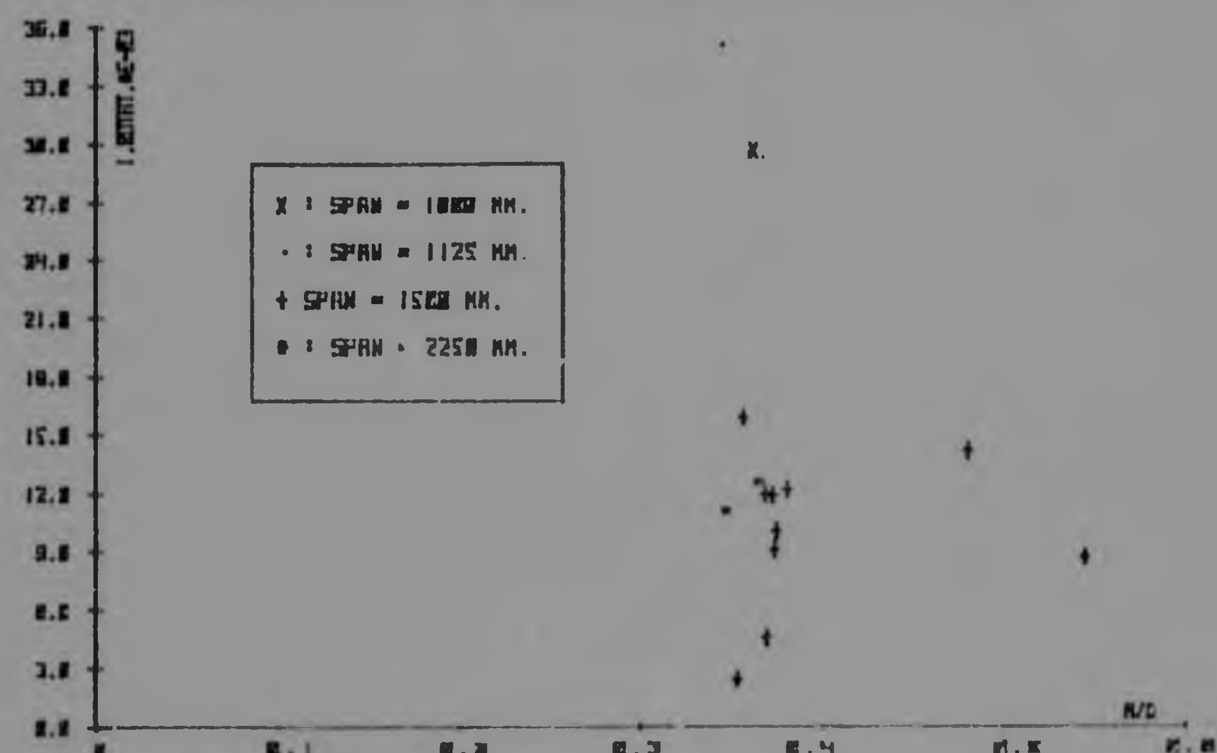

FIGURE 4.20

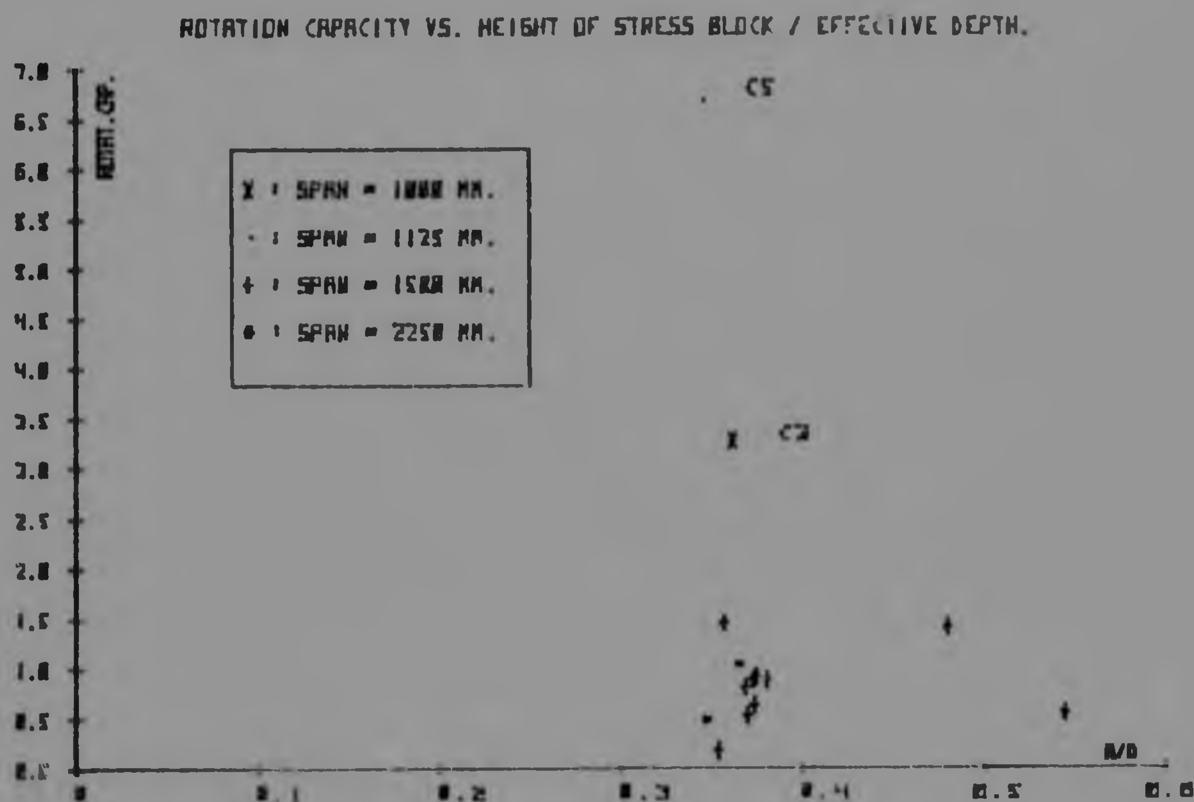
ROTATION CAPACITY VS. HEIGHT OF STRESS BLOCK / EFFECTIVE DEPTH.
ROTAT.CAP.
X : SPAN = 1000 MM.
· : SPAN = 1125 MM.
+ : SPAN = 1500 MM.
• : SPAN = 2250 MM.
C5
C3
A/D
7.0
6.5
6.0
5.5
5.0
4.5
4.0
3.5
3.0
2.5
2.0
1.5
1.0
0.5
0.0
0
0.1
0.2
0.3
0.4
0.5
0.6

FIGURE 4.21a

ROTATION CAPACITY VS. HEIGHT OF STRESS BLOCK / EFFECTIVE DEPTH.

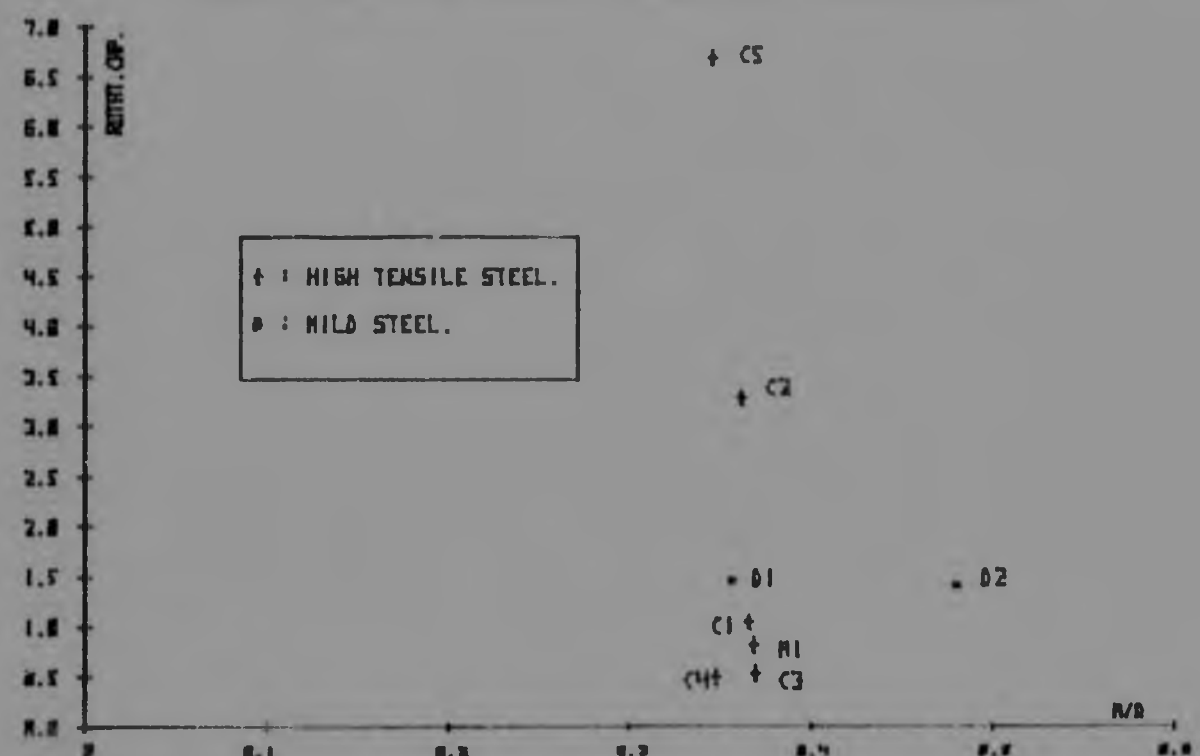

FIGURE 4.21b

INELASTIC ROTATION VS. HEIGHT OF STRESS BLOCK / EFFECTIVE DEPTH.

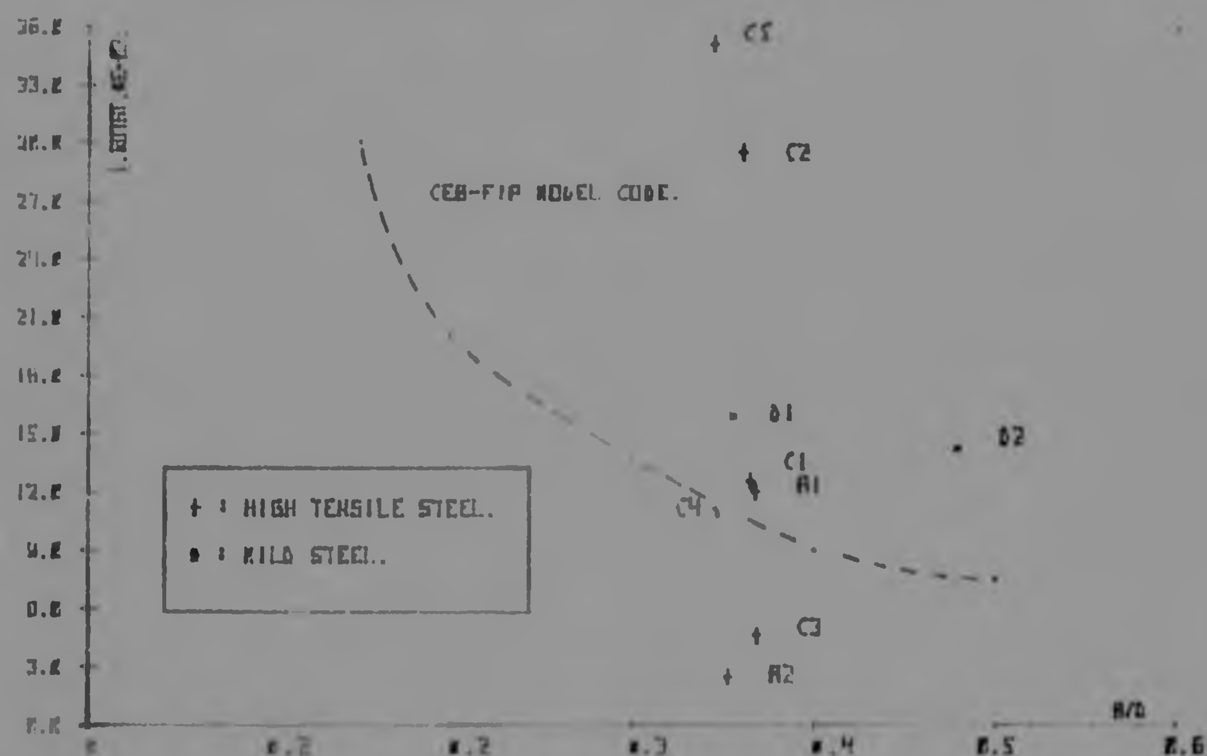

FIGURE 4.22

with twice the minimal amount of binders according to CP110 code design (B1), there is not very much difference in rotation capacity as a function of quantity of binders. More tests were needed with much closer links and with different diameters of steel to be able to establish a clear trend. Comparing beam A1 with minimal binders and beam B2 with no links, indicates that the maximum compressive strain of the concrete appears to be higher as links are used (Table 4.2).

Only two beams, B3 and B4 were tested so as to gain a feeling for the effect of width on rotation capacity. No clear trend emerged but it should be noted that the provision of binders in beam B3 did not influence the maximum compressive strain (Table 4.2) or the ductility (Tables 4.5 and 4.6) when compared to beam B4 without binders. This may imply that at the very low depths of compressive stress block which occur in wide beams with small percentages of reinforcement, links do not have a beneficial effect because the critical concrete in compression is largely located at the level of, or outside the concrete contained by the stirrups. It is of interest that unlike earlier tests by Corley[8] and Mattock[14], the significant influence of links on rotation capacity was not observed in these tests and that this could probably be ascribed to the fact that no compression reinforcement was provided in this series of tests.

4.5.6 Effect of Concrete Strength

One of the disconcerting results obtained in the tests was the reduction in rotation capacity from 0,81 in A1 and to 0,18 in test A2 in which the ratio of stress block height to effective depth was maintained effectively constant while the area of reinforcement and concrete strength were increased by 50%. This is contrary to established theory which would predict equal ductility in these two beams. It is recognized that one test is insufficient to draw firm conclusions but the extent of the reduction in both rotation capacity and maximum compressive strain (Table 4.2) certainly justifies a more detailed investigation of concrete strength.

CHAPTER 5

CONCLUSIONS

5.1 Experimental Review

The purpose of the tests performed was to investigate the behaviour of some variables affecting rotation capacity, the main variables are :

(i) Effect of type of tension reinforcement;
(ii) Effect of span;
(iii) Effect of binders and width of specimens.

It is recognized that within the scope of a six-month project, it is not possible to provide firm conclusions on the influence of each of these variables. The intention was rather to provide a survey of the relative importance of each of these effects which are not considered in design codes.

5.2 Test Results

The maximum concrete compressive strain at a section of maximum moment may be well over values assumed by various design codes. Consequently, the ultimate curvature and plastic rotation also can be much greater than that calculated on the assumed value of maximum concrete compressive strain specified by codes.

In this investigation, Corley's and Mattock's equation for maximum concrete compressive strain (Eqn. 2.2) seemed to be too optimistic, while the CEB-FIP expression (Eqn. 4.4) and the theoretical program's values were definitely too conservative; also the low value of 0,003 established by the ACI code is too conservative. A precise formula to assess a true value of the maximum concrete compressive strain may be difficult to establish since this parameter is a function of several variables including : concrete strength, stress-strain characteristics of the concrete, tensile steel strength and its strain-hardening properties, amount of tension and compression reinforcement, rate of loading and other important parameters such as span and influence of binders. It appears from Table 4.2 that Corley and Mattock's formula is most in error in predicting the effect of concrete strength and stress block depth.

An increase in the tension steel content $A_s f_y / f_c bd$ will increase the strength of the section of a member but decreases the flexural ductility as measured by the rotation capacity and maximum compressive strain of the member. Beams reinforced with mild steel bars display higher inelastic rotations than beams with high tensile steel for the same tension steel content as measured by $A_s f_y / f_c bd$.

The experimental and theoretical values of the ductility ratio (Table 4.6) are very different and this is caused by the high maximum concrete compressive strains observed in the tests compared to the theoretical values assumed by various codes or obtained from the theoretical moment-curvature relationships. One possible explanation could be local bond failure in the cracked region resulting in a non-linear strain distribution through the depth as illustrated in Figure 4.5 and reflecting the differences in the moment-curvature relationships in Appendix 3.

Rotation capacity appears to be a function of span rather than span to depth ratio, or span to height of stress block or span to effective depth. This is an important result of the tests and is related to the influence of strain gradient along the span on the maximum concrete compression strain. It appears that maximum compressive strain in the concrete is inversely proportional to span and influenced by the depth of the stress block.

The ductility of a section may be expressed either in terms of the ratio of ultimate curvature to curvature at first yield of the reinforcement or as a function of the ratio of neutral axis depth to effective depth. It was found that the CEB-FIP's model code for the ratio neutral axis to effective depth vs. inelastic rotation represents a fairly good lower boundary for the expected inelastic rotations. It should be adjusted to allow for the influence of span.

Corley's and Mattock's expression for spread of plasticity (l_p) (Eqn.2.21 in Chapter 2) appears not to be an effective formula to be regarded as a general expression. Apparently effective depth and span alone are not the only variables affecting the spread of plasticity.

Although shear reinforcement must be adequate to ensure that the strength in shear exceeds the strength in flexure, binders alone, without compression reinforcement, seem not to have an effective beneficial effect on rotation capacity especially for wide beams since the compressive stress block for these beams are small, and therefore the critical concrete in compression is mainly located at or above the level of the concrete contained by the stirrups. Most reinforced concrete beams contain some compression reinforcement even when not needed, mainly because of construction or code requirements, so that the available ductility and rotational capacity is increased. This does not apply to slabs but width of concrete will compensate in this case. A disconcerting result was the substantial drop in both ductility and maximum concrete compressive strain in a test in which both areas of reinforcement and concrete strength were increased by 50% while maintaining the same ratio of stress block depth to effective depth. This requires further investigation.

5.3 Further areas of research

Lateral reinforcement helps to prevent premature shear failure. It would be of great advantage to analyze the influence of shear on rotation capacity since it is felt that the total amount of rotation is a function of the shearing stresses in the member. If the shear is large enough for inclined cracks to occur the inelastic rotations may be fairly large, provided stirrups prevent a shear failure, because greater concrete compressive strains can develop, and also because steel can yield at several sections displaying a larger yielded zone. If, on the other hand, the shear is so small that inclined cracks do not occur, the yield stress of steel may be only reached at the crack at the point of maximum moment and the inelastic rotation will be smaller.

Another interesting area of study would be that of the ratio width to effective depth of a member, because differences in behaviour between broad (slab) type sections and narrow (beam) type sections may be established and used to confirm or extend other conclusions.

This would also assist in establishing the influence of stress-block height on maximum concrete compressive strain.

LIST OF REFERENCES

1. Comité Euro-International du Be'ton; CEB-FIP model code for concrete structures, 1978, p.94.

2. British Standards Institution; 'The Structural use of concrete", CP110 : Part 1: 1982, p.19.

3. Cohn, M.Z. and Ghosh, S.K., "The flexural ductility of reinforced concrete sections", International Association for Bridge and Structural Engineering, (IABSE), Vol. 32-11, 1972, pp.53-82.

4. ACI Committee 318, "Building Code Requirements for Reinforced Concrete", (ACI 318-77), American Concrete Institute, Detroit, 1977, pp. 33-38.

5. Base, G.B. and Read, J.B., "Effectiveness of helical binding in the compression zone of concrete beams", Journal ACI, Vol. 62, No.7, July 1965, pp. 763-781.

6. Chandrasekhar, C.S., and Falkner, H.A., "Influence of the width of loading plate on the rotation capacity of reinforced concrete members", Journal ACI, Proceedings, Vol.71 No.6, June 1974, pp.49-54.

7. Burnett, E.,"Flexural rigidity, curvature and rotation and their significance in reinforced concrete design", Magazine of Concrete Research, June 1954, pp. 67-72.

8. Corley, W.G. "Rotation capacity of reinforced concrete beams", Journal of Structural Division, American Society of Civil Engineers, (ASCE), Vol. 92, ST5, October 1966, pp. 121-144.

9. Mattock, A.H. "Discussion of rotational capacity of reinforced concrete beams by Corley, W.G.", Journal of Structural Division, ASCE, Vol.93 ST2, April 1967, pp. 519-522.

10. Clements, S.W., Cranston, W.B. and Symons, M.G., "The influence of section breadth on rotation

LIST OF REFERENCES (CONT')

capacity", Cement and Concrete Association, Technical Report 553, September 1980, pp.1-27.

11. SABS 920, Standard Specification for Steel Bars for Concrete Reinforcement, Pretoria, Council of the South African Bureau of Standards, 1969, pp.7-8.

12. Baker, A.L.L., "Limit-state design of reinforced concrete", London, Cement and Concrete Association, 1970, p.20.

13. Kemp, A.R., "Ductility and moment redistribution in reinforced concrete beams", The Civil Engineer in South Africa, May 1981, pp. 175-181.

14. Mattock, A.H., "Rotational capacity of hinging regions in reinforced concrete beams", Proceedings of the International Symposium on the Flexural Mechanics of Reinforced Concrete, ASCE-ACI, Miami, 1965, pp. 143-180.

BIBLIOGRAPHY

1. ACI Committee 318C, Commentary of Building Code requirements for reinforced concrete, ACI 318C, American Concrete Institute, Detroit, 1977.

2. Burnett, E.F.P. and Yu, C.W., "Reinforced concrete linear structures at ultimate load", Proceedings of the International Symposium on the Flexural Mechanics of Reinforced Concrete, ASCE-ACI, Miami, 1965, pp. 29-47.

3. Chan, W.W.L.,"The rotation of reinforced concrete plastic hinges at ultimate load", Magazine of Concrete Research, London, Vol. 14, No.41, July 1982, pp. 63-72.

4. Cohn, M.Z., and Petcu, V.A., "Moment redistribution and rotation capacity of plastic hinges in redundant reinforced concrete beams", Indian Concrete Journal, Vol.37, No.8, Bombay, August 1963, pp. 282-290.

5. Fintel, M., "Handbook of concrete engineering", Van Nostrand Binhold Company, New York, 1974.

6. Kemp, A.R., "Ductility and moment redistribution in reinforced concrete beams", The Civil Engineer in South Africa, May 1981, pp. 175-181.

7. Kong, F.K., Evans, R.H., Cohen, E., and Roll, F., "Handbook of structural concrete", Pitman Advanced Publishing Program, 1983.

8. Mattock, A.H., "Rotational capacity of hinging regions in reinforced concrete beams", Proceedings of the International Symposium on the Flexural Mechanics of Reinforced Concrete, ASCE-ACI, Miami, 1965, pp. 143-180.

BIBLIOGRAPHY

1. ACI Committee 318C, Commentary of Building Code requirements for reinforced concrete, ACI 318C, American Concrete Institute, Detroit, 1977.

2. Burnett, E.F.P. and Yu, C.W., "Reinforced concrete linear structures at ultimate load", Proceedings of the International Symposium on the Flexural Mechanics of Reinforced Concrete, ASCE-ACI, Miami, 1965, pp. 29-47.

3. Chan, W.W.L.,"The rotation of reinforced concrete plastic hinges at ultimate load", Magazine of Concrete Research, London, Vol. 14, No.41, July 1982, pp. 63-72.

4. Cohn, M.Z., and Petcu, V.A., "Moment redistribution and rotation capacity of plastic hinges in redundant reinforced concrete beams", Indian Concrete Journal, Vol.37, No.8, Bombay, August 1963, pp. 282-290.

5. Fintel, M., "Handbook of concrete engineering", Van Nostrand Binhold Company, New York, 1974.

6. Kemp, A.R., "Ductility and moment redistribution in reinforced concrete beams", The Civil Engineer in South Africa, May 1981, pp. 175-181.

7. Kong, F.K., Evans, R.H., Cohen, E., and Roll, F., "Handbook of structural concrete", Pitman Advanced Publishing Program, 1983.

8. Mattock, A.H., "Rotational capacity of hinging regions in reinforced concrete beams", Proceedings of the International Symposium on the Flexural Mechanics of Reinforced Concrete, ASCE-ACI, Miami, 1965, pp. 143-180.

BIBLIOGRAPHY (CONT')

9. Park, R., and Paulay, T., "Reinforced concrete structures", Canada, Wiley-Interscience Publication, 1975, Chapter 6.

10. Regan, P.E., "Limit-state design of structural concrete, London, Chatto and Windus Ltd., 1973.

11. Roy, H.E.H. and Dozen, M.A., "Ductility of concrete", Proceedings of the International Symposium on the Flexural Mechanics of Reinforced Concrete, Miami, November 1964, pp. 213-224.

APPENDIX 1

UNIVERSITY OF THE WITWATERSRAND

MATERIALS LABORATORY

TRIAL MIX DESIGN SHEET

MIX FOR Roberto Donoso JOB Thesis

Cement Ordinary Portland Cement DATE 23-November-1983.

14th day Compressive strenth of 31.2Mpa.

Sand 1) Granite R D 2.65 F M 3.5 C B D 1520 L B D 1520

2) ____ ____ ____ ____ ____

Stone 1) Quartzite ~~(13mm)~~ R D 2.7 F M ____ C B D ____ L B D ____

2) ____ ____ ____ ____ ____

Mix proportions per m³

	CALCULATED	USED		
C/W	1.84	1.8		
Water	215 lts.	225 lts.		
Cement	396 kg.	405 kg.		
Stone	838 kg.	840 kg.		
Sand	925 kg.	890 kg.		

LABORATORY MIX (0.135 m³)

Water		30.38 lts.		
Cement		54.68 kg..		
Stone		113.40 kg		
Sand		120.15 kg.		
Slump				

UNIVERSITY OF THE WITWATERSRAND

DEPARTMENT OF CIVIL ENGINEERING - MATERIALS LABORATORY

AGGREGATE GRADING ANALYSIS

DATE: 23-November-83

PROJECT :Rotation Capacity of Reinforced Concrete Beams.

SAMPLE NO. ______________ DESCRIPTION ______________

COARSE MECHANICAL ANALYSIS (STONE)

	TOTAL MASS OF SAMPLE = g				
Size mm	Mass Retained g	% Retained	% Passing	CUMULATIVE % Retained	CUMULATIVE % Passing
75					
37,5					
19					
9,5					
4,75					
PAN					
TOTALS					

FINE MECHANICAL ANALYSIS (SAND)

WEATHERED GRANITE.

	TOTAL MASS OF SAMPLE = 999.40 g.					
Sieve No.	Size mm	Mass Retained g	% Retained	%Passing	CUMULATIVE %Retained	CUMULATIVE %Passing
3½	4,75	134.30	13.44		13.44	86.56
7	2,36	209.70	20.98		34.42	65.58
14	1,18	280.70	28.09		62.51	37.49
25	0,600	197.80	19.79		82.30	17.70
52	0,300	92.80	9.29		91.59	8.41
100	0,150	41.30	4.13		95.72	4.28
200	0,075	17.50	1.75			2.53
PAN M1		23.30	2.53			
	TOTALS	999.40	100.00		379.98	

UNIVERSITY OF THE WITWATERSRAND

DEPARTMENT OF CIVIL ENGINEERING – MATERIALS LABORATORY

AGGREGATE GRADING ANALYSIS

DATE 23-NOV-1984

PROJECT THESIS: ROTATION CAPACITY OF REINFORCED CONCRETE BEAMS SAMPLE No WEATHERED GRANITE. DESCRIPTION:

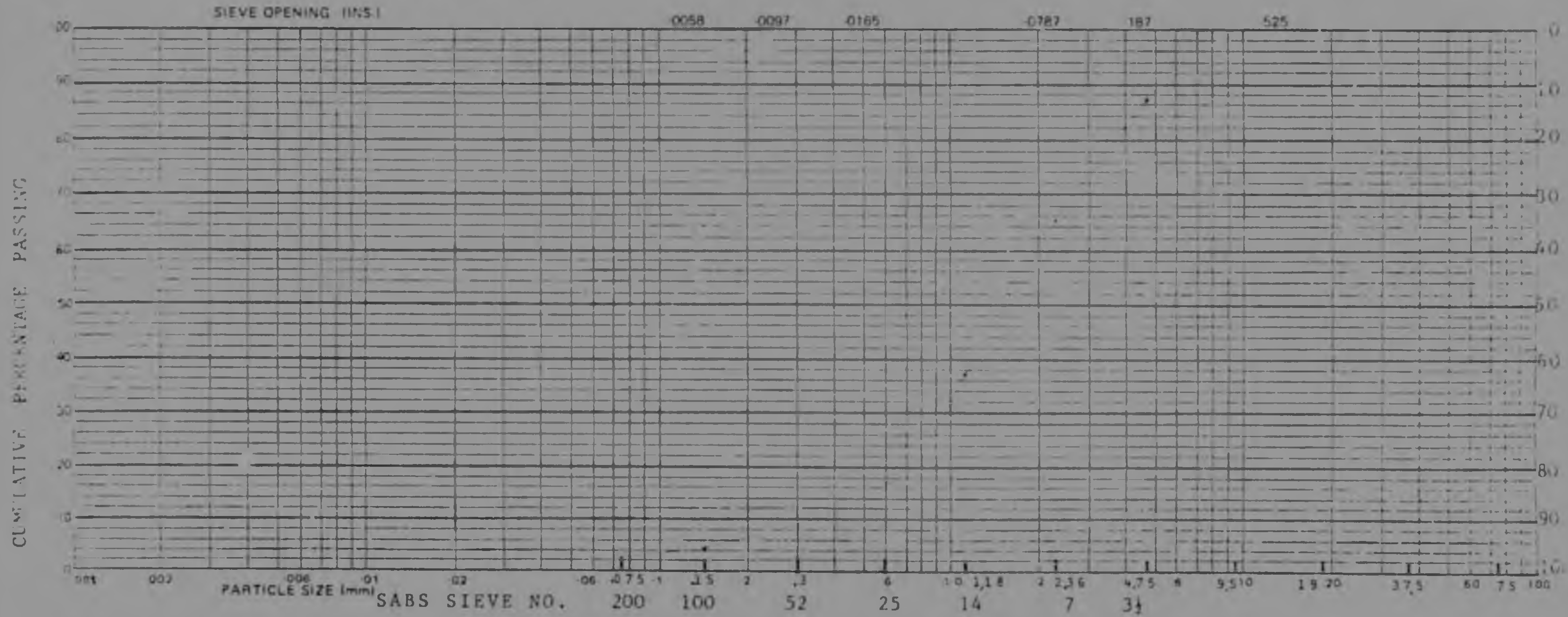

	FINE	MEDIUM	COARSE	FINE	MEDIUM	COARSE ✓	
CLAY	SILT FRACTION			SAND FRACTION ✓			STONE FRACTION

RELATIVE DENSITY OF SAND

SIEVE 200mm

2.4.1 Density - bottle method

W1 = density bottle weighted while dig.

W2 = sand plus bottle

W3 = sand plus bottle + de-aired distilled water

W4 = bottle + de-aired distilled water

$$Gs = \frac{W2 - W1}{(W4-W1)-(W3-W2)}$$

Gs = SPECIFIC GRAVITY

	1st	2nd	3rd	4th
W1	30,513	30,153	31,378	31,701
W2	42,747	40,681	40,835	41,595
W3	287,127	285,706	285,113	285,817
W4	279,619	279,218	279,362	279,884
Gs	2,5886	2,6059	2,5518	2,4978

$Gs_{av.} = 2,561$

BEAM	CONCRETE TESTS AT 7 DAYS			CONCRETE TESTS AT 14 DAYS						CONCRETE TESTS AT 28 DAYS		
	CYLINDER STRENGTH			CYLINDER STRENGTH			CUBE STRENGTH			CYLINDER STRENGTH		
	No.of Tests	f'_c (MPa)	Coeff.of Varn.(%)	No.of Tests	f'_c (MPa)	Coeff. of Varn.(%)	No.of Tests	f_{cu} (MPa)	Coeff.of Varn.(%)	No.of Tests	f'_c (MPa)	Coeff.of Varn.(%)
A1	5	19,071	5,36	5	23,942	6,56	3	29,78	3,90	5	27,316	8,92
B1	5	17,93	7,06	5	22,28	12,87	3	30,53	21,65	5	27,28	11,07
B2	5	15,89	4,29	5	20,03	4,56	3	25,51	5,87	5	25,78	12,01
B3	5	17,40	6,80	5	20,94	4,13	3	27,23	2,52	5	24,71	6,22
B4	4	15,86	6,14	5	21,21	8,84	3	27,44	1,51	5	24,54	5,07
C1	5	16,08	5,90	5	21,23	8,95	3	25,95	3,97	5	24,92	9,12
C2	5	18,65	4,31	5	25,51	5,94	3	31,03	3,53	5	30,00	8,26
C3	5	15,33	11,15	5	20,56	3,56	3	26,29	6,35	5	27,50	12,50
C4	5	17,06	7,65	5	19,52	9,70	3	27,48	2,24	5	28,26	7,40
C5	5	15,26	4,88	5	20,38	9,59	3	27,59	4,29	5	23,83	7,22
D1	5	13,09	1,73	5	19,67	11,99	3	24,60	1,98	5	26,41	2,22
D2	5	16,16	4,35	5	23,07	14,10	3	29,88	1,36	5	23,95	6,82
D3	5	15,99	8,56	5	22,23	9,51	3	26,09	8,47	5	25,99	15,39
Ex*	5	18,44	5,99	5	22,35	10,30	3	26,01	7,00	5	26,69	5,90
MEAN		16,587			21,64			27,53			26,227	
S.DEVIATION		1,616			1,713			2,02			1,767	
Coeff.of Varn.(%)		9,7			7,9			7,3			6,7	

* EXTRA CYLINDERS AND CUBES

TABLE 1 :STRENGTH OF CONCRETE FOR BEAMS TESTED AT 14 DAYS

		CONCRETE TESTS FOR DIFFERENT DAYS				
		14 DAYS	28 DAYS	42 DAYS	57 DAYS	59 DAYS
CYLINDER STRENGTH	No.of Tests	3	3	3	2	3
	f'_c (MPa)	21,77	28,78	32,08	32,485	33,78
	Coeff of Varn. (%)	2,36	1,64	8,97	8,42	8,39
CUBE STRENGTH	No. of Tests	-	-	-	-	3
	f_{cu} (MPa)	-	-	-	-	42,36
	Coeff.of Varn. (%)	-	-	-	-	2,79

TABLE 2 : STRENGTH OF CONCRETE FOR BEAM A2 TESTED AT 59 DAYS

		CONCRETE TESTS FOR DIFFERENT DAYS				
		14 DAYS	28 DAYS	42 DAYS	57 DAYS	59 DAYS
CYLINDER STRENGTH	No.of Tests	3	3	3	2	3
	f'_c (MPa)	21,77	28,78	32,08	32,485	33,78
	Coeff.of Varn. (%)	2,36	1,64	8,97	8,42	8,39
CUBE STRENGTH	No. of Tests	-	-	-	-	3
	f_{cu} (MPa)	-	-	-	-	42,36
	Coeff.of Varn. (%)	-	-	-	-	2,79

TABLE 2 : STRENGTH OF CONCRETE FOR BEAM A2 TESTED AT 59 DAYS

APPENDIX 2

STRESS - STRAIN CURVE FOR THE TRANSVERSE REINFORCEMENT USED IN ALL LINKS

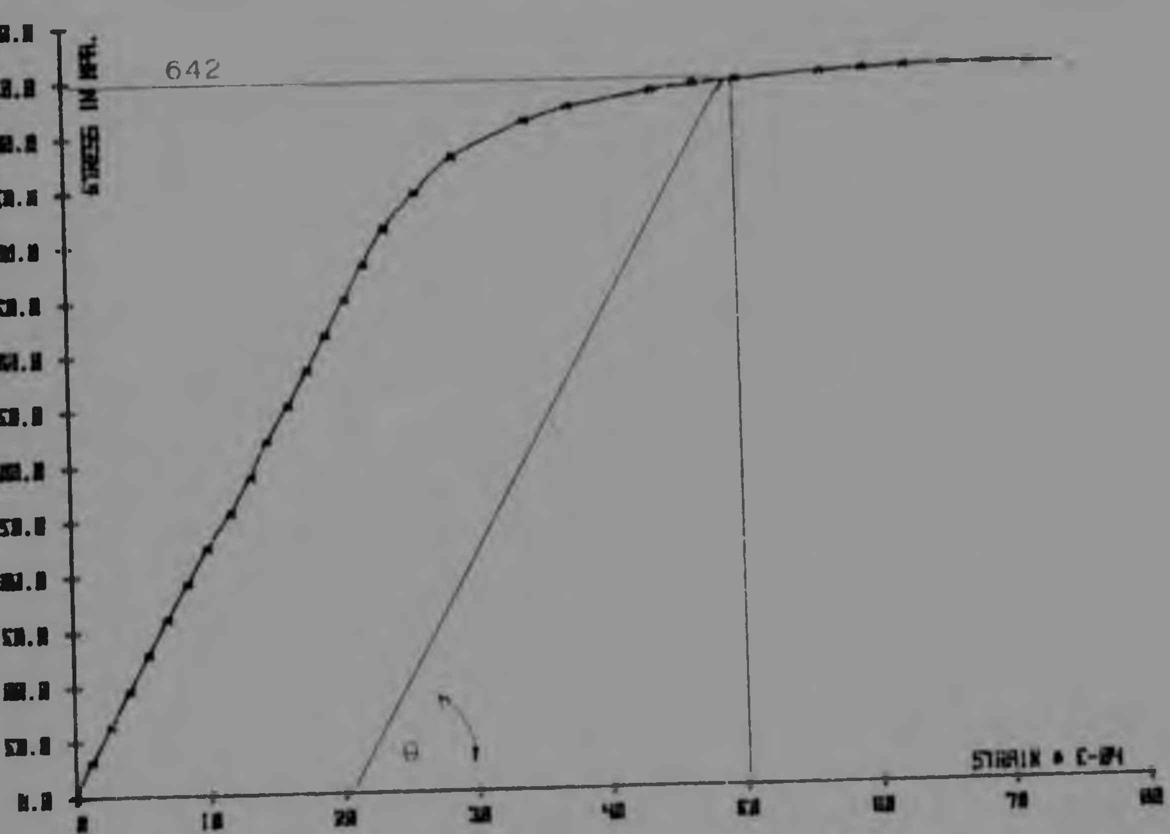

$f_y = 642$ $\qquad E_s = \dfrac{642}{30 \times 10^{-4}} = 193\,\text{GPa}$

STRESS - STRAIN CURVE FOR A STEEL BAR Y10 USED IN BEAM A1

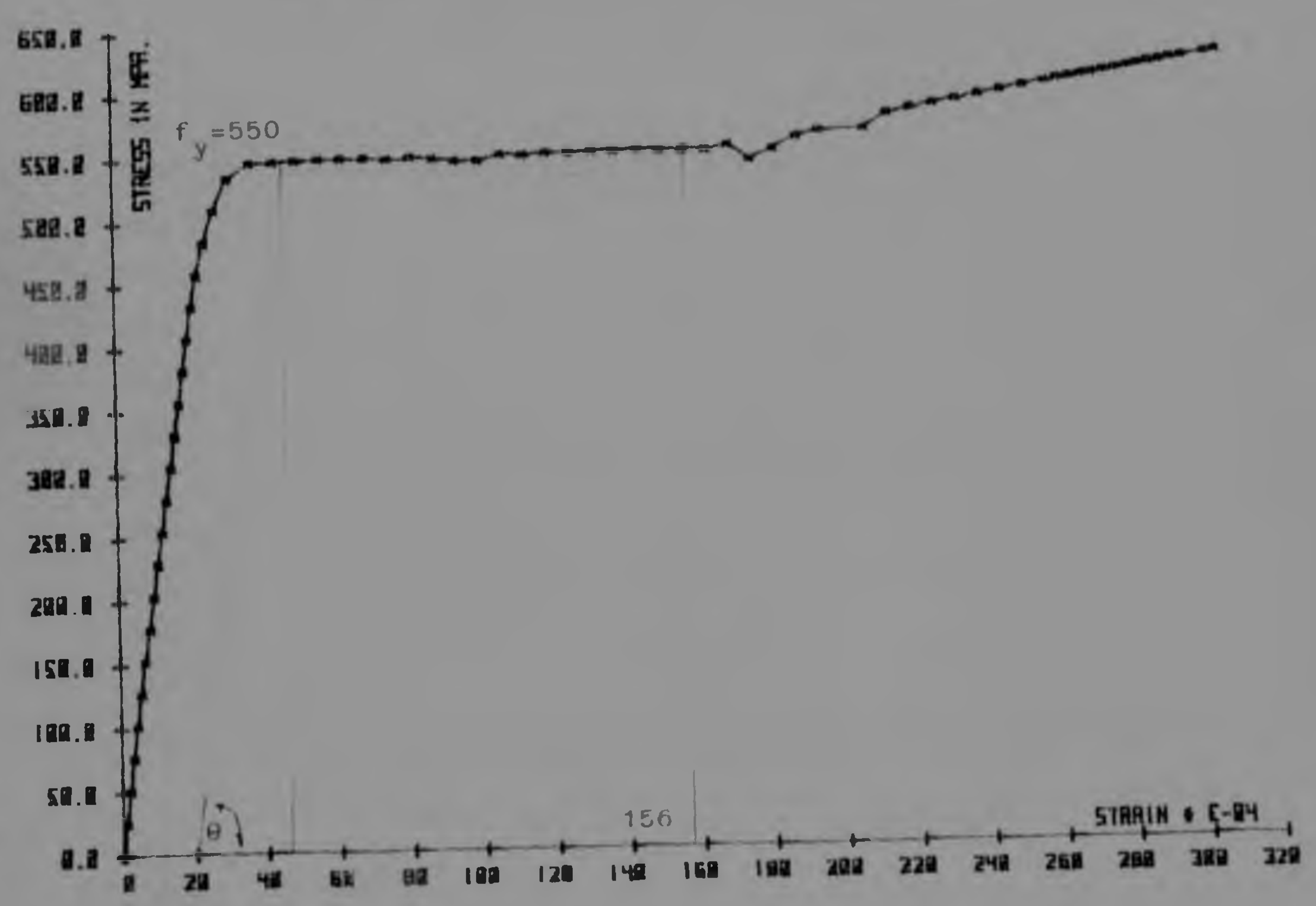

E's=4480

0,2%

$f_y = 550MPa$

$Es = \tan \theta = \frac{550}{26 \times 10^{-4}} = 211,5GPa$

STRESS - STRAIN CURVE FOR A STEEL BAR Y10 USED IN BEAM A2

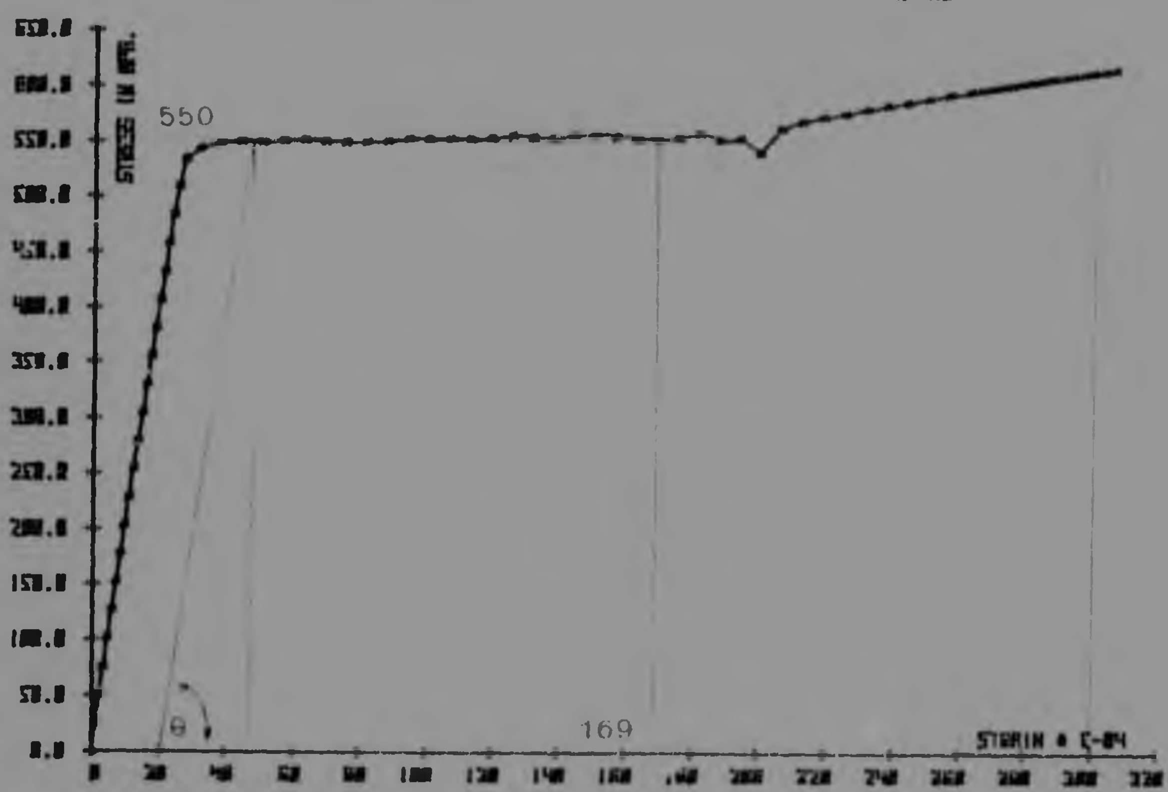

E's = 4552

$f_y = 550 \qquad Es = \tan\theta = \frac{550}{27{,}06 \times 10^{-4}} = 203GPa$

STRESS - STRAIN CURVE FOR A STEEL BAR Y13 USED IN BEAM A2

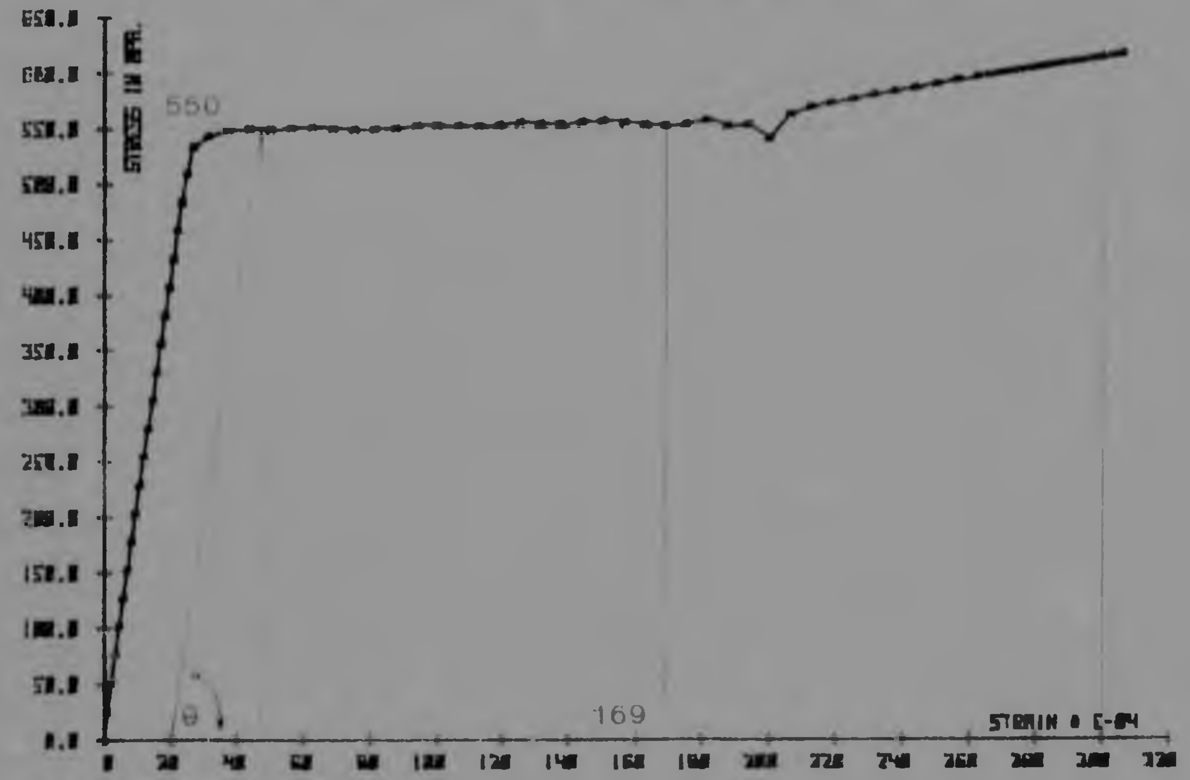

E's = 4552

$f_y = 550$ $\qquad$ $Es = \text{Tan}\,\theta = \dfrac{550}{27{,}06 \times 10^{-4}} = 203\text{GPa}$

STRESS - STRAIN CURVE FOR A STEEL BAR Y10 IN BEAM B1

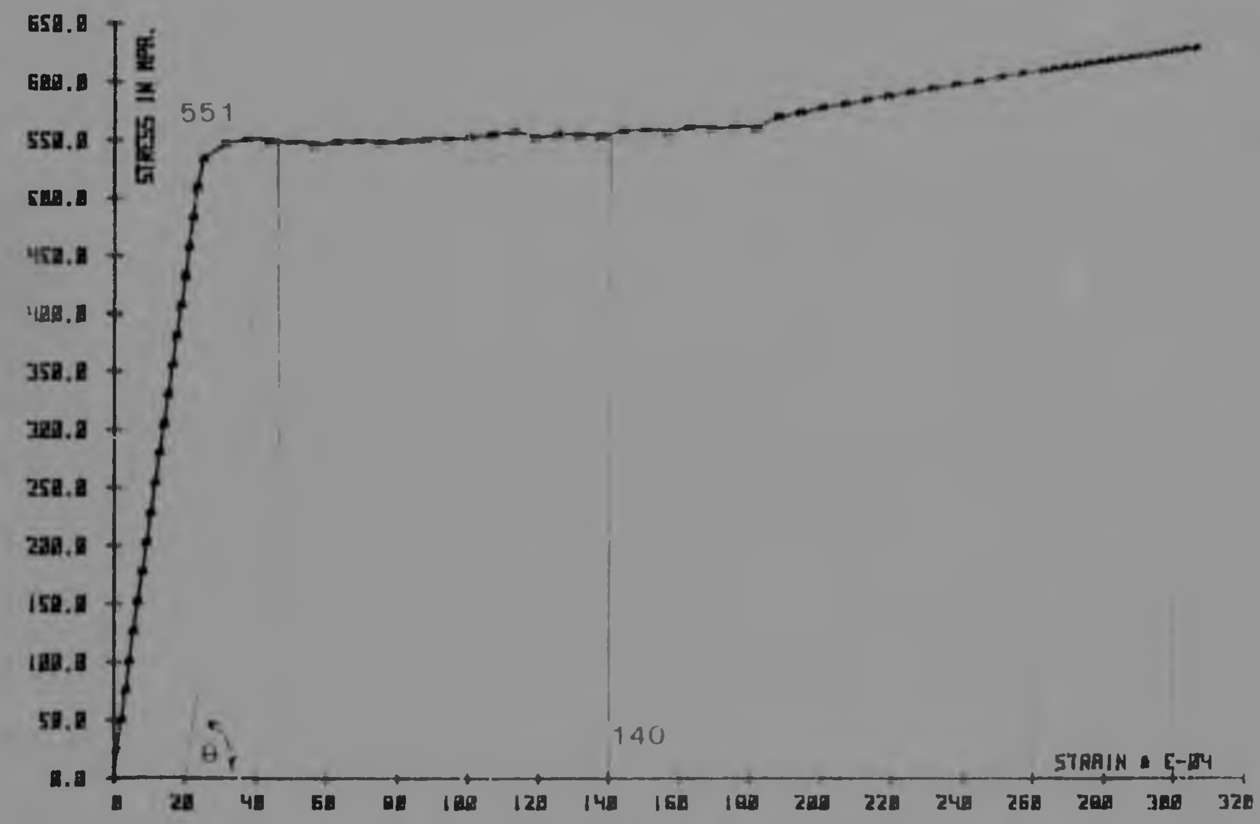

$f_y = 551MPa$ $\quad Es = \tan\theta = \dfrac{551}{26,49 \times 10^{-4}} = 208GPa$

STRESS - STRAIN CURVE FOR A STEEL BAR Y10 USED IN BEAM B2

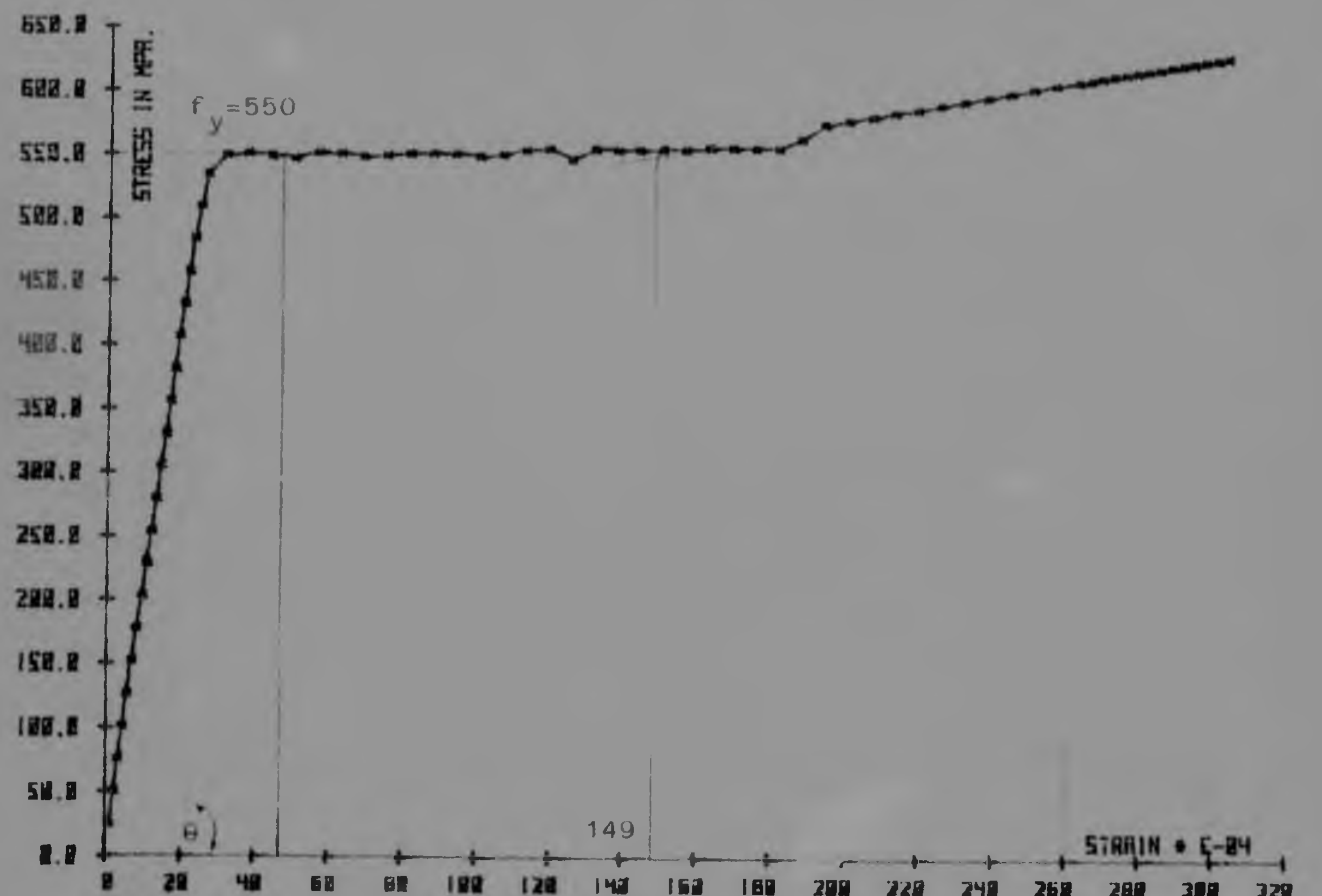

E's=4616

0,2%

f_y = 550MPa

$$Es = \tan\theta = \frac{550}{27,0\times 10^{-4}} = 203,7GPa$$

STRESS - STRAIN CURVE FOR A STEEL BAR Y10 IN BEAM B3

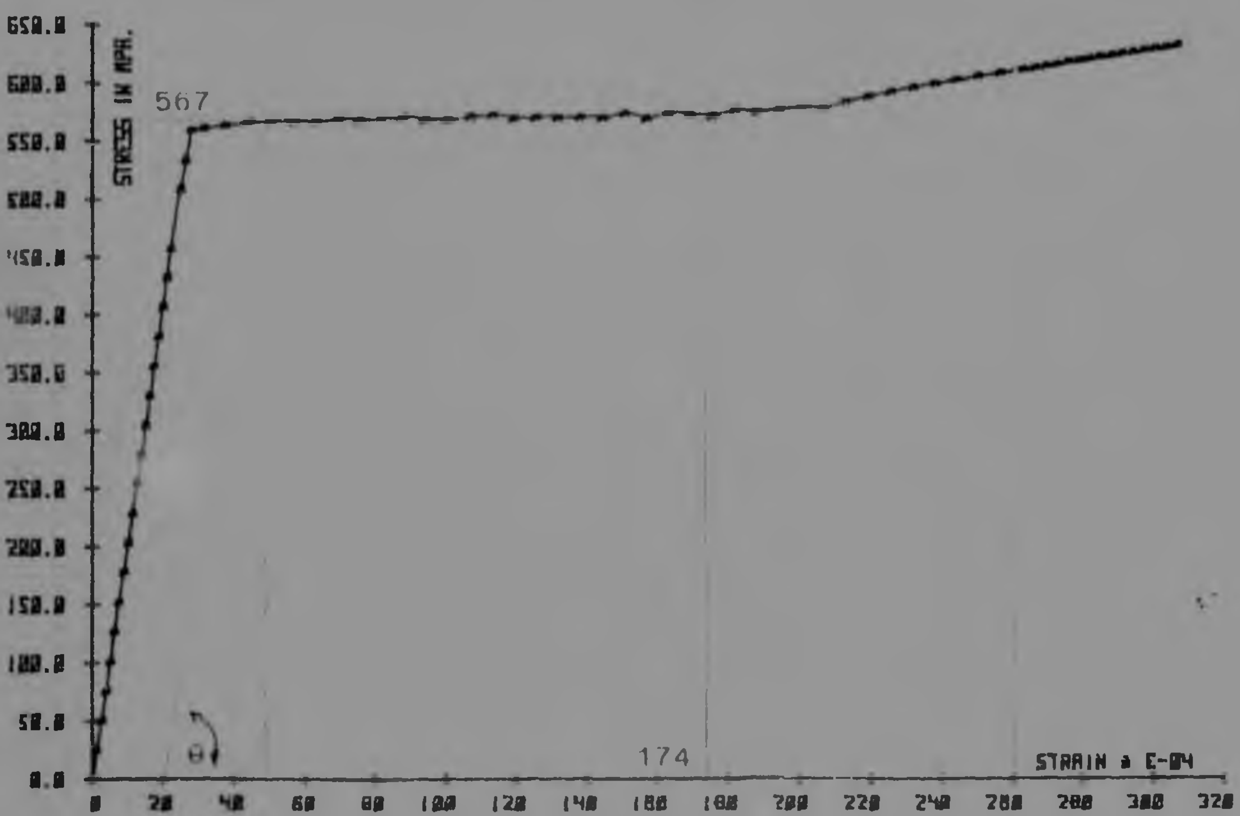

E's=4619

$f_y = 567$ $\quad E_s = \tan\theta = \dfrac{567}{28,6\times10^{-4}} = 198GPa$

STRESS - STRAIN CURVE FOR A STEEL BAR Y10 USED IN BEAM B4

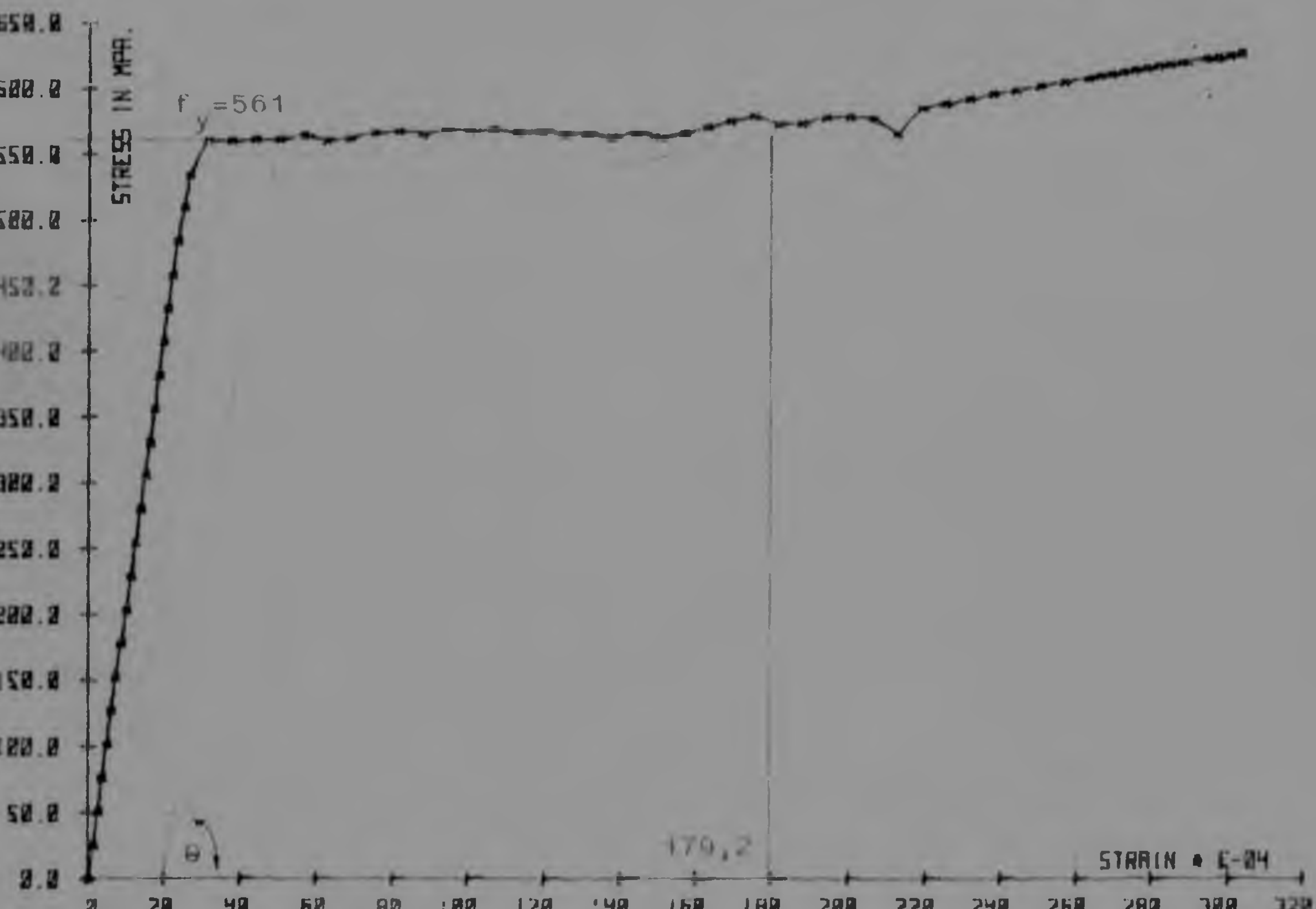

E's =4515

0,2% $f_y = 561$ $Es = \tan\theta = \frac{561}{28\times10^{-4}} = 200,3GPa$

STRESS - STRAIN CURVE FOR A STEEL BAR Y10 IN BEAM C1

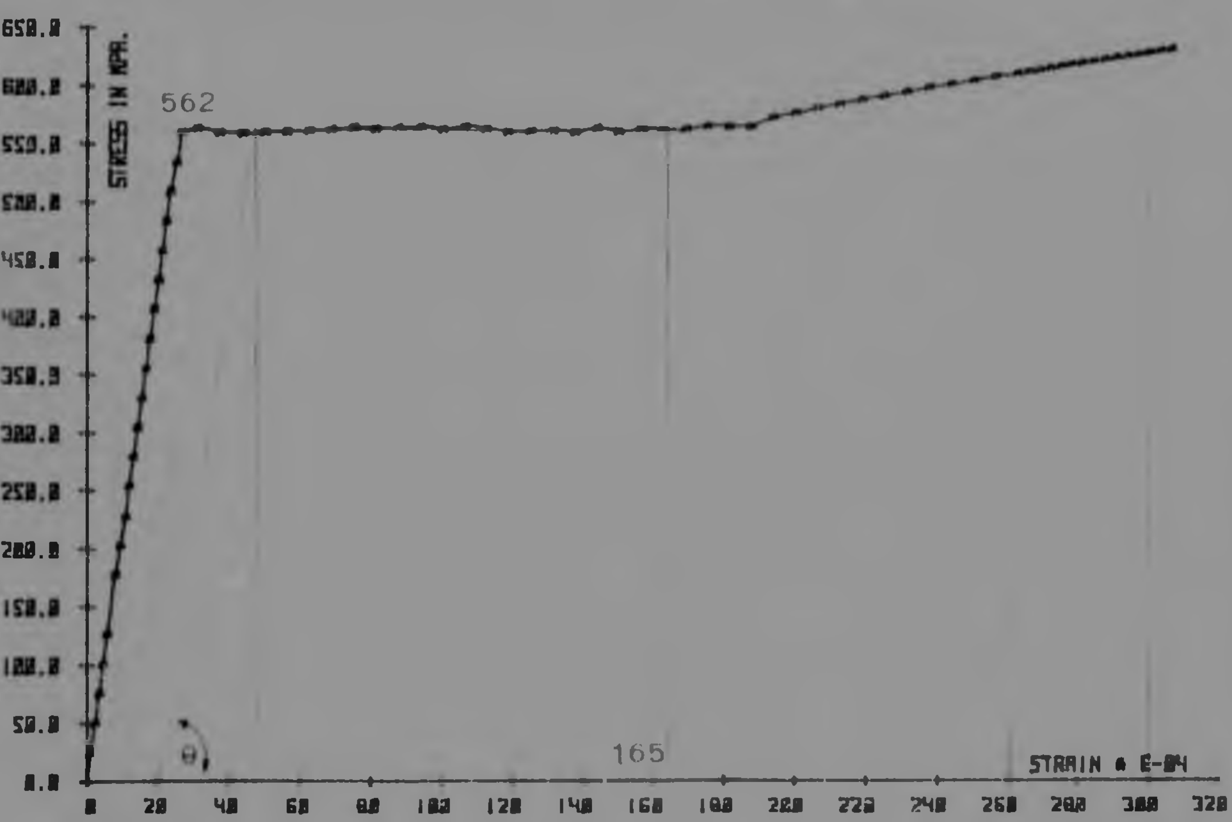

E's = 4584

f_y = 562 $\quad$ $\tan\theta = \dfrac{562}{27.78 \times 10^{-4}} = 202\text{GPa}$

STRESS - STRAIN CURVE FOR A STEEL BAR Y10 USED IN BEAM C2

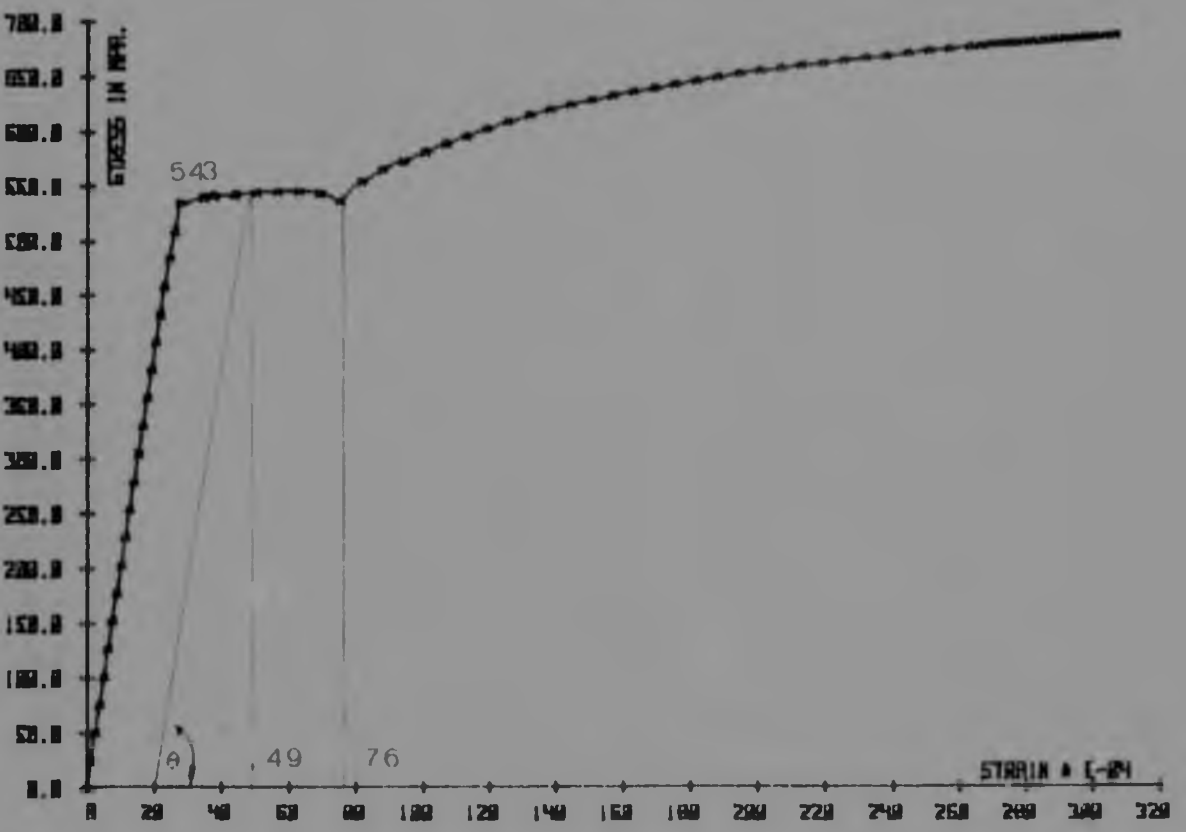

E's= 2341,33

$f_y = 543$ $\qquad$ $Es = Tan\ \theta = \dfrac{543}{29,14 \times 10^{-4}} = 186GPa$

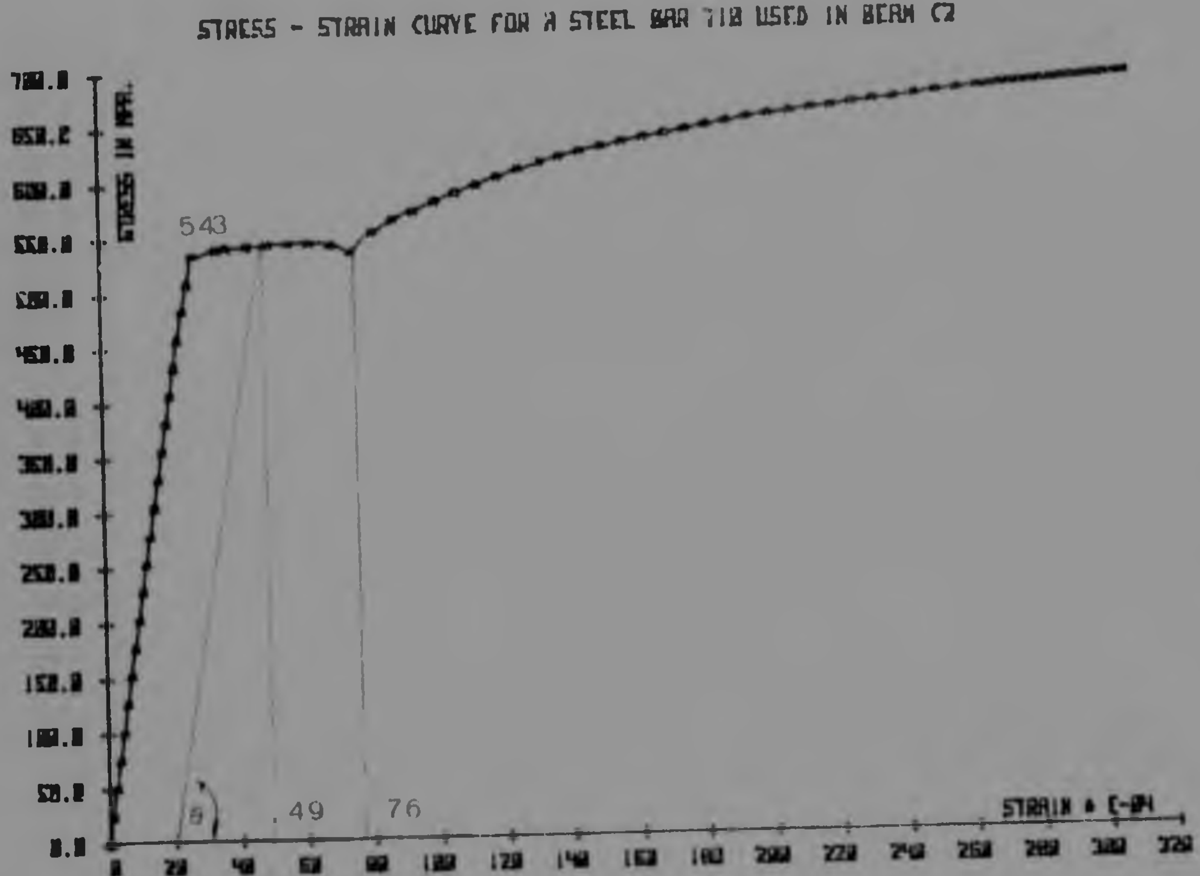

E's= 2341,33

$f_y = 543$ $\quad$ $E_s = \tan\theta = \dfrac{543}{29,14 \times 10^{-4}} = 186\,GPa$

STRESS - STRAIN CURVE FOR A STEEL BAR USED IN BEAM C3

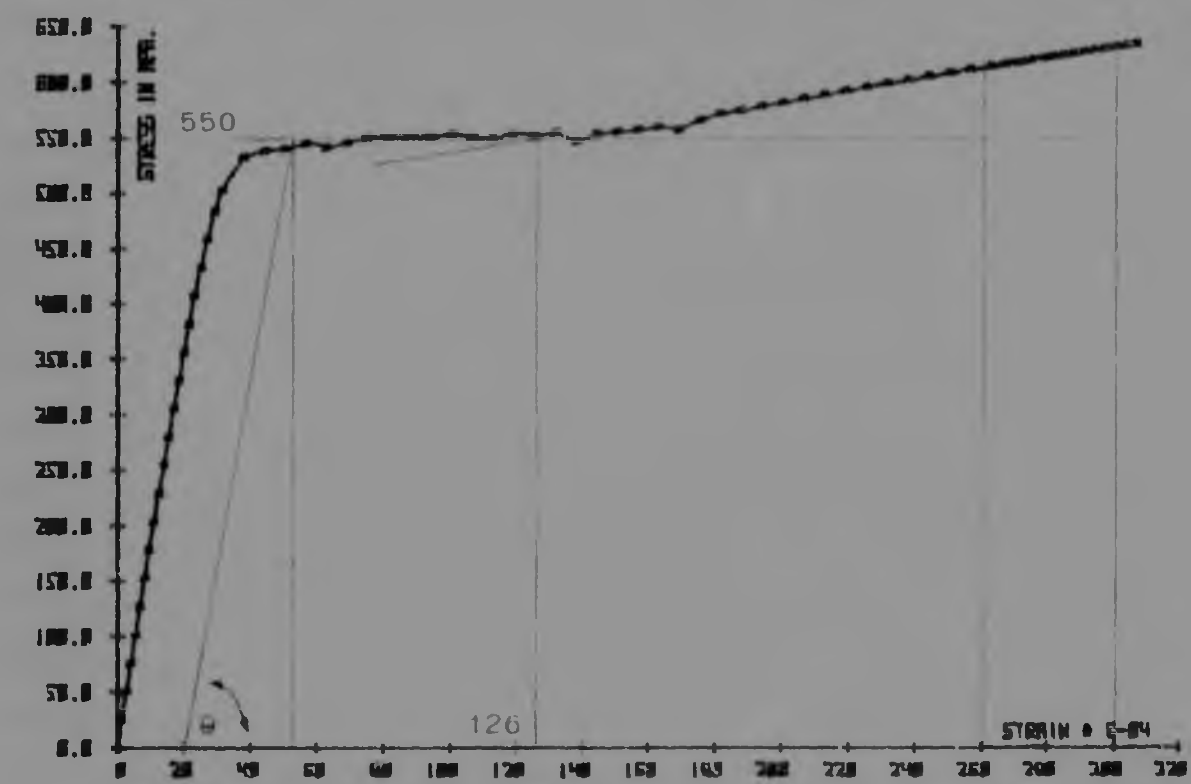

E's = 4549

$f_y = 550 \quad Es = \tan\theta = \frac{550}{32,94 \times 10^{-4}} = 167 GPa$

STRESS - STRAIN CURVE FOR A STEEL BAR Y10 IN BEAM C4

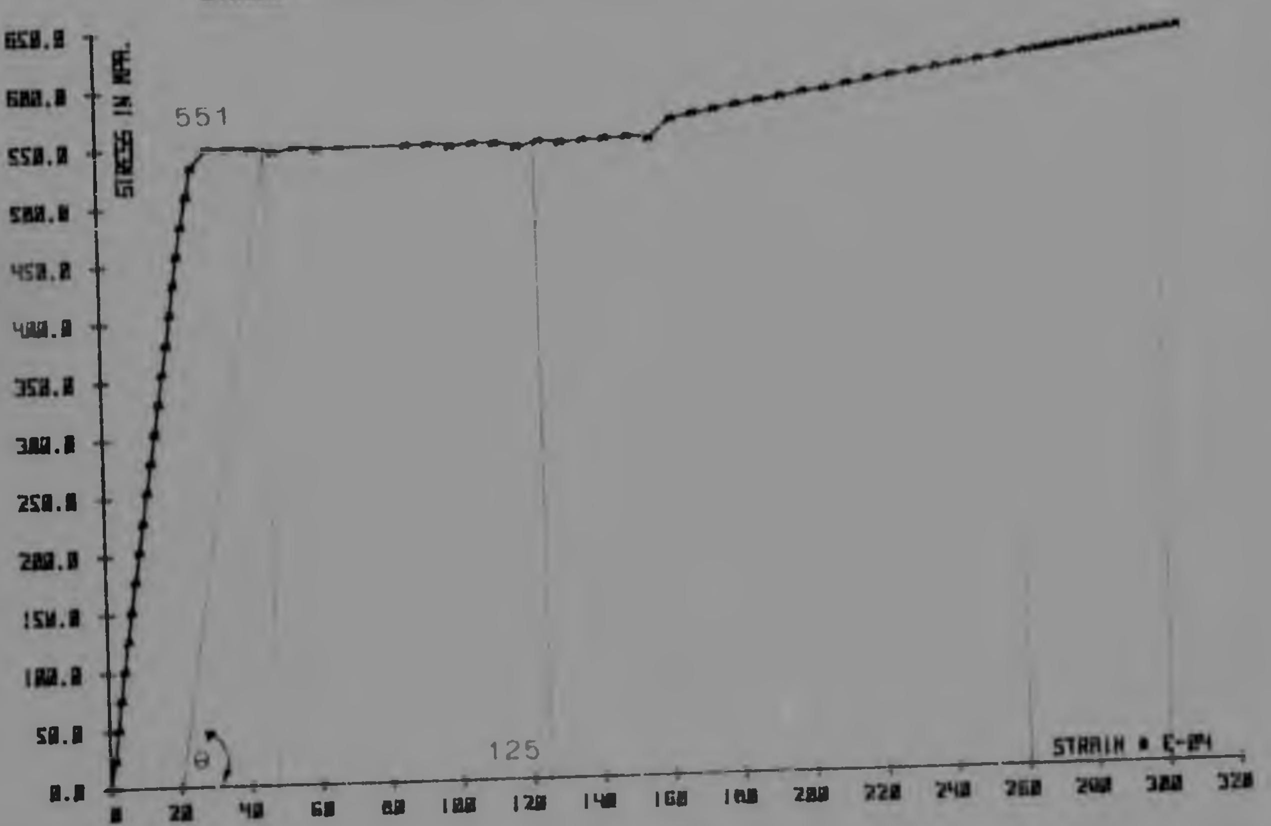

E's = 4176

$f_y = 551$ Es = Tan θ = $\frac{551}{27,03 \times 10^{-4}}$ = 203,8GPa

STRESS - STRAIN CURVE FOR A STEEL BAR Y10 IN BEAM C5

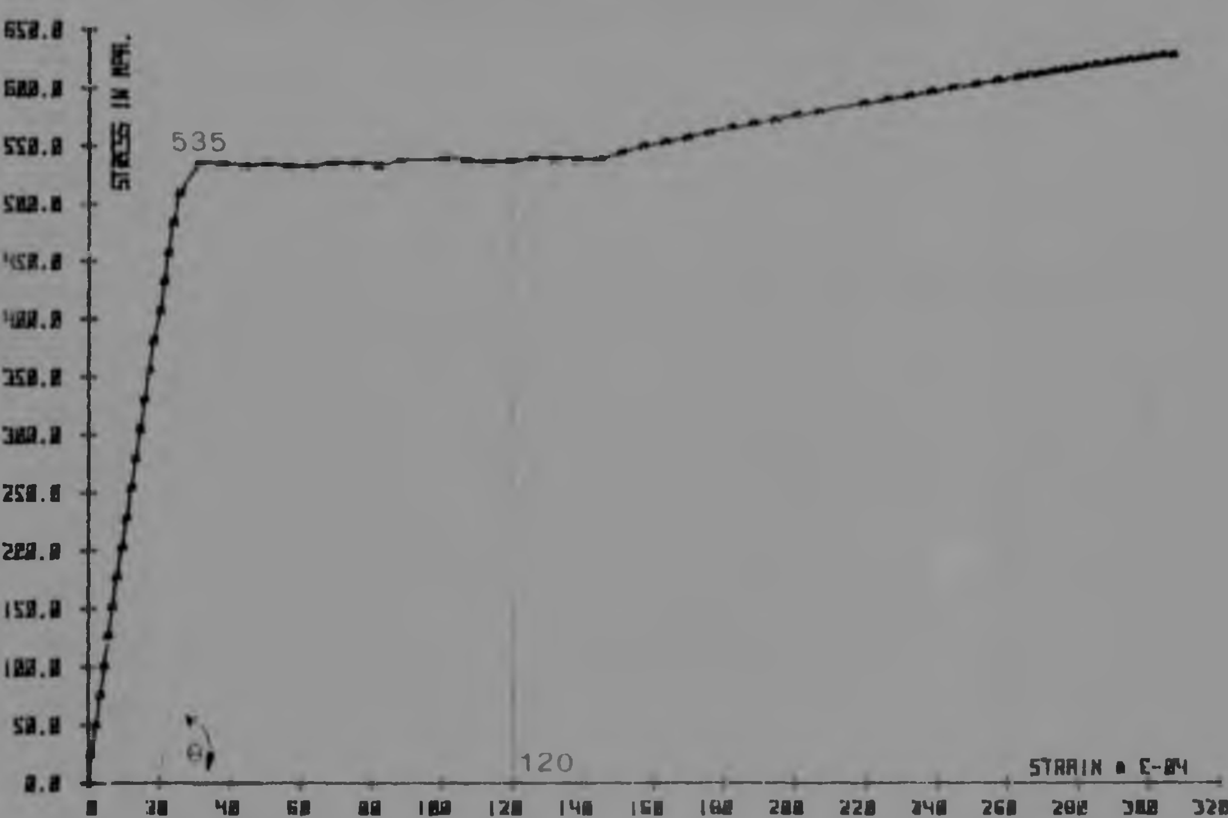

E's = 4584

$f_y = 535 \quad E_s = \tan\theta = \dfrac{535}{27{,}57 \times 10^{-4}} = 194 GPa$

STRESS - STRAIN CURVE FOR A STEEL BAR RA USED IN BEAM D1

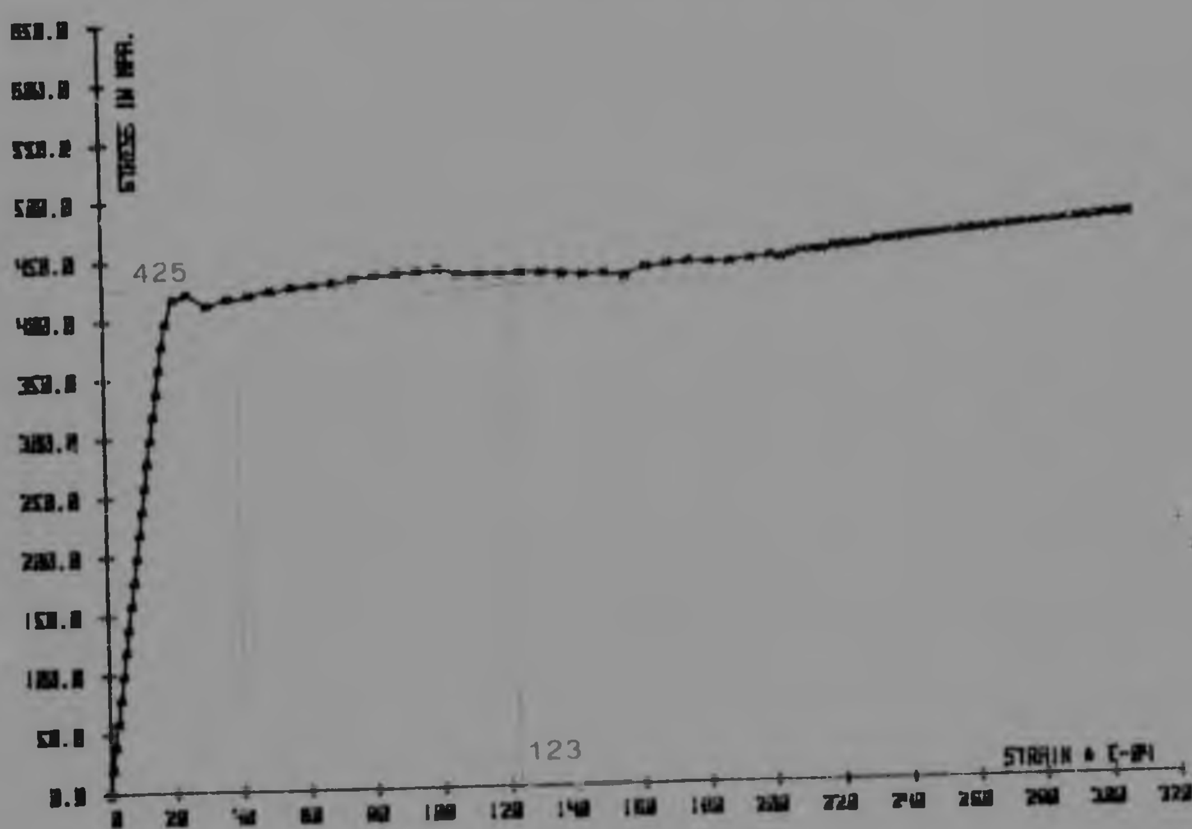

E's = 2387

$F_y = 425 \quad \tan\theta = \frac{425}{20 \times 10} = 212{,}5\text{GPa}$

STRESS - STRAIN CURVE FOR A STEEL BAR R8 USED IN BEAM D2

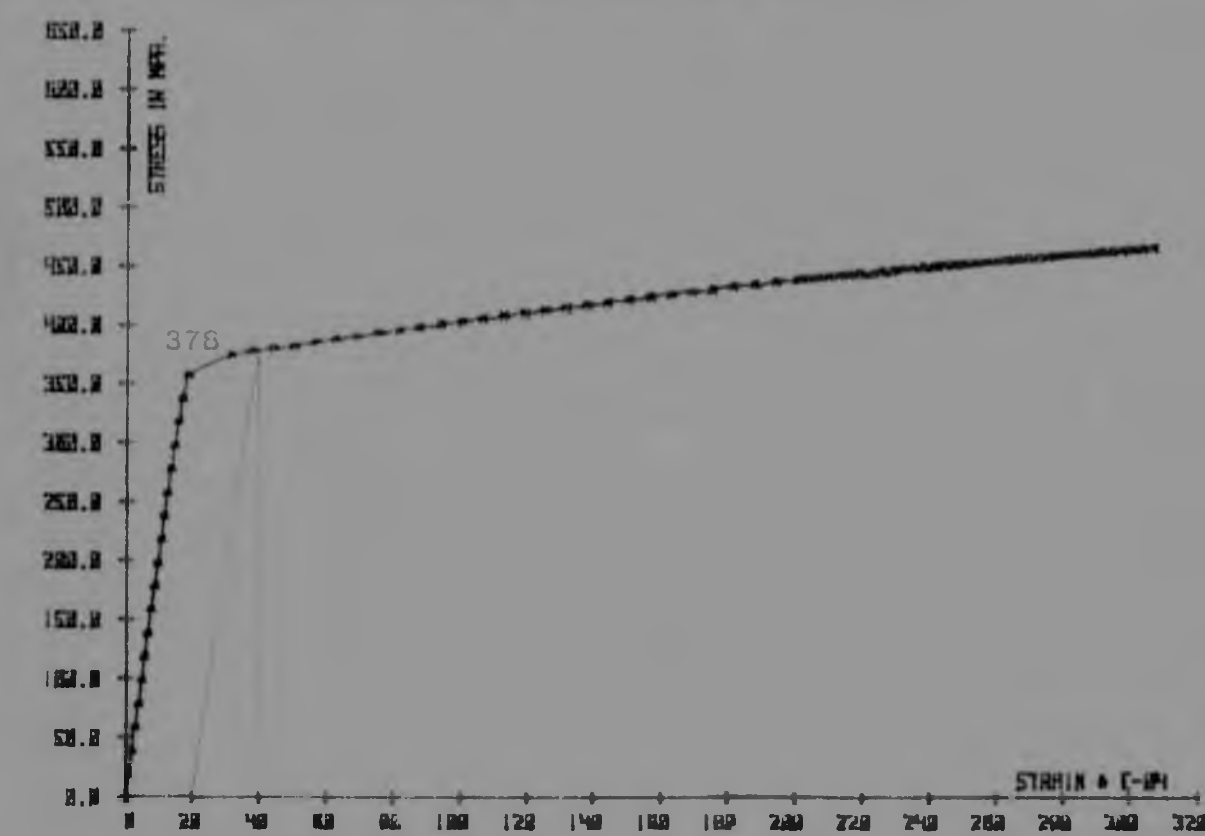

E's = 2493

$f_y = 378 \quad E_s = \frac{378}{20 \times 10^{-4}} = 189GPa$

STRESS - STRAIN CURVE FOR A STEEL BAR Y10 USED IN BEAM D3

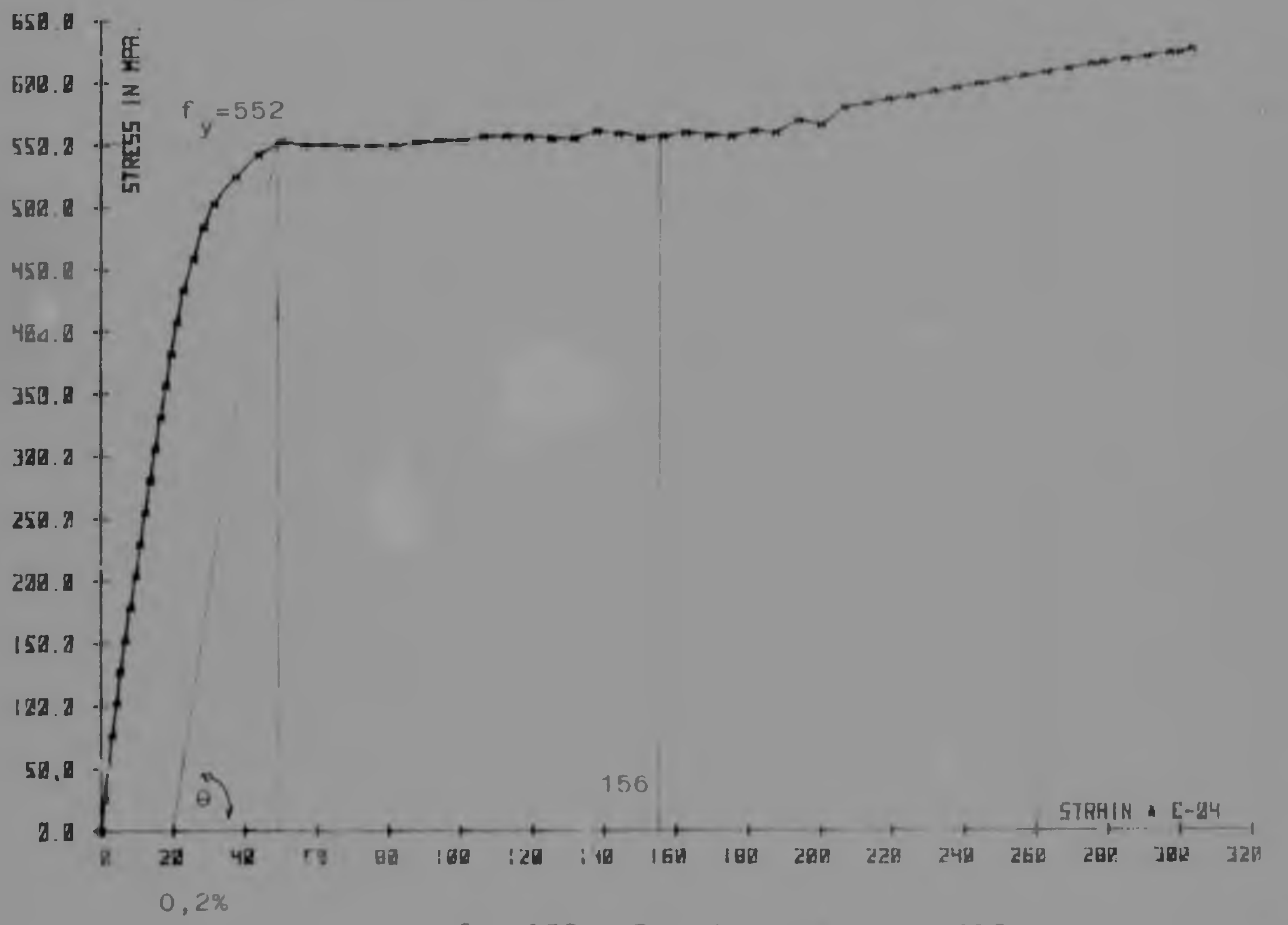

$f_y = 552 \quad E_s = \tan\theta = \dfrac{552}{29\times10^{-4}} = 190{,}3\,GPa$

APPENDIX 3

LOAD-DEFLECTION CURVES AT MIDSPAN

LOAD - DEFLECTION CURVE AT MIDSPAN FOR BEAM A2

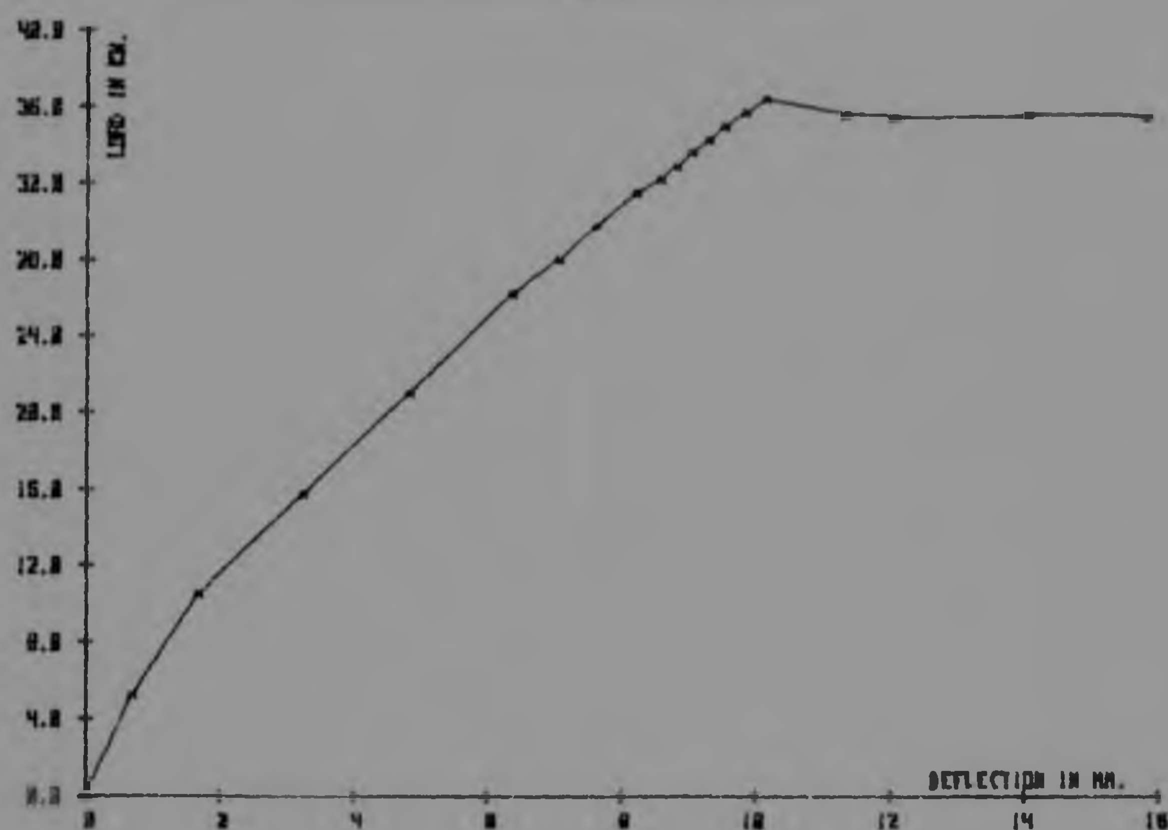

LOAD - DEFLECTION AT MIDSPAN FOR BEAM B1

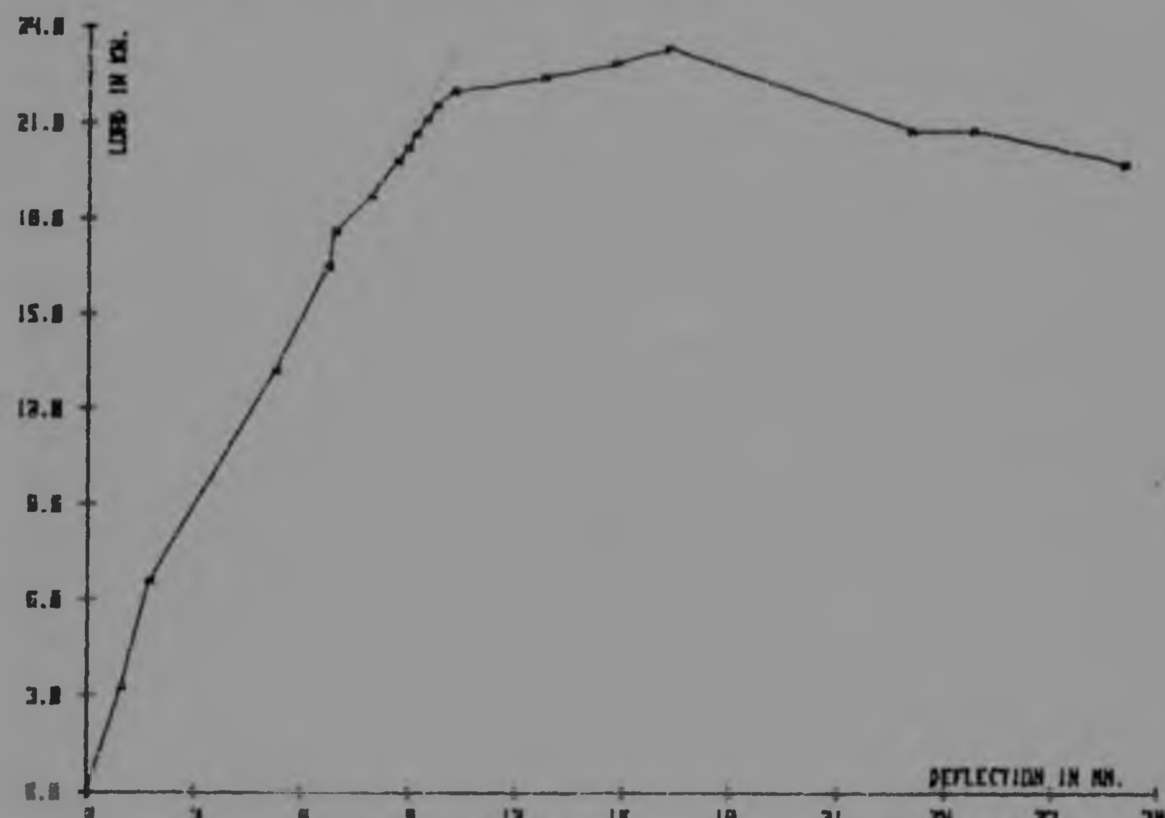

LOAD - DEFLECTION CURVE AT MIDSPAN FOR BEAM B2

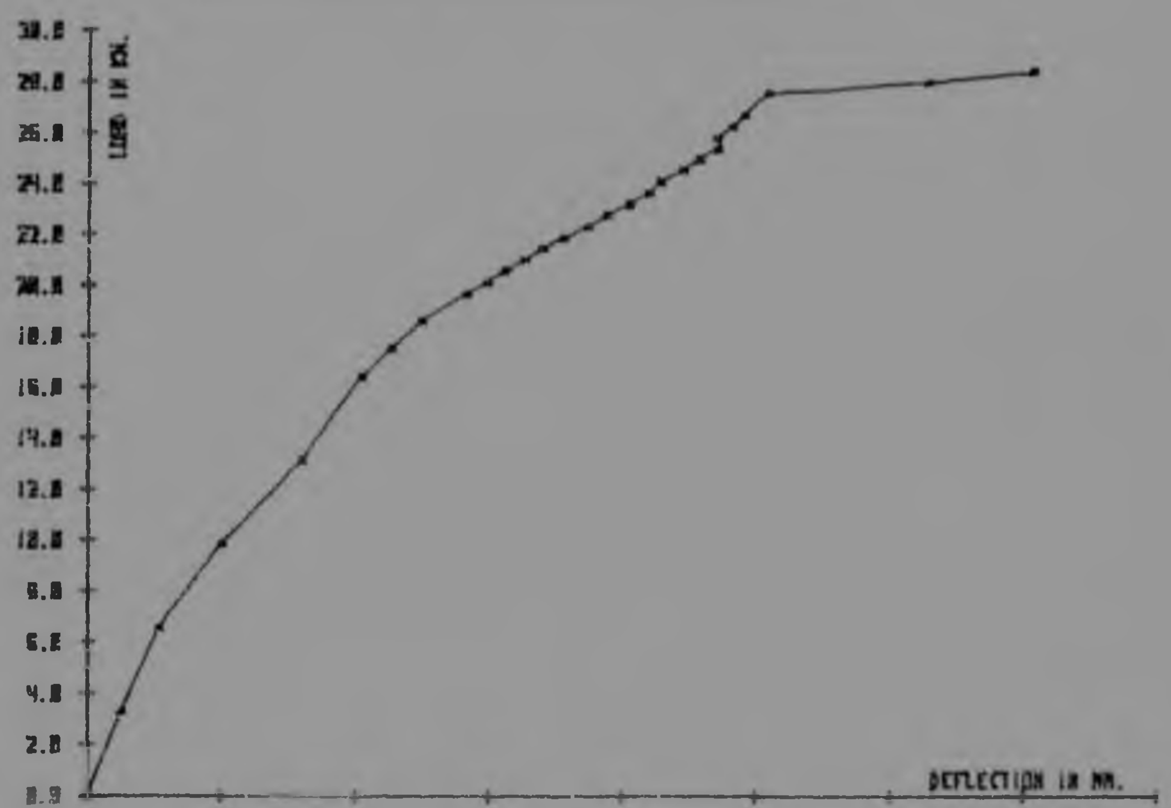

LOAD - DEFLECTION CURVE AT MIDSPAN FOR BEAM B3

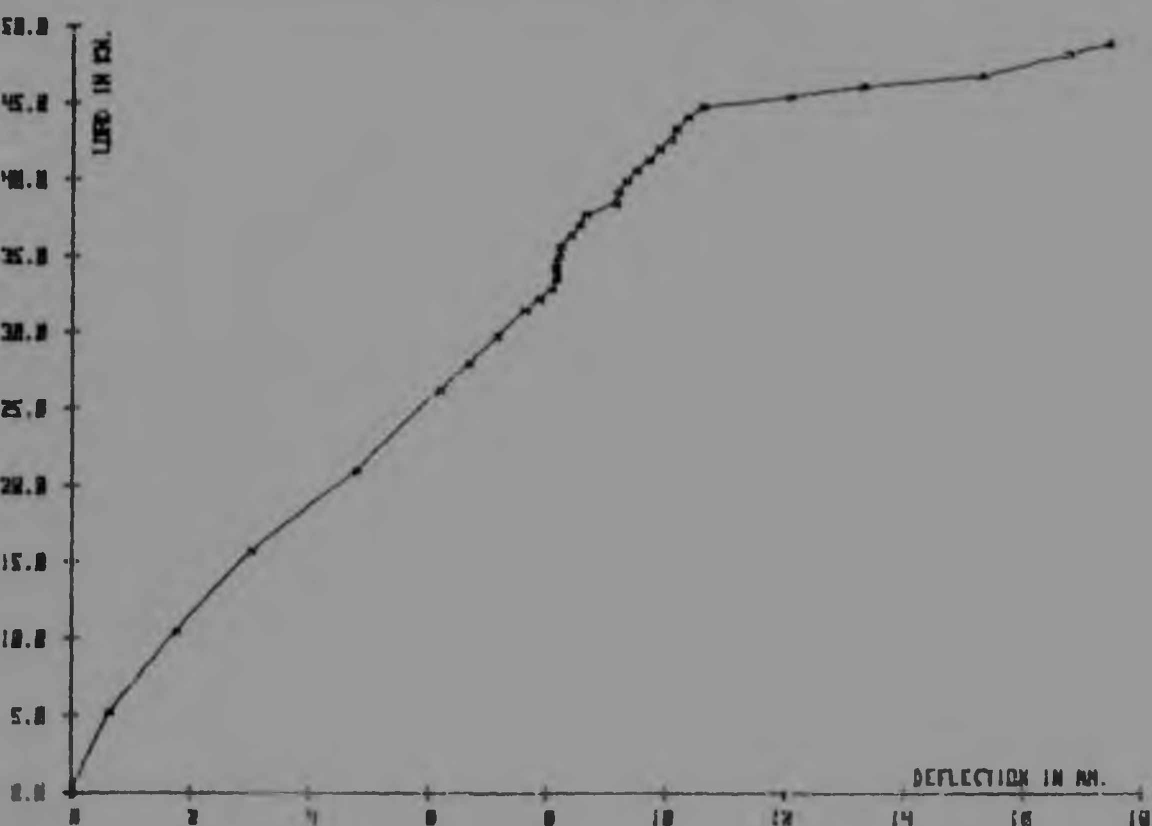

LOAD - DEFLECTION CURVE AT MIDSPAN FOR BEAM B4

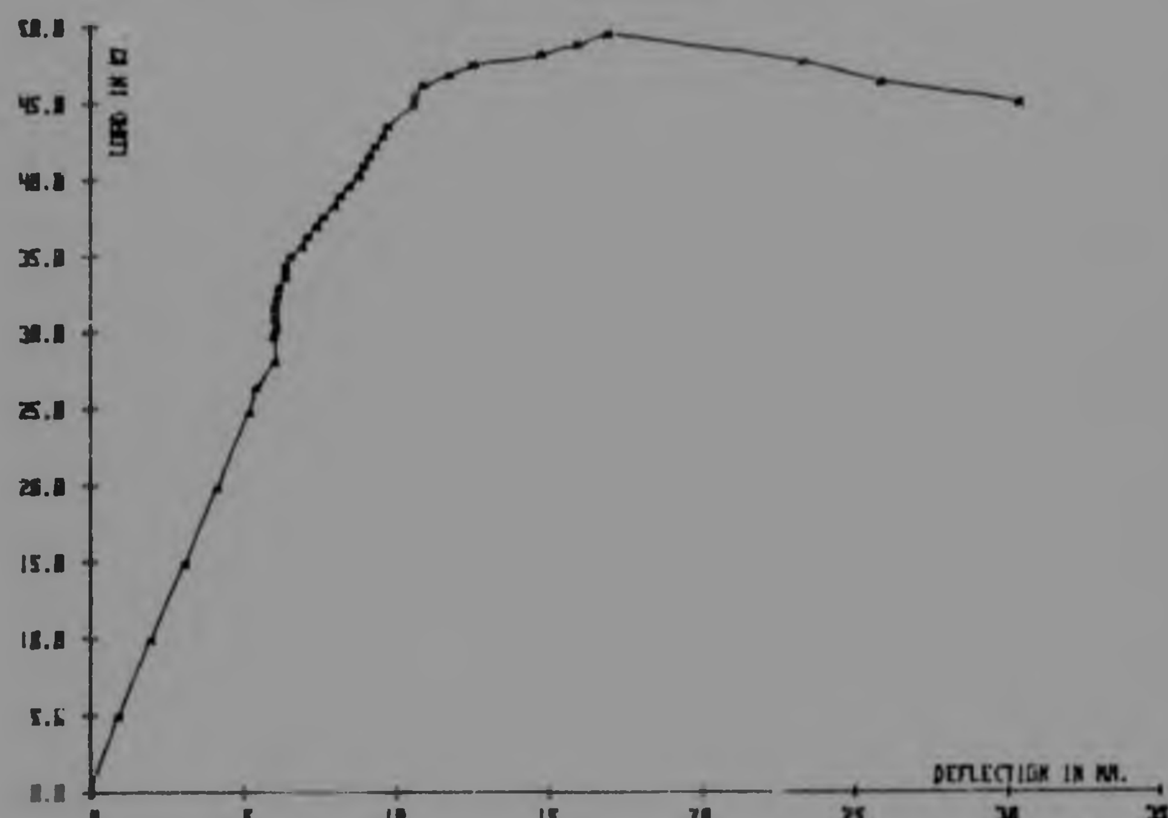

LOAD - DEFLECTION CURVE AT MIDSPAN FOR BEAM C1

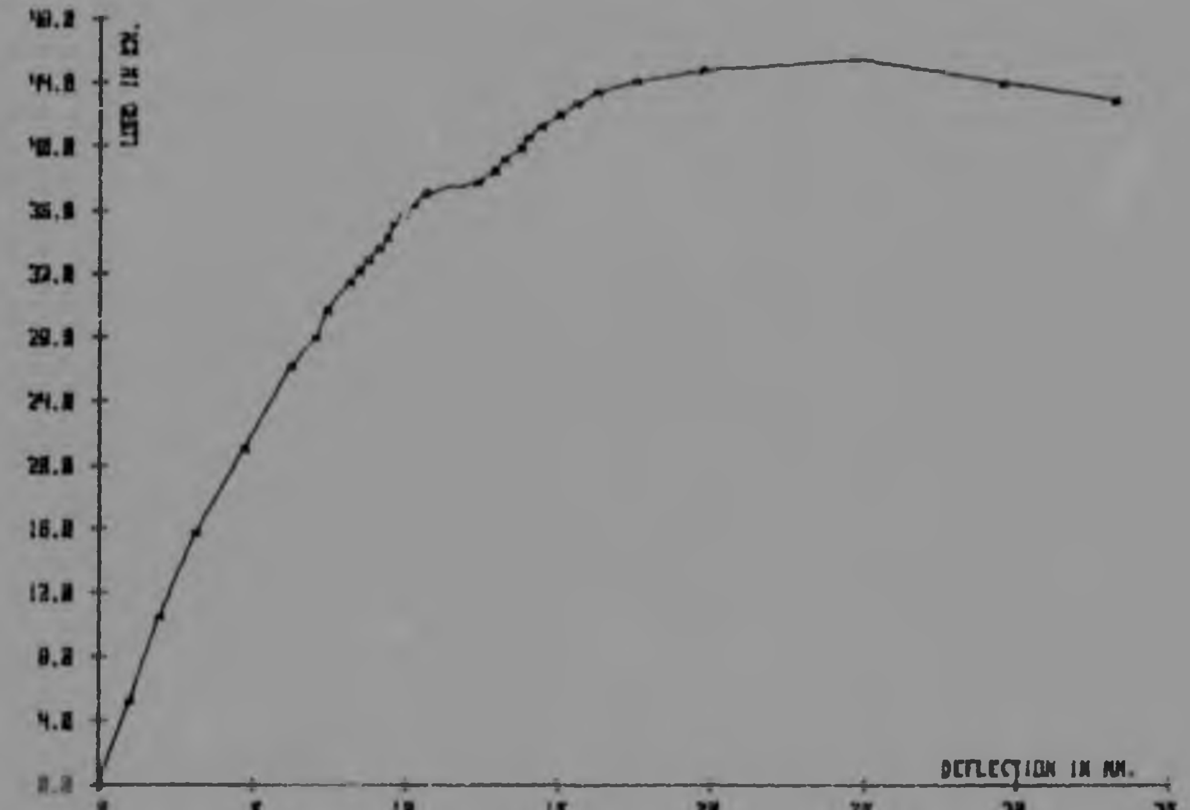

LOAD - DEFLECTION CURVE AT MIDSPAN FOR BEAM C2

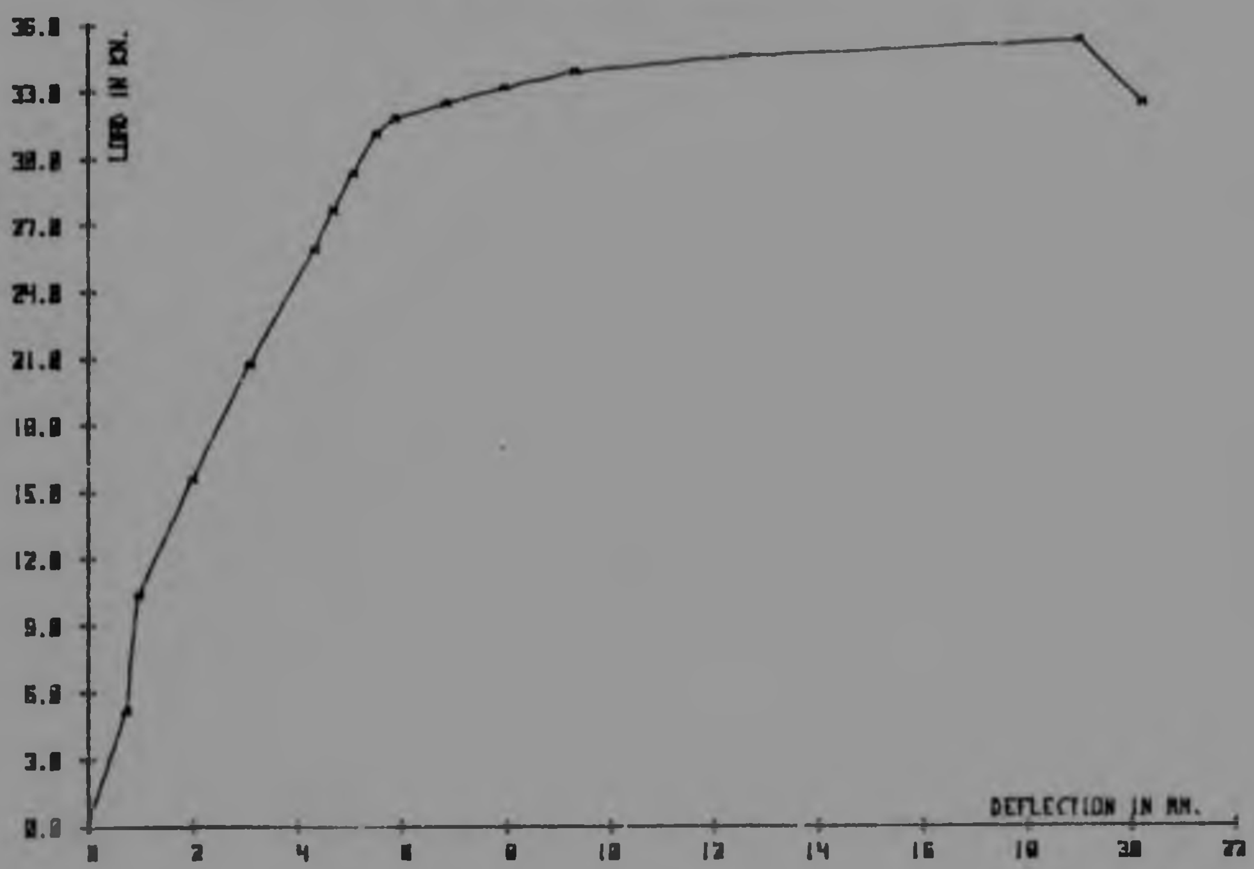

LOAD - DEFLECTION CURVE AT MIDSPAN FOR BEAM C3

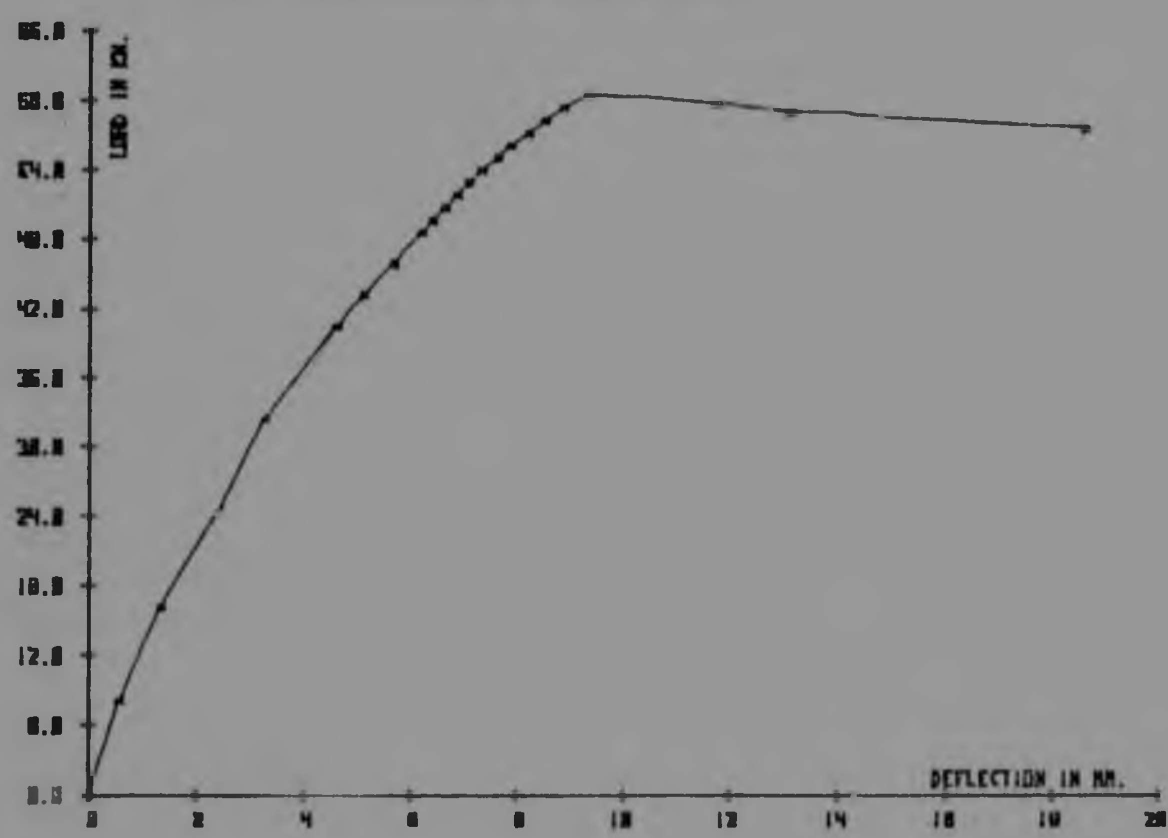

LOAD - DEFLECTION CURVE AT MIDSPAN FOR BEAM C4

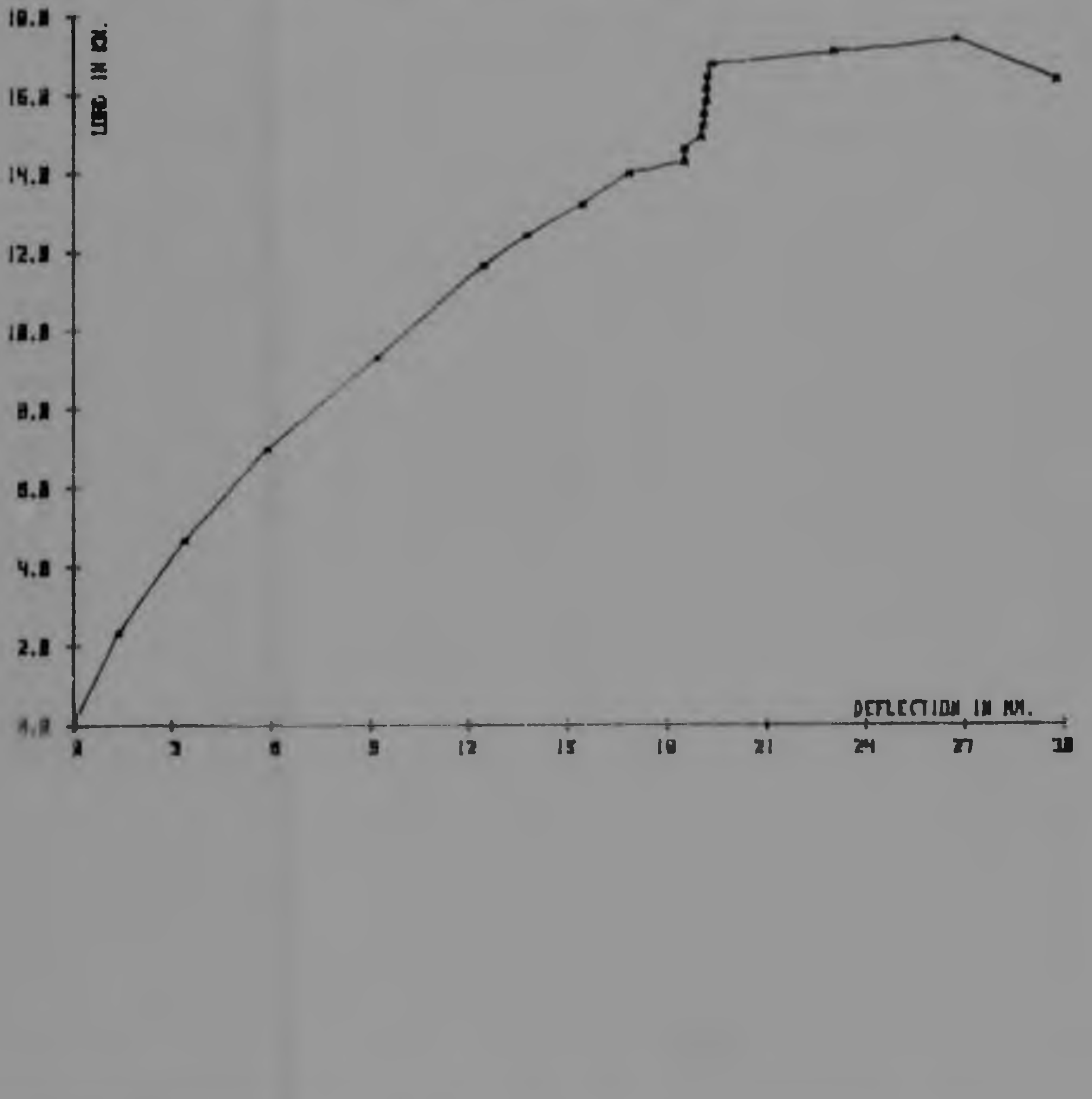

LOAD - DEFLECTION CURVE AT MIDSPAN FOR BEAM C6

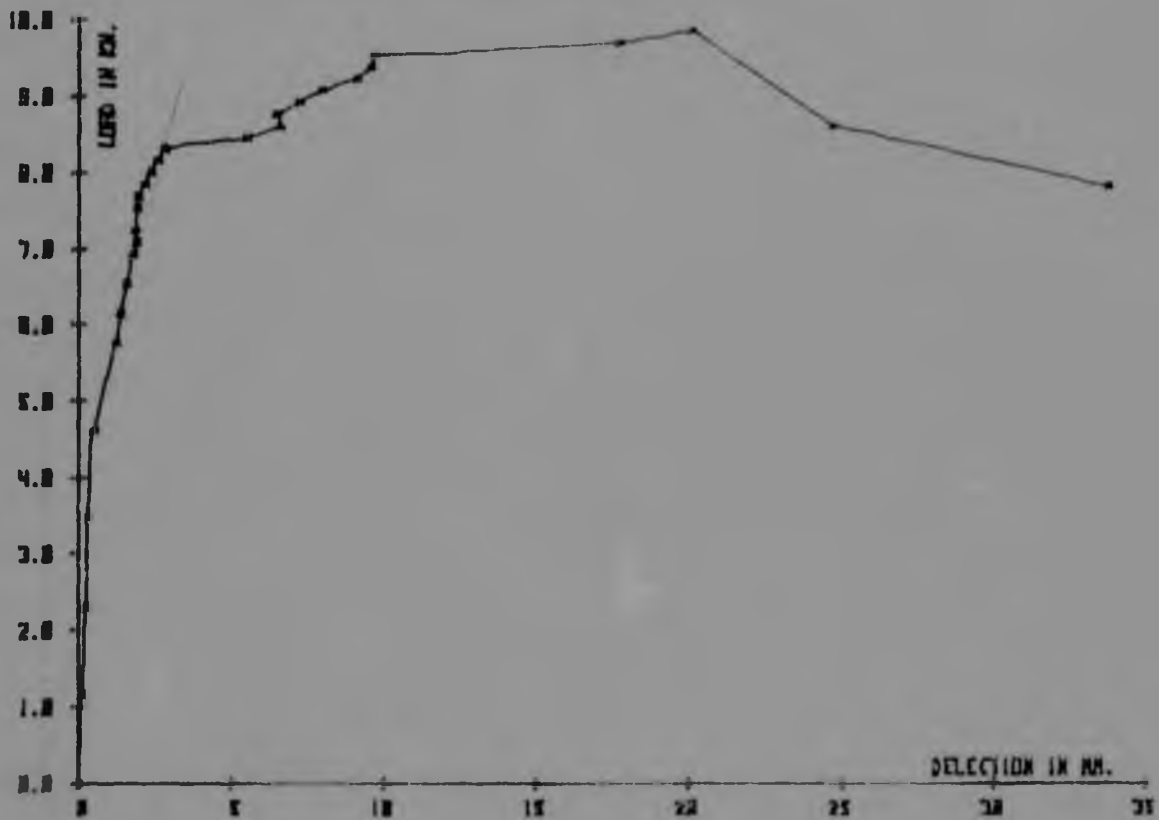

LOAD - DEFLECTION CURVE AT MIDSPAN FOR BEAM D1

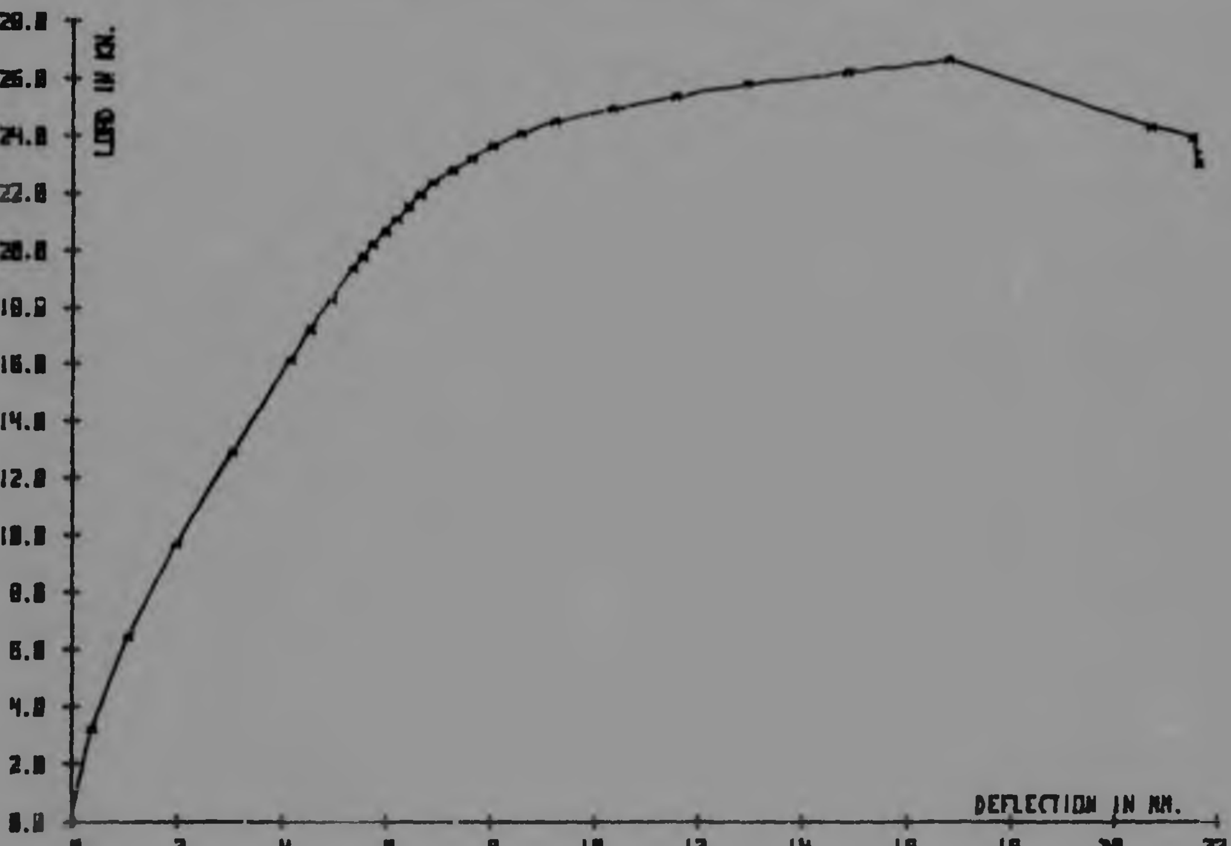

LOAD - DEFLECTION CURVE AT MIDSPAN FOR BEAM D2

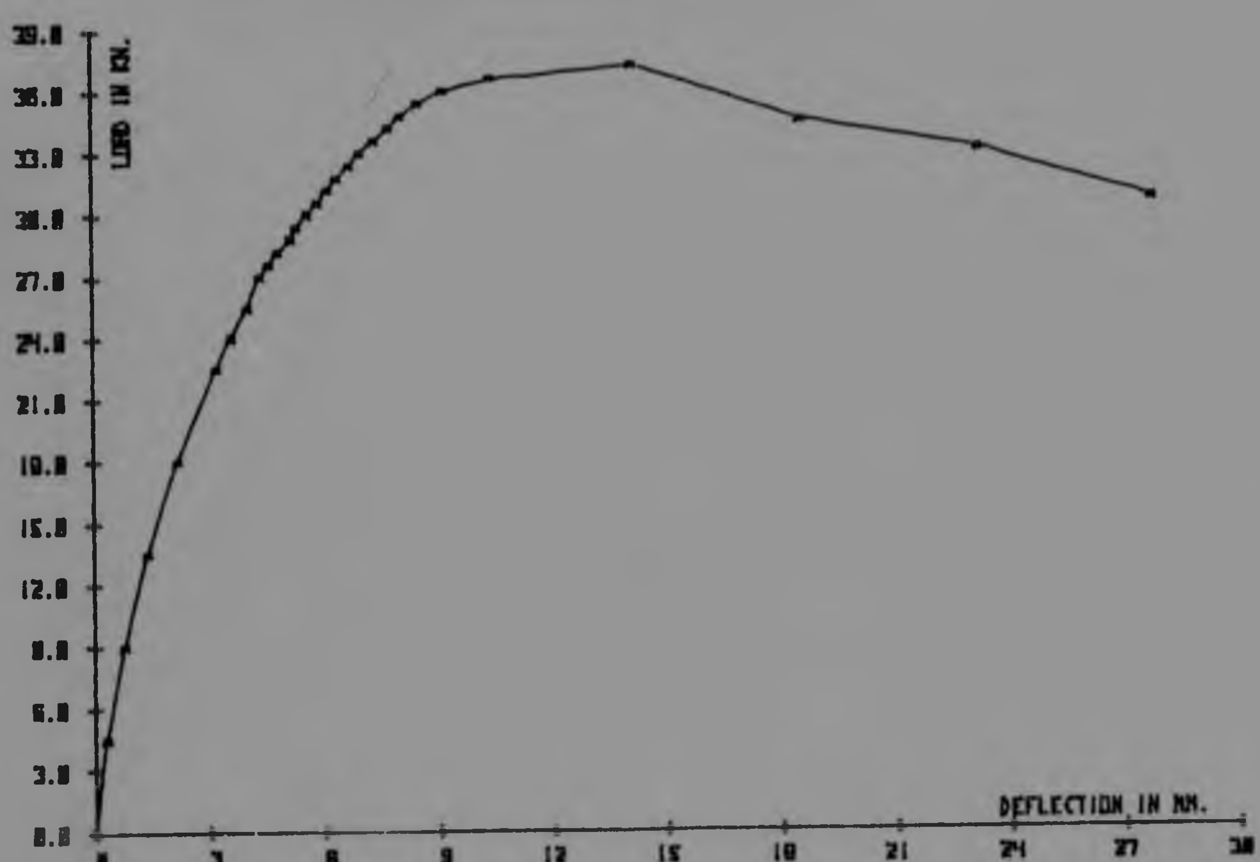

LOAD - DEFLECTION CURVE AT MIDSPAN FOR BEAM D3

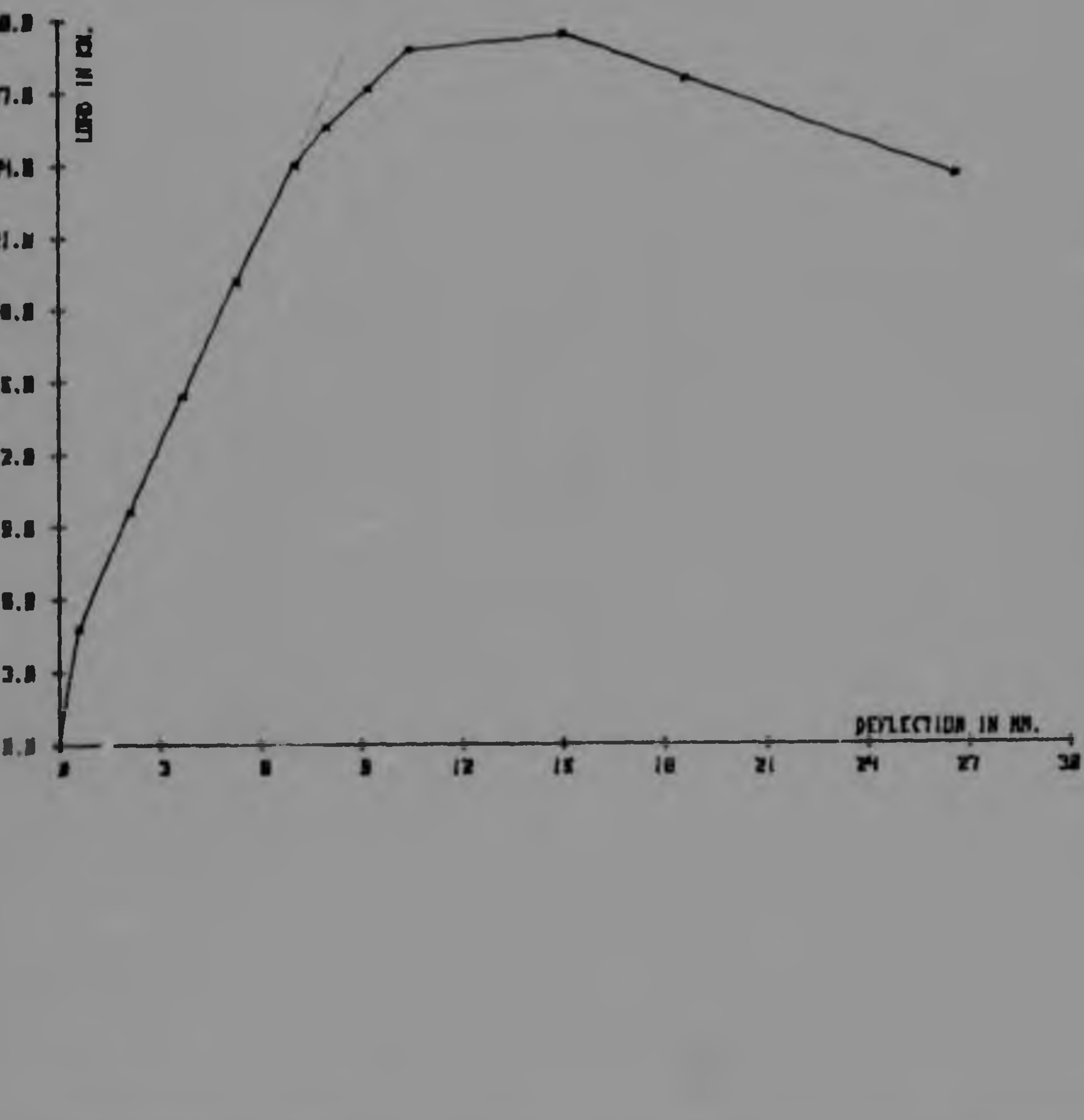

MOMENT-ROTATION CURVES FOR HALF SPAN

MOMENT - ROTATION CURVE FOR HALF SPAN FOR BEAM A2

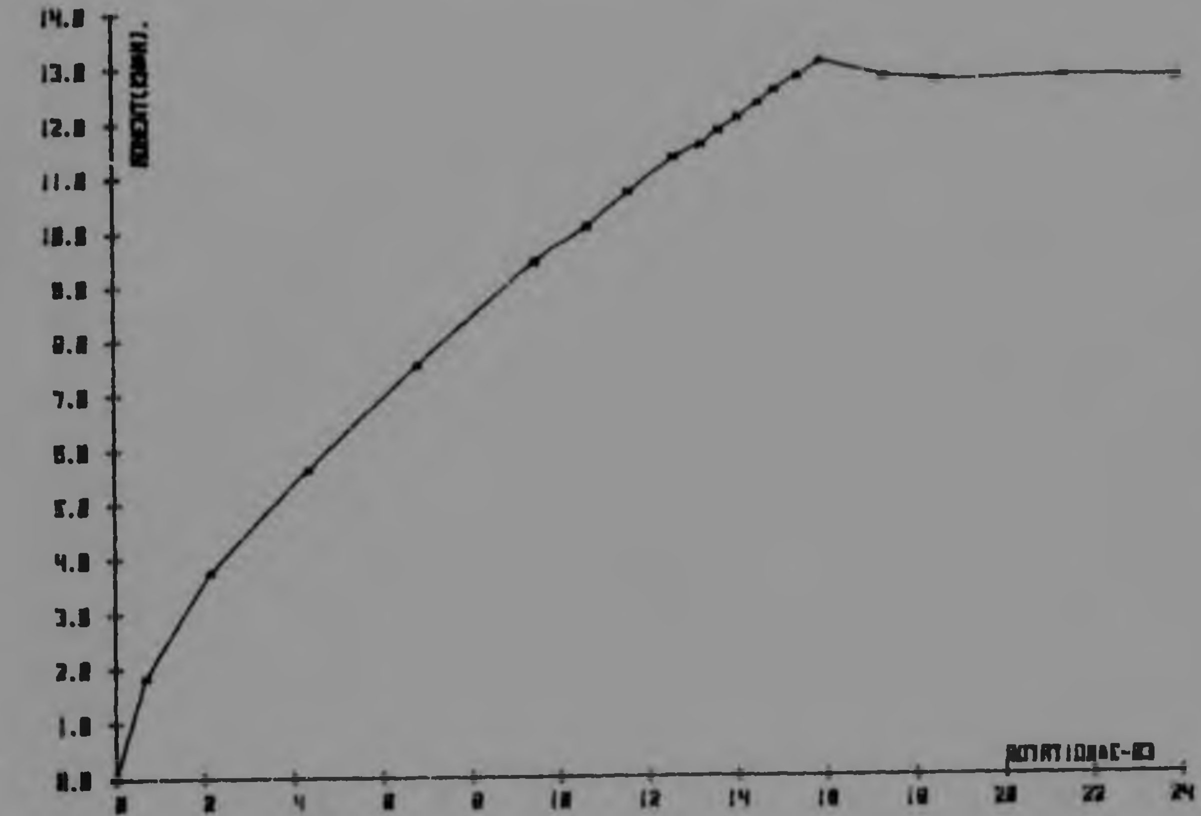

MOMENT - ROTATION CURVE FOR HALF SPAN FOR BEAM B1

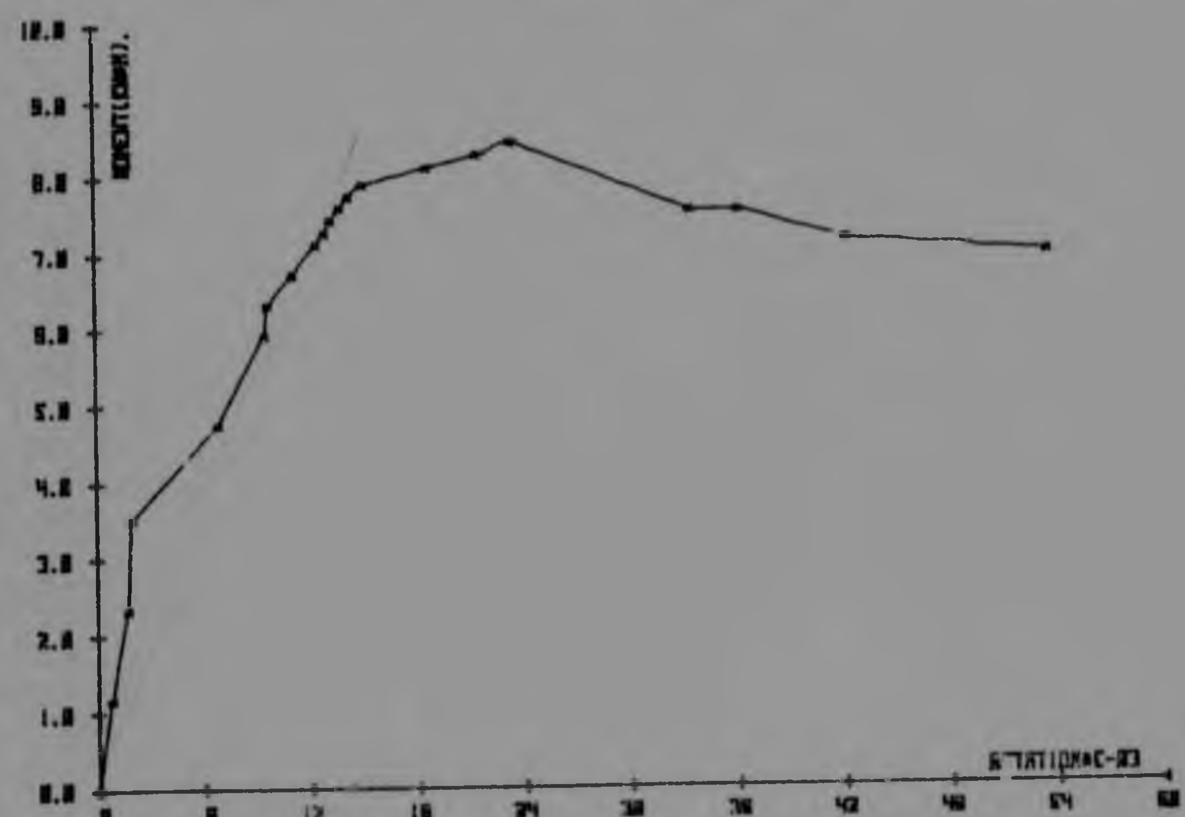

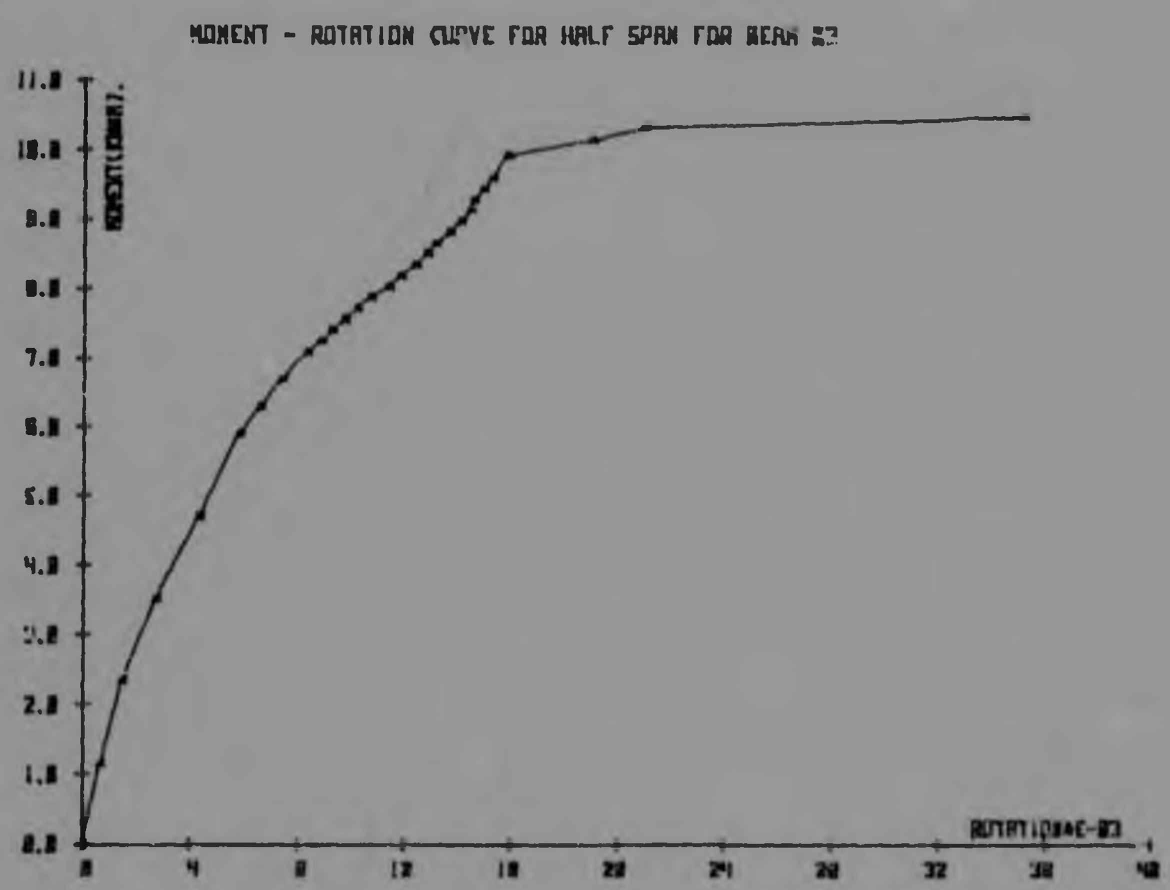
MOMENT - ROTATION CURVE FOR HALF SPAN FOR BEAM B3
11.0
10.0
9.0
8.0
7.0
6.0
5.0
4.0
3.0
2.0
1.0
0.0
0
4
8
12
16
20
24
28
32
36
40

MOMENT - ROTATION CURVE FOR HALF SPAN FOR BEAM B3

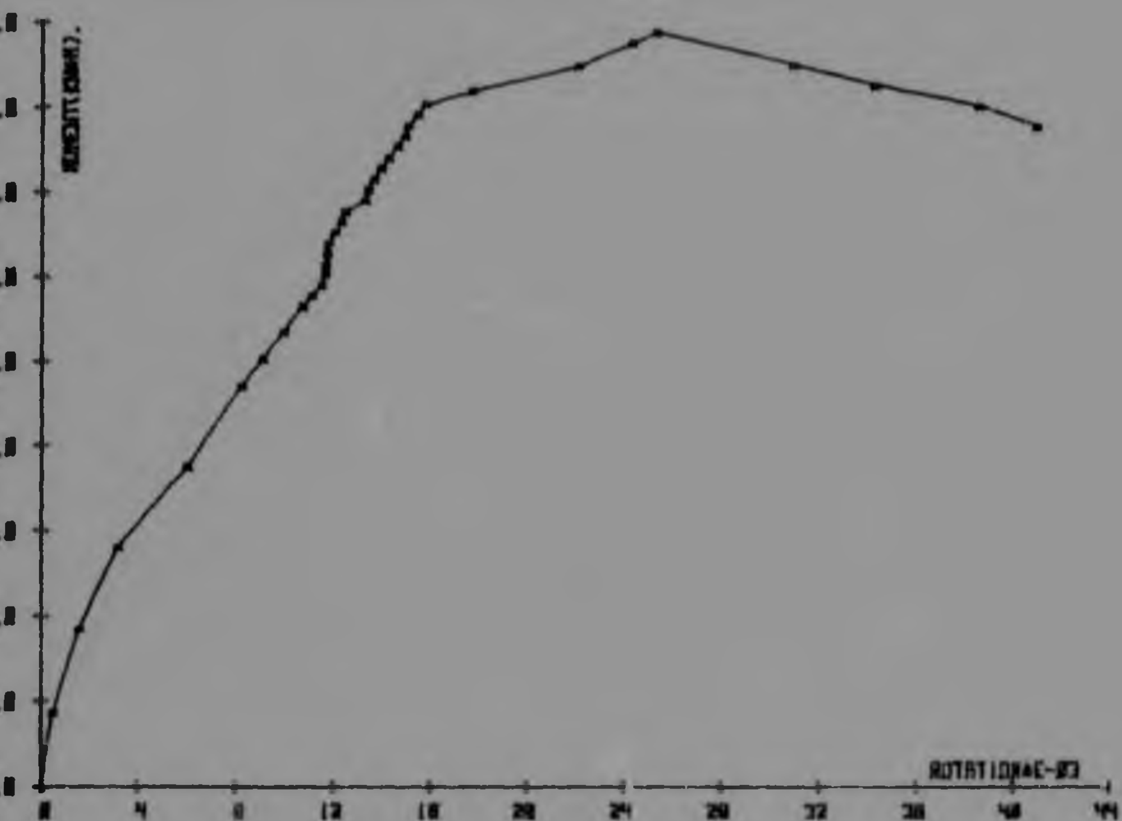

MOMENT - ROTATION CURVE FOR HALF SPAN FOR BEAM B4

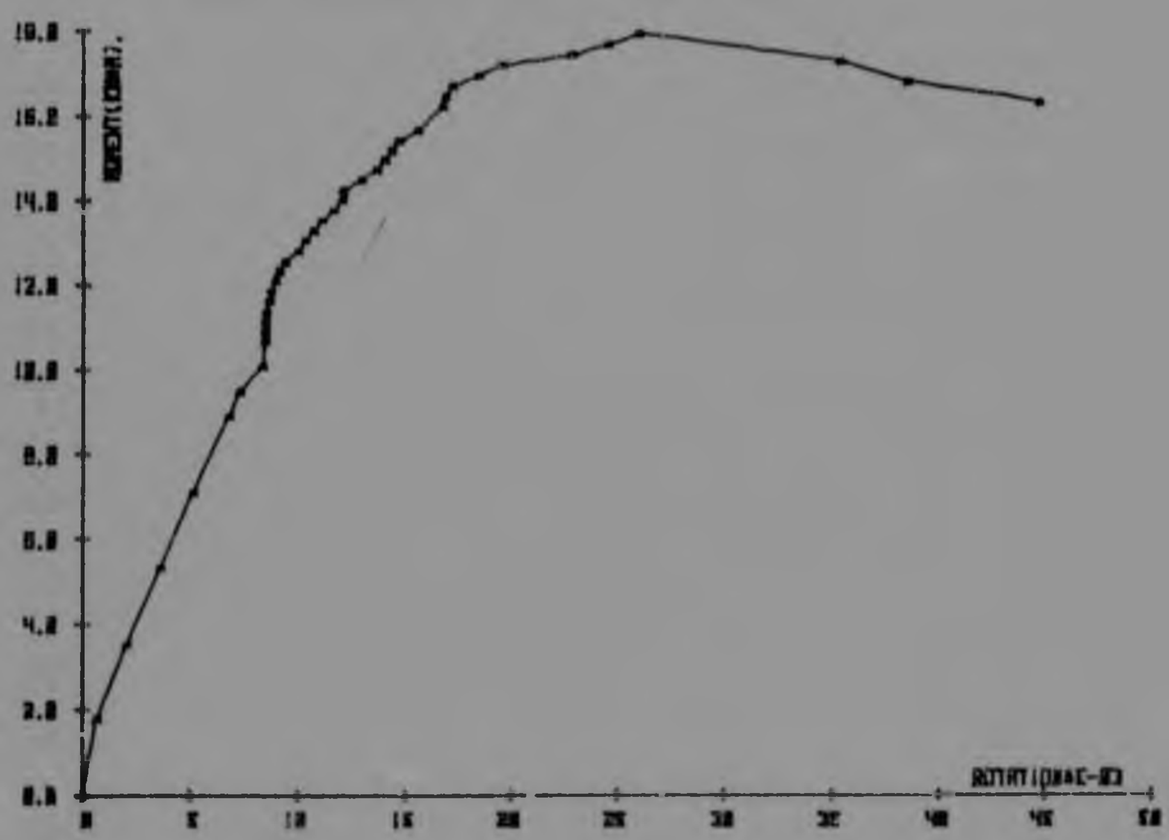

MOMENT - ROTATION CURVE FOR HALF SPAN FOR BEAM C1

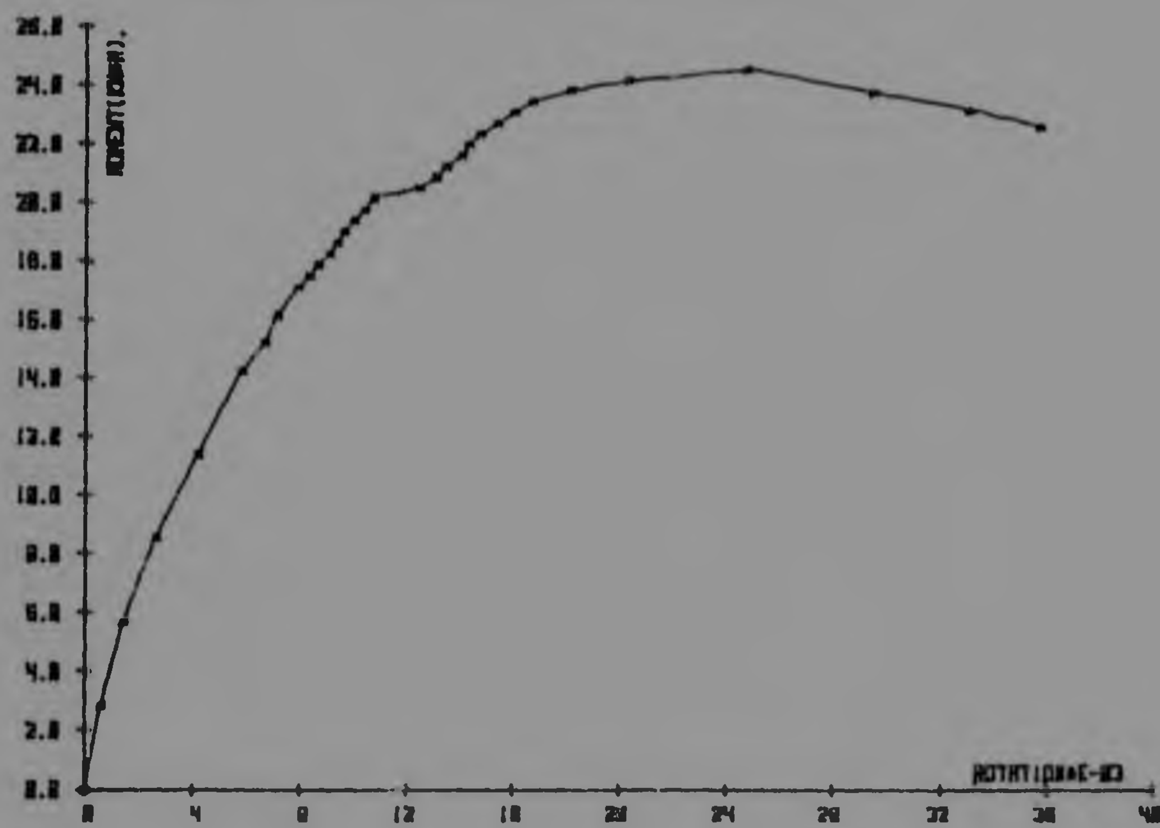

MOMENT - ROTATION CURVE FOR HALF SPAN FOR BEAM C2

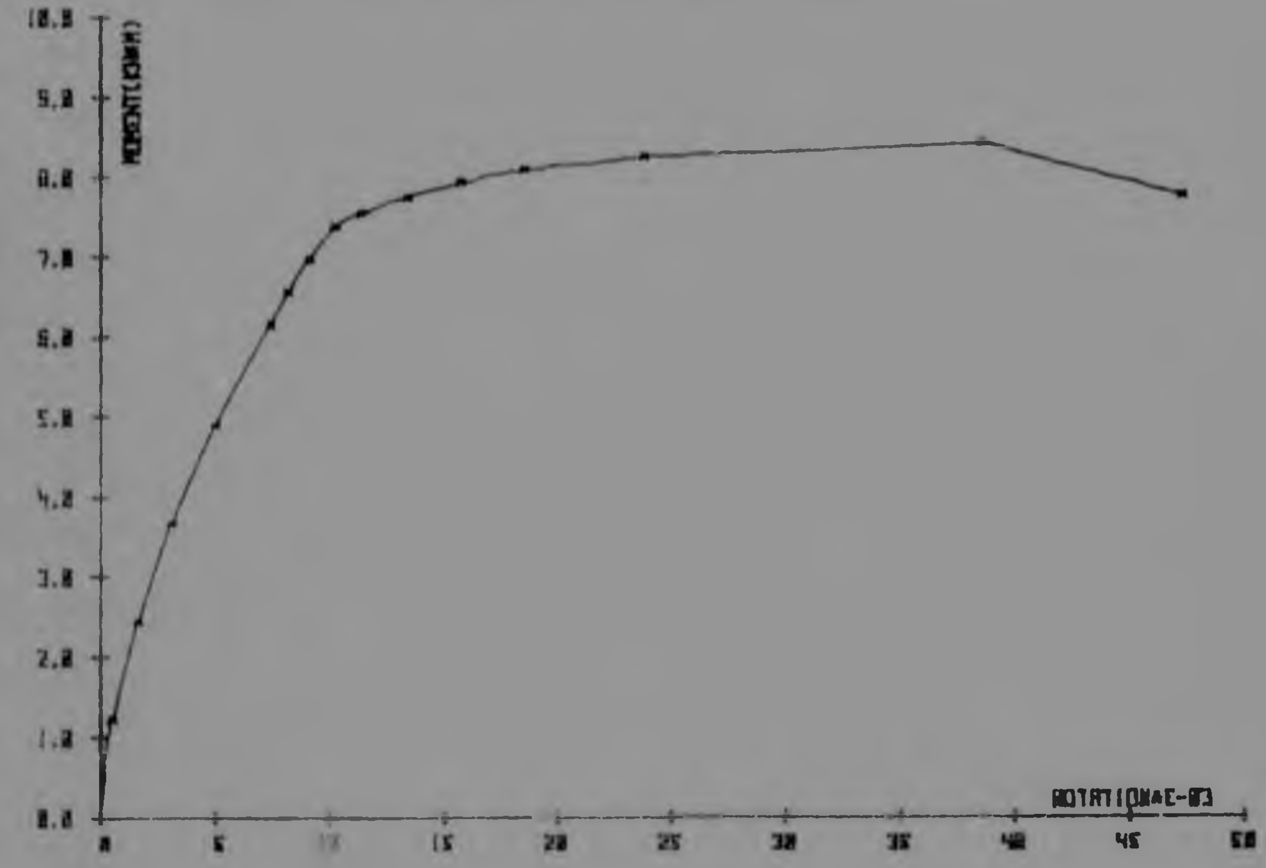

MOMENT - ROTATION CURVE FOR HALF SPAN FOR BEAM C3

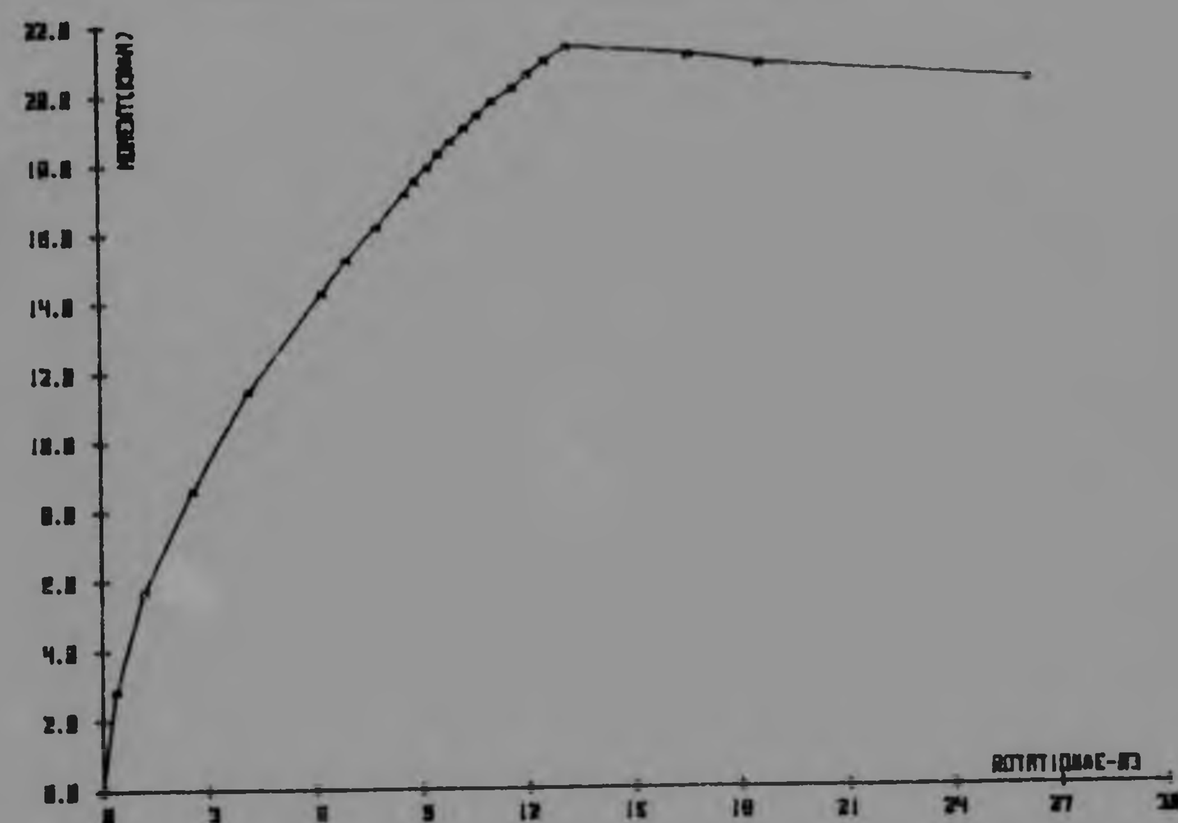

MOMENT - ROTATION CURVE FOR HALF SPAN FOR BEAM C4

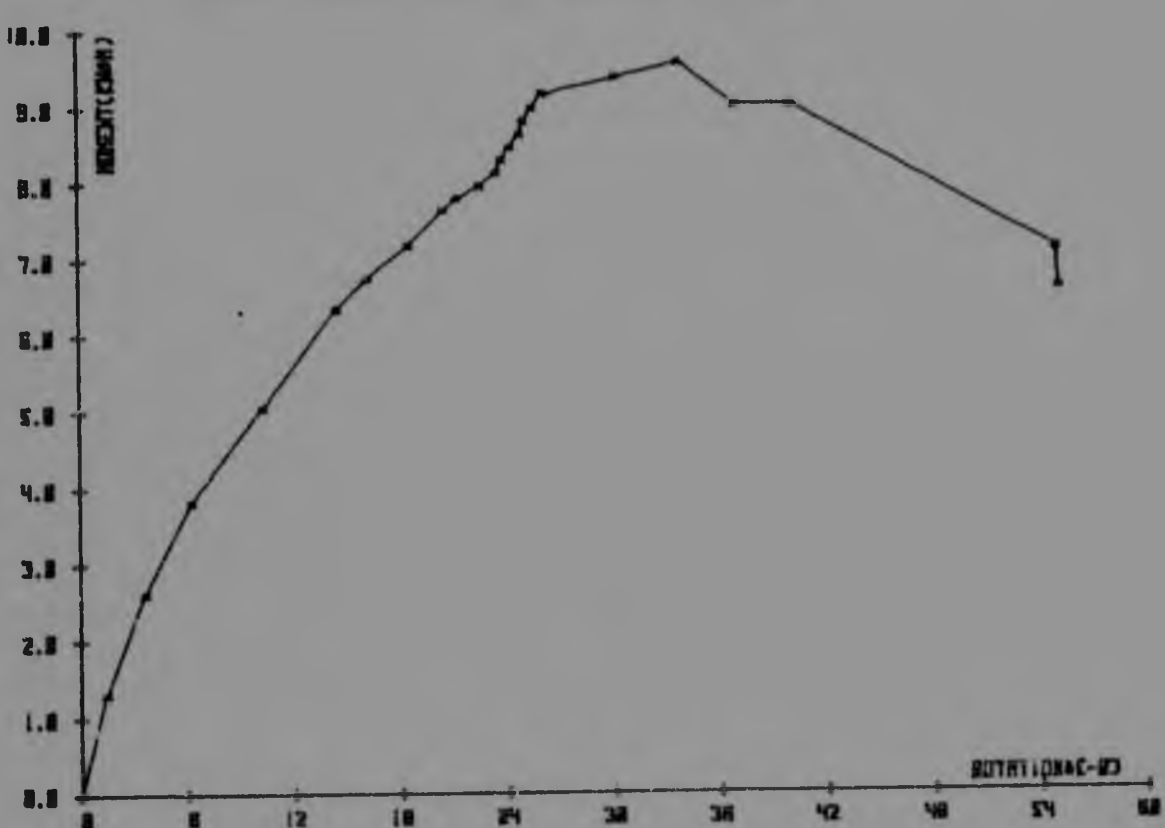

MOMENT - ROTATION CURVE FOR HALF SPAN FOR BEAM C5

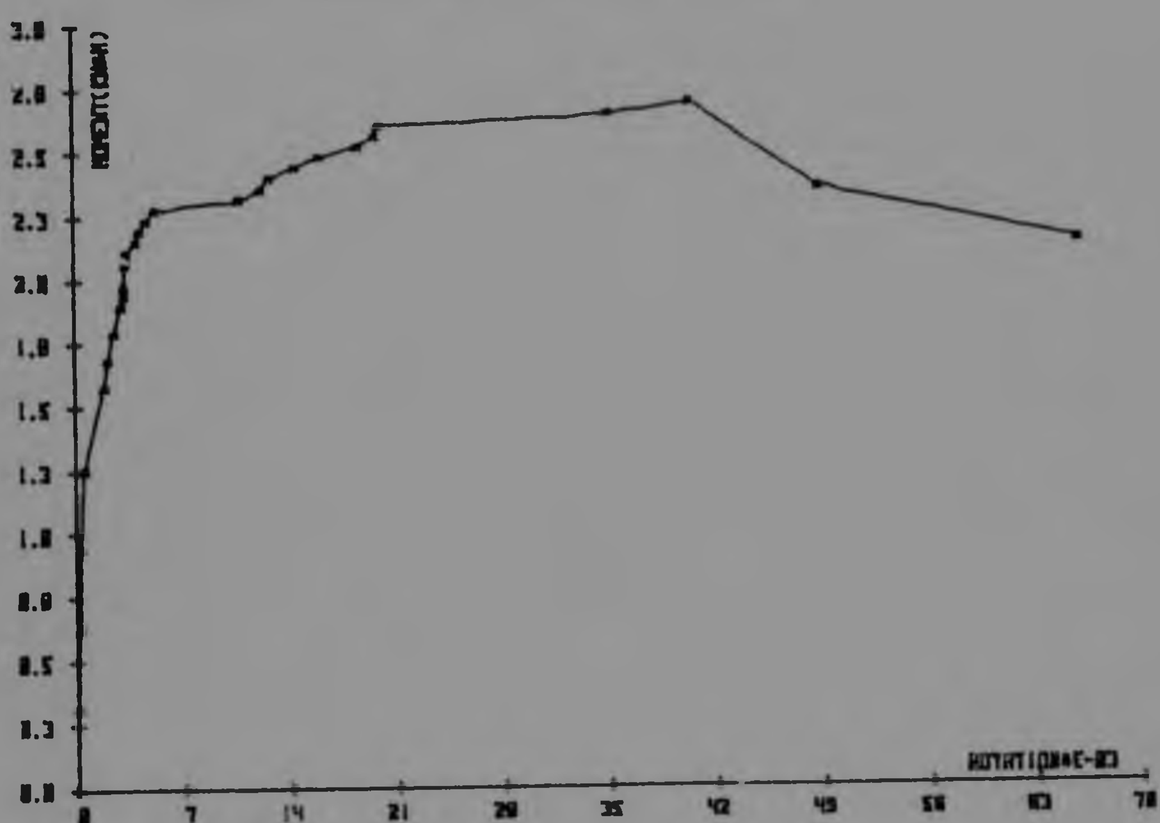

MOMENT - ROTATION CURVE FOR HALF SPAN FOR BEAM D1

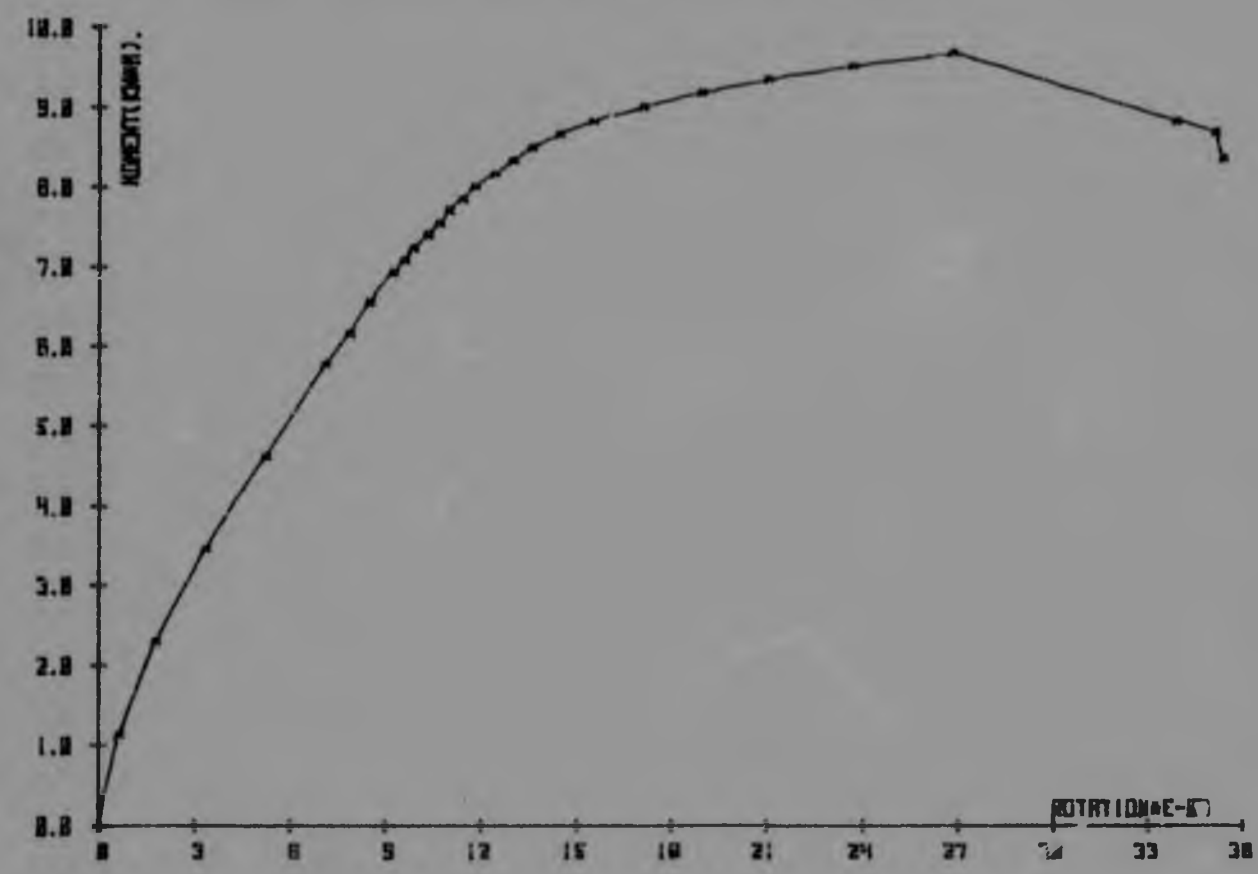

MOMENT - ROTATION CURVE FOR HALF SPAN FOR BEAM D2

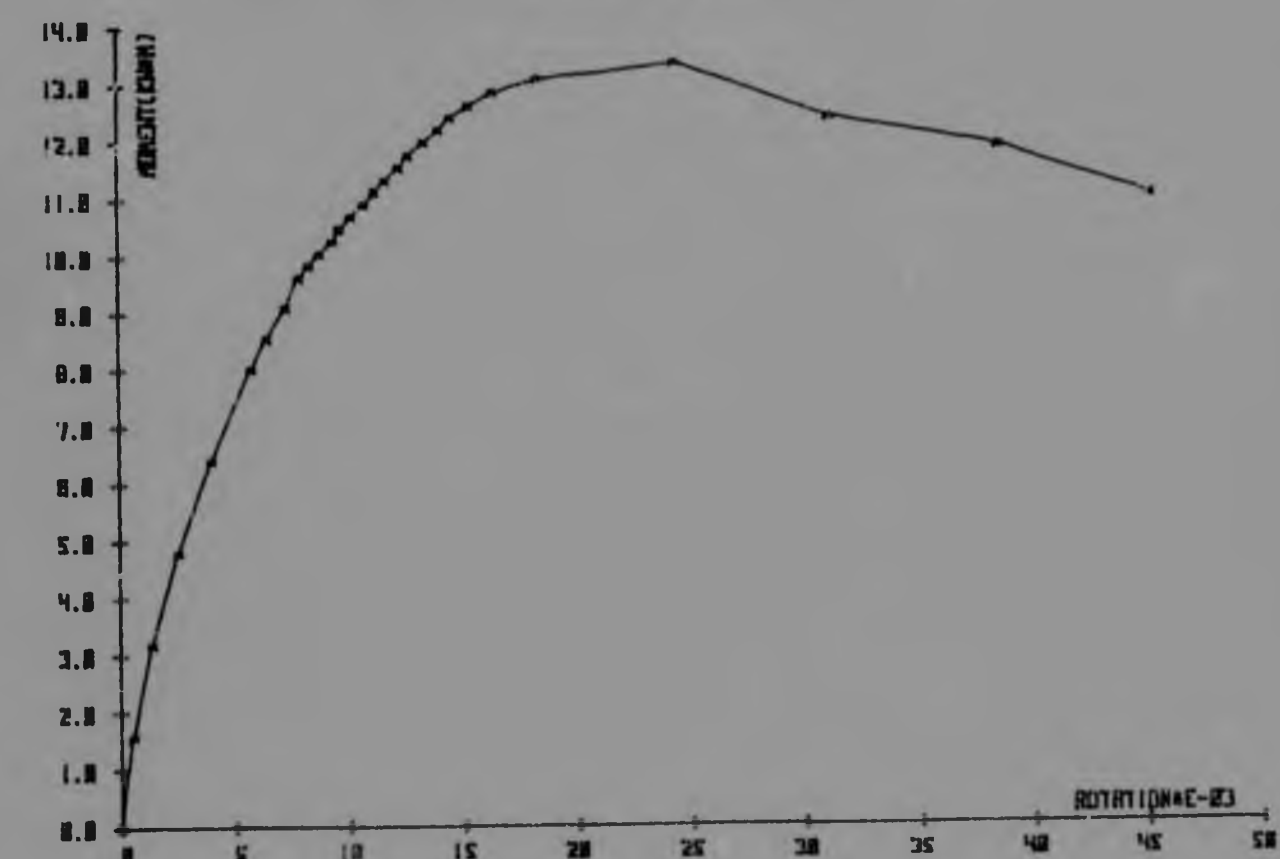

MOMENT - ROTATION CURVE FOR HALF SPAN FOR BEAM D3

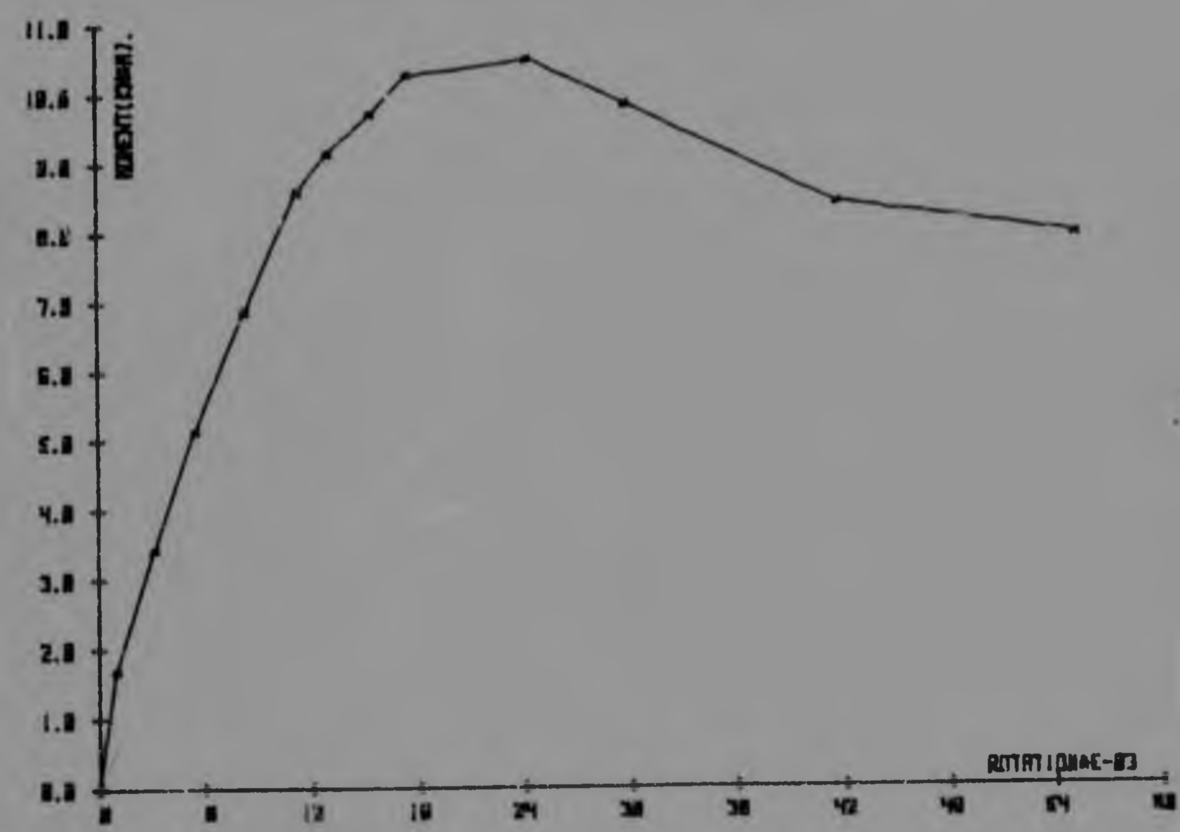

THEORETICAL AND EXPERIMENTAL MOMENT AND
NEUTRAL AXIS HEIGHT RATIOS-CURVATURE CURVES

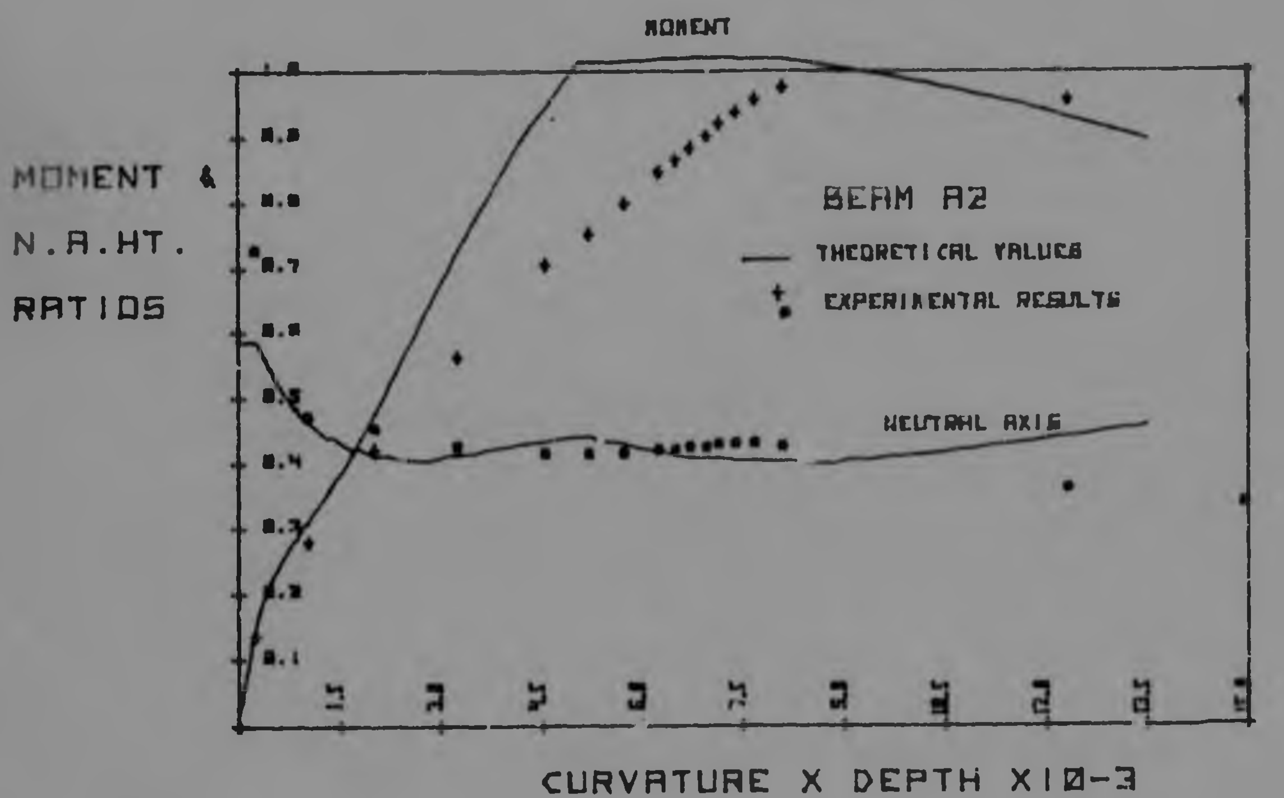
MOMENT
MOMENT &
N.A.HT.
RATIOS
BEAM A2
THEORETICAL VALUES
EXPERIMENTAL RESULTS
NEUTRAL AXIS
CURVATURE X DEPTH X10-3

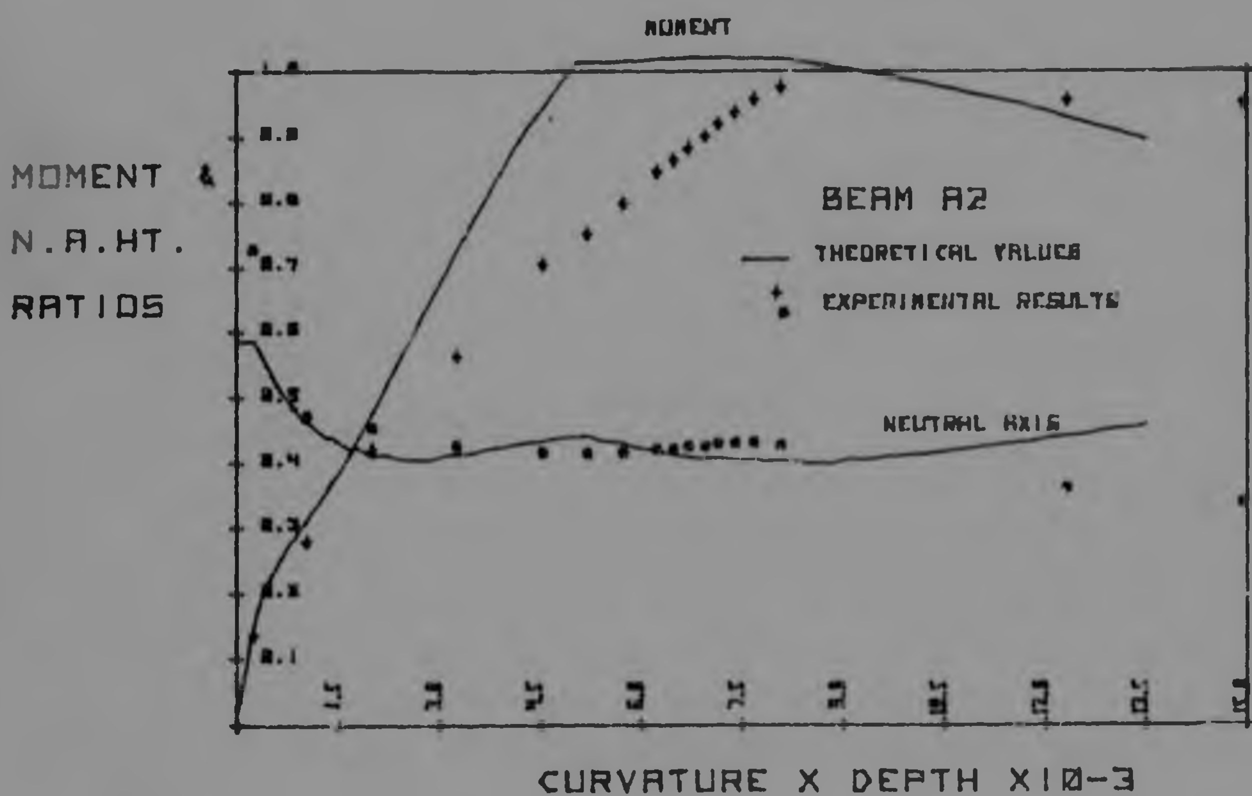
MOMENT
MOMENT &
N.A.HT.
RATIOS
BEAM A2
THEORETICAL VALUES
EXPERIMENTAL RESULTS
NEUTRAL AXIS
CURVATURE X DEPTH X10-3

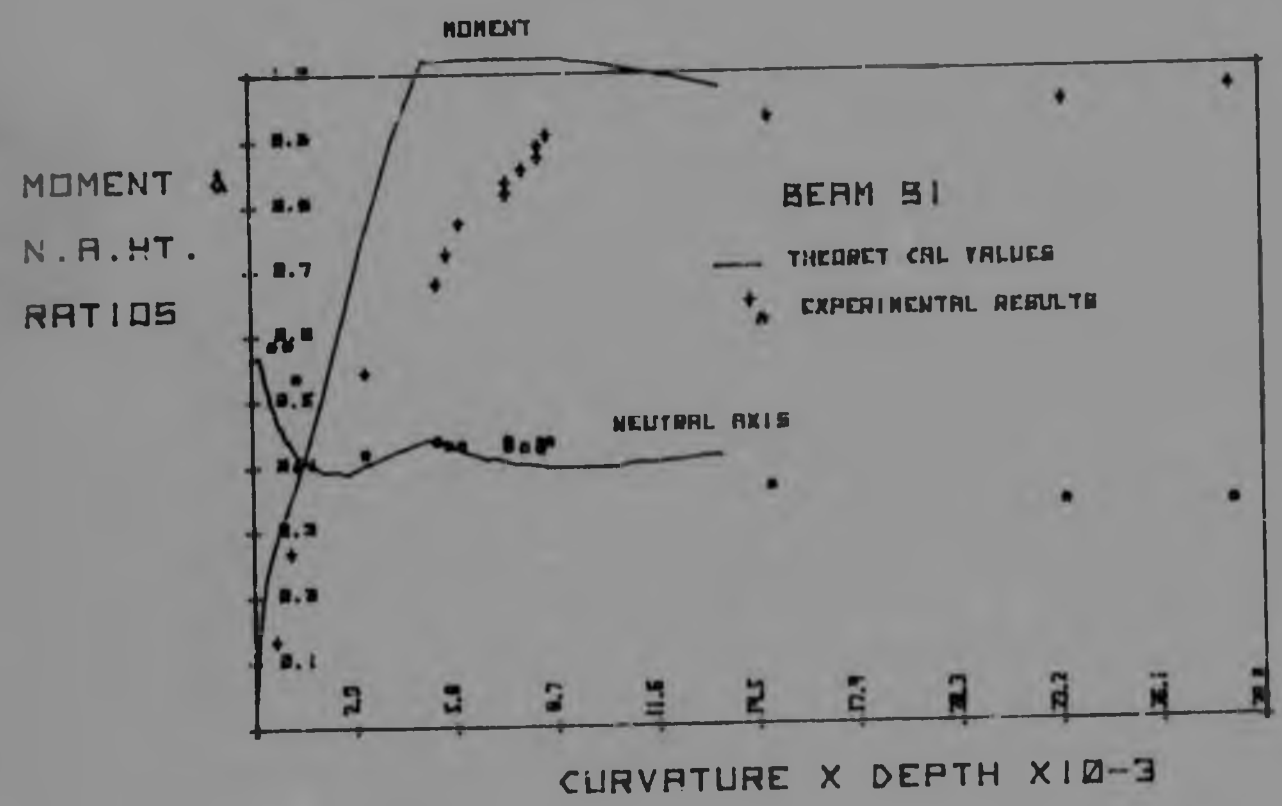
MOMENT
MOMENT &
N.A.HT.
RATIOS
BEAM B1
THEORETICAL VALUES
EXPERIMENTAL RESULTS
NEUTRAL AXIS
CURVATURE X DEPTH X10-3

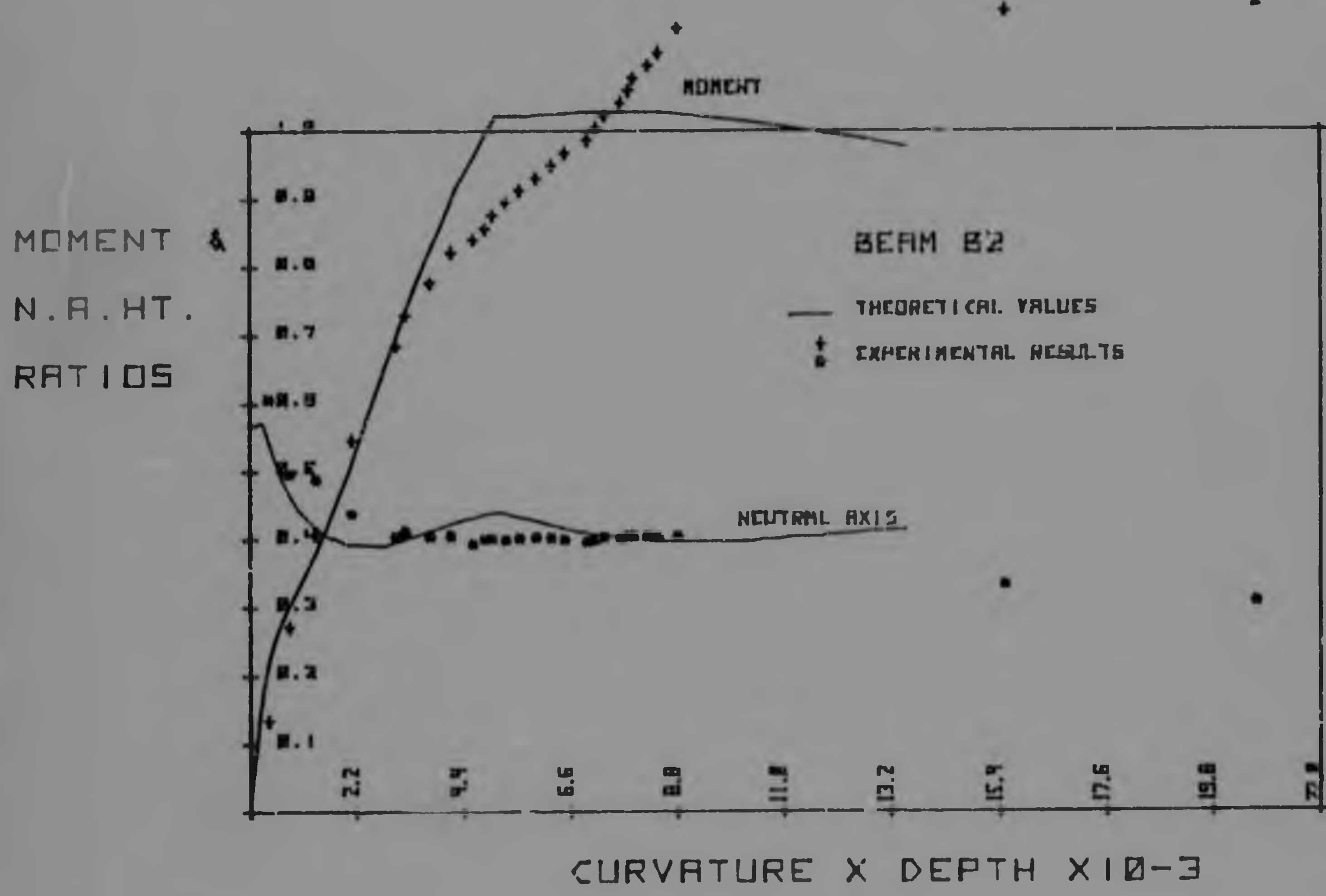
MOMENT &
N.A.HT.
RATIOS
BEAM B2
THEORETICAL VALUES
EXPERIMENTAL RESULTS
MOMENT
NEUTRAL AXIS
CURVATURE X DEPTH X10-3

162

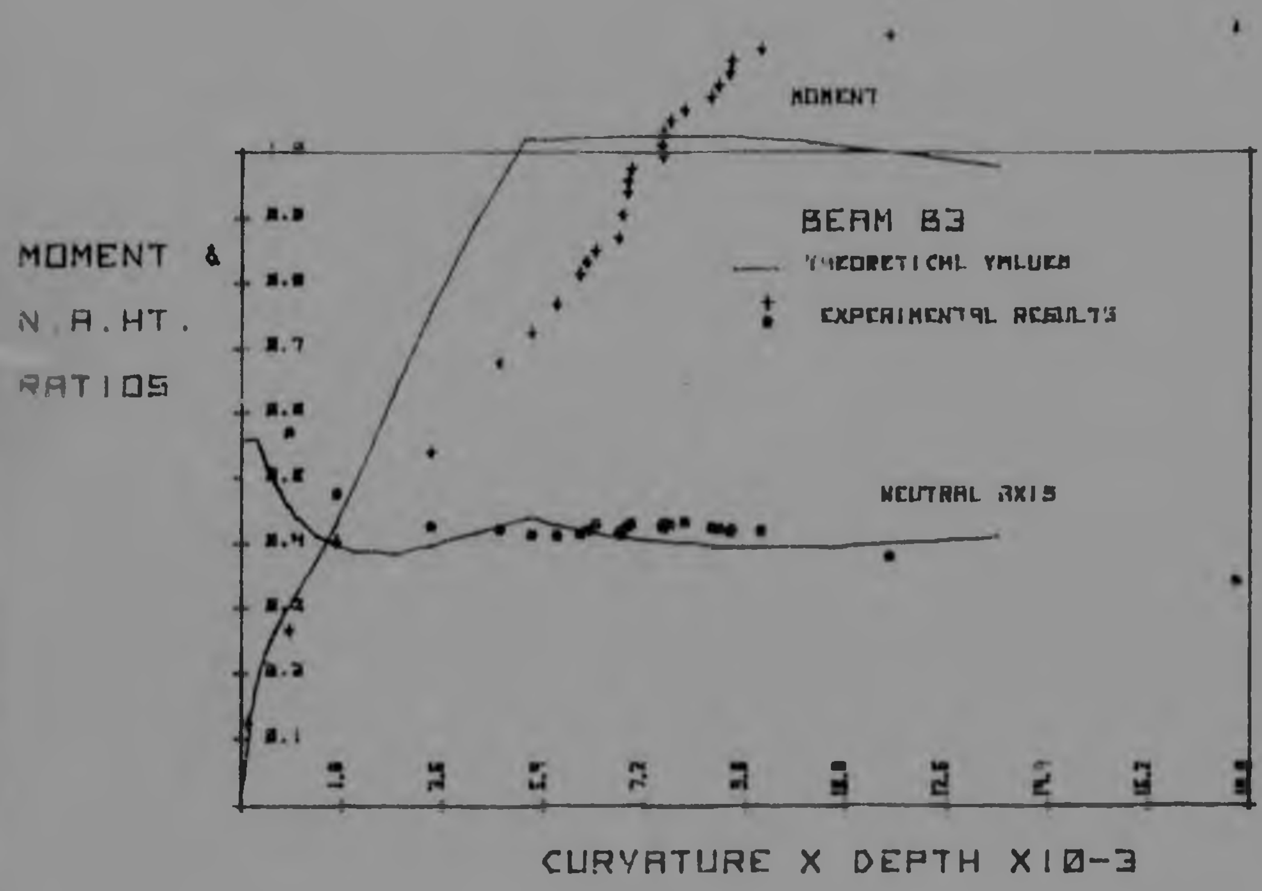
MOMENT
BEAM B3
THEORETICAL VALUES
EXPERIMENTAL RESULTS
NEUTRAL AXIS
MOMENT &
N.A.HT.
RATIOS
CURVATURE X DEPTH X10-3

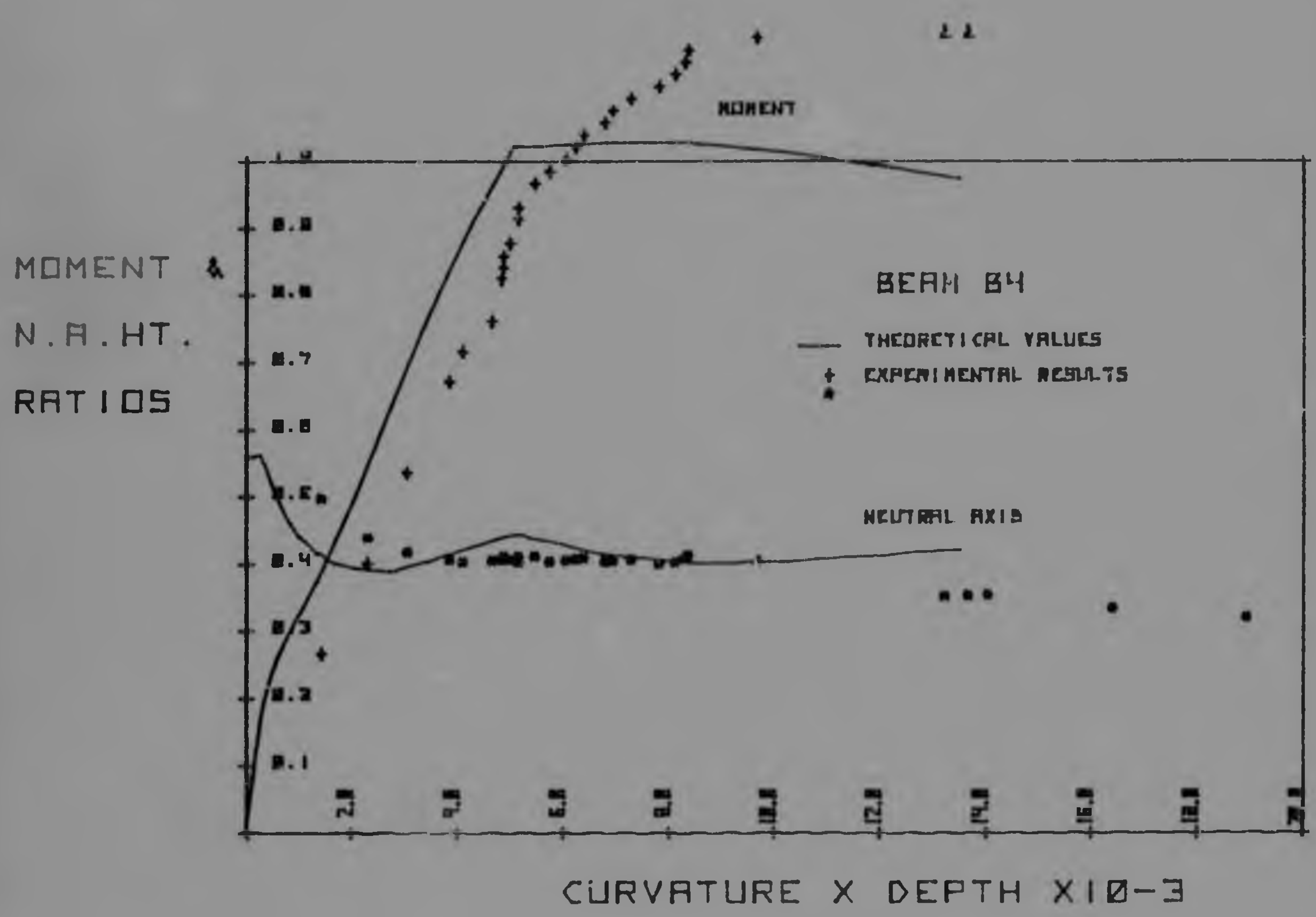
MOMENT & N.A.HT. RATIOS
MOMENT
BEAM B4
THEORETICAL VALUES
EXPERIMENTAL RESULTS
NEUTRAL AXIS
CURVATURE X DEPTH X10-3

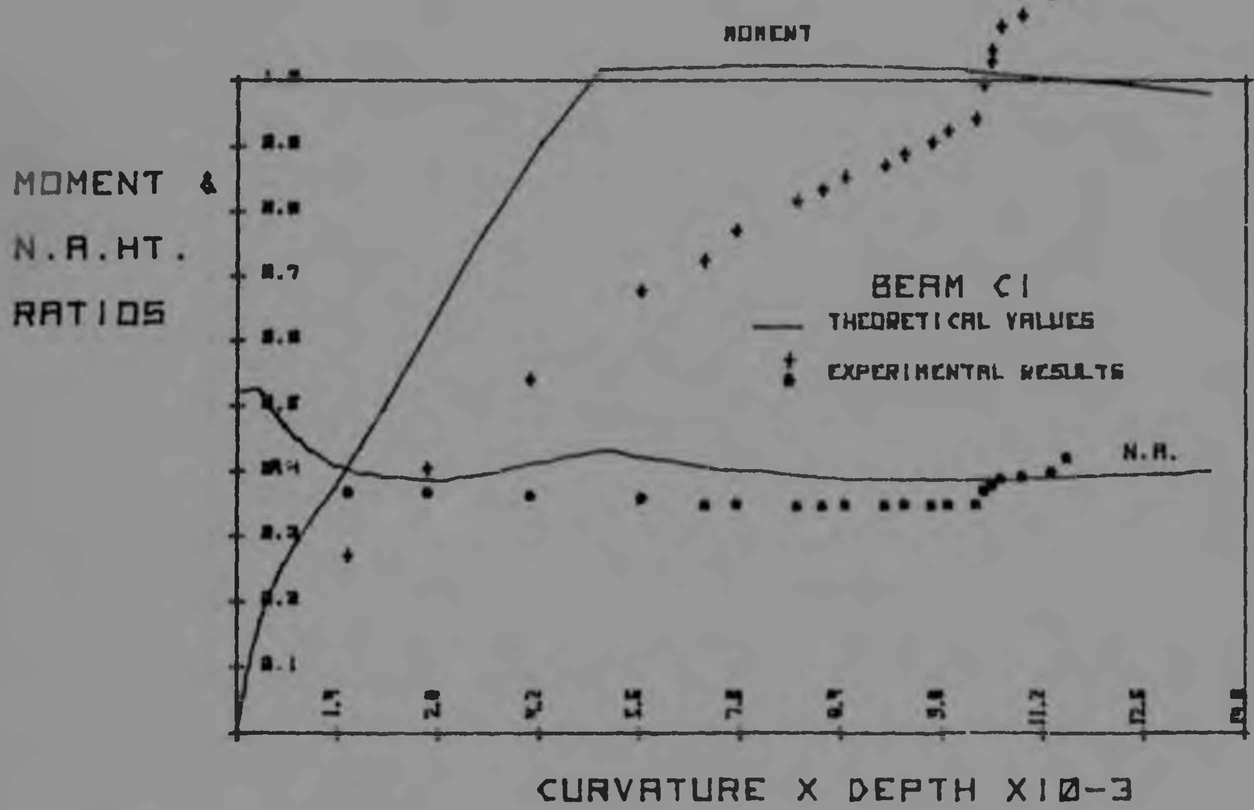
MOMENT
MOMENT & N.A.HT. RATIOS
BEAM C1
THEORETICAL VALUES
EXPERIMENTAL RESULTS
N.A.
CURVATURE X DEPTH X10-3

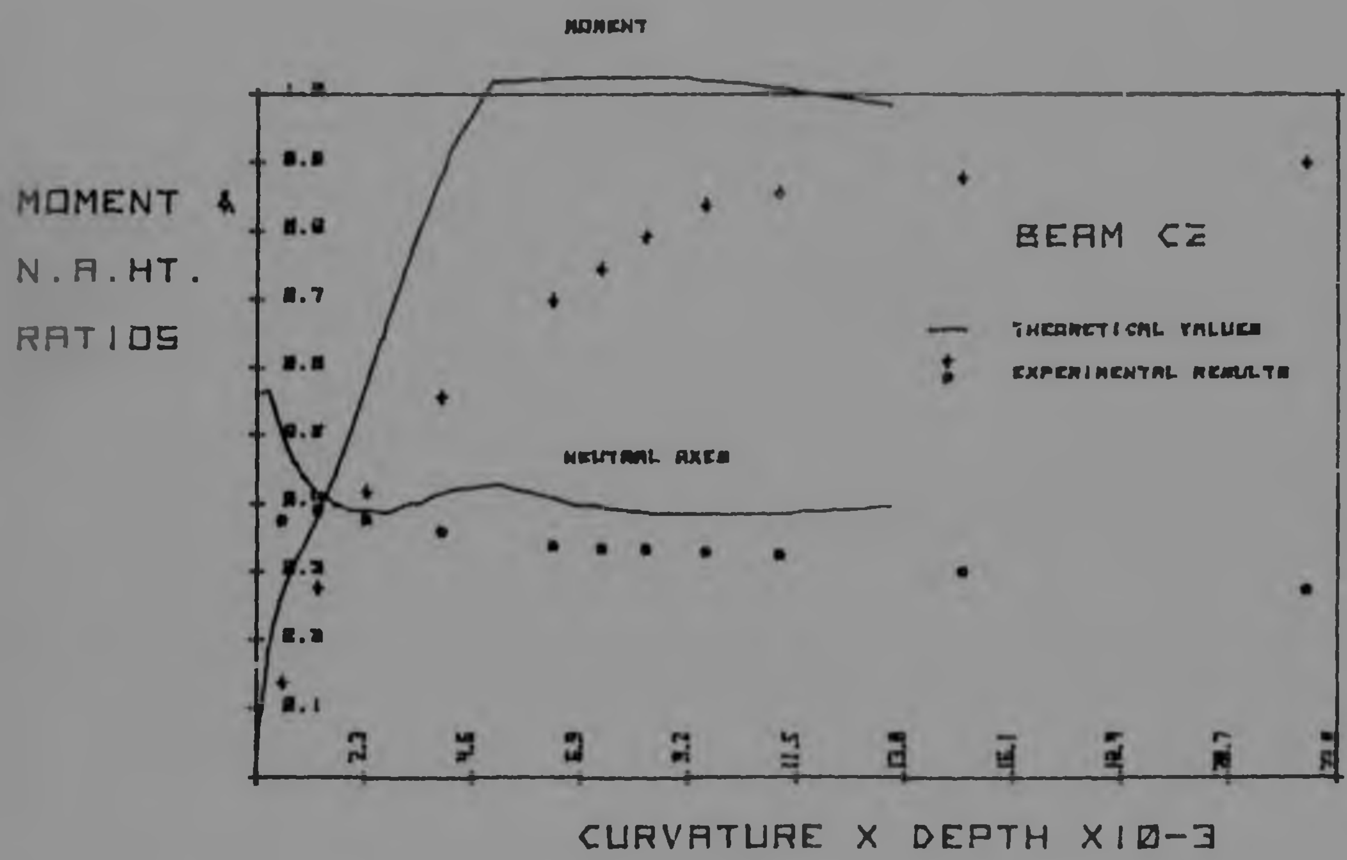
MOMENT
MOMENT &
N.A.HT.
RATIOS
BEAM C2
THEORETICAL VALUES
EXPERIMENTAL RESULTS
NEUTRAL AXES
2.3
4.6
6.9
9.2
11.5
13.8
16.1
18.4
20.7
23.0
CURVATURE X DEPTH X10-3

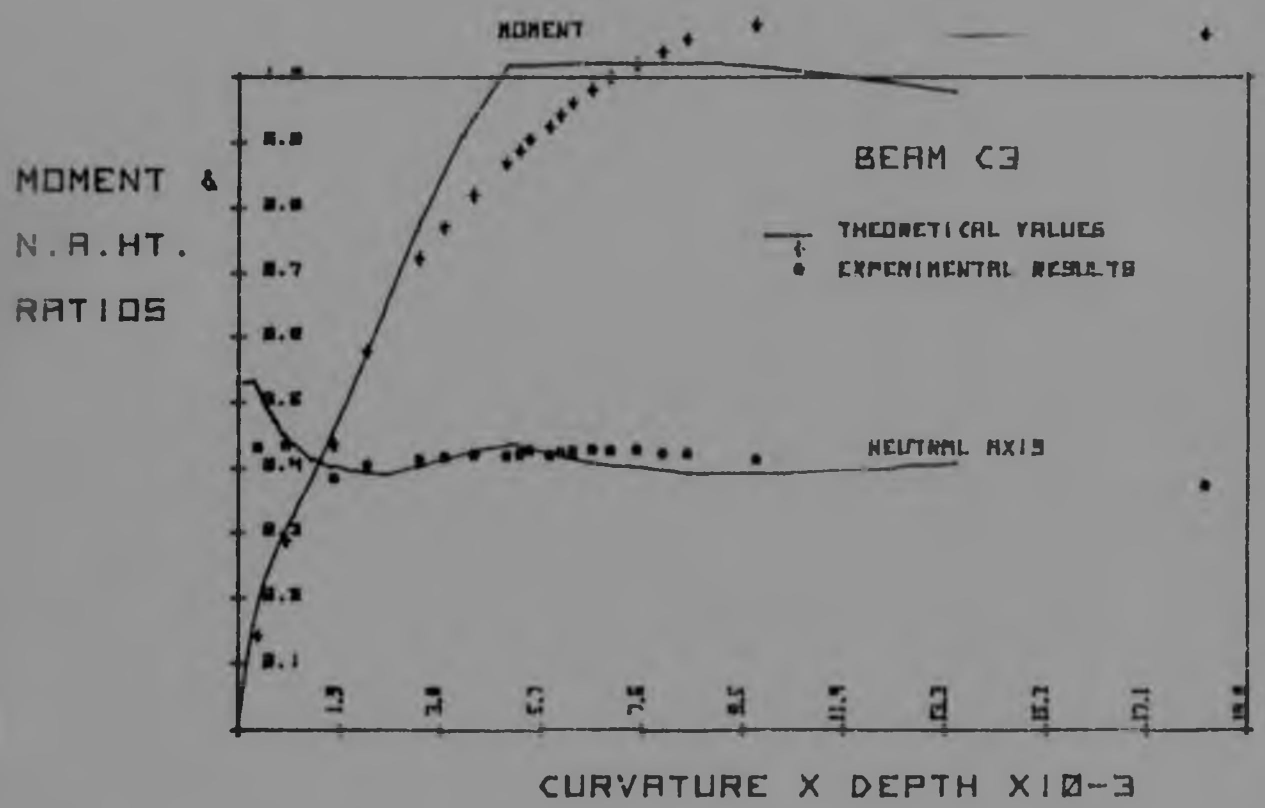
MOMENT
BEAM C3
THEORETICAL VALUES
EXPERIMENTAL RESULTS
NEUTRAL AXIS
MOMENT &
N.A.HT.
RATIOS
CURVATURE X DEPTH X10-3

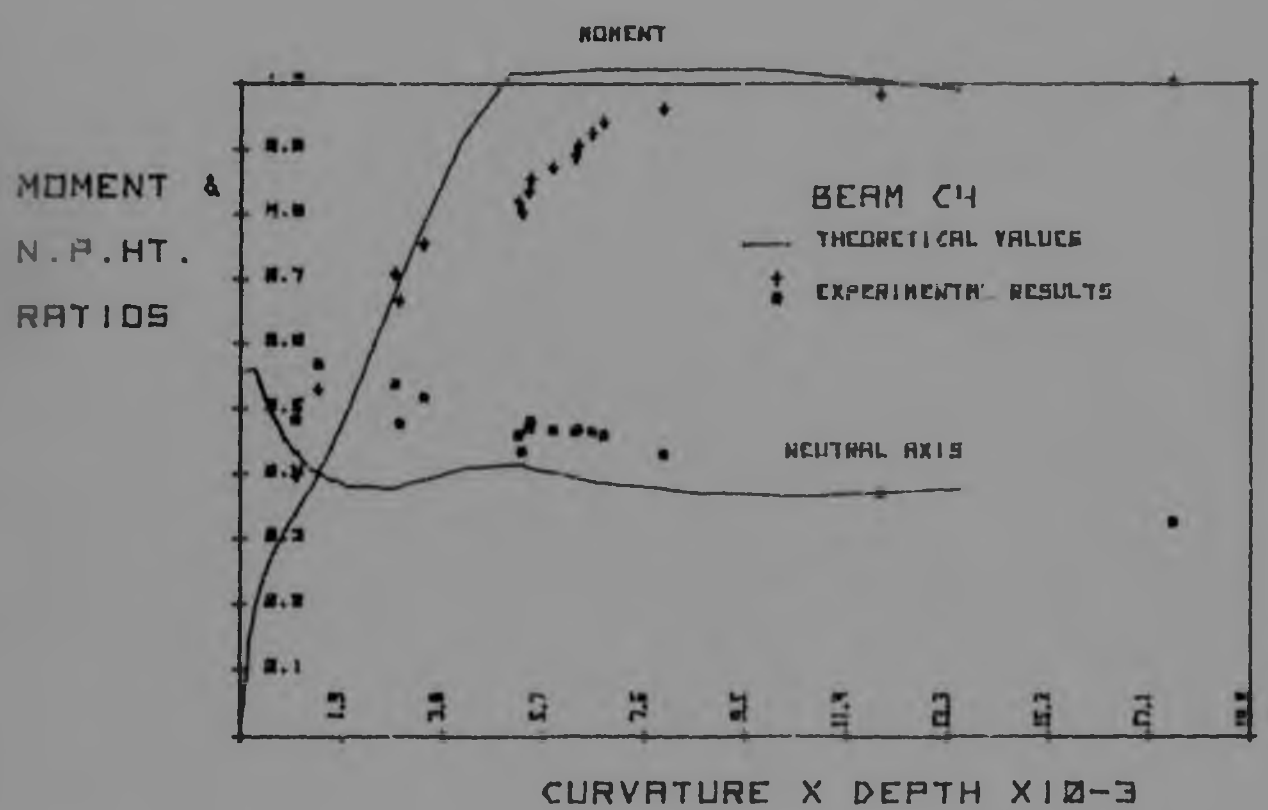
MOMENT
MOMENT &
N.P.HT.
RATIOS
BEAM C4
THEORETICAL VALUES
EXPERIMENTAL RESULTS
NEUTRAL AXIS
CURVATURE X DEPTH X10-3

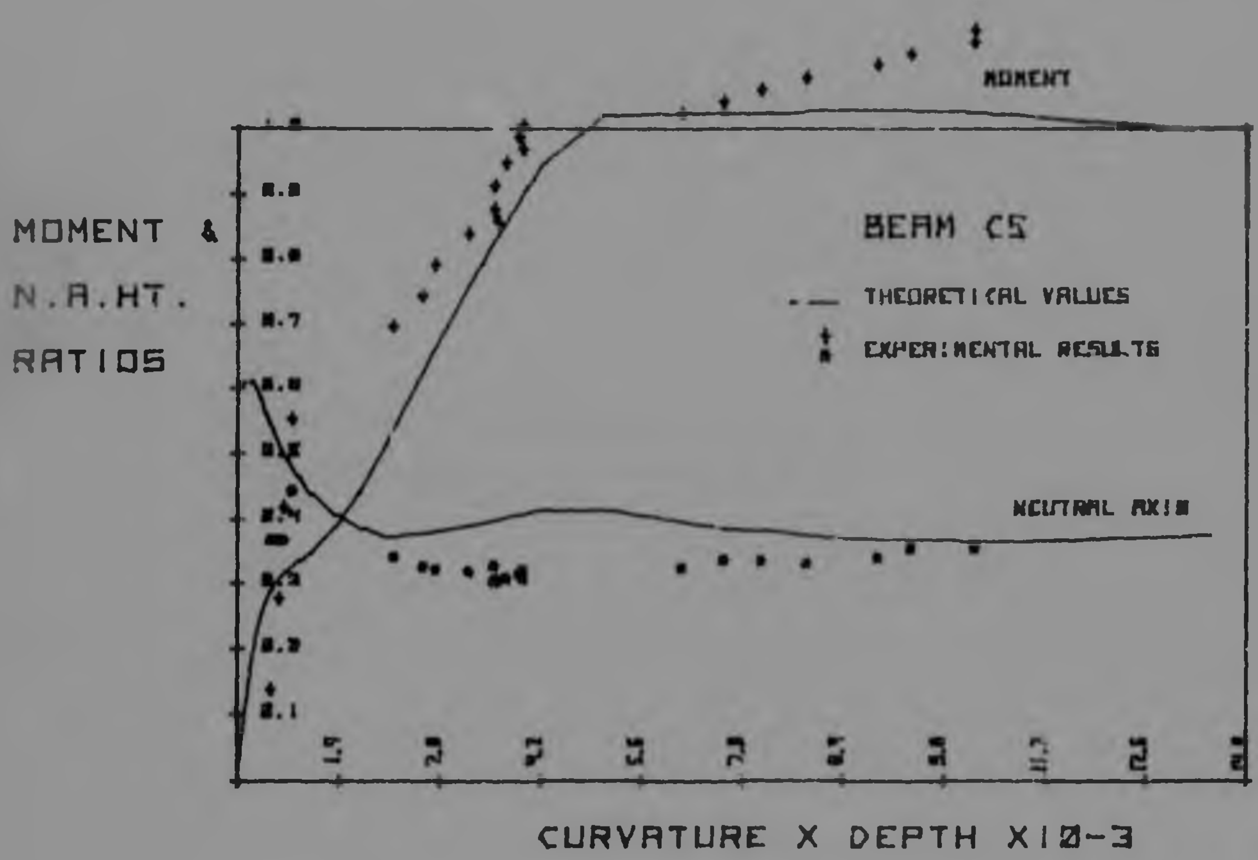
MOMENT & N.A.HT. RATIOS
BEAM C5
THEORETICAL VALUES
EXPERIMENTAL RESULTS
MOMENT
NEUTRAL AXIS
CURVATURE X DEPTH X10-3

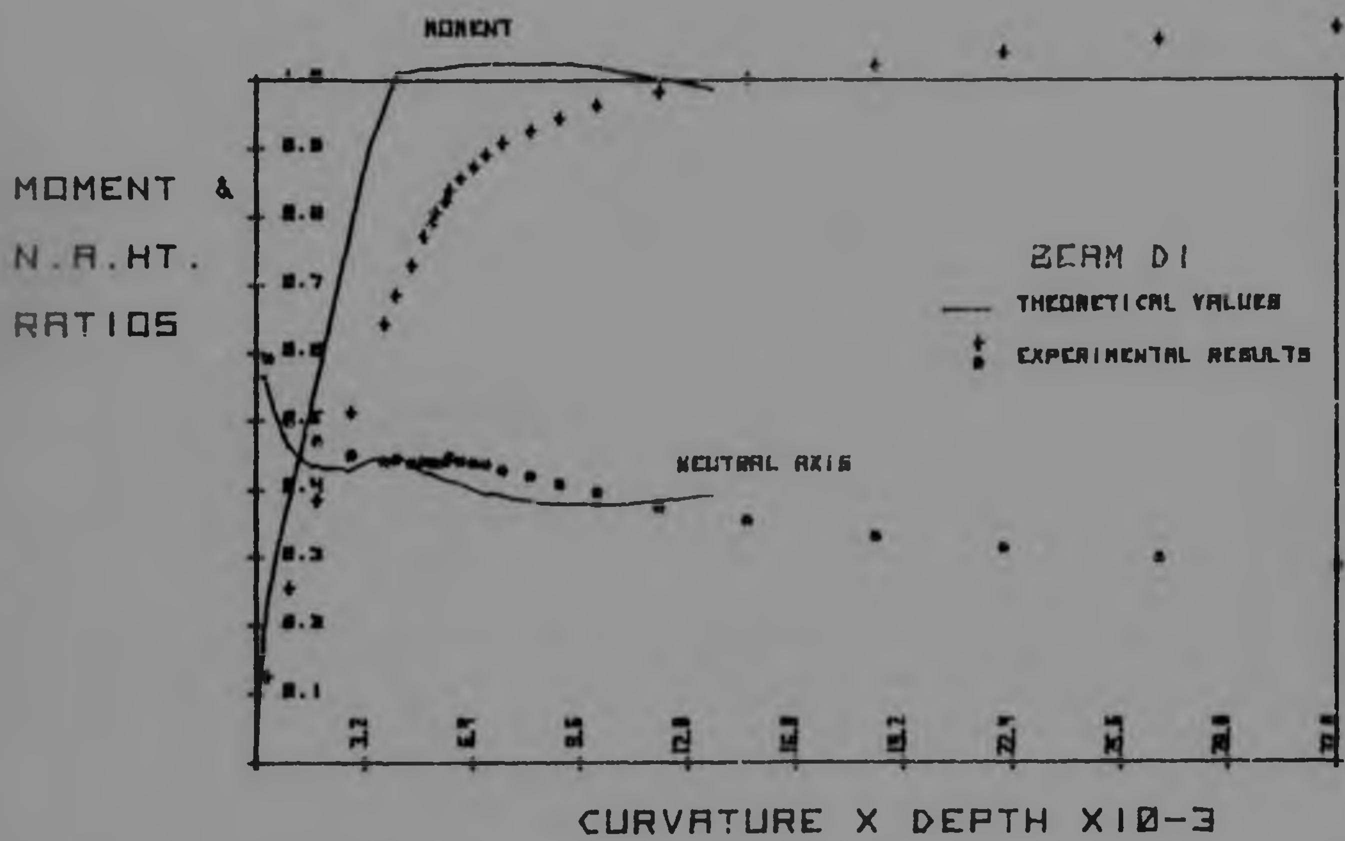
MOMENT & N.A.HT. RATIOS
MOMENT
NEUTRAL AXIS
BEAM D1
THEORETICAL VALUES
EXPERIMENTAL RESULTS
CURVATURE X DEPTH X10-3

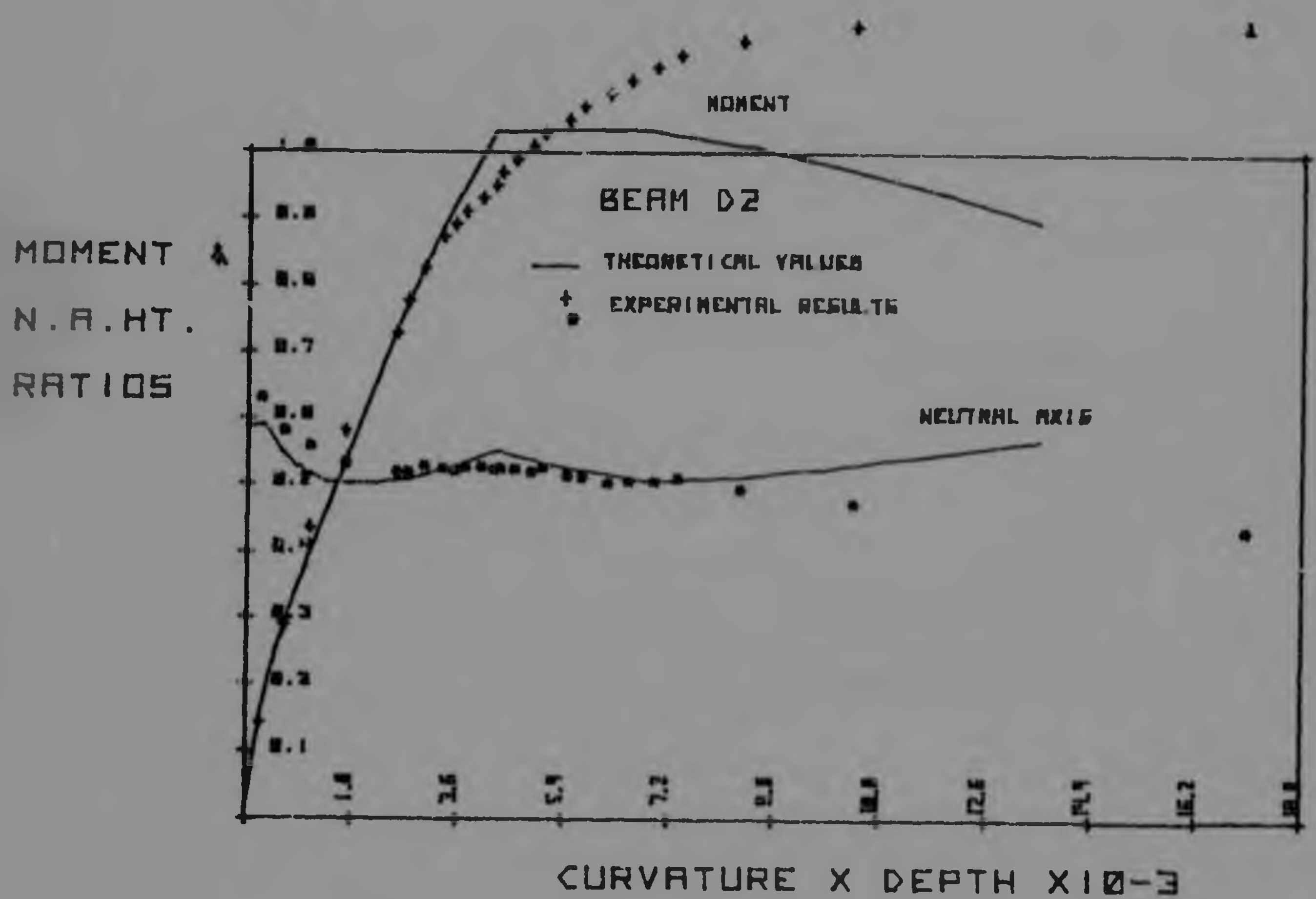
MOMENT
BEAM D2
THEORETICAL VALUES
EXPERIMENTAL RESULTS
NEUTRAL AXIS
MOMENT &
N.A.HT.
RATIOS
CURVATURE X DEPTH X10-3

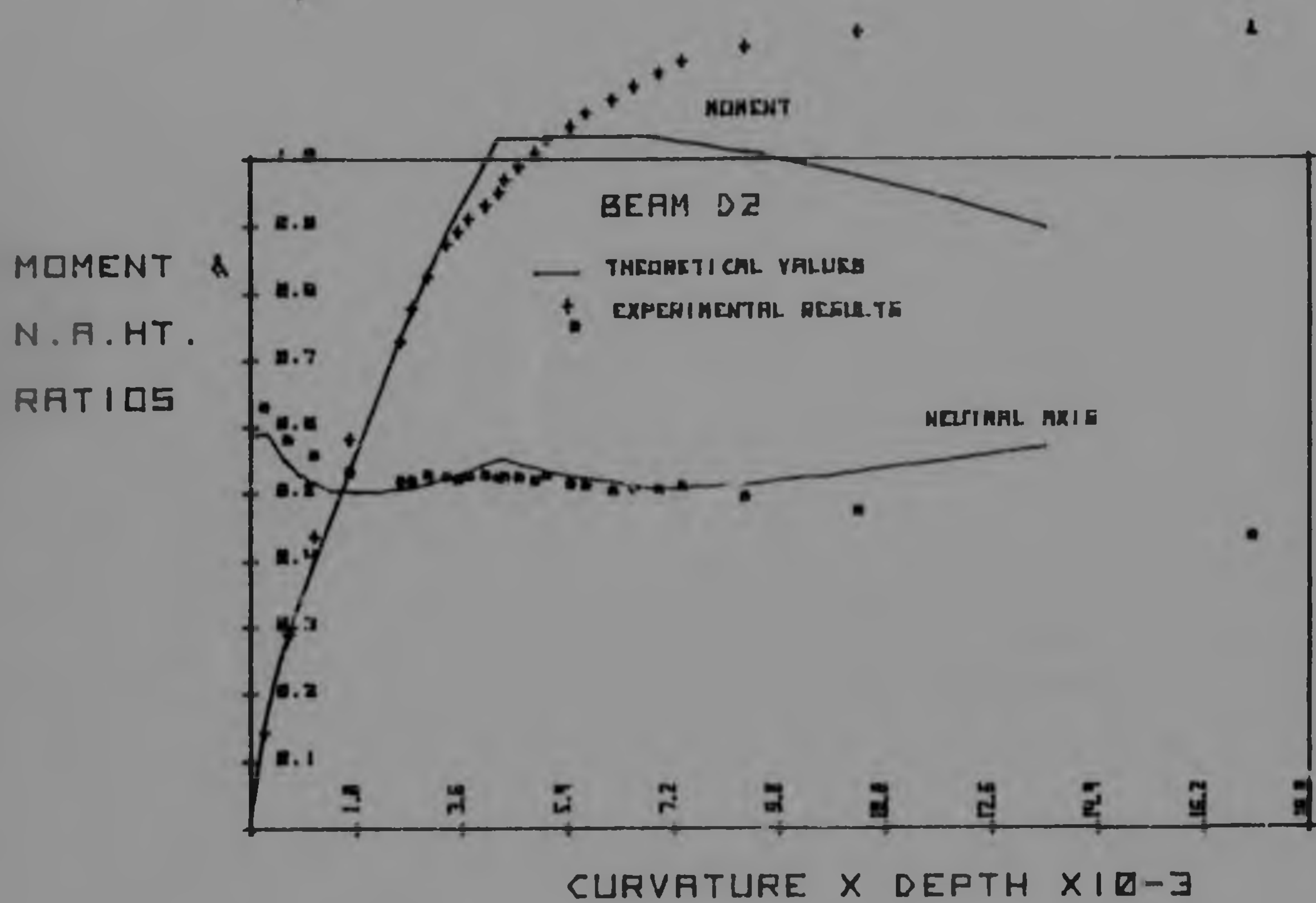
MOMENT
BEAM D2
THEORETICAL VALUES
MOMENT &
N.A.HT.
RATIOS
CURVATURE X DEPTH X10-3

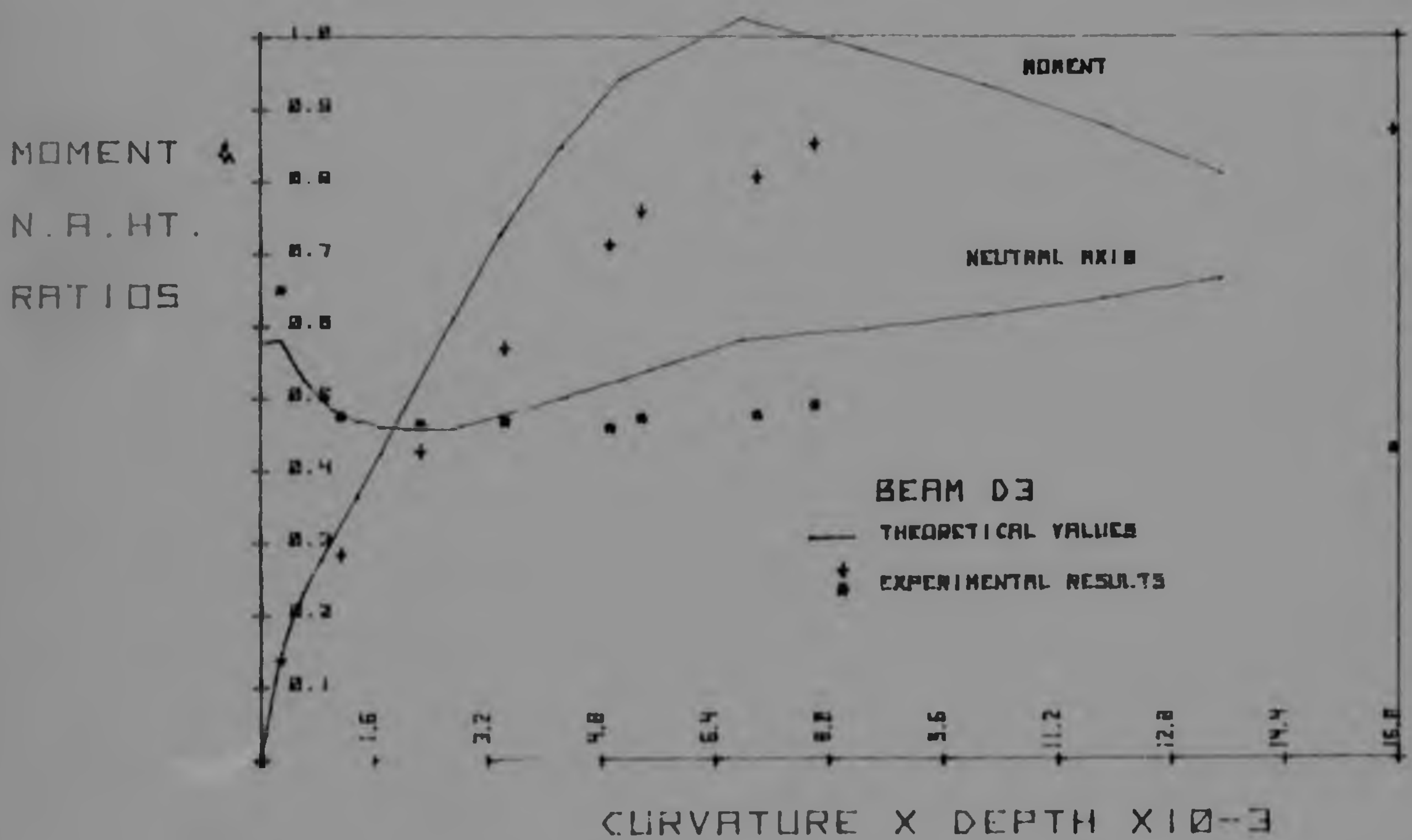
MOMENT &
N.A.HT.
RATIOS
MOMENT
NEUTRAL AXIS
BEAM D3
THEORETICAL VALUES
EXPERIMENTAL RESULTS
CURVATURE X DEPTH X10-3